doi.org/10.26434/chemrxiv.7828769.v3

Chemoenzymatic ortho-quinone methide formation

Tyler Doyon, Jonathan Perkins, Summer A. Baker Dockrey, Evan O. Romero, Kevin Skinner, Paul M. Zimmerman, Alison Narayan

Submitted date: 26/10/2019 • Posted date: 29/10/2019

Citation information: Doyon, Tyler; Perkins, Jonathan; Dockrey, Summer A. Baker; Romero, Evan O.; Skinner, Kevin; Zimmerman, Paul M.; et al. (2019): Chemoenzymatic ortho-quinone methide formation. ChemRxiv. Preprint.

Generation of reactive intermediates and interception of these fleeting species in a cascade is a common strategy employed by Nature. However, formation of these species under mild conditions using traditional synthetic techniques can present a challenge. Here, we demonstrate the utility of biocatalysis in generating ortho-quinone methide intermediates under aqueous conditions and at reduced temperatures. Specifically, we applied an α-ketoglutarate-dependent non-heme iron enzyme, CitB, in the selective modification of benzylic C–H bonds of ortho-cresol substrates to afford a benzylic alcohol product which, under the reaction conditions, is in equilibrium with the corresponding ortho-quinone methide. Interception of the ortho-quinone methide by a nucleophile or a dienophile allows for one-pot conversion of benzylic C–H bonds into C–C, C–N, C–O, and C–S bonds in a chemoenzymatic cascade.

File list (2)

Chemoenzymatic *ortho*-quinone methide formation

Tyler J. Doyon,[1,2+] Jonathan C. Perkins,[1,3+] Summer A. Baker Dockrey,[1,3] Evan O. Romero,[1,3] Kevin C. Skinner,[1,3] Paul M. Zimmerman,[3] Alison R. H. Narayan[1,2,3*]

[1]Life Sciences Institute, University of Michigan, Ann Arbor, Michigan 48109, USA. [2]Program in Chemical Biology, University of Michigan, Ann Arbor, Michigan 48109, USA. [3]Department of Chemistry, University of Michigan, Ann Arbor, Michigan 48109, USA.

[+] These authors contributed equally to this work.

*Corresponding author, email: arhardin@umich.edu

KEYWORDS: biocatalysis, C–H functionalization, ortho-quinone methide

ABSTRACT: Generation of reactive intermediates and interception of these fleeting species under physiological conditions is a common strategy employed by Nature to build molecular complexity. However, formation of these species under mild conditions using traditional synthetic techniques can present a challenge. Here, we demonstrate the utility of biocatalysis in generating *ortho*-quinone methide intermediates under aqueous conditions and at reduced temperatures. Specifically, we applied α-ketoglutarate-dependent non-heme iron enzymes, CitB and ClaD, in the selective modification of benzylic C–H bonds of *ortho*-cresol substrates. In this transformation, these biocatalysts directly hydroxylate a benzylic C–H bond to afford a benzylic alcohol product which, under the reaction conditions, is in equilibrium with the corresponding *ortho*-quinone methide. Interception of the *ortho*-quinone methide by a nucleophile or a dienophile allows for one-pot conversion of benzylic C–H bonds into C–C, C–N, C–O, and C–S bonds in a chemoenzymatic cascade. The versatility of this method is demonstrated through preparative-scale reactions, selective modification of peptides, and chemoenzymatic synthesis of the chroman natural product (–)-xyloketal D.

INTRODUCTION

Nature has developed strategies for the generation of highly reactive intermediates for the control of reactions in the synthesis of complex secondary metabolites.[1-2] Synthetic approaches that mimic biosynthetic pathways often encounter challenges in reproducing the elegance of these evolved methods, at times requiring blocking groups to achieve site-selectivity, protection of sensitive functional groups, and harsh or forcing conditions to access reactive intermediates.[3-6] *Ortho*-quinone methide species (*o*-QM, **4**) have been implicated in the biosynthesis of multiple families of natural products, as these versatile intermediates can readily participate in inverse electron-demand Diels-Alder (IEDDA) or 1,4-addition reactions.[3-5] These valuable and reactive intermediates have been used in the synthesis of a diverse array of natural products and bioactive compounds.[3-6] Several synthetic strategies have been developed to access *o*-QMs through the oxidative functionalization of phenolic substrates to generate *o*-QM precursors (Fig. 1A, **2**-**3**).[3-6] These methods typically involve the installation of a benzylic leaving group, followed by prolonged heating of the precursor to generate the corresponding *o*-QM.[7-9] This route can also require super-stoichiometric reagents to activate the benzylic leaving-group, leading to reduced atom economy.[7] Efforts to access *o*-QMs more efficiently have led to direct oxidation methods using transition metals or organic oxidants, to generate *o*-QMs in a one-pot system without the need for pre-functionalization of the substrate (Fig. 1A, **5**-**6**).[3-6, 10-16] However, this approach is generally restricted to electron-rich compounds and does not provide control over the site-selectivity of the benzylic oxidation.[3-6, 10-16] Furthermore, one-pot generation and functionalization of *o*-QMs requires a delicate balance between reactivity of the oxidant and compatibility with reagents for *o*-QM diversification.[3, 15] Often, the harsh oxidizing reagents which are required for *o*-QM generation can interfere with downstream functionalization of *o*-QMs or prove incompatible with sensitive moieties on the substrate.[3] As a result, significant reagent screening campaigns are often necessary to optimize direct oxidation reactions, creating additional constraints on the application of this approach.[3, 10-11, 13-15] Therefore, a one-pot method for the chemo- and site-selective generation and diversification of *o*-QMs would address key challenges in exploiting these useful synthetic intermediates in synthesis.

Inspired by the efficiency of Nature's approach for the generation of *o*-QMs, we sought to exploit enzymatic mechanisms for *o*-QM creation.[17] In these systems, the *o*-QM is proposed to arise from *ortho*-cresol precursors (see **7**, **9**, Fig. 1B) through hydroxylation of the benzylic position, followed by loss of water to directly form an *o*-QM under mild

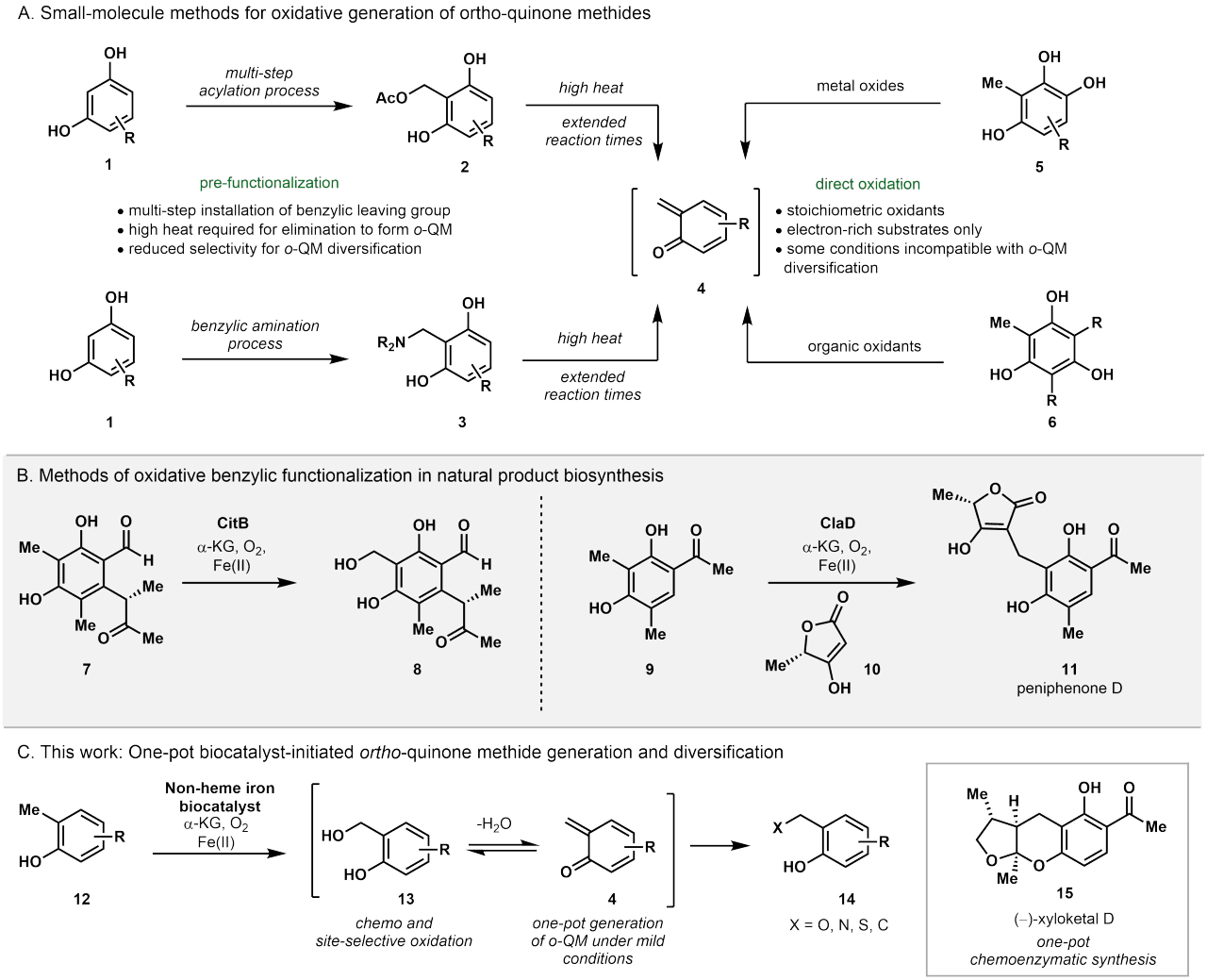

Figure 1. A. Oxidative methods for generation of *ortho*-quinone methides (*o*-QMs). B. Biocatalytic oxidative benzylic functionalization. C. This work: One-pot biocatalyst-initiated *o*-QM generation and diversification.

intracellular conditions.[17] These intermediates are subsequently functionalized with bioavailable dienophiles or nucleophiles, generating the associated natural products, such as peniphenone D (**11**).[17] We anticipated that a biocatalytic approach to oxidative *o*-QM generation could afford numerous advantages in the development of a selective and sustainable method (Fig. 1C). This approach would combine the selectivity advantages of biocatalytic pre-functionalization with the ability to generate and diversify the *o*-QM in the same vessel under mild conditions. We also anticipated that the reactive nature of *o*-hydroxybenzylic alcohols would reduce required reaction times and temperatures, leading to efficient functionalization of the resulting *o*-QM.

Nature has evolved numerous tools for the oxidation of benzylic C–H bonds. Several reports have highlighted the utility of whole microorganism biotransformations in accomplishing this challenging transformation.[18-23] These methods rely on native monooxygenases present in microbes to accomplish benzylic oxidation on a range of substrates.[18-23] Several cytochromes P450 have also been identified as promising *in vitro* catalysts for benzylic C–H oxygenation.[24-32] Whereas these biocatalytic methods do not offer complete control over the final oxidation state of the product, they successfully reduce the overall environmental impact of the transformation by using earth-abundant iron as the catalytic metal, molecular oxygen as the stoichiometric oxidant, and water as the bulk solvent.[24-32]

Motivated by the advantages of an enzymatic approach to benzylic hydroxylation, we sought to demonstrate the site- and chemoselectivity of biocatalytic C–H functionalization and opportunities for cascade reactions under biocatalytic reaction conditions. We anticipated that an α-ketoglutarate-dependent (α-KG) non-heme iron oxygenase could be employed for the selective oxidation of primary benzylic C–H bonds. This well-studied family of enzymes has precedent for both scalability[33] and substrate scope tunability through protein engineering.[34]

By coupling the activation of molecular oxygen to the decarboxylation of inexpensive α-oxoacid co-substrates, these enzymes generate an iron(IV)-oxo species capable of H-atom abstraction (Fig. 1C).[35-36] α-KG-dependent non- heme iron oxygenases catalyze a wide variety of site-selective transformations following this conserved mechanism of oxygen activation, including hydroxylation, halogenation, epoxidation, desaturation, epimerization, endo-peroxidation, ring-contraction, and ring-expansion.[35-37] Unlike many P450s, α-KG-dependent non-heme iron oxygenases do not

require an exogenous reductase to complete their catalytic cycle.[35-36] We anticipated that the relatively simple reaction requirements of α-KG-dependent non-heme iron oxygenases would provide distinct advantages in developing a widely applicable and practical approach to biocatalytic benzylic C–H hydroxylation and subsequent *o*-QM generation.

Our search for biocatalysts for selective benzylic C–H hydroxylation led us to two homologous fungal NHI oxygenases (sharing 54% sequence identity): (1) CitB, from *Monascus ruber* and (2) ClaD, native to *Penicillium crustosum*.[38] Cox and coworkers demonstrated through *in vivo* experiments that CitB performs a benzylic hydroxylation in the biosynthesis of the mycotoxin citrinin (**8**, Fig. 1B).[38] ClaD was shown by Li and coworkers to perform a similar transformation in the biosynthesis of peniphenones and penilactones (Fig. 1B, **9**-**11**).[17] We envisioned employing CitB and ClaD as general catalysts for benzylic hydroxylation of *ortho*-cresol substrates. We anticipated that, following benzylic C–H bond oxidation, an *o*-QM intermediate (see **12**-**14** Fig. 1C) could be accessed and intercepted with a variety of nucleophiles or dienophiles to form benzylic C–O, C–N, C–S, and C–C bonds in a biomimetic fashion.[17] Here, we demonstrate this approach with two biocatalysts, but we anticipate this chemoenzymatic platform could be executed with a plethora of wild-type enzymes to access more diverse substrates and complementary selectivity.

RESULTS AND DISCUSSION

Toward developing a chemoenzymatic method for benzylic C–H functionalization, we tested the feasibility of biocatalytic C–H hydroxylation, coupled with *o*-QM formation and derivatization with a model substrate (see **16**, Fig. 2) that captures the conserved methyl resorcinol core of CitB and ClaD's native substrates. This model compound maintained the redox-sensitive aldehyde moiety and hydroxyl groups present in the citrinin biosynthetic intermediate (**7**). This model compound, **16**, was completely consumed in 3 h upon exposure to 0.4 mol % CitB in the presence of α-KG, an iron(II) source and sodium ascorbate in 50 mM TES buffer at pH 7.5 (Fig. 2). From this reaction, a single benzylic alcohol product (**17**) was isolated in 82% yield without any evidence of oxidation of either the aldehyde or the resorcinol core. This result demonstrated that CitB could function on a non-native substrate with the robustness needed for preparative-scale synthesis with precise chemo- and site-selectivity. As a comparative measure, we subjected substrate **16** to several chemical oxidation conditions and did not observe conversion to desired benzylic alcohol **17** (see Supporting Information, Table S1). For example, attempts to oxidize **16** with DDQ[39] resulted in over-oxidation to the bisaldehdye and exposure of **16** to MnO_2[40] or Ag_2O[41] resulted in no observed reaction. Efforts to perform a benzylic hydroxylation with $K_2S_2O_8$[42] or cerium ammonium nitrate[43] led to decomposition of the substrate. Radical bromination with AIBN/NBS resulted in aromatic bromination and did not generate the desired benzylic halide for subsequent hydrolysis to the benzyl alcohol.[44] These results capture the challenge in accomplishing this seemingly simple benzylic hydroxylation in the presence of redox-sensitive aldehyde and phenolic groups, as well as the advantages provided by biocatalytic benzylic C–H hydroxylation. Next, the reactivity

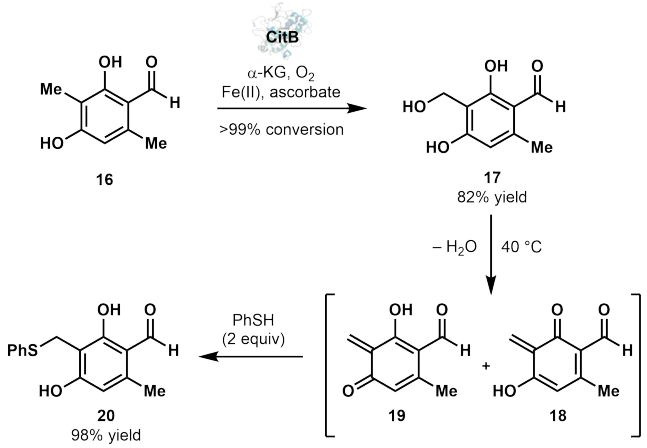

Figure 2. Initial experiments to assess feasibility of NHI biocatalyst-initiated *ortho*-quinone methide formation and functionalization.

of benzylic alcohol **17** was investigated under aqueous conditions. Gratifyingly, upon gentle heating in the presence of thiophenol, alcohol **17** was quantitatively transformed into thioether **20** through an anticipated *o*-QM intermediate (**18**-**19**). These experiments provided evidence for *o*-QM formation under remarkably mild conditions compared to previous reports for the generation of *o*-QMs from *ortho*-hydroxy benzylic alcohols.[4, 45-46]

Evidence that CitB is sufficiently robust to perform preparative-scale reactions and provide access to *o*-QMs under mild conditions spurred further investigation of this chemoenzymatic strategy for benzylic functionalization, including studies with the homologous NHI enzyme, ClaD. To investigate the substrate scope of CitB and ClaD, a panel of substrates was synthesized possessing an *ortho*-cresol core (Fig. 3).[47] This panel was designed to define the electronic and steric parameters of substrates that undergo a productive reaction with the NHI biocatalysts. Compounds **9**, **16**, and **23**-**42** were subjected to analytical-scale reactions with CitB and ClaD, using standard conditions for α-KG-dependent non-heme iron oxygenases.[37] These analytical-scale reactions were performed *in vitro* with purified enzyme (Supporting Information, Fig. S5), as well as in whole cell or crude cell lysate format (Fig. 3). For CitB, a whole cell reaction platform was shown to affect benzylic C–H hydroxylation in an efficient manner. However, whole cell reactions were not effective for ClaD, leading us to perform reactions using filtered crude cell lysate. Both of these reaction platforms provide an operationally-simple method for preparing and using NHI biocatalysts in a manner that is amenable to preparative-scale reactions, avoiding arduous protein purification steps.[48-50] Analytical-scale reactions revealed that CitB and ClaD each selectively hydroxylate compounds with a variety of steric and electronic properties (Fig. 3). Introducing bulky, electron-withdrawing or electron-donating groups at either the C5 or C6 position did not prevent productive reactions with CitB. However, ClaD demonstrated limitations in its ability to accept larger groups, such as phenyl substituents at C5 and C6. The complementarity of substrate scopes between CitB and ClaD is also observed in the substitution at C4. For CitB, the formyl group at C4 can be substituted with alternative electron-withdrawing substituents such as a nitro group (**25**) or

imine (**24**). However, substrates with greater steric bulk at C4, such as ketone substrates, were generally not hydroxylated by CitB. In contrast, ClaD can productively react with a variety of ketones (see **9**, **27**-**30**). The importance of this C4 substituent is also highlighted by the lack of reaction observed with 2,5-dimethylresorcinol (**23**). Based on preliminary analysis of models of these biocatalysts, we anticipate that a hydrogen bond acceptor is critical at the C4 position to achieve a catalytically active conformation of the substrate-enzyme complex. Current efforts are focused on obtaining engineered enzyme variants that do not require substrates bearing a hydrogen bond acceptor, such as an aldehyde, for a productive reaction to occur. To probe the substrate scope of our biocatalysts beyond resorcinol substrates, phenolic compounds **39** and **S5** (see Supporting Information) were subjected to CitB hydroxylation conditions. Phenol **39** was converted to the corresponding benzylic alcohol; however, the position of the hydroxyl group proved to be important for catalysis as phenol **S5** was not oxidized by either CitB or ClaD. These results motivated us to synthesize an additional panel of phenolic substrates to further assess the scope of NHI biocatalytic hydroxylation (**40**-**42**). In the case of CitB, increasing the steric bulk at the C5 position increased the conversion of substrates to hydroxylated products except for 2-naphthyl substrate **42**, which demonstrated decreased conversion, possibly reflecting the steric limitations of the CitB active site. ClaD was unable to hydroxylate phenolic substrates **40**-**42**.

As a next step in the evaluation of the synthetic utility of the NHI dioxygenase-catalyzed benzylic C–H hydroxylation, we performed reactions on preparative-scale using whole cell (CitB) and crude cell lysate (ClaD) conditions (Fig. 4). This method enabled routine performance of reactions on >500 mg scale without the requirement for protein purification. Isolation and characterization of C5-substituted benzylic alcohol products **17** and **46**-**48** was achieved with yields that corresponded to starting material consumption. For example, benzylic alcohol **17** was isolated in 82% yield. However, poor isolated yields were obtained for substrates with C6-substituents, despite nearly complete consumption of starting material (see **49**-**53**). Further analysis of the crude product mixture from these reactions revealed a second product, in which a molecule of ascorbic acid had been incorporated, presumably through interception of an intermediate *o*-QM (see Supporting Information Fig. S63).

The observed reactivity of C6-substituted alcohols was explored computationally and can be explained by thermodynamics of the reaction sequence of **43** to **45** (Fig. 4A), which includes hypothetical substrates to explore the electronic effects at both the C5 and C6 positions (see Supporting Information Part XIV for detailed analysis). We identified a relationship between inductive effects and Gibbs free energy. The thermodynamic trends indicated that benzylic alcohols with electron-withdrawing substituents at the C6-position were less thermodynamically stable, making these substrates more reactive and prone to generation of an *o*-QM. This computational data supported our experimental observations. Therefore, we hypothesized that higher yields could be achieved if the reactive benzylic alcohol products were first transformed into more stable benzylic thioethers by interception of intermediate *o*-QMs with thiophenol. The corresponding thermodynamic analysis of thiophenol adducts **49**-**53** revealed that, regardless of substitution, the benzylic thioethers are lower in energy than their respective benzylic alcohol precursor (Fig. 4C and Supporting Information Figs. S88 and S89). To test this hypothesis, we developed an *in situ* functionalization protocol, demonstrating that increasing the reaction temperature to 40 °C and adding two equivalents of thiophenol led to the isolation of the desired benzylic thioethers **49**-**53** and **62** as the sole product in each reaction.

Motivated by this initial success in generating and diversifying *o*-QMs under mild conditions, we assessed the range of products accessible through this biocatalyst-initiated cascade. First, a panel of nucleophiles was evaluated in 1,4-additions to the *in situ*-generated *o*-QMs (Fig. 5, **18** and **19**). Both linear and branched alcohols were competent nucleophiles, affording the desired products (**73**-**75**) in good yields. A secondary amine nucleophile was also well tolerated (**77**); however, reactions with several primary amines resulted in an undesired condensation reaction with the pendant aldehyde to form imines. Thiol nucleophiles reacted smoothly to provide the desired conjugate addition products (**20** and **76**) in excellent yields. The comparatively high yield of thioether adducts relative to alkyl ether adducts is likely due to the increased nucleophilicity of sulfur as well as stability of the sulfur adducts compared to the alcohol precursor.

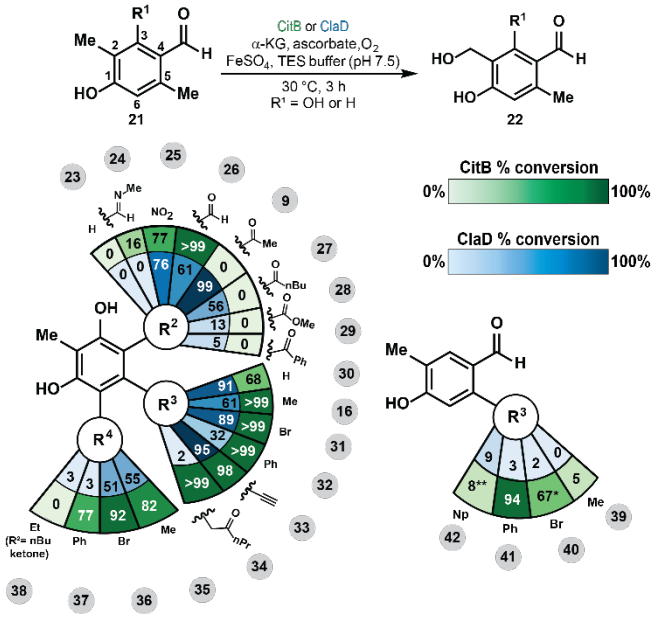

Figure 3. Substrate scope for CitB and ClaD-catalyzed benzylic C–H hydroxylation. Reaction conditions: 2.5 mM substrate, 45 mg/mL CitB wet cell pellet or 10% v/v ClaD crude cell lysate, 50 mM TES pH 7.5, 5 mM α-ketoglutaric acid (α-KG), 8 mM sodium ascorbate (NaAsc), 0.1 mM ferrous sulfate ($FeSO_4$), 30 °C, 100 rpm shaking, 3 h. [*] with 15% acetonitrile as cosolvent. [**] with 15% tetrahydrofuran as cosolvent. Conversion to product was quantified by UPLC-DAD analysis.

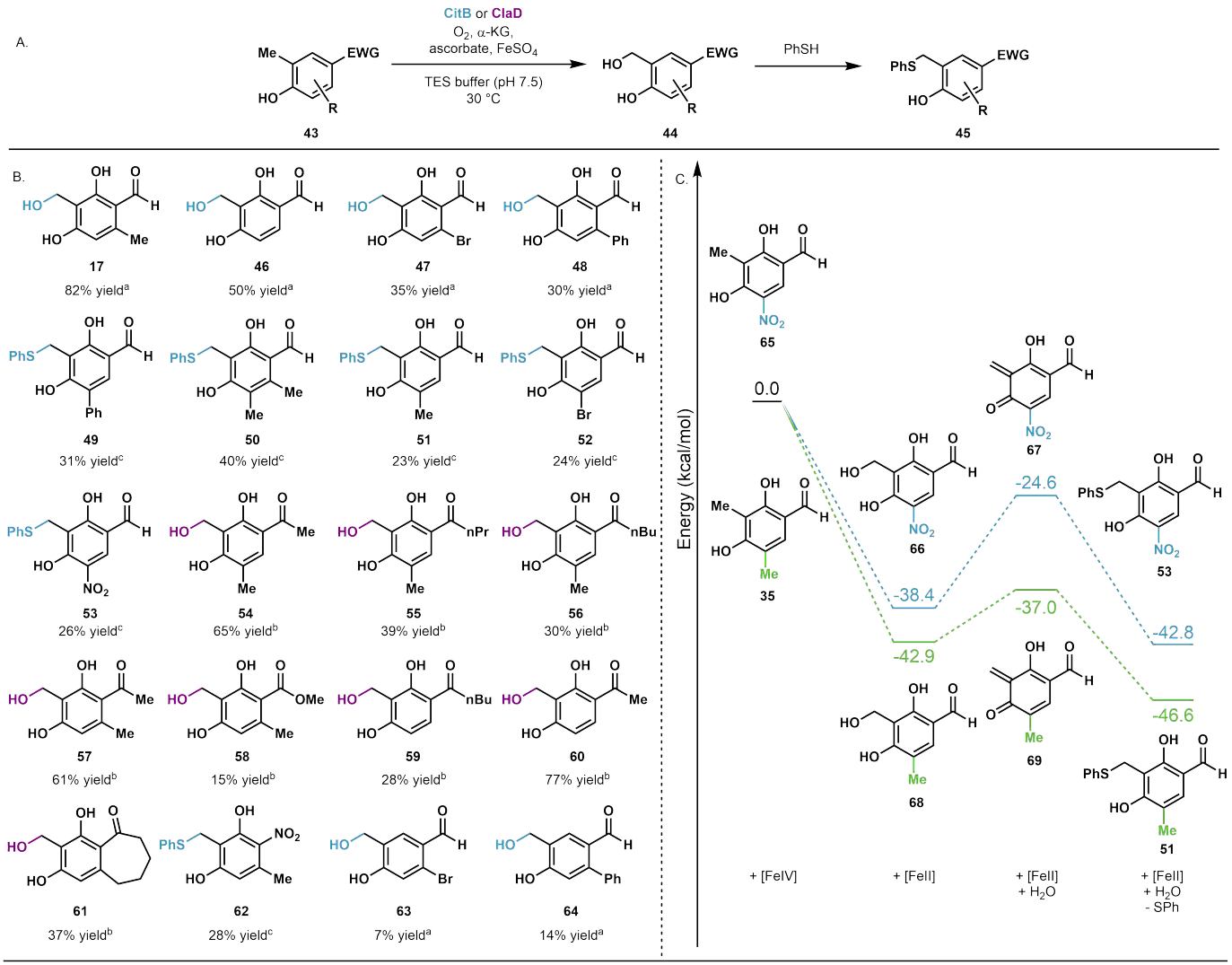

Figure 4. A. General scheme for CitB and ClaD-catalyzed benzylic hydroxylation and in situ functionalization with thiophenol. B. Preparative scale reaction isolated yields for CitB-catalyzed hydroxylation and functionalization. Reaction conditions: 2.5 mM substrate, [a]45 mg/mL CitB wet cell pellet or [b]10% v/v ClaD clarified cell lysate, 50 mM TES pH 7.5, 5 mM α-ketoglutaric acid (α-KG), 8 mM sodium ascorbate (NaAsc), 0.1 mM ferrous sulfate ($FeSO_4$), 30 °C, 100 rpm shaking, 3 h. [c] PhSH was added directly to reaction mixture after conversion to benzylic alcohol and incubated at 40 °C, 3 h, 100 rpm shaking. C. Thermodynamic analysis of C6-methyl (green) and C6-nitro (blue) substrates. Structures represent the starting material, benzylic alcohol product, *o*-QM, and thiophenol adducts (left to right). The energies are mass balanced with a truncated 2-His-1-Asp non-heme iron system (see Supporting Information Fig. S86). Geometry optimizations and frequency calculations were performed at B3LYP 6-311++G** and 6-31G** for iron.

The feasibility of benzylic C–C bond formation was probed through inverse electron-demand Diels-Alder (IEDDA) reactions. The reactivity of biocatalyst-generated benzyl alcohol **17** with various dienophiles was evaluated through a one-pot reaction sequence. Following generation of **17** by CitB, the reaction mixture was heated to 45 °C in the presence of ethyl vinyl ether. Gratifyingly, chroman products **78** and **79** were produced in 64% and 27% yield, respectively. Reactions with electron-rich dienophiles (**78**-**83**) proceeded smoothly to deliver mixtures of two isomeric products derived from the two possible *o*-QM intermediates (**18** and **19**). Reactions employing electron-rich dienophiles typically afforded 4:1 mixtures of isomeric products, favoring the product derived from reaction with the C1 *o*-QM (**19**). Reactions with styrenes **84**-**89** were also carried out. Due to the electron-deficient character of these dienophiles, these reactions required a higher temperature, 65 °C, to undergo a productive reaction. The major products of these IEDDA reactions resulted from reaction with the *o*-QM formed at the C3 hydroxyl group (**18**), while the minor isomers were formed from reaction with the C1 *o*-QM species (**19**). This operationally-simple, one-pot protocol accomplishes the direct conversion of benzylic C–H bonds to C–O, C–N, C–S and C–C bonds, allowing for direct access to diverse chemical scaffolds and demonstrating the synthetic utility of this biocatalyst.

Upon the observation that *o*-QM generation occurs at reduced temperatures, we hypothesized that these reactions likely proceed through low barrier processes. This was assessed and confirmed computationally using benzylic alcohol **17**. We generated models for both C1 and C3 *o*-QMs and

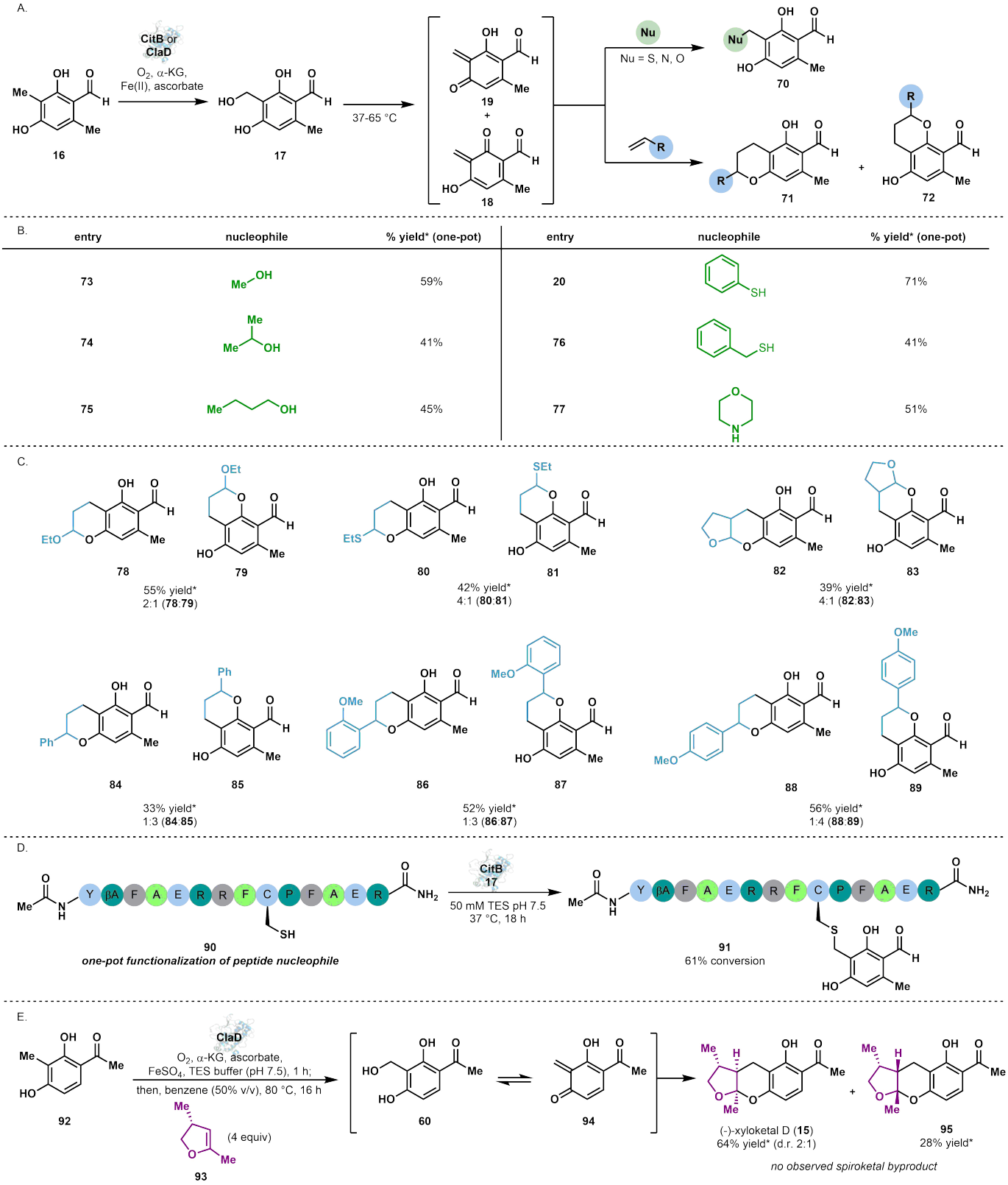

Figure 5. One-pot NHI biocatalyst-initiated *o*-QM generation and diversification. A. Yields of one-pot Michael addition reactions. B. Yields of one-pot IEDDA reactions. C. One-pot functionalization of cysteine-containing peptide. D. One-pot chemoenzymatic synthesis of (–)-xyloketal D (**15**). HPLC yields determined by analysis of isolated product standard curves.

modelled the subsequent IEDDA reactions (Supporting Information Fig. S82). In this model, *o*-QM generation was found to proceed through a concerted, low barrier transition state, while reactions with ethyl vinyl ether and styrene were found to proceed through concerted, asynchronous transition states that are typically proposed for IEDDA mechanisms (Supporting Information Figs. S83 and S84).

Additionally, we envisioned that this method could be extended to the functionalization of biomolecules under physiological conditions to selectively modify cysteine residues in peptides and proteins. Two complementary peptides were synthesized: one peptide that contained a cysteine residue (**90**) and another in which the cysteine was replaced with a lysine residue (**S14**). Substrate **16** was subjected to *in vitro* CitB-catalyzed hydroxylation conditions in the presence of either peptide **90** or **S14**. After an 18 h incubation the cysteine-containing peptide was converted to singly-modified peptide **91** (61% conversion). Under the same conditions, the peptide containing a lysine in place of cysteine (**S14**) was not modified through imine condensation or through addition to the *o*-QM. These cascade reactions demonstrate the utility of this biocatalytic method in providing a platform for *in situ* functionalization of peptides.

Finally, to demonstrate the utility of this biocatalytic method for the synthesis of a secondary metabolite, we aimed to develop a chemoenzymatic route to the chroman natural product (–)-xyloketal D (**15**). Xyloketal D is a fungal natural product from *Xylaria* sp. found in the South China Sea.[51] Synthetic strategies have been developed previously for the synthesis of (–)-xyloketal D including a Diels-Alder cycloaddition by Wilson and co-workers,[7] a sequential Michael-addition ketalization sequence by Flörke and co-workers[52] and, more recently, a gold-catalyzed cycloisomerization reported by Sarkar and co-workers in 2013.[53] The latter two syntheses report high diastereoselectivity (19:2 and >20:1, respectively); however, the Michael-addition ketalization yields a mixture of regioisomers and the gold-catalyzed cycloisomerization requires a lengthy precursor synthesis. The approach developed by Wilson and co-workers provided the required *o*-QM precursor in a single step; however, their conditions for *o*-QM generation led to a low overall yield due in part to undesired isomerization of the dienophile under the requisite conditions for *o*-QM formation. Ultimately, this approach provided a 2:1 mixture of the desired chroman ketal and undesired chroman spiroketal products.[7] Our chemoenzymatic strategy controls the site-selectivity of the oxidation and provides a more active *o*-QM precursor (see Supporting Information Fig. S93) allowing for more mild cycloaddition conditions and circumventing any dienophile isomerization challenges. After synthesis of chiral dienophile **93,** according to Wilson's established procedure, we subjected methyl ketone **92** to our conditions for biocatalytic benzylic C–H hydroxylation with ClaD crude lysate, obtaining complete conversion to benzylic alcohol **60**. Following the enzymatic C–H benzylic hydroxylation step, benzene was added directly to the biocatalytic reaction mixture, along with dienophile **93**. The reaction tube was sealed and heated to 80 °C for 16 h. This process generated (–)-xyloketal D (**15**) in a 64% yield (2:1 ratio) with the diastereomer (**95**, 28% yield) and no detectable formation of unwanted spiroketal products. Thus, our approach enabled a one-pot chemoenzymatic synthesis of (–)-xyloketal D (**15**), with improved yields and under milder conditions compared to a previous *o*-QM-based approach to this molecule.[7] We anticipate this one-pot chemoenzymatic strategy will facilitate the streamlined synthesis of a variety of natural products.

CONCLUSIONS

We have demonstrated the utility of biocatalysis for chemo- and site-selective C–H functionalization through NHI biocatalyst-initiated benzylic functionalization of *ortho*-cresol substrates. This was accomplished by establishing scalable biocatalytic reaction methods to provide an inexpensive and highly accessible platform for benzylic hydroxylation. Using this platform, we have leveraged NHI dioxygenase-catalyzed hydroxylation for further diversification of phenolic scaffolds. Chemoenzymatic formation of *o*-QM intermediates was followed by reactions with small-molecule and peptide nucleophiles as well as electron-rich dienophiles, leading to the synthesis of the fungal natural product (–)-xyloketal D. Thus, direct access to a diverse set of compounds though this simple chemoenzymatic cascade is possible. We anticipate that our method for biocatalyst-initiated *o*-QM generation can be broadly applied to other chemoenzymatic systems capable of performing benzylic C–H hydroxylation and will enable transformations complementary to small molecule catalysts and reagents.

ASSOCIATED CONTENT

Supporting Information. Experimental details, NMR spectra, full compound characterization, UPLC and LCMS traces, details of protein expression and purification and peptide synthesis. This material is available free of charge via the Internet at http://pubs.acs.org.

AUTHOR INFORMATION

Corresponding Author

*arhardin@umich.edu

Author Contributions

[+] These authors contributed equally.

Notes

The authors declare no competing financial interest.

ACKNOWLEDGMENT

This work was supported by funds from the University of Michigan Life Sciences Institute and Department of Chemistry. T.J.D. thanks the National Science Foundation for a Graduate Research Fellowship. S.A.B.D. acknowledges a National Institutes of Health Chemistry Biology Interface Training Grant (T32 GM 008597). K.C.S acknowledges a Rackham Merit Fellowship from the University of Michigan Rackham Graduate School. P.M.Z. acknowledges partial support from NIH R35GM128830. The authors thank Dr. Steven Sturlis (University of Michigan) for his assistance in peptide synthesis and purification. The authors also thank Shuri Francis (University of Michigan) for her assistance in substrate synthesis and Attabey Rodríguez Benítez for her assistance in figure design.

ABBREVIATIONS

TES: N-[Tris(hydroxymethyl)methyl]-2-aminoethanesulfonic acid, UPLC: ultra performance liquid chromatography, LCMS: liquid chromatography mass spectrometry.

REFERENCES

1. Ueberbacher, B. T.; Hall, M.; Faber, K., Electrophilic and nucleophilic enzymatic cascade reactions in biosynthesis. *Nat. Prod. Rep.* **2012,** *29* (3), 337-50.
2. Hashimoto, T.; Kuzuyama, T., Mechanistic insights into Diels-Alder reactions in natural product biosynthesis. *Curr. Opin. Chem. Biol.* **2016,** *35*, 117-123.
3. Bai, W. J.; David, J. G.; Feng, Z. G.; Weaver, M. G.; Wu, K. L.; Pettus, T. R., The domestication of ortho-quinone methides. *Acc. Chem. Res.* **2014,** *47* (12), 3655-64.
4. Singh, M. S.; Nagaraju, A.; Anand, N.; Chowdhury, S., ortho-Quinone methide (o-QM): a highly reactive, ephemeral and versatile intermediate in organic synthesis. *RSC Adv.* **2014,** *4* (99), 55924-55959.
5. Van De Water, R. W.; Pettus, T. R. R., o-Quinone methides: intermediates underdeveloped and underutilized in organic synthesis. *Tetrahedron* **2002,** *58* (27), 5367-5405.
6. Willis, N. J.; Bray, C. D., ortho-Quinone Methides in Natural Product Synthesis. *Chemistry – A European Journal* **2012,** *18* (30), 9160-9173.
7. Pettigrew, J. D.; Freeman, R. P.; Wilson, P. D., Total synthesis of (-)-xyloketal D and its enantiomer: Confirmation of absolute stereochemistry. *Can. J. Chem.* **2004,** *82* (11), 1640-1648.
8. Spence, J. T.; George, J. H., Total Synthesis of Peniphenones A-D via Biomimetic Reactions of a Common o-Quinone Methide Intermediate. *Org. Lett.* **2015,** *17* (24), 5970-3.
9. Spence, J. T. J.; George, J. H., Biomimetic Total Synthesis of ent-Penilactone A and Penilactone B. *Org. Lett.* **2013,** *15* (15), 3891-3893.
10. Basha, R. S.; Chen, C. W.; Reddy, D. M.; Lee, C. F., Iodine-Mediated Direct Generation of o-Quinone Methides at Room Temperature: A Facile Protocol for the Synthesis of ortho-Hydroxybenzyl Thioethers. *Chem. Asian J.* **2018,** *13* (17), 2475-2483.
11. Zhou, D.; Yu, X.; Zhang, J.; Wang, W.; Xie, H., Organocatalytic Asymmetric Formal [4 + 2] Cycloaddition of in Situ Oxidation-Generated ortho-Quinone Methides and Aldehydes. *Org. Lett.* **2018,** *20* (1), 174-177.
12. Reichl, K. D.; Smith, M. J.; Song, M. K.; Johnson, R. P.; Porco, J. A., Jr., Biomimetic Total Synthesis of (+/-)-Griffipavixanthone via a Cationic Cycloaddition-Cyclization Cascade. *J. Am. Chem. Soc.* **2017,** *139* (40), 14053-14056.
13. More, A. A.; Ramana, C. V., o-Quinone Methides via Oxone-Mediated Benzofuran Oxidative Dearomatization and Their Intramolecular Cycloaddition with Carbonyl Groups: An Expeditious Construction of the Central Tetracyclic Core of Integrastatins, Epicoccolide A, and Epicocconigrone A. *Org. Lett.* **2016,** *18* (3), 612-615.
14. Gebauer, K.; Reuss, F.; Spanka, M.; Schneider, C., Relay Catalysis: Manganese(III) Phosphate Catalyzed Asymmetric Addition of beta-Dicarbonyls to ortho-Quinone Methides Generated by Catalytic Aerobic Oxidation. *Org Lett* **2017,** *19* (17), 4588-4591.
15. Wong, Y. F.; Wang, Z.; Hong, W.-X.; Sun, J., A one-pot oxidation/cycloaddition cascade synthesis of 2,4-diaryl chromans via ortho -quinone methides. *Tetrahedron* **2016,** *72* (22), 2748-2751.
16. Lam, H. C.; Spence, J. T.; George, J. H., Biomimetic Total Synthesis of Hyperjapones A-E and Hyperjaponols A and C. *Angew. Chem. Int. Ed. Engl.* **2016**, *55* (35), 10368-71.
17. Fan, J.; Liao, G.; Kindinger, F.; Ludwig-Radtke, L.; Yin, W. B.; Li, S. M., Peniphenone and Penilactone Formation in Penicillium crustosum via 1,4-Michael Additions of ortho-Quinone Methide from Hydroxyclavatol to gamma-Butyrolactones from Crustosic Acid. *J. Am. Chem. Soc.* **2019**, *141*, (10), 4225-4229.
18. Lie, F.; Chen, Y.; Wang, Z.; Li, Z., Enantioselective benzylic hydroxylation of indan and tetralin with Pseudomonas monteilii TA-5. *Tetrahedron: Asymmetry* **2009,** *20* (10), 1206-1211.
19. Yongzheng, C.; Felicia, L.; Zhi, L., Enantioselective Benzylic Hydroxylation with Pseudomonas monteilii TA-5: A Simple Method for the Syntheses of (R)-Benzylic Alcohols Containing Reactive Functional Groups. *Adv. Synth. & Catal.* **2009,** *351* (13), 2107-2112.
20. Limberger, R. P.; Ursini, C. V.; Moran, P. J. S.; Rodrigues, J. A. R., Enantioselective benzylic microbial hydroxylation of indan and tetralin. *J. Mol. Catal. B: Enzym.* **2007,** *46* (1), 37-42.
21. Dai, S.; Wu, J.; Wang, Z.; Chen, Y.; Li, Z., Highly chemo- and regioselective hydroxylations of o- and m-substituted toluenes to benzyl alcohols with Cellulosimicrobium cellulans EB-8-4. *Tetrahedron* **2010,** *66* (34), 6919-6923.
22. Uzura, A.; Katsuragi, T.; Tani, Y., Stereoselective oxidation of alkylbenzenes by fungi. *J. Biosci. Bioengin.* **2001,** *91* (2), 217-221.
23. Yadav, S.; Yadav, R. S. S.; Yadava, S.; Yadav, K. D. S., Stereoselective hydroxylation of ethylbenzene to (R)-1-phenylethanol using mycelia of Aspergillus niger as catalyst. *Catal. Commun.* **2011,** *12* (9), 781-784.
24. Alexander, D.; Maria, W. A.; Tsvetan, K.; Andrea, M. C.; Erika, T.; Martin, S.; Joëlle, R. A.; Ulrich, S., An Enzymatic Route to α-Tocopherol Synthons: Aromatic Hydroxylation of Pseudocumene and Mesitylene with P450 BM3. *Chem. Eur. J.* **2017,** *23* (71), 17981-17991.
25. Anja, E.; Łukasz, G.; Susanne, H.; P., K. P.; J., T. N.; Jürgen, P.; L., F. S., Enantioselective Benzylic Hydroxylation Catalysed by P450 Monooxygenases: Characterisation of a P450cam Mutant Library and Molecular Modelling. *ChemBioChem* **2016,** *17* (5), 426-432.
26. Driscoll, J. P.; Kornecki, K.; Wolkowski, J. P.; Chupak, L.; Kalgutkar, A. S.; O'Donnell, J. P., Bioactivation of Phencyclidine in Rat and Human Liver Microsomes and Recombinant P450 2B Enzymes: Evidence for the Formation of a Novel Quinone Methide Intermediate. *Chem. Res. Toxicol.* **2007,** *20* (10), 1488-1497.
27. Du, L.; Dong, S.; Zhang, X.; Jiang, C.; Chen, J.; Yao, L.; Wang, X.; Wan, X.; Liu, X.; Wang, X.; Huang, S.; Cui, Q.; Feng, Y.; Liu, S.-J.; Li, S., Selective oxidation of aliphatic C–H bonds in alkylphenols by a chemomimetic biocatalytic system. *Proc. Nat'l. Acad. Sci.* **2017,** *114* (26), E5129-E5137.
28. Kelly, P. P.; Eichler, A.; Herter, S.; Kranz, D. C.; Turner, N. J.; Flitsch, S. L., Active site diversification of P450cam with indole generates catalysts for benzylic oxidation reactions. *Beilstein J. Org. Chem.* **2015,** *11*, 1713-1720.
29. Li, A.; Wu, S.; Adams, J. P.; Snajdrova, R.; Li, Z., Asymmetric epoxidation of alkenes and benzylic hydroxylation with P450tol monooxygenase from Rhodococcus coprophilus TC-2. *Chem. Commun.* **2014,** *50* (63), 8771-8774.
30. Neufeld, K.; Marienhagen, J.; Schwaneberg, U.; Pietruszka, J., Benzylic hydroxylation of aromatic compounds by P450 BM3. *Green Chem.* **2013,** *15* (9), 2408-2421.
31. Suzuki, K.; Stanfield, J. K.; Shoji, O.; Yanagisawa, S.; Sugimoto, H.; Shiro, Y.; Watanabe, Y., Control of stereoselectivity of benzylic hydroxylation catalysed by wild-type cytochrome P450BM3 using decoy molecules. *Catal. Sci. & Technol.* **2017,** *7* (15), 3332-3338.
32. Hall, E. A.; Sarkar, M. R.; Bell, S. G., The selective oxidation of substituted aromatic hydrocarbons and the observation of uncoupling via redox cycling during naphthalene oxidation by the CYP101B1 system. *Catal. Sci. & Technol.* **2017,** *7* (7), 1537-1548.
33. Zwick, C. R.; Renata, H., Evolution of Biocatalytic and Chemocatalytic C–H Functionalization Strategy in the Synthesis of Manzacidin C. *J. Org. Chem.* **2018,** *83* (14), 7407-7415.
34. Dror, A.; Fishman, A., Engineering non-heme mono- and dioxygenases for biocatalysis. *Comput. Struct. Biotechnol. J.* **2012,** *2* (3), e201209011.
35. Herr, C. Q.; Hausinger, R. P., Amazing Diversity in Biochemical Roles of Fe(II)/2-Oxoglutarate Oxygenases. *Trends Biochem. Sci.* **2018**.

36. Martinez, S.; Hausinger, R. P., Catalytic Mechanisms of Fe(II)- and 2-Oxoglutarate-dependent Oxygenases. *J. Biol. Chem.* **2015,** *290* (34), 20702-11.
37. Nakamura, H.; Matsuda, Y.; Abe, I., Unique chemistry of non-heme iron enzymes in fungal biosynthetic pathways. *Nat. Prod. Rep.* **2018,** *35* (7), 633-645.
38. He, Y.; Cox, R. J., The molecular steps of citrinin biosynthesis in fungi. *Chem. Sci.* **2016,** *7* (3), 2119-2127.
39. Takuya, M.; Pal, S. I.; Hideo, E.; Hitoshi, T., The First Total Synthesis of Grandinal, a New Phloroglucinol Derivative Isolated from Eucalyptus grandis. *Chem. Lett.* **2001,** *30* (3), 210-211.
40. Carter, D. V.; Charlton, P. T.; Fenton, A. H.; Housley, J. R.; Lessel, B., The preparation and the antibacterial and antifungal properties of some substituted benzyl alcohols. *J. Pharm. Pharmacol.* **1958,** *10* (S1), 149T-159T.
41. Li, L.; Liu, Y.; Wang, Q., Regioselective Oxidative Dehydrogenation under Nonenzymatic Conditions: A Synthetic Route to Gossypol. *Eur. J. Org. Chem.* **2013,** *2013* (35), 8014-8021.
42. Cort, A. D.; Mandolini, L.; Panaioli, S., Selective One-Pot Oxidation of Methylarenes to Benzyl Alcohols with the Copper(II)-Peroxydisulfate System. *Synth. Commun.* **1988,** *18* (6), 613-616.
43. Baciocchi, E.; Mandolini, L.; Rol, C., Oxidation by metal ions. 6. Intramolecular selectivity in the side-chain oxidation of p-ethyltoluene and isodurene by cobalt(III), cerium(IV), and manganese(III). *J. Org. Chem.* **1980,** *45* (19), 3906-3909.
44. Vece, V.; Jakkepally, S.; Hanessian, S., Total Synthesis and Absolute Stereochemical Assignment of the Insecticidal Metabolites Yaequinolones J1 and J2. *Org. Lett.* **2018,** *20* (14), 4277-4280.
45. Yang, B.; Gao, S., Recent advances in the application of Diels–Alder reactions involving *o*-quinodimethanes, aza-*o*-quinone methides and *o*-quinone methides in natural product total synthesis. *Chem. Soc. Rev.* **2018,** *47* (21), 7926-7953.
46. Arumugam, S.; Popik, V. V., Photochemical Generation and the Reactivity of o-Naphthoquinone Methides in Aqueous Solutions. *J. Am. Chem. Soc.* **2009,** *131* (33), 11892-11899.
47. Baker Dockrey, S. A.; Lukowski, A. L.; Becker, M. R.; Narayan, A. R. H., Biocatalytic site- and enantioselective oxidative dearomatization of phenols. *Nat. Chem.* **2017,** *10*, 119.
48. de Carvalho, C. C. C. R., Whole cell biocatalysts: essential workers from Nature to the industry. *Microb. Biotechnol.* **2017,** *10* (2), 250-263.
49. Wachtmeister, J.; Rother, D., Recent advances in whole cell biocatalysis techniques bridging from investigative to industrial scale. *Curr. Opin. Biotechnol.* **2016,** *42*, 169-177.
50. Baker Dockrey, S. A.; Doyon, T. J.; Perkins, J. C.; Narayan, A. R. H., Whole-cell biocatalysis platform for gram-scale oxidative dearomatization of phenols. *Chem. Biol. & Drug Des.* **2018**, *93*, 1207-1213.
51. Lin, Y.; Wu, X.; Feng, S.; Jiang, G.; Luo, J.; Zhou, S.; Vrijmoed, L. L. P.; Jones, E. B. G.; Krohn, K.; Steingröver, K.; Zsila, F., Five Unique Compounds: Xyloketals from Mangrove Fungus Xylaria sp. from the South China Sea Coast. *The Journal of Organic Chemistry* **2001,** *66* (19), 6252-6256.
52. Krohn, K.; Riaz, M.; Flörke, U., Synthesis of Xyloketals, Natural Products from the Mangrove Fungus Xylaria sp. *European Journal of Organic Chemistry* **2004**, *2004* (6), 1261-1270.
53. Panda, B.; Sarkar, T. K., Gold catalysis: regio- and stereoselective total synthesis of xyloketals D and G and the related natural product alboatrin. *J Org Chem* **2013**, *78* (6), 2413-21.

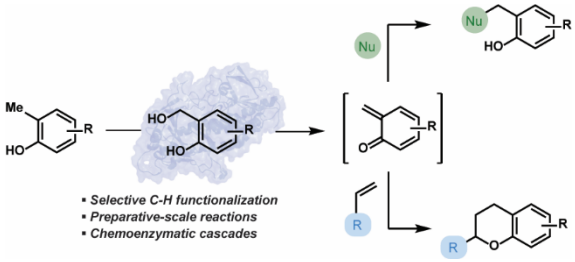
Me
R
HO
HO
HO
R
Nu
Nu
HO
R
O
R
R
O
R
▪ Selective C-H functionalization
▪ Preparative-scale reactions
▪ Chemoenzymatic cascades

Chemoenzymatic *ortho*-quinone methide formation

Supporting Information

Tyler J. Doyon,[1,2 +] Jonathan C. Perkins,[1,3 +] Summer A. Baker Dockrey,[1,3] Evan O. Romero,[1,3] Kevin C. Skinner,[1,3] Paul M. Zimmerman,[1,3] Alison R. H. Narayan[1,2,3]*

[1]Life Sciences Institute, University of Michigan, Ann Arbor, Michigan 48109, USA. [2]Program in Chemical Biology, University of Michigan, Ann Arbor, Michigan 48109, USA. [3]Department of Chemistry, University of Michigan, Ann Arbor, Michigan 48109, USA.

[+] These authors contributed equally to this work.

[*]Corresponding author, email: arhardin@umich.edu

Table of Contents

Part I. Substrate and peptide synthesis

General Information: All reagents were used as received unless otherwise noted. Reactions were carried out under a nitrogen atmosphere using standard Schlenk techniques unless otherwise noted. Solvents were degassed and dried over alumina columns on an MBraun solvent system (Innovative Technology, Inc., Model PS-00-3). Reactions were monitored by thin layer chromatography using Millipore 60 F254 pre-coated silica TLC plates (0.25 mm) which were visualized using UV, *p*-anisaldehyde, CAM, DNP, or bromocresol green stains. Flash column chromatography was performed using Machery-Nagel 60 µm (230-400 mesh) silica gel. All compounds purified by column chromatography were sufficiently pure for use in further experiments unless otherwise indicated. ^{1}H and ^{13}C NMR spectra were obtained in $CDCl_3$ at rt (25 °C), unless otherwise noted, on Varian 400 MHz or Varian 600 MHz spectrometers. Chemical shifts of ^{1}H and ^{13}C NMR spectra were recorded in parts per million (ppm) on the δ scale. High resolution electrospray mass spectra were obtained on an Agilent 1290 Series Infinity II HPLC with a 6230 Series Time-of-Flight mass spectrometer or an Agilent 1290 Series Infinity HPLC with a 6545 Series Quadrupole-Time-of-Flight mass spectrometer. UPLC-PDA spectrometric traces were obtained on a Waters Aquity H-class instrument. IR spectra were recorded on a Perkin-Elmer Spectrum BX FT-IR spectrometer.

Compounds **8**, **16**, **23**, **26**-**28**, **30**-**36**, and **39** were prepared and characterized by our lab previously.[1] Details of this characterization can be found in the Supplementary Information of the provided reference. Compound **29** (methyl atratate) was purchased from Sigma Aldrich and used without further purification.

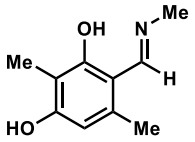

24

2,5-dimethyl-4-((methylimino)methyl)benzene-1,3-diol (24)

A flame-dried vial equipped with a stir bar was charged with 2,4-dihydroxy-3,6-dimethylbenzaldehyde (100 mg, 0.604 mmol, 1.00 equiv), methylamine hydrochloride (80 mg, 1.2 mmol, 2.0 equiv), and MeOH (1.2 mL, 0.50 M). The reaction was heated at 65 °C with stirring for 18 h during which time a pink solid precipitated out of the reaction. After cooling to room temperature, EtOAc (5 mL) was added to the reaction mixture. The reaction mixture was filtered to collect the pink solid. The pink solid was dissolved in water (5 mL) and added to a separatory funnel followed by the addition of saturated $NaHCO_3$ (10 mL). This mixture was extracted with EtOAc (3 x 15 mL). The combined organic layers were washed with brine, dried over Na_2SO_4, and concentrated under reduced pressure to afford 107 mg (99% yield) of the title compound as a pink solid. The material was used without further purification. **^{1}H NMR** (599 MHz, $CDCl_3$) δ 8.37 (s, 1H), 6.09 (s, 1H), 3.39 (s, 3H), 2.32 (s, 3H), 2.09 (s, 3H); **^{13}C NMR** (151 MHz, $CDCl_3$) δ 168.1, 162.5, 158.1, 137.3, 110.1, 109.3, 108.0, 42.8, 18.7, 7.4; **HRMS (ESI)** *m/z*: $[M-H]^-$ calculated for $C_{10}H_{12}NO_2^-$ 178.0874, found 178.0877; **IR** (thin film): 2925, 2652, 1733, 1643, 1606, 1502, 1457, 1392, 1351, 1256, 1148, 1111, 1029, 1005 cm^{-1}.

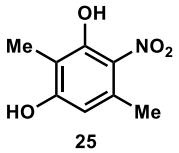

25

2,5-dimethyl-4-nitrobenzene-1,3-diol (25)

A flame-dried round-bottom flask equipped with a stir bar was charged with 2,5-dimethylbenzene-1,3-diol (100 mg, 0.724 mmol, 1.00 equiv) and $Cu(NO_3)_2$•$2.5H_2O$ (101 mg, 0.434 mmol, 0.600 equiv). The flask was cooled to 0 °C and Ac_2O (1 mL, 0.7 M) was added to the reaction. The reaction was stirred for 3 h before water (5 mL) was added to the reaction and the mixture extracted with EtOAc (3 x 10 mL). The combined organic layers were washed with brine, dried over Na_2SO_4, and concentrated under reduced pressure. Purification on silica gel (gradient elution 1% to 75% EtOAc in hexanes) afforded 64 mg (35% yield) of the title compound as a yellow solid. All spectroscopic data for the compound was in accordance with literature

values.[2] **^{1}H NMR** (599 MHz, CD_3OD) δ 6.32 (s, 1H), 2.49 (s, 3H), 2.06 (s, 3H); **HRMS (ESI)** *m/z*: $[M-H]^-$ calculated for $C_8H_8NO_4^-$ 182.0459, found 182.0460.

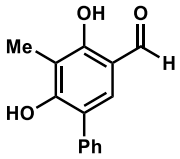

37

4,6-dimethoxy-5-methyl-[1,1'-biphenyl]-3-carbaldehyde (37)

A flame-dried round-bottom flask equipped with a magnetic stir bar was charged with 5-bromo-2,4-dimethoxy-3-methylbenzaldehyde (200 mg, 0.772 mmol, 1.00 equiv), K_2CO_3 (267 mg, 1.93 mmol, 2.50 equiv) and 1,4-dioxane (4 mL, 0.25 M). Phenylboronic acid (188 mg, 1.54 mmol, 2.00 equiv) and $Pd(PPh_3)_4$ (89 mg, 0.077 mmol, 0.10 equiv) were added to the flask. The reaction mixture was stirred and heated at 80 °C for 24 h before being cooled to rt and quenched by addition of 5 mL of saturated $NaHCO_3$. The reaction mixture was extracted with EtOAc (3 x 20 mL). The combined organic layers were washed with brine, dried over Na_2SO_4, and concentrated under reduced pressure. The crude solid was transferred to a flame-dried round-bottom flask equipped with a magnetic stir bar and dichloromethane (3 mL, 0.25 M) was added. The flask was cooled to -78 °C before BBr_3 (183 µL, 1.92 mmol, 2.50 equiv) was added to the reaction dropwise by syringe over 5 min. The reaction was removed from the cooling bath, allowed to warm to room temperature, and stirred for 18 h. Next, the reaction was cooled to 0 °C and quenched by slow addition of ice water (5 mL) by syringe followed by stirring for 10 min. The reaction mixture was extracted with EtOAc (3 x 10 mL). The combined organic layers were washed with brine, dried over Na_2SO_4, and concentrated under reduced pressure. Purification on silica gel (gradient elution 5% to 40% EtOAc in hexanes) afforded 148 mg (84% yield) of the title compound as a white solid. **^{1}H NMR** (599 MHz, CD_3OD) δ 9.70 (s, 1H), 7.45 (d, *J* = 7.3 Hz, 2H), 7.41 (t, *J* = 7.6 Hz, 2H), 7.35 (s, 1H), 7.33 (t, *J* = 7.4 Hz, 1H), 2.14 (s, 3H); **^{13}C NMR** (151 MHz, CD_3OD) δ 196.7, 162.1, 161.4, 138.9, 134.9, 130.5, 129.5, 128.2, 124.2, 116.0, 112.8, 7.9; **HRMS (ESI)** *m/z*: $[M-H]^-$ calculated for $C_{14}H_{11}O_3^-$ 227.0714, found 227.7011; **IR** (thin film): 2926, 1625, 1425, 1377, 1305, 1188, 1073, 746, 703, 573 cm^{-1}.

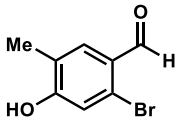

40

2-bromo-4-hydroxy-5-methylbenzaldehyde (40)

A flame-dried round-bottom flask equipped with a magnetic stir bar was charged with 5-bromo-2-methylphenol (2.00 g, 10.7 mmol, 1.00 equiv) and dichloromethane (107 mL, 0.1 M). The reaction was cooled to 0 °C and $TiCl_4$ (1.41 mL, 12.8 mmol, 1.20 equiv) was added dropwise. The reaction was stirred at 0 °C for 30 min before dichloromethyl methyl ether (1.06 mL, 11.8 mmol, 1.10 equiv) was added dropwise. The reaction mixture was allowed to warm to room temperature over 18 h with stirring. The reaction mixture was transferred to a separatory funnel and quenched by addition of saturated $NaHCO_3$ (150 mL). The mixture was extracted with dichloromethane (3 x 100 mL). The combined organic layers were washed with brine, dried over Na_2SO_4, and concentrated under reduced pressure. Purification on silica gel (gradient elution 5% to 40% EtOAc in hexanes) afforded 528 mg (23% yield) of the title compound as a white solid. **^{1}H NMR** (599 MHz, CD_3OD) δ 10.08 (s, 1H), 7.66 (s, 1H), 7.03 (s, 1H), 2.17 (s, 3H); **^{13}C NMR** (151 MHz, CD_3OD) δ 191.9, 163.6, 132.9, 126.9, 126.8, 126.7, 119.8, 15.7; **HRMS (ESI)** *m/z*: $[M-H]^-$ calculated for $C_8H_6O_2Br^-$ 212.9557, found 212.9576; **IR** (thin film): 3083, 1650, 1580, 1494, 1263, 1139, 981, 901, 850, 641, 447 cm^{-1}.

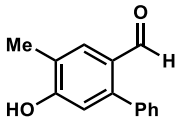

41

4-hydroxy-5-methyl-2-phenylbenzaldehyde (41)

A flame-dried round-bottom flask equipped with a magnetic stir bar was charged with 2-bromo-4-hydroxy-5-methylbenzaldehyde (25 mg, 0.12 mmol, 1.0 equiv), K_2CO_3 (48 mg, 0.35 mmol, 3.0 equiv), and 1,4-dioxane (1.0 mL, 0.12 M). Phenylboronic acid (28 mg, 0.23 mmol, 2.0 equiv) and $Pd(PPh_3)_4$ (27 mg, 0.023 mmol, 0.20 equiv) were added to the flask. The reaction mixture was stirred and heated at 80 °C for 24 h before being cooled to room temperature and quenched by addition of 3 mL of saturated $NaHCO_3$. The reaction mixture was extracted with EtOAc (3 x 10 mL). The combined organic layers were washed with brine, dried over Na_2SO_4, and concentrated under reduced pressure. Purification on silica gel (gradient elution 5% to 40% EtOAc in hexanes) afforded 15 mg (48% yield) of the title compound as a yellow solid. **^{1}H NMR** (599 MHz, CD_3OD) δ 9.66 (s, 1H), 7.76 (s, 1H), 7.50-7.38 (m, 3H), 7.38-7.31 (m, 2H), 6.75 (s, 1H), 2.26 (s, 3H); **^{13}C NMR** (151 MHz, CD_3OD) δ 192.5, 162.5, 148.4, 139.4, 131.4, 131.0, 129.4, 129.0, 127.0, 126.3, 116.9, 15.8; **HRMS (ESI)** *m/z*: $[M-H]^-$ calculated for $C_{14}H_{11}O_2^-$ 211.0765, found 211.0766. **IR** (thin film): 2923, 2329, 1742, 1650, 1578, 1487, 1276, 1138, 979, 872, 768, 703, 649 cm^{-1}.

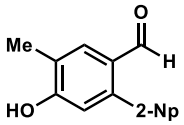

42

4-hydroxy-5-methyl-2-(naphthalen-2-yl)benzaldehyde (42)

A flame-dried round-bottom flask equipped with a magnetic stir bar was charged with 2-bromo-4-hydroxy-5-methylbenzaldehyde (25 mg, 0.12 mmol, 1.0 equiv), K_2CO_3 (48 mg, 0.35 mmol, 3.0 equiv), and 1,4-dioxane (1.0 mL, 0.12 M). Naphthalene-2-boronic acid (42 mg, 0.23 mmol, 2.0 equiv) and $Pd(PPh_3)_4$ (27 mg, 0.023 mmol, 0.20 equiv) were added to the flask. The reaction mixture was stirred and heated at 80 °C for 24 h before being cooled to room temperature and quenched by addition of 3 mL of saturated $NaHCO_3$. The reaction mixture was extracted with EtOAc (3 x 10 mL). The combined organic layers were washed with brine, dried over Na_2SO_4, and concentrated under reduced pressure. Purification on silica gel (gradient elution 5% to 40% EtOAc in hexanes) afforded 14.6 mg (48% yield) of the title compound as a white solid. **^{1}H NMR** (599 MHz, CD_3OD) δ 9.72 (s, 1H), 7.96-7.87 (m, 3H), 7.81 (s, 1H), 7.80 (s, 1H), 7.56-7.51 (m, 2H), 7.49 (dd, *J* = 8.3, 1.5 Hz, 1H), 6.86 (s, 1H), 2.28 (s, 3H); **^{13}C NMR** (151 MHz, CD_3OD) δ 192.5, 162.5, 148.2, 136.8, 134.5, 134.2, 131.6, 130.0, 129.1, 128.9, 128.8, 128.7, 127.8, 127.6, 127.3, 126.4, 117.2, 15.9; **HRMS (ESI)** *m/z*: $[M-H]^-$ calculated for $C_{18}H_{13}O_2^-$ 261.0921, found 261.0917; **IR** (thin film): 2991, 2913, 1732, 1436, 1373, 1241, 1042, 952, 696 cm^{-1}.

Peptide Synthesis

Sequence of peptides used in this study:

A. Ac-Tyr-βAla-Phe-Ala-Glu-Arg-Arg-Phe-Cys-Pro-Phe-Ala-Glu-Arg-NH_2
B. Ac-Tyr-βAla-Phe-Ala-Glu-Arg-Arg-Phe-Lys-Pro-Phe-Ala-Glu-Arg-NH_2

Peptide design and synthesis: The peptides listed above were designed from a sequence reported to have a ligandable cysteine residue, based on screens with cysteine-reactive probes.[3] The peptides synthesized using standard FMOC solid-phase synthesis methods on a Liberty Blue Microwave Synthesizer (CEM). Rink Amide ProTide resin (CEM) was utilized for peptide synthesis, providing C-terminal amide protection upon cleavage of the peptide. Amino acid coupling reactions were performed by mixing diisopropylcarbodiimide (7 equiv relative to resin, ChemImpex), Oxyma Pure (5 equiv, CEM), and amino acid (5 equiv) in *N*,*N*-dimethylformamide, followed by irradiation to maintain a temperature of 90 °C for 4 min. FMOC protecting groups were removed by suspending the resin in 20% piperidine in *N*,*N*-dimethylformamide with 0.2 M Oxyma Pure and irradiating to maintain a temperature of 90 °C for 1 min. The resin was rinsed (4 times each cycle) with *N*,*N*-dimethylformamide between deprotection and coupling steps. The final peptide was FMOC deprotected and was incubated with acetic anhydride in the presence of triethylamine for N-terminal acetylation. The resulting peptide was cleaved from the resin with 95% trifluoroacetic acid (Sigma Aldrich), 2.5% ddH_2O, and 2.5% triisopropylsilane (Sigma Aldrich). The resin was incubated in the resulting solution for 4 h at RT under continuous mixing conditions before filtration to remove resin. The resin was rinsed with three volumes dichloromethane and the resulting solution was concentrated to 1 mL total volume under a stream of nitrogen gas in a 15 mL Falcon tube. The peptide was precipitated by the addition of 10 mL of cold diethyl ether, followed by overnight incubation at -20 °C. The precipitate was collected by centrifugation and dried under a stream of nitrogen gas. After drying, the crude peptide mixture was dissolved in 1:1 MeCN/ddH_2O containing 1% formic acid (2 mL total volume).

Peptide purification: The peptide was purified by reverse-phase HPLC using an Agilent 1260 Series LC-DAD with a 150 x 30 mm Luna Omega 5 µm PS C_{18} column (Phenomenex) under the following conditions: mobile phase (solvent A: ddH_2O + 0.1% trifluoroacetic acid; solvent B: acetonitrile) gradient elution over 40 min (10% to 50% solvent B). The purity of the peptides was assessed by analytical LC/MS on an Agilent 1290 Series Infinity II HPLC with a 6230 Series Time-of-Flight (TOF) mass spectrometer. Samples were analyzed on a Phenomenex Aeris 3.6 µm WIDEPORE C4 column (2.1 x 50 mm) under the following conditions: mobile phase (solvent A: ddH_2O + 0.1% trifluoroacetic acid; solvent B: acetonitrile + 0.1% trifluoroacetic acid) gradient elution over 6 min (5% to 100% solvent B). The purified peptide fractions were combined and concentrated to dryness under a stream of nitrogen gas. The peptide was then resuspended in minimal DMSO (20 µL) and the concentration quantified by UV-vis spectrometry on a Nanodrop spectrophotometer based on the absorbance of the N-terminal tyrosine at 280 nm (ε_{280} = 1280 $M^{-1}cm^{-1}$). The peptide stock was then diluted to 2.5 mM in DMSO and stored at -20 °C.

Part II. Plasmid and protein information

Plasmids: The gene encoding *citB* (KT781075.1) was codon-optimized for overexpression in *E. coli* and synthesized by GeneArt (ThermoFisher). The synthesized sequence was cloned by GeneArt into a pET-151 vector containing the T7 expression system, ampicillin resistance, and N-terminal 6 x His-tag encoded upstream from the insert gene. No further modifications to this plasmid construct were necessary.

The gene encoding *claD* (QBK15042.1) was codon-optimized for overexpression in *E. coli* and synthesized by Twist Bioscience. The synthesized sequence was cloned by Twist Bioscience into a pET-28a vector containing the T7 expression system, kanamycin resistance, and N-terminal 6 x His tag encoded upstream from the insert gene. No further modifications to this plasmid construct were necessary.

Codon-Optimized *citB* Sequence (including 6 x His Tag)

ATGCATCATCACCATCACCATGGTAAGCCTATCCCTAACCCTCTCCTCGGTCTCGATTCTACGGAAAACCTGTATTT
TCAGGGAATTGATCCCTTCACCATGCCGATTAGCACCAAAAGCAGCTTTTATCTGCCTGCAGTTGATATTAGCCCGT
ATCTGCAGGATCCGAATAGTGATGCAGCACGTAAAGTTATTGATGATGTTCGTGCAGCATGTACCAGCACCGGTTTT
TTTCAGCTGTTAGGTCATGGTATTAGTCCGGCACTGCAGCAGAGCGTTTTTGCAGCAGCAGCAAAATTCTTTGCACT
GCCGAGTGATGTTAAAAGCCGTTGTCGTAATGTTGGTTTTCGTGGTTATGATCCGATGGCAAGCCAGAGCTATGAAC
TGGGTGTTCTGCCGGATCTGAAAGAAGGTTTTATTGCCGGTAAAGATATTCCGCTGGATGATCCGCGTGTTGCAAGC
CAGCGCTTTTTTATGGGTCAGAATGCATGGCCTCCGAGCGAACTGCTGCCGGAAGCAAATTTTCGTCGTCCGATTGA
AGAATATTATCAGGCAATGCTGAAACTGTGTTGGGTTGTTCTGGATCTGGTTGCAGCAACCCTGCCGTATGGTCCGC
ATGTTTTTGATGAATTCAAAGAAAATGATCCGGCATGTCCGCTGCGTCTGCTGCATTATCCGCCTGCACCGGCACCG
GATGTTGCAAAAGGTCGTCAGCTGGGTAGCAGCGCACATACCGATTTTGGTGCAATTACCCTGCTGTTACAGGATGA
TCATAGCGGTCTGGAAGTTCAGGATTGTGAAACCGGTGAATGGATTGGTGTTCCGCCTAATAAAGATGCCTATGTTG
TTAATCTGGGCGATATGATGAGCCGTATTACCCGTGGTCACTATAAAAGCAGCATTCATCGTGTGATTAACCAGAAT
CTGACCGATCGTTATAGCGTGGTGTTTTTTTTCGATGGCAATCTGGATTATCGTCTGCGTCCTCTGGATCGTGTTGG
TCAGAATTGGGATGAAGAAGATACCCTGACCGTTGAAGAACATATGCTGGAACGTACCACCACCACCTATAATCTGA
AAGTGAAATAA

CitB Protein Sequence (including 6 x His Tag)

MHHHHHHGKPIPNPLLGLDSTENLYFQGIDPFTMPISTKSSFYLPAVDISPYLQDPNSDAARKVIDDVRAACTSTGF
FQLLGHGISPALQQSVFAAAAKFFALPSDVKSRCRNVGFRGYDPMASQSYELGVLPDLKEGFIAGKDIPLDDPRVAS
QRFFMGQNAWPPSELLPEANFRRPIEEYYQAMLKLCWVVLDLVAATLPYGPHVFDEFKENDPACPLRLLHYPPAPAP
DVAKGRQLGSSAHTDFGAITLLLQDDHSGLEVQDCETGEWIGVPPNKDAYVVNLGDMMSRITRGHYKSSIHRVINQN
LTDRYSVVFFFDGNLDYRLRPLDRVGQNWDEEDTLTVEEHMLERTTTYNLKVK

Codon-Optimized *claD* Sequence (including 6 x His Tag)

ATGGGCAGCAGCCATCATCATCATCATCACAGCAGCGGCCTGGTGCCGCGCGGCAGCCATATGATGCCGGTGCTGTC
GAATCCGAGCTTTTATCTGCCACTGGTGGATATCACCCCGTTCCTGGAGAACCCGCATGGCGCAGCGGCGCAGGATG
TCATCGAAAGCGTGCGTACCGCCTGCAAAAGCACCGGTTTTTTTTCAGATCAAAGGTCATCAGGTGCCGCTGCGTTTG
CAAAAATCGGTGTTCGAAGCCAGCGCGCGTTTCTTTGCGCTGCCTCTCAAAAACAAACTCGAACTCGACAGCCGCAA
AACCGTTGGCTTCCGCGGTTACGATGTCATGGAAACGCAAAGCTACGAACTGGAATTTGGCGCGGTGCAGGAAGCGG
ATGCGTTGCGCGATATCAAAGAAGGCTTTTTTATTGCCACCGACCTGCCGCCGGATCATCCGCATGTCGCCAACGGT
CGTTTTTTGCAGGGCCCGAACGTCTGGCCGAAACCAGAACAGCTGGCGCCGGAAGATTTCCAGAGCGTACTGGAAGA
ATATTACACCGAAATGCAGCGTCTGTCTCATGTGGTGTTGTCGCTGCTGGCAGCAACGCTGCCGTATGGTCCGCACG
TTTTCGACGAGCTGGAAACCTGCGATCCGATGTCGTTGCTGCGCCTGCTGCATTATCCGCGCGGCTTGGAAAAACAG
GATGGCAAAAAACTGCAACTGGGTGCCGGGGAACATACCGATTTTGGTACCTTTACCCTGTTACTGCAGGACGAGCA
TCCTGGCCTGGAAGTGCAAGACAGTGTCACCGGCGAATGGCACGGCGTGCCACCGCAGGAGGATGTTTATATCGTCA
ACGTTGCCGATATTCTGTCCACCATGACCGAGGGCGATTACAAGTCTTCTGTGCATCGCGTGTGGAACATCAAGAGC
AACGATCGCTACAGCGTCGTGTTTTTCTACGACGGCAACCTGGATTACAAAGTCAAACCGTTACGCAGCAGCGGTCA
GGACGAAAACGAAGAAATCGATGCACCGACCATCGAAGAGCACGTCCGTTCGCGTCTCACTGCCAGTTATGCCATTT
AA

ClaD Protein Sequence (including 6 x His Tag)

MGSSHHHHHHSSGLVPRGSHMMPVLSNPSFYLPLVDITPFLENPHGAAAQDVIESVRTACKSTGFFQIKGHQVPLRL
QKSVFEASARFFALPLKNKLELDSRKTVGFRGYDVMETQSYELEFGAVQEADALRDIKEGFFIATDLPPDHPHVANG

RFLQGPNVWPKPEQLAPEDFQSVLEEYYTEMQRLSHVVLSLLAATLPYGPHVFDELETCDPMSLLRLLHYPRGLEKQ
DGKKLQLGAGEHTDFGTFTLLLQDEHPGLEVQDSVTGEWHGVPPQEDVYIVNVADILSTMTEGDYKSSVHRVWNIKS
NDRYSVVFFYDGNLDYKVKPLRSSGQDENEEIDAPTIEEHVRSRLTASYAI

Protein overexpression and purification: The plasmid containing *citB* or *claD* was transformed using a standard heat-shock protocol for chemically competent *E. coli* into BL21(DE3) cells. Overexpression of *citB* and *claD* was achieved using 4% glycerol (v/v) Terrific Broth (TB) in 2.8 L flasks. 500 mL portions of autoclaved media were inoculated with 5 mL of overnight culture prepared from a single colony in Luria Broth (LB) and 100 µg/mL ampicillin or 50 µg/mL kanamycin (Gold Biotechnology). Cultures were grown at 37 °C and 200 rpm until the optical density (at 600 nm) reached 0.8. The cultures were then cooled to 20 °C for 1 h and protein expression was induced with 0.2 mM isopropyl-β-D-1-thiogalactopyranoside (IPTG, Gold Biotechnology). Expression was continued at 20 °C overnight (approx. 18 h) at 200 rpm. The typical yield for one 500 mL culture cell pellet (wet cell pellet) was ~25 g.

General purification procedure: 50-60 g of cell pellet containing CitB or ClaD was resuspended in 250 mL of lysis buffer containing 50 mM Tris HCl (pH 7.4), 300 mM NaCl, 10 mM imidazole and 10% glycerol. The mixture was homogenized using a handheld dounce homogenizer. Approximately 1 mg/mL lysozyme (Gold Biotechnology) was added prior to 1 h incubation on a rocker held at 4 °C. Cells were lysed by sonication of the total cell lysate in 100 mL batches on ice. Each cycle of sonication was 10 s sonication, followed by a 20 s rest period, for a total of 6 min at 60% power. The total cell lysate was centrifuged at 45,000 x g for 30 min and the supernatant was removed. The cell lysate was incubated with 3 mL of Ni-NTA resin (Thermo) for 1 h at 4 °C with gentle rocking. The supernatant was filtered through a fritted 50 mL plastic column (Gold Biotechnologies) to isolate the Ni-NTA resin. The resin was washed with 100 mL of wash buffer containing 50 mM Tris HCl (pH 7.4), 300 mM NaCl, 25 mM imidazole and 10% glycerol. The protein was then eluted using 15 mL of an elution buffer containing 50 mM Tris HCl (pH 7.4), 300 mM NaCl, 250 mM imidazole and 10% glycerol. The eluted protein was concentrated to a volume of 2.5 mL using a 30 KDa molecular weight cutoff ultrafiltration device (Amicon). The concentrated protein was desalted using a PD-10 desalting column that was pre-equilibrated with a storage buffer containing 50 mM Tris HCl (pH 7.4), 300 mM NaCl, and 10% glycerol. The protein was eluted from the column with 3.5 mL of storage buffer, before flash freezing in liquid nitrogen and storage at -80 °C. Protein concentration was determined by the A280 absorbance method using a Nanodrop spectrophotometer. The concentration was corrected using the estimated extinction coefficient from the ProtParam tool on the Expasy server (CitB: ε = 1.128; ClaD ε = 0.890). **Average yield:** 60 mg/L of CitB; 41 mg/L of ClaD.

Preparation of clarified crude cell lysate (ClaD only): 50-60 g of cell pellet containing ClaD was resuspended to a volume of 45 mg/mL in lysis buffer containing 50 mM Tris HCl (pH 7.4), 150 mM NaCl, and 10% glycerol. The mixture was homogenized using a handheld dounce homogenizer. Approximately 1 mg/mL lysozyme (Gold Biotechnology) was added prior to 1 h incubation on a rocker held at 4 °C. Cells were lysed by sonication of the total cell lysate in 100 mL batches on ice. Each cycle of sonication was 10 s sonication, followed by a 20 s rest period, for a total of 6 min at 60% power. The total cell lysate was centrifuged at 45,000 x g for 30 min and the supernatant was removed. The resulting supernatant was clarified by filtration through a 0.4 µm sterile filtration device. Aliquots of lysate were flash frozen in liquid nitrogen and stored at -80 °C until needed.

Supplementary Figure S1. SDS-PAGE gel of purified CitB (40.61 kDa with 6x His tag)

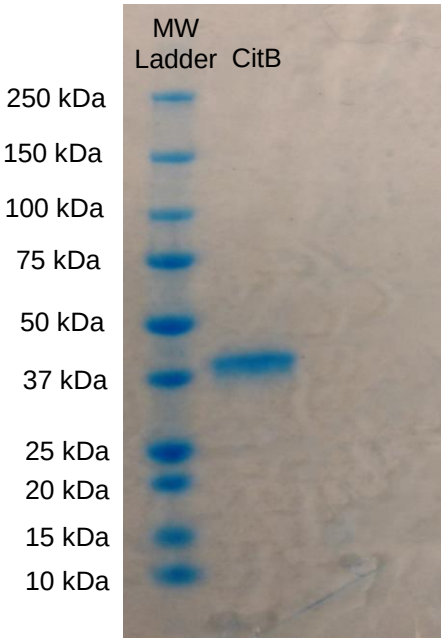

Supplementary Figure S2. SDS-PAGE gel of purified ClaD (40.40 kDa with 6x His tag)

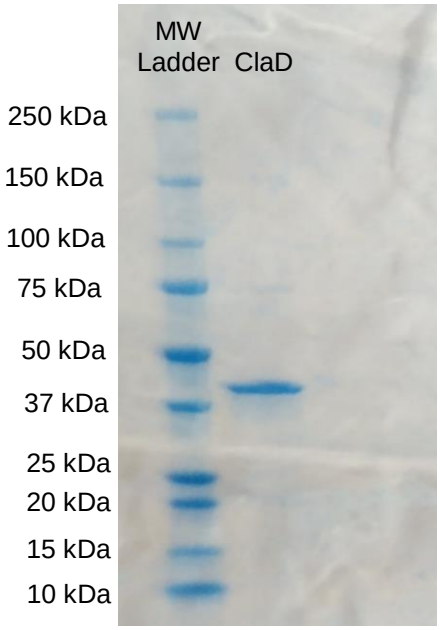

Part III. Biocatalytic reactions and products

Stock solutions: Stock solutions of each substrate (50 mM) were prepared by dissolving the substrate in DMSO (analytical grade). Stock solutions of α-ketoglutaric acid (125 mM), ferrous sulfate (10 mM) and sodium ascorbate (50 mM) were freshly prepared before each use, stored on ice, and used within 3 h. Aliquots of CitB (124 μM) and ClaD (80 μM) were stored at -80 °C until needed.

***In vitro* analytical-scale reactions (CitB and ClaD):** Each reaction contained 50 mM TES buffer pH 7.5 (2.5 μL of a 1 M solution), 2.5 mM substrate (2.5 μL, 50 mM), 10 μM CitB (4 μL, 124 μM) or ClaD (6.25 μL, 80 μM), 5 mM α-ketoglutaric acid (2 μL, 125 mM), 0.1 mM ferrous sulfate heptahydrate (0.5 μL, 10 mM), 8 mM sodium ascorbate (8 μL, 50 mM) and Milli-Q water to a final volume of 50 μL. Reactions were carried out at 30 °C for 3 h and quenched by the addition of 3 volumes of acetonitrile containing 3.5 mM pentamethyl benzene as an internal standard. Precipitated biomolecules were pelleted by centrifugation (17,000 x g, 20 min). The supernatant was analyzed by UPLC-DAD and conversion obtained by comparison to calibration curves of each substrate.

Whole cell analytical-scale reactions (CitB): Except where otherwise noted, each reaction contained 50 mM TES buffer pH 7.5 (25 μL of a 1M solution), 2.5 mM substrate (25 μL, 50 mM), 22.5 mg CitB wet cell pellet (45 mg/mL), 5 mM α-ketoglutaric acid (20 μL, 125 mM), 0.1 mM ferrous sulfate (5 μL, 10 mM), 8 mM sodium ascorbate (80 μL, 50 mM) and Milli-Q water to a final volume of 500 μL. Reactions were carried out at 30 °C for 3 h and quenched by the addition of 3 volumes of acetonitrile containing 3.5 mM pentamethylbenzene as an internal standard. The supernatant was analyzed by UPLC-DAD and conversion obtained by comparison of remaining starting material to calibration curves of each substrate.

Crude cell lysate analytical-scale reactions (ClaD): Each reaction contained 50 mM TES buffer pH 7.5 (2.5 μL of a 1 M solution), 2.5 mM substrate (2.5 μL, 50 mM), 10% v/v ClaD (5 μL) or 5 mM α-ketoglutaric acid (2 μL, 125 mM), 0.1 mM ferrous sulfate heptahydrate (0.5 μL, 10 mM), 8 mM sodium ascorbate (8 μL, 50 mM) and Milli-Q water to a final volume of 50 μL. Reactions were carried out at 30 °C for 1 h and quenched by the addition of 3 volumes of acetonitrile containing 3.5 mM pentamethyl benzene as an internal standard. Precipitated biomolecules were pelleted by centrifugation (17,000 x g, 20 min). The supernatant was analyzed by UPLC-DAD and conversion obtained by comparison to calibration curves of each substrate.

Determination of percent conversion: Percent conversion was determined by analysis of each reaction after 3 h. PDA spectrometric analysis was performed on a Waters Aquity H-Class instrument, using a Phenomenex Kinetex (1.7 μm C18, 2.1 x 150 mm) column under the following conditions: mobile phase (Solvent A: deionized water + 0.1% formic acid; Solvent B: acetonitrile + 0.1% formic acid) 5% to 100% solvent B over 2 min, 100% solvent B for 1 min; flow rate: 0.5 mL/min. Based on the calibration curves of the starting materials, the percent conversion of the substrate to hydroxylated product was calculated with $AUC_{substrate}$ (300 nm)/$AUC_{internal\ standard}$ (270 nm). *In vitro* reactions were performed and analyzed in triplicate, while whole cell reactions were performed and analyzed in duplicate with reported conversions as an average of those trials.

General procedure for whole cell milligram-scale reactions: Except where otherwise noted, preparative-scale enzymatic reactions were conducted on 20-40 mg of each substrate under the following conditions: 2.5 mM substrate, 50 mM TES buffer pH 7.5, 5 mM α-ketoglutaric acid, 0.1 mM ferrous sulfate, 8 mM sodium ascorbate, 45 mg/mL CitB wet cell pellet. Reactions were performed in Erlenmeyer flasks of appropriate volume to achieve proper oxygenation (at least 3 times reaction volume) and shaken at 100 rpm at 30 °C. Reaction progress was monitored at hourly intervals by analysis of a 50 μL aliquot by UPLC-DAD. The aliquot was processed in the manner described for *in vitro* analytical scale determination of reaction conversion. Upon satisfactory conversion of the substrate, the product(s) were isolated in the following manner. **Isolation procedure:** The reaction mixture was transferred to a 50 mL falcon tube and 2 volumes of acetone were added. The mixture was centrifuged at 4,500 x g for 10 min to separate the biomolecule components from the aqueous reaction mixture. The supernatant was removed and acetone removed under reduced pressure. The supernatant was acidified to pH 2.0 with 0.1 M HCl. The organic materials were extracted from the aqueous layer with ethyl acetate (3 x 50 mL). The organic fractions were

pooled and concentrated under reduced pressure to yield a crude mixture. To ensure maximal product recovery, the pelleted wet cell components were extracted with hexanes and ethyl acetate. These fractions were concentrated under reduced pressure to yield a separate crude mixture. These mixtures were purified by either preparative HPLC or flash silica gel chromatography (Biotage).

General procedure for crude cell lysate milligram-scale reactions: Except where otherwise noted, preparative-scale enzymatic reactions were conducted on 20-100 mg of each substrate under the following conditions: 2.5 mM substrate, 50 mM TES buffer pH 7.5, 5 mM α-ketoglutaric acid, 0.1 mM ferrous sulfate, 8 mM sodium ascorbate, 10% v/v ClaD clarified crude lysate (prepared from 45 mg/mL wet whole cell suspension). Reactions were performed in Erlenmeyer flasks of appropriate volume to achieve proper oxygenation (at least 3 times reaction volume) and incubated at 30 °C. Reaction progress was monitored at hourly intervals by analysis of a 50 µL aliquot by UPLC-DAD. The aliquot was processed in the manner described for *in vitro* analytical scale determination of reaction conversion. Upon satisfactory conversion of the substrate, the product(s) were isolated in the following manner. **Isolation procedure:** The reaction mixture was acidified to pH 2.0 with 0.1 M HCl. The organic materials were extracted from the aqueous layer with ethyl acetate (3 x 50 mL). The organic fractions were pooled and concentrated under reduced pressure to yield a crude mixture. These fractions were concentrated under reduced pressure to yield a separate crude mixture. These mixtures were purified by either preparative HPLC or flash silica gel chromatography (Biotage).

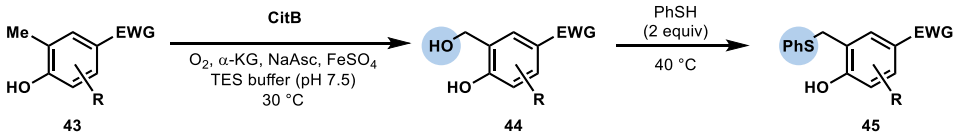

Supplementary Figure S3. Whole-cell milligram-scale CitB reactions with *in situ* functionalization.

Modified procedure for whole-cell milligram-scale reactions with *in situ* functionalization: Preparative-scale reactions with *in situ* functionalization using thiophenol were set up using a protocol identical to the general procedure for whole cell milligram-scale reactions, except that after 1 h, 2 equiv of thiophenol was added and the temperature increased to 40°C.

Procedure for one-pot whole-cell chemoenzymatic cascade reactions (nucleophile addition): Analytical scale whole-cell cascade reactions were performed in 15 mL Falcon tubes (in duplicate trials) in a manner analogous to analytical-scale CitB reactions, except that after 3 h, cell pellet was spun down at 4,000 x g for 5 min. 2 equiv of nucleophile (**17** and **20**,**73**-**77**) were added directly to the supernatant. Each Falcon tubes was shaken at 400 rpm and 37 °C for 16 h. 50 µL of the reaction was removed and diluted 10x with acetonitrile containing 3.5 mM pentamethyl benzene as internal standard. For reactions run neat in nucleophilic solvent, 50 µL of sample was concentrated to dryness under reduced pressure. The dried film was then diluted 10 x with acetonitrile and internal standard, plus 50 µL of ddH_2O to dissolve associated reaction salts. Samples were analyzed by UPLC using the method for determination of conversion percentage described previously, except for morpholine adduct **77**, which was analyzed using a hydrophilic interaction column (HILIC) under the following conditions: mobile phase (Solvent A: deionized water + 0.1% formic acid; Solvent B: acetonitrile + 0.1% formic acid) 85% to 40% solvent B over 7 min, 85% solvent B for 6 min; flow rate: 0.45 mL/min. HILIC column = Waters Acquity 1.7 µm UPLC BEH Amide HILIC 2.1 x

100 mm. Samples were quenched by the addition of 3 equiv solution containing 1:1 deionized water and acetonitrile, with 3.5 mM L-tryptophan as internal standard.

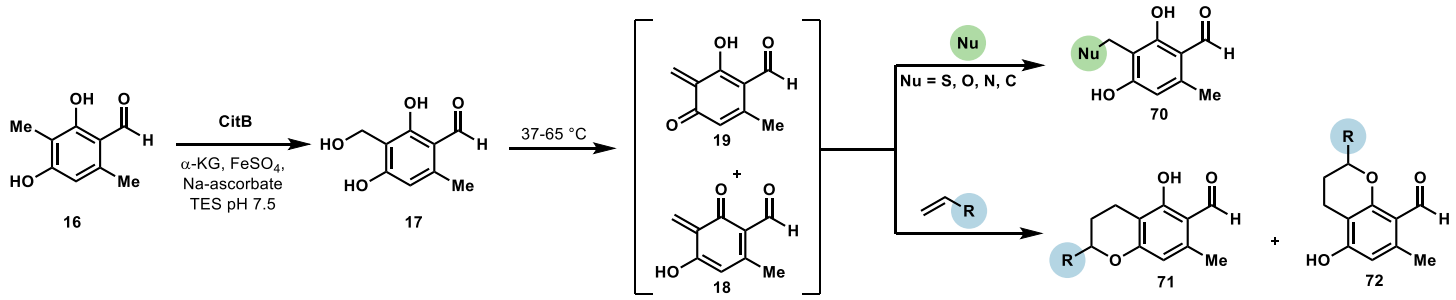

Supplementary Figure S4. One-pot whole-cell chemoenzymatic cascade reactions

Procedure for one-pot whole-cell chemoenzymatic cascade reactions (Diels-Alder reactions): Analytical scale whole-cell cascade reactions were performed in 1 dram reaction vials (duplicate) in a manner analogous to analytical scale CitB reactions, except that the reactions were stirred at 100 rpm using a Teflon stir bar for 3 h at 30 °C. After 3 h, 10 equiv of dienophile was added to the vial which was sealed with an air-tight cap and heated to 60 °C (65 °C for styrene and 2,3-dihydrofuran) for 16 h. For reactions using styrenes as a dienophile, 50 µL of the reaction was removed and diluted 10x with acetonitrile containing 3.5 mM pentamethyl benzene as an internal standard. For reactions with all other dienophiles, 50 µL of sample was reduced to dryness under reduced pressure. The dried film was then diluted 10 x with acetonitrile and internal standard, plus 50 µL of ddH_2O to dissolve associated reaction salts. Samples were analyzed by UPLC using the method for determination of conversion percentage described above. Reactions were performed in triplicate, with reported conversions as an average of those trials.

Purification by preparative HPLC: For purification of milligram-scale reactions, the resulting crude mixture was taken up in a 60:40 mixture of milli-Q water:acetonitrile (2 mL). The product(s) were purified from this mixture by preparative HPLC using a Phenomenex Kinetex 5 µm C18, 150 x 21.2 mm column under the following conditions: mobile phase (Solvent A: deionized water + 0.1% formic acid; Solvent B: acetonitrile + 0.1% formic acid) 5% to 100% solvent B over 13 min, 100% solvent B for 4 min; flow rate: 11.5 mL/min.

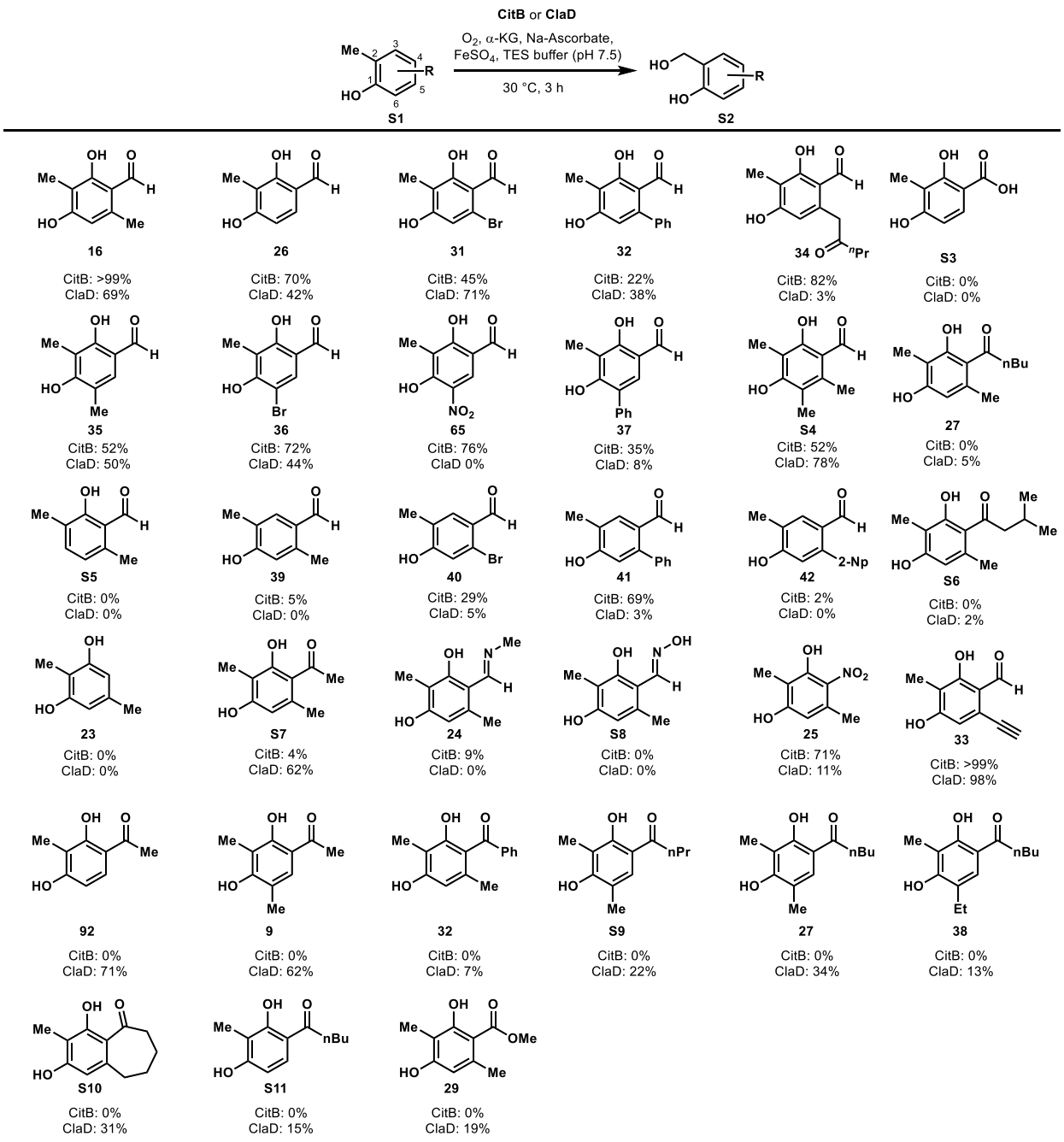

Supplementary Figure S5. *In vitro* conversion of phenolic substrates in CitB- and ClaD-catalyzed benzylic hydroxylation. Reaction conditions: 2.5 mM substrate, 10 µM CitB or ClaD, 50 mM TES pH 7.5, 5 mM α-ketoglutaric acid (α-KG), 8 mM sodium ascorbate (Na Asc), 0.1 mM ferrous sulfate ($FeSO_4$), 30 °C, 3 h. Np = 2-naph Conversion to product was quantified by UPLC-DAD analysis using 3.5 mM pentamethylbenzene as internal standard.

Products of biocatalytic benzylic C–H hydroxylation

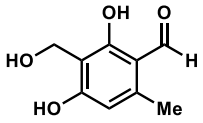

17

2,4-dihydroxy-3-(hydroxymethyl)-6-methylbenzaldehyde (17)
The title compound was synthesized according to the general procedure for milligram-scale whole cell enzymatic hydroxylation with CitB. The reaction was performed with 500 mg of starting material. Purification by flash chromatography afforded 460 mg (84% yield) of the title compound as a white solid. **^{1}H NMR** (400 MHz, MeOD) δ 10.07 (s, 1H), 6.26 (s, 1H), 4.68 (s, 2H), 2.50 (s, 3H); **^{13}C NMR** (150 MHz, MeOD) δ 194.5, 165.5, 165.4, 145.5, 113.7, 112.8, 111.2, 53.7, 18.2; **HR-ESI-MS**: m/z calcd for $C_9H_{11}O_4^+$ $[M+H-H_2O]^+$: 165.0546, found: 165.0544; **IR** (thin film): 3268, 2922, 1605, 1484, 1438, 1244, 1115, 966, 840, 565 cm^{-1}.

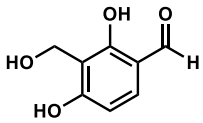

46

2,4-dihydroxy-3-(hydroxymethyl)benzaldehyde (46)
The title compound was synthesized according to the general procedure for milligram-scale whole cell enzymatic hydroxylation with CitB. The reaction was performed with 20 mg of starting material. Purification by preparative HPLC afforded 10.6 mg (50% yield) of the title compound as a white solid. **^{1}H NMR** (400 MHz, CD_3OD) δ 9.68 (s, 1H), 7.46 (d, *J* = 8.8, 1H), 6.50 (d, J = 8.8, 1H), 4.73 (s, 2H); **^{13}C NMR** (150 MHz, CD_3OD) δ 196.2, 165.7, 163.5, 136.4, 115.8, 114.6, 109.4, 53.7; **HR-ESI-**MS: m/z calcd for $C_8H_{11}O_4^+$ $[M+H-H_2O]^+$: 151.0390, found: 151.0393; **IR** (thin film): 3254, 2920, 2530, 2274, 1608, 1495, 1435, 1383, 1321, 1249, 1077 cm^{-1}.

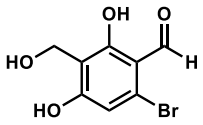

47

6-bromo-2,4-hydroxy-3-(hydroxymethyl)benzaldehyde (47)
The title compound was synthesized according to the general procedure for milligram-scale whole cell enzymatic hydroxylation with CitB. The reaction was performed with 20 mg of starting material. Purification by preparative HPLC afforded 7.4 mg (35% yield) of the title compound as a tan film. **^{1}H NMR** (400 MHz, CD_3OD) δ 10.07 (s, 1H), 6.73 (s, 1H), 4.68 (s, 2H); **^{13}C NMR** (150 MHz, CD_3OD) δ 195.3, 165.0, 164.7, 128.6, 113.0, 111.2, 110.8, 61.3; **HR-ESI-MS**: m/z calcd for $C_8H_9O_4Br^+$ $[M+H-H_2O]^+$: 228.9495, found: 228.9493; **IR** (thin film): 3129, 2831, 1617, 1460, 1425, 1248, 1109, 1019 cm^{-1}.

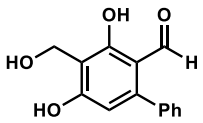

48

3,5-dihydroxy-4-(hydroxymethyl)-[1,1'-biphenyl]-2-carbaldehyde (48)
The title compound was synthesized according to the general procedure for milligram-scale whole cell enzymatic hydroxylation with CitB. The reaction was performed with 20 mg of starting material, using 30 mg/mL CitB wet cell pellet. Purification by preparative HPLC afforded 6.8 mg (30% yield) of the title

compound as a white film. **^{1}H NMR** (400 MHz, CD_3OD) δ 9.53 (s, 1H), 7.43 (m, 3 H), 7.38 (m, 2H), 6.38 (s, 1H), 2.58 (s, 2H); **^{13}C NMR** (150 MHz, CD_3OD) δ 195.9, 165.1, 150.4, 139.0, 130.8, 130.7, 130.1, 129.4, 129.3, 129.0, 114.0, 113.0, 111.0, 53.7; **HR-ESI-MS**: m/z calcd for $C_{14}H_{13}O_4^+$ $[M+H-H_2O]^+$: 227.0703, found: 227.0705; **IR** (thin film): 3296, 2924, 1616, 1428, 1381, 1254, 1107, 1022, 855 cm^{-1}.

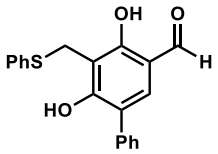

49

2,4-dihydroxy-3-((phenylthiol)methyl)-5-phenylbenzaldehyde (49)
The title compound was synthesized according to the modified procedure for milligram-scale whole cell enzymatic hydroxylation with CitB and *in situ* functionalization with thiophenol. The reaction was performed with 20 mg of starting material. Purification by flash chromatography afforded 9.2 mg (31% yield) of the title compound as a white solid. **^{1}H NMR** (400 MHz, CD_3OD) δ 9.67 (s, 1H), 7.78 (s, 1H), 7.37 (m, 10H), 4.28 (s, 2H); **^{13}C NMR** (150 MHz, CD_3OD) δ 196.2, 162.3, 138.4, 138.1, 136.4, 131.8, 129.7, 128.5, 127.4, 124.6, 115.7, 113.4, 27.9; **HR-ESI-MS**: m/z calcd for $C_{20}H_{17}O_3S^+$ $[M+H]^+$: 337.0893, found: 337.0903; **IR** (thin film): 3057, 2926, 2854, 1606, 1549, 1456, 1438, 1306, 1087 cm^{-1}.

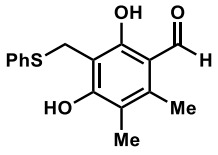

50

2,4-hydroxy-3-(hydroxymethyl)-5,6-dimethylbenzaldehyde (50)
The title compound was synthesized according to the general procedure for milligram-scale whole cell enzymatic hydroxylation with CitB. The reaction was performed with 20 mg of starting material, using 30 mg/mL CitB wet cell pellet. Purification by preparative HPLC afforded 12.8 mg (40% yield) of the title compound as a white solid. **^{1}H NMR** (400 MHz, CD_3OD) δ 10.15 (s, 1H), 7.37 (d, J = 8.0, 2H), 7.23 (t, J = 8.0, 2H), 7.15 (t, J = 8.0, 1H) 4.23 (s, 2H), 2.46 (s, 3H), 2.11 (s, 3H); **^{13}C NMR** (150 MHz, CD_3OD) δ 195.3, 163.0, 163.0, 142.1, 138.4, 131.2, 129.6, 127.1, 117.3, 113.9, 109.9, 27.5, 14.0, 11.66; **HR-ESI-MS**: m/z calcd for $C_{16}H_{17}O_3S^+$ $[M+H]^+$: 289.0893, found: 289.0882; **IR** (thin film): 3337, 2943, 2831, 1606, 1447, 1269, 1225, 1173, 1116, 1022 cm^{-1}.

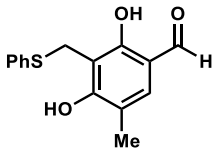

51

2,4-dihydroxy-5-methyl-3-((phenylthio)methyl)benzaldehyde (51)
The title compound was synthesized according to the general procedure for milligram-scale whole cell enzymatic hydroxylation with CitB and *in situ* functionalization with thiophenol. The reaction was performed with 40 mg of starting material. Purification by flash chromatography afforded 14.8 mg (23% yield) of the title compound as a white solid. **^{1}H NMR** (400 MHz, CD_3OD) δ 9.63 (s, 1H), 7.31 (s, 1H), 4.87 (s, 2H), 2.16 (s, 3H); **^{13}C NMR** (150 MHz, CD_3OD) δ 196.3, 164.5, 160.5, 135.7, 119.1, 115.1, 112.5, 56.8, 15.3; **HR-ESI-MS**: m/z calcd for $C_{15}H_{15}O_3S^+$ $[M+H]^+$: 275.0736, found: 275.0737; **IR** (thin film): 3335, 2925, 1619, 1479, 1438, 1387, 1332, 1273, 1175, 1121 cm^{-1}.

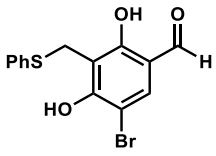

52

5-bromo-2,4-dihydroxy-3-((phenylthiol)methyl)benzaldehyde (52)

The title compound was synthesized according to the modified procedure for milligram-scale whole cell enzymatic hydroxylation with CitB and *in situ* functionalization with thiophenol. The reaction was performed with 20 mg of starting material. Purification by flash chromatography afforded 6.8 mg (24% yield) of the title compound as a white film. **^{1}H NMR** (400 MHz, CD_3OD) δ 9.64 (s, 1H), 7.75 (s, 1H), 7.39 (m, 2H), 7.23 (m, 3H), 4.23 (s, 2H); **^{13}C NMR** (150 MHz, CD_3OD) δ 195.4, 167.5, 137.6, 137.5, 131.6, 129.4, 127.2, 116.6, 114.8, 102.1, 27.9, 16.8; **HR-ESI-MS**: m/z calcd for $C_{14}H_{12}O_3SBr^+$ $[M+H]^+$: 338.9685, found: 338.9710; **IR** (thin film): 3299, 3058, 2927, 2854, 1603, 1549, 1455, 1438, 1304, 1173, 1084 cm^{-1}.

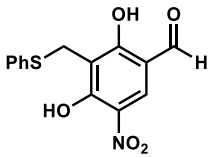

53

2,4-dihydroxy-5-nitro-3-((phenylthiol)methyl)benzaldehyde (53)

The title compound was synthesized according to the modified procedure for milligram-scale whole cell enzymatic hydroxylation with CitB and *in situ* functionalization with thiophenol. The reaction was performed with 20 mg of starting material. Purification by flash chromatography afforded 8.0 mg (26% yield) of the title compound as a yellow film. **^{1}H NMR** (599 MHz, $(CD_3)_2CO$) δ 10.04 (s, 1H), 8.75 (s, 1H), 7.49-7.26 (m, 5H), 4.29 (s, 2H); **^{13}C NMR** (150 MHz, $(CD_3)_2CO$) δ 196.0, 173.6, 132.6, 130.5, 129.6, 128.8, 128.4, 126.5, 125.5, 114.5, 107.8, 25.9; **HR-ESI-MS**: m/z calcd for $C_{14}H_{12}NO_5S^+$ $[M+H]^+$: 306.0431, found: 306.0426; **IR** (thin film): 2924, 2854, 1709, 1625, 1540, 1456, 1267, 1158, 1092 cm^{-1}.

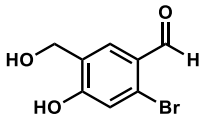

63

2-bromo-4-hydroxy-5-(hydroxymethyl)benzaldehyde (63)

The title compound was synthesized according to the general procedure for milligram-scale whole cell enzymatic hydroxylation with CitB. The reaction was performed with 40 mg of starting material. Purification by preparative HPLC afforded 2.7 mg (7% yield) of the title compound as a tan film. **^{1}H NMR** (400 MHz, CD_3OD) δ 10.14 (s, 1H), 7.94 (s, 1 H), 7.07 (s, 1H), 4.60 (s, 2H); **^{13}C NMR** (150 MHz, CD_3OD) δ 191.6, 162.4, 130.3, 130.2, 128.0, 126.8, 120.0, 59.5; **HR-ESI-MS** m/z calcd for $C_8H_8BrO_3^+$ $[M+H]^+$: 230.9651, found: 230.9657; **IR** (thin film): 3258, 2925, 2855, 1621, 1433, 1381, 1256, 1106 cm^{-1}.

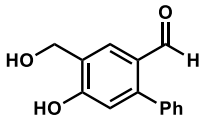

64

4-hydroxy-5-(hydroxymethyl)-2-phenylbenzaldehyde (64)

The title compound was synthesized according to the modified procedure for milligram-scale whole cell enzymatic hydroxylation with CitB and *in situ* functionalization with thiophenol. The reaction was performed with 40 mg of starting material. Purification by preparative HPLC afforded 6.0 mg (14% yield) of the title compound as a white film. **^{1}H NMR** (400 MHz, CD_3OD) δ 9.71 (s, 1H), 8.04 (s, 1H), 7.46-7.38 (m, 5H), 6.79 (s, 1H), 4.70 (s, 2H); **^{13}C NMR** (150 MHz, $(CD_3)_2CO$) δ 189.4, 138.0, 129.8, 128.3, 128.2, 128.0, 127.8, 127.1, 116.5, 59.8; **HR-ESI-MS**: m/z calcd for $C_{14}H_{13}O_3^+$ $[M+H]^+$: 229.0859, found: 229.0855; **IR** (thin film): 3266, 2925, 1659, 1602, 1484, 1282, 1015 cm^{-1}.

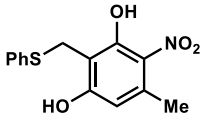

62

5-methyl-4-nitro-2-((phenylthio)methyl)benzene-1,3-diol (62)

The title compound was synthesized according to the modified procedure for milligram-scale whole cell enzymatic hydroxylation with CitB and *in situ* functionalization with thiophenol. The reaction was performed with 20 mg of starting material. Purification by preparative HPLC afforded 8.1 mg (28% yield) of the title compound as a yellow solid. **^{1}H NMR** (600 MHz, $(CD_3)_2CO$) δ 11.40 (s, 1H), 10.02 (s, 1H), 7.44 (d, *J* = 7.4, 2H), 7.29 (t, *J* = 7.4, 2H), 7.20 (t, *J* = 7.4, 1H), 6.50 (s, 1H), 4.27 (s, 2H), 2.52 (s, 3H); **^{13}C NMR** (150 MHz, $(CD_3)_2CO$) δ 160.9, 156.0, 137.7, 137.4, 129.5, 129.1, 128.7, 125.9, 111.5, 110.9, 26.6, 22.0; **HR-ESI-MS**: m/z calcd for $C_{14}H_{13}O_3^+$ $[M+H]^+$: 292.0268, found: 292.0261; **IR** (thin film): 3356, 2931, 1603, 1549, 1455, 1415, 1306, 1173, 1006 cm^{-1}.

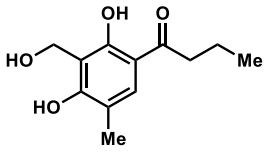

55

1-(2,4-dihydroxy-3-(hydroxymethyl)-5-methylphenyl)butan-1-one (55)

The title compound was synthesized according to the procedure for milligram-scale crude cell reactions with ClaD. The reaction was performed with 20 mg of starting material. Purification by flash chromatography afforded 8.5 mg (39% yield) of the title compound as a white solid. **^{1}H NMR** (600 MHz, CD_3CN) δ 13.15 (s, 1H), 7.60 (s, 1H), 4.92 (s, 2H), 2.91 (t, *J* = 7.4, 2H), 2.14 (s, 3H), 1.70 (sxt, *J* = 7.4, 2H), 0.99 (t, *J* = 7.4, 3H); **^{13}C NMR** (150 MHz, CD_3CN) δ 205.8, 162.2, 159.7, 131.1, 111.9, 110.9, 57.4, 39.5, 39.4, 18.0, 14.4, 13.1; **HR-ESI-MS**: m/z calcd for $C_{12}H_{15}O_3^+$ $[M+H-H_2O]^+$: 207.1016, found: 207.1024; **IR** (thin film): 3333, 2957, 2358, 1622, 1168, 997, 661 cm^{-1}.

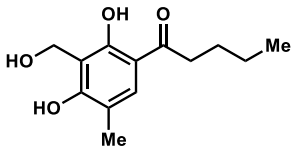

56

1-(2,4-dihydroxy-3-(hydroxymethyl)-5-methylphenyl)pentan-1-one (56)

The title compound was synthesized according to the procedure for milligram-scale crude cell reactions with ClaD. The reaction was performed with 20 mg of starting material. Purification by flash chromatography afforded 6.5 mg (30% yield) of the title compound as a white solid. **^{1}H NMR** (600 MHz, CD_3CN) δ 13.15 (s, 1H), 7.60 (s, 1H), 4.92 (s, 2H), 2.94 (t, *J* = 7.4, 2H), 2.14 (s, 3H) 1.66 (p, *J* = 7.4, 2H), 1.40 (sxt, *J* = 7.4, 2H), 0.95 (t, *J* = 7.4, 3H); **^{13}C NMR** (150 MHz, CD_3CN) δ 206.0, 162.2, 159.7, 131.1, 116.7, 111.8, 110.5, 57.5, 37.3, 26.7, 22.1, 14.4, 13.2; **HR-ESI-MS**: m/z calcd for $C_{13}H_{17}O_3^+$ $[M+H-H_2O]^+$: 221.1172, found: 221.1178; **IR** (thin film): 3394, 2955, 2352, 2025, 1225, 961, 740 cm^{-1}.

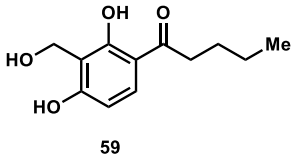

59

1-(2,4-dihydroxy-3-(hydroxymethyl)phenyl)pentan-1-one (59)

The title compound was synthesized according to the procedure for milligram-scale crude cell reactions with ClaD. The reaction was performed with 20 mg of starting material. Purification by flash chromatography afforded 6.1 mg (28% yield) of the title compound as a white solid. **^{1}H NMR** (600 MHz, CD_3CN) δ 7.71 (d, *J* = 8.9, 1H), 6.40 (d, *J* = 8.9, 1H), 4.72 (s, 2H), 2.91 (t, *J* = 7.5, 2H), 1.67 (m, 2H), 1.40 (m, 2H), 0.95 (t, *J* = 3H); **^{13}C NMR** (150 MHz, CD_3CN) δ 205.5, 163.2, 131.4, 113.4, 112.2, 106.9, 52.7, 48.1,. 37.0, 26.9, 22.0, 12.8; **HR-ESI-MS**: m/z calcd for $C_{12}H_{15}O_3^+$ $[M+H-H_2O]^+$: 207.1016, found: 207.1019; **IR** (thin film): 3301, 2512, 1654, 1441, 982 cm^{-1}.

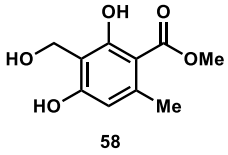

58

Methyl-2,4-dihydroxy-3-(hydroxymethyl)-6-methylbenzoate (58)

The title compound was synthesized according to the procedure for milligram-scale crude cell reactions with ClaD. The reaction was performed with 20 mg of starting material. Purification by flash chromatography afforded 4 mg (7% yield) of the title compound as a white solid. **^{1}H NMR** (600 MHz, CD_3OD) δ 6.25 (s, 1H), 4.71 (s, 2H), 3.91 (s, 3H), 2.46 (s, 3H); **^{13}C NMR** (150 MHz, CD_3CN) δ 172.3, 163.3, 160.9, 142.3, 111.2, 110.5, 53.2, 50.8, 22.9; **HR-ESI-MS**: m/z calcd for $C_{12}H_{11}O_4^+$ $[M+H-H_2O]^+$: 195.0652, found: 195.0667; **IR** (thin film): 3388, 2954, 2364, 1719, 1647, 1439, 1317, 1276, 1198, 1165, 981 cm^{-1}.

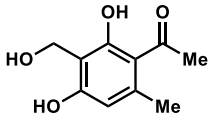

57

1-(2,4-dihydroxy-3-(hydroxymethyl)-6-methylphenyl)ethan-1-one (57)

The title compound was synthesized according to the procedure for milligram-scale crude cell reactions with ClaD. The reaction was performed with 20 mg of starting material. Purification by flash chromatography afforded 13.2 mg (61% yield) of the title compound as a white solid. **^{1}H NMR** (600 MHz, CD_3CN) δ 13.90 (s, 1H), 6.26 (s, 1H), 4.80 (s, 2H), 2.61 (s, 3H), 2.53 (s, 3H); **^{13}C NMR** (150 MHz, CD_3CN) δ 205.0, 163.4, 161.4, 141.8, 114.3, 111.7, 109.9, 56.6, 32.4, 23.9; **HR-ESI-MS**: m/z calcd for $C_{10}H_{11}O_3^+$ $[M+H-H_2O]^+$: 179.0703, found: 179.0703; **IR** (thin film): 3283, 2357, 1963, 1607, 1428, 1268, 1001 cm^{-1}.

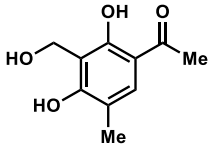

54

1-(2,4-dihydroxy-3-(hydroxymethyl)-5-methylphenyl)ethan-1-one (54)

The title compound was synthesized according to the procedure for milligram-scale crude cell reactions with ClaD. The reaction was performed with 20 mg of starting material. Purification by flash chromatography afforded 14.1 mg (65% yield) of the title compound as a white solid. **^{1}H NMR** (600 MHz, CD_3CN) δ 13.01 (s, 1H), 7.57 (s, 1H), 4.92 (s, 2H), 2.52 (s, 3H), 2.14 (s, 3H); **^{13}C NMR** (150 MHz, CD_3CN) δ 203.6, 162.3, 159.5, 131.8, 116.7, 112.3, 110.4, 57.4, 25.6, 14.4; **HR-ESI-MS**: m/z calcd for $C_{10}H_{11}O_3^+$ $[M+H-H_2O]^+$: 179.0703, found: 179.0707; **IR** (thin film): 3270, 2356, 2013, 1713, 1486, 1371, 1333, 1269, 1190, 1083, 1004 cm^{-1}.

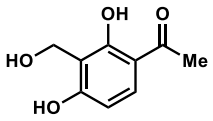

60

1-(2,4-dihydroxy-3-(hydroxymethyl)phenyl)ethan-1-one (60)

The title compound was synthesized according to the procedure for milligram-scale crude cell reactions with ClaD. The reaction was performed with 20 mg of starting material. Purification by flash chromatography afforded 76 mg (69% yield) of the title compound as a white solid. **^{1}H NMR** (600 MHz, CD_3CN) δ 13.17 (s, 1H), 7.68 (d, *J* = 8.8, 1H), 6.41 (d, *J* = 8.8, 1H), 4.82 (s, 1H), 2.53 (s, 1H); **^{13}C NMR** (150 MHz, CD_3CN) δ 203.7, 163.4, 161.8, 132.2, 112.9, 112.1, 107.9, 55.9, 25.6; **HR-ESI-MS**: m/z calcd for $C_9H_9O_3^+$ $[M+H-H_2O]^+$: 165.0546, found: 165.0557; **IR** (thin film): 3320, 2956, 2360, 2341, 1981, 1615, 987 cm^{-1}.

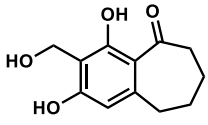

61

2,4-dihydroxy-3-(hydroxymethyl)-6,7,8,9-tetrahydro-5H-benzo[7]annulen-5-one (61)

The title compound was synthesized according to the procedure for milligram-scale crude cell reactions with ClaD. The reaction was performed with 10 mg of starting material. Purification by flash chromatography afforded 4.1 mg (37% yield) of the title compound as a white solid. **^{1}H NMR** (600 MHz, CD_3CN) δ 13.70 (s, 1H), 6.27 (s, 1H), 4.80 (s, 2H), 2.93-2.85 (m, 2H), 2.83-2.76 (m, 2H), 1.88-1.75 (m, 4H). **^{13}C NMR** (150 MHz, CD_3CN) δ 208.7, 163.1, 162.1, 147.2, 113.2, 109.8, 56.2, 40.9, 32.9, 27.1, 24.2, 20.4; **HR-ESI-MS**: m/z calcd for $C_{12}H_{13}O_3^+$ $[M+H-H_2O]^+$: 205.0859, found: 205.0856; **IR** (thin film): 3282, 2281, 1617, 1182 cm^{-1}.

Part IV. Chemical oxidation reactions of substrate 16

Supplementary Table S1. Chemical oxidation reactions of substrate **16**.

Reaction[4-9]	Result
CitB	benzylic alcohol
MnO_2	starting material
DDQ	quinone
$K_2S_2O_8$	decomposition
CAN, AcOH	decomposition
AIBN, NBS	aromatic bromination
Ag_2O, MeOH	starting material

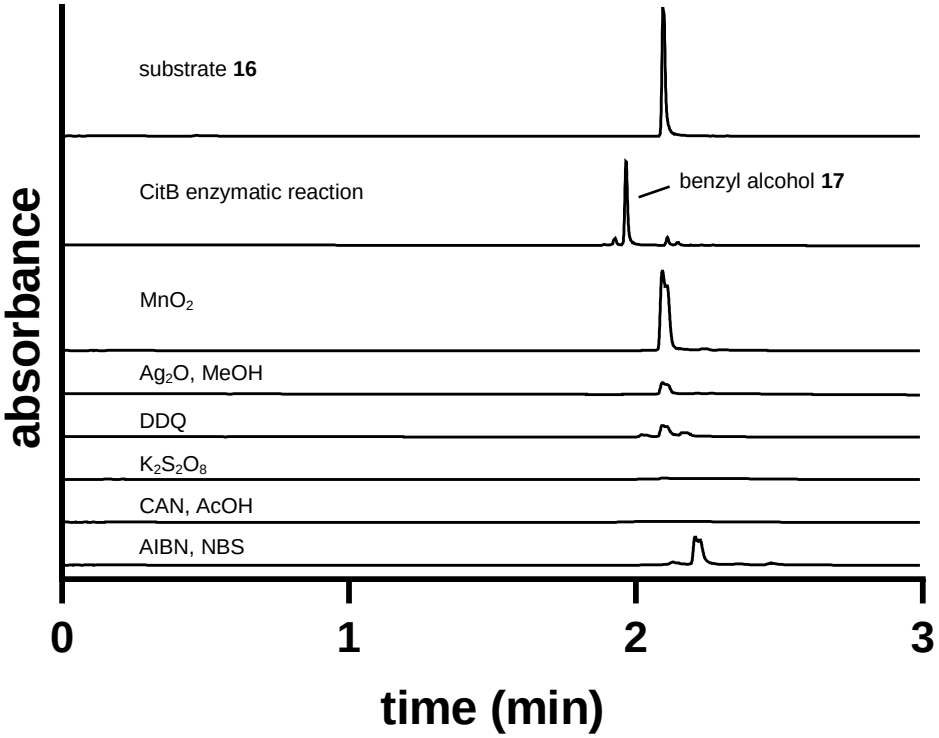

Supplementary Figure S6. Chemical oxidation reactions of substrate **16**.

Each chemical oxidation reaction was performed according to the general procedure in the given references.[4-9]

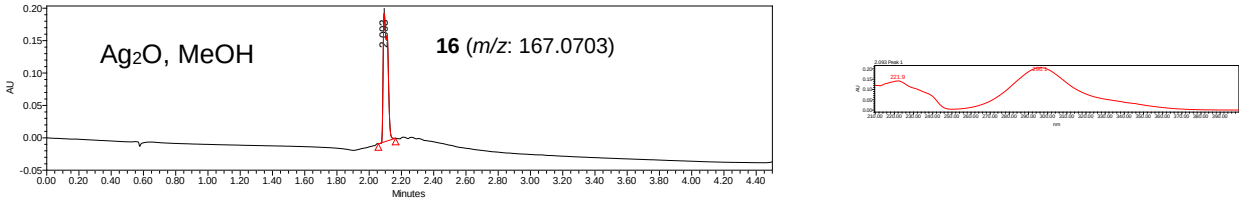

Supplementary Figure S7. Ag_2O oxidation reaction of substrate **16**.[4] PDA trace of reaction analyzed at 300 nm.

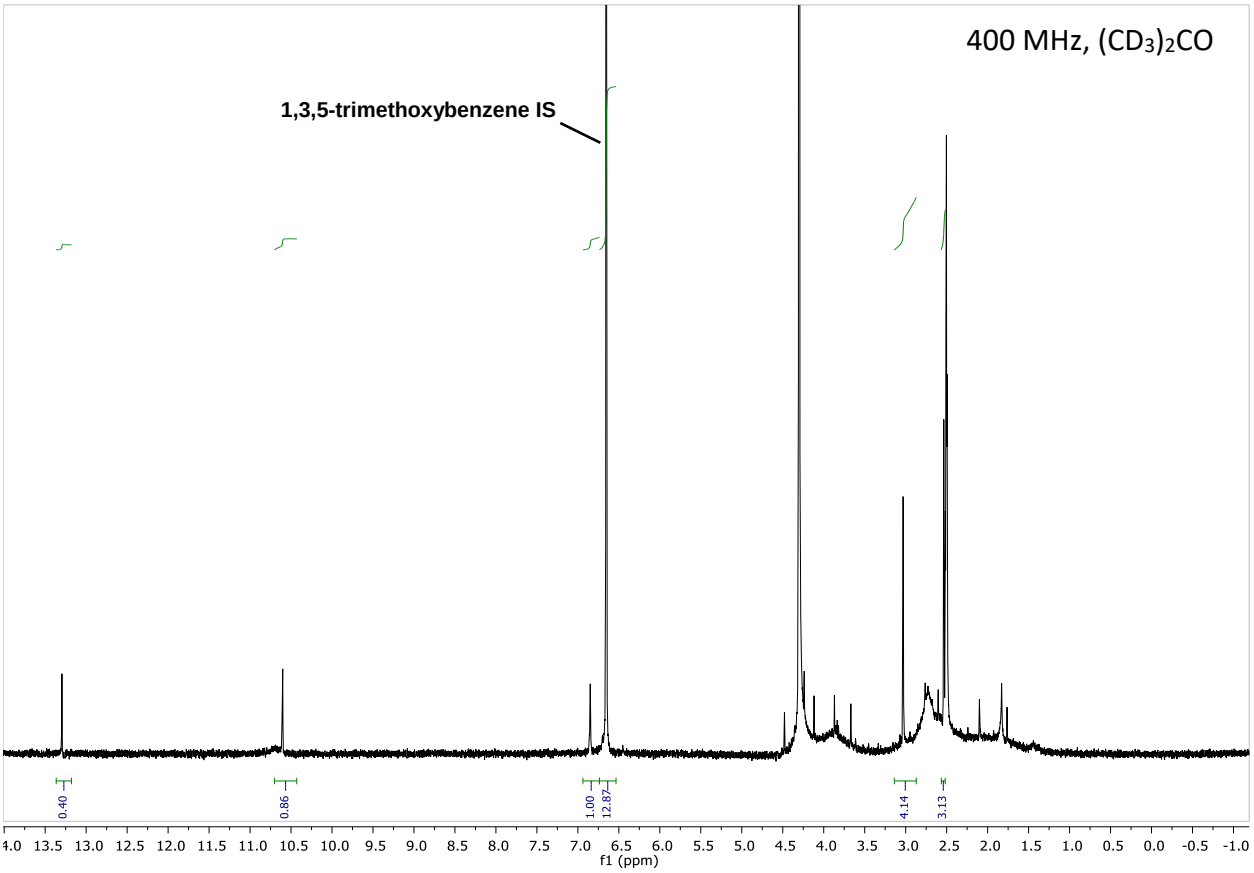

Supplementary Figure S8. Crude NMR of Ag_2O oxidation reaction of substrate **16**. Spectrum recorded on 400 MHz NMR in DMSO with 50 mM 1,3,5-trimethoxybenzene as internal standard.

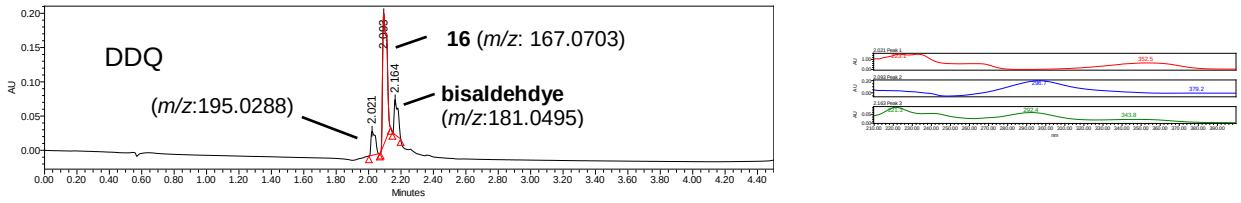

Supplementary Figure S9. DDQ oxidation reaction of substrate **16**.[5] PDA trace of reaction analyzed at 300 nm.

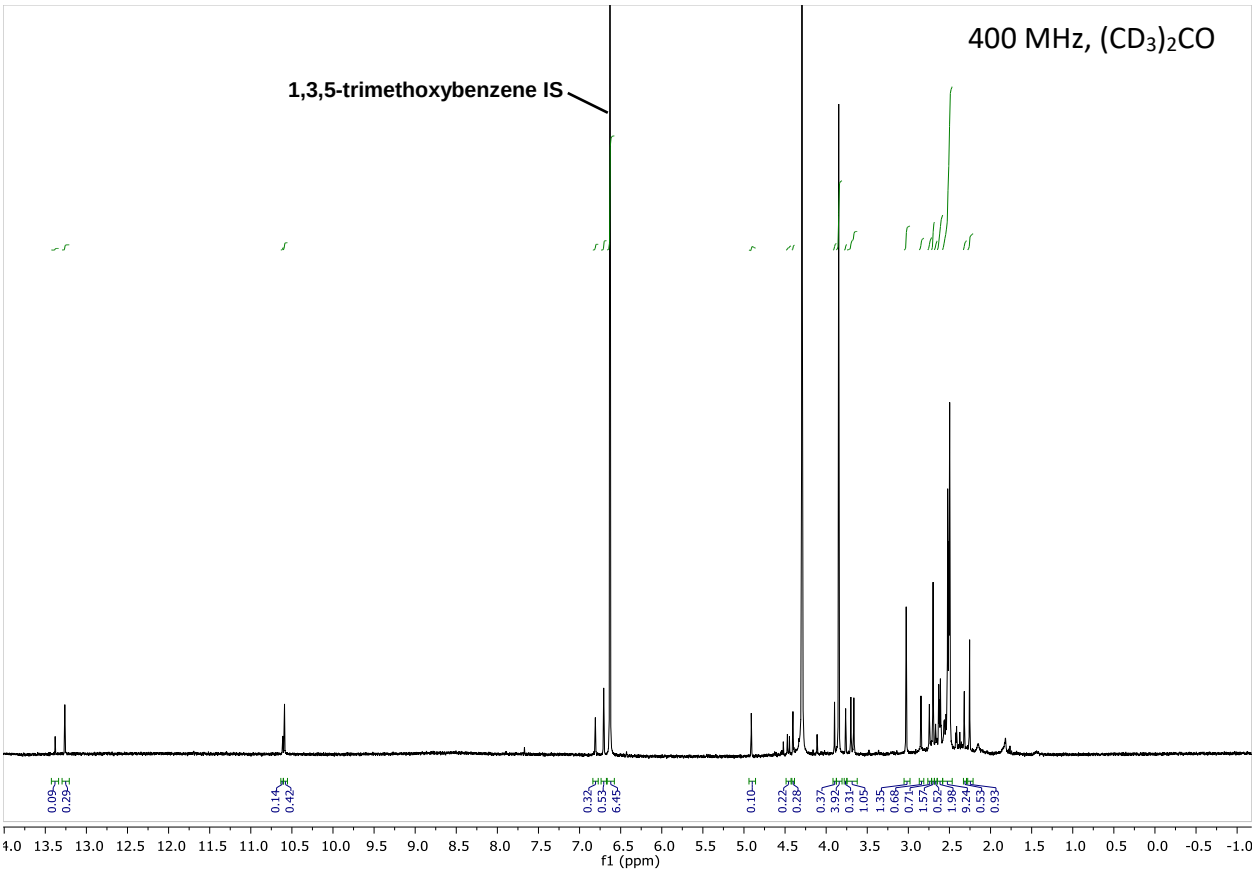

Supplementary Figure S10. Crude NMR of DDQ oxidation reaction of substrate **16**. Spectrum recorded on 400 MHz NMR in DMSO with 50 mM 1,3,5-trimethoxybenzene as internal standard.

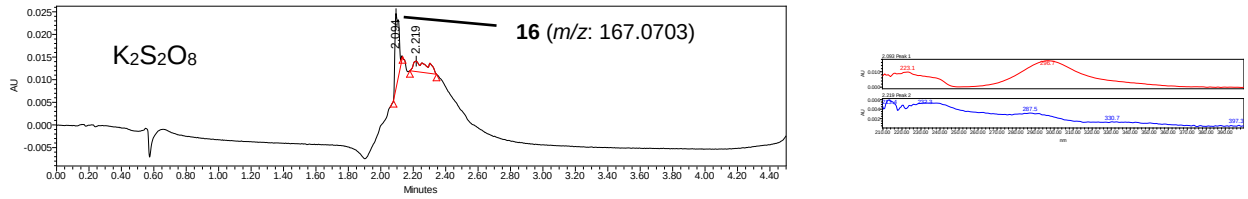

Supplementary Figure S11. $K_2S_2O_8$ oxidation reaction of substrate **16**.[6] PDA trace of reaction analyzed at 300 nm.

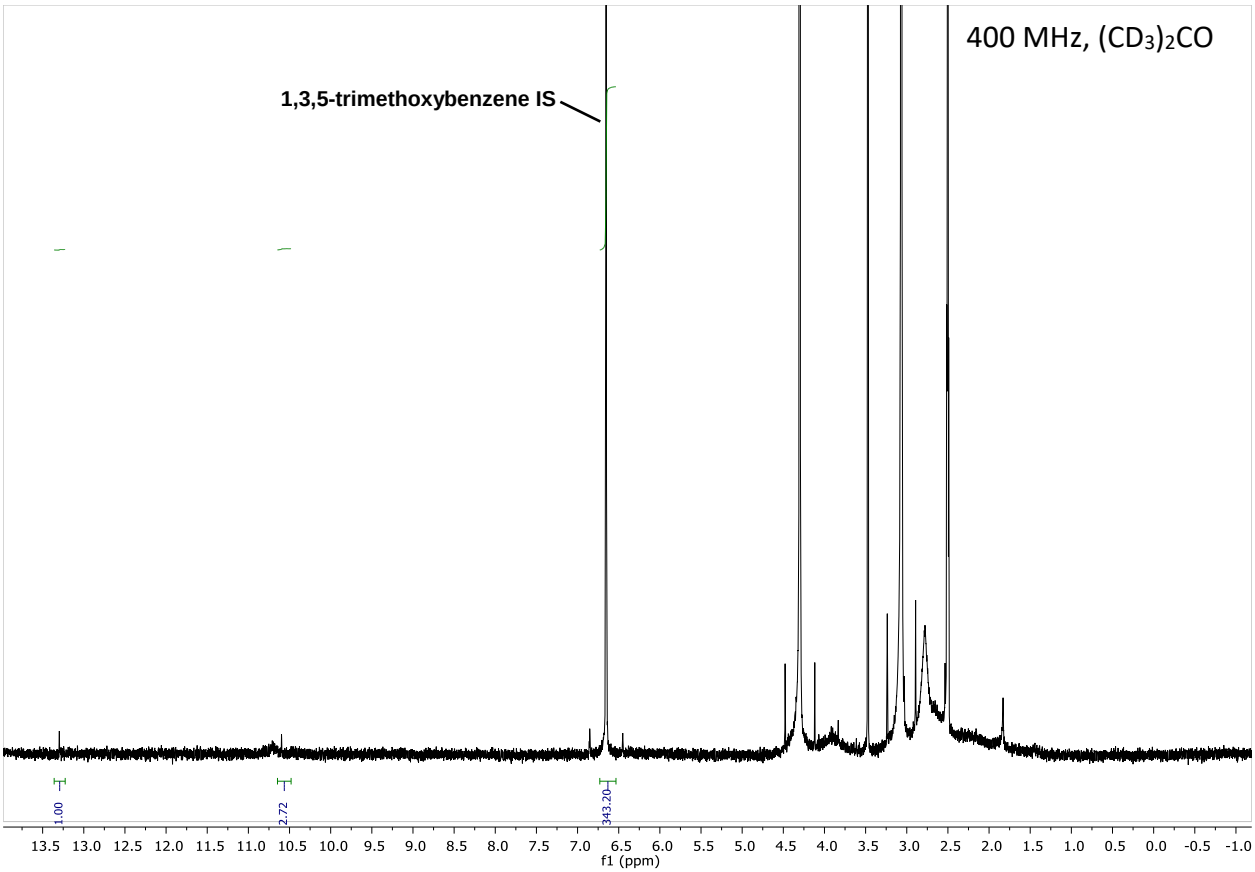

Supplementary Figure S12. Crude NMR of $K_2S_2O_8$ oxidation reaction of substrate **16**. Spectrum recorded on 400 MHz NMR in DMSO with 50 mM 1,3,5-trimethoxybenzene as internal standard.

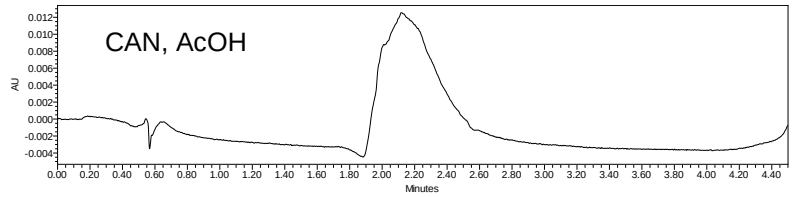

Supplementary Figure S13. Ceric ammonium nitrate (CAN) oxidation reaction of substrate **16**.[7] PDA trace of reaction analyzed at 300 nm.

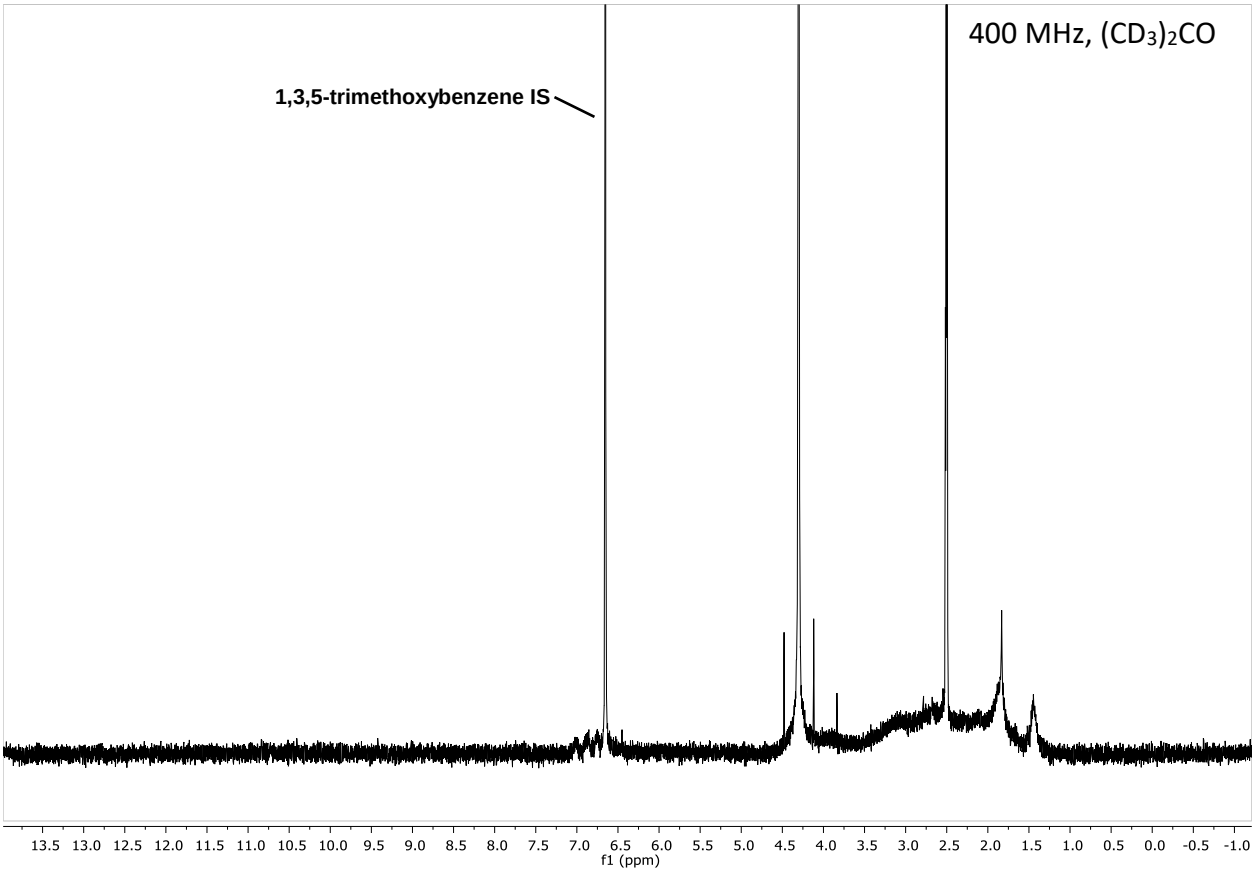

Supplementary Figure S14. Crude NMR of CAN oxidation reaction of substrate **16**. Spectrum recorded on 400 MHz NMR in DMSO with 50 mM 1,3,5-trimethoxybenzene as internal standard.

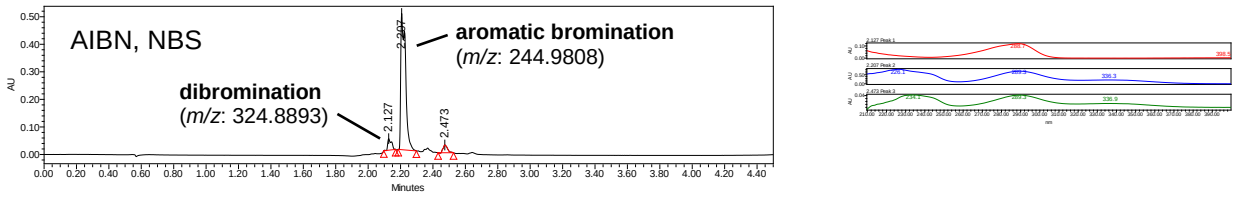

Supplementary Figure S15. AIBN, NBS oxidation reaction of substrate **16**.[8] PDA trace of reaction analyzed at 300 nm.

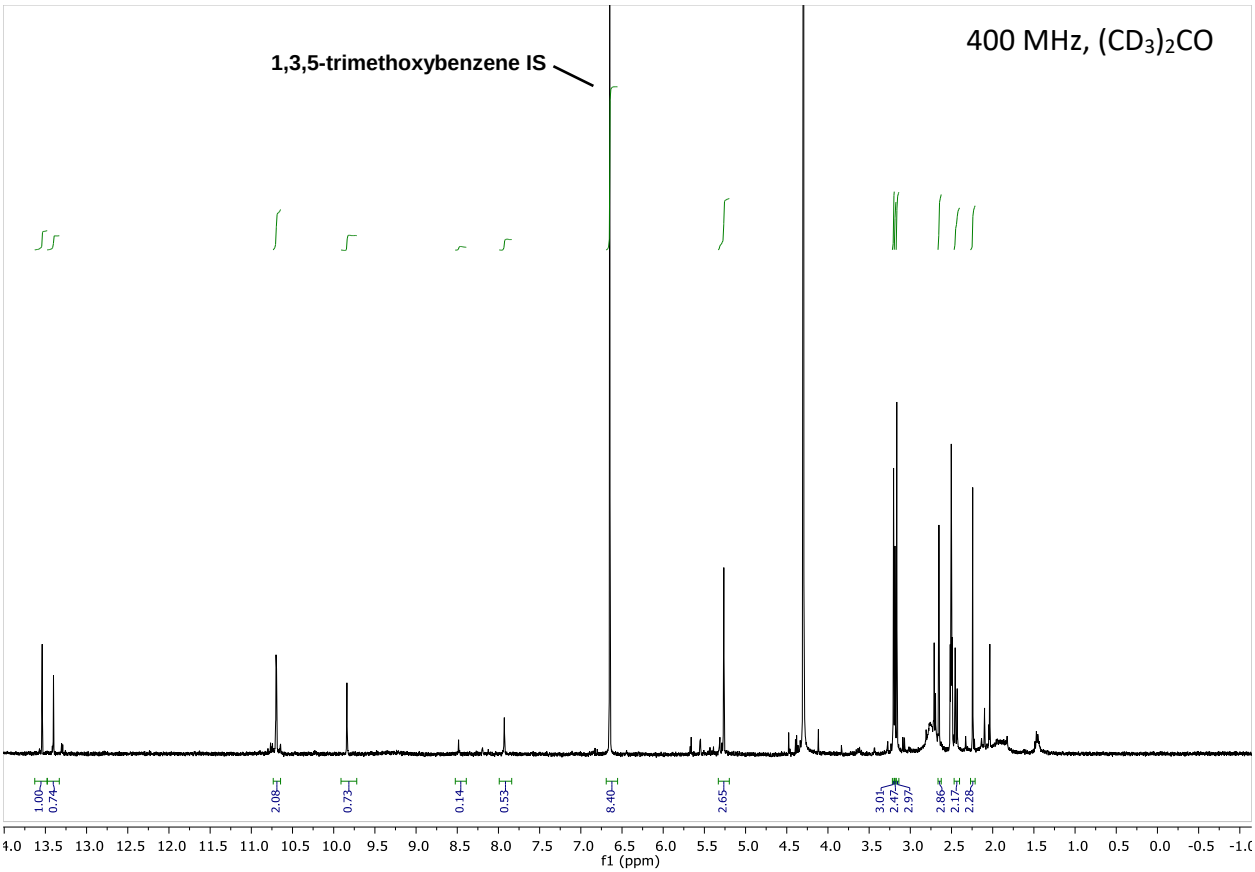

Supplementary Figure S16. Crude NMR of AIBN, NBS oxidation reaction of substrate **16**. Spectrum recorded on 400 MHz NMR in DMSO with 50 mM 1,3,5-trimethoxybenzene as internal standard.

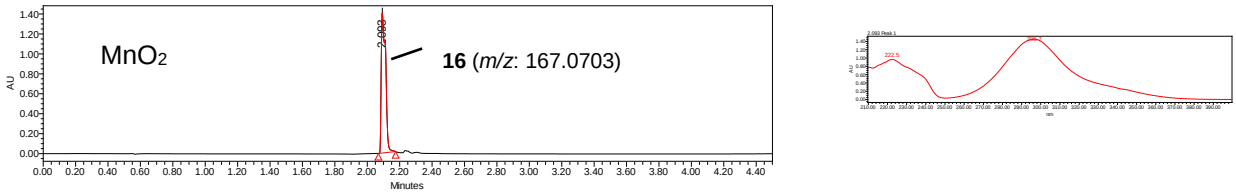

Supplementary Figure S17. MnO_2 oxidation reaction of substrate **16**.[9] PDA trace of reaction analyzed at 300 nm.

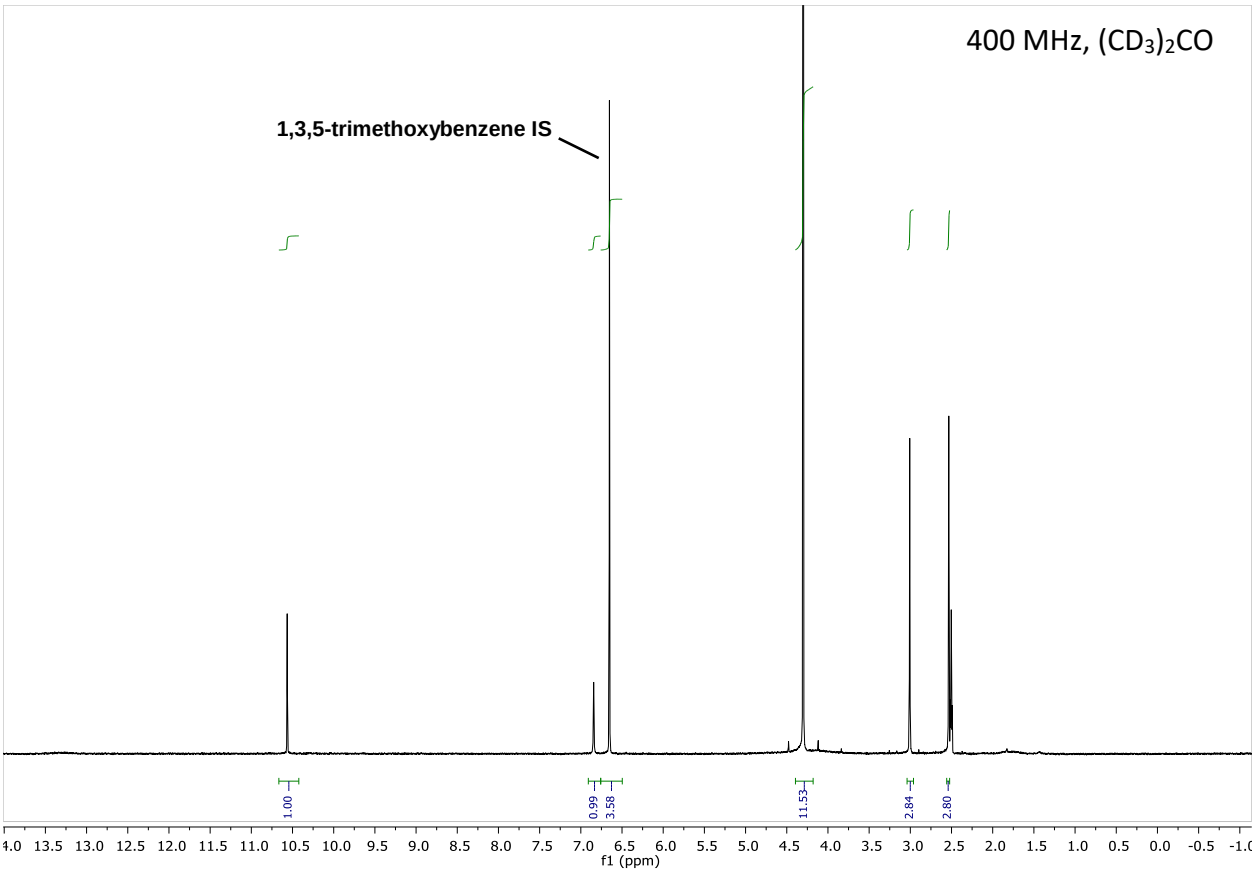

Supplementary Figure S18. Crude NMR of MnO_2 oxidation reaction of substrate **16**. Spectrum recorded on 400 MHz NMR in DMSO with 50 mM 1,3,5-trimethoxybenzene as internal standard.

Part V. Benzylic functionalization of NHI enzyme-generated benzylic alcohols

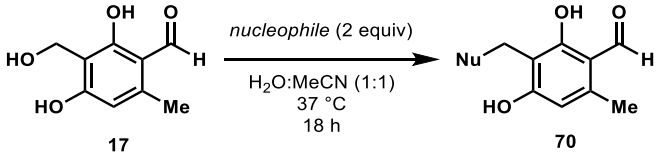

Supplementary Figure S19. Benzylic functionalization of benzylic alcohol **17** with nucleophiles.

General procedure for *ortho*-quinone methide conjugate addition reactions: Benzylic alcohol **17** (20 mg, 0.11 mmol, 1.0 equiv) was added to an oven-dried 1 dram vial equipped with a stir bar and dissolved in 1 mL of 1:1 H_2O:MeCN. Nucleophile (2.0 equiv) was then added to the vial and the reaction heated at 37 °C for 18 h. The solvent and excess nucleophile were removed under reduced pressure. Purification on silica gel afforded the desired 1,4-addition product.

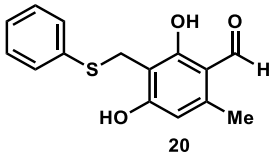

2,4-dihydroxy-6-methyl-3-((phenylthio)methyl)benzaldehyde (20)
The title compound was synthesized according to the general procedure for *ortho*-quinone methide conjugate addition reactions using thiophenol (22 µL, 0.22 mmol) as the nucleophile. Purification on silica gel (gradient elution 1% to 75% EtOAc in hexanes) afforded 30 mg (98% yield) of **20** as an off-white solid. **^{1}H NMR** (400 MHz, CD_3OD) δ 10.02 (s,1H), 7.39 (d, *J* = 7.3 Hz, 2H), 7.23 (t, *J* = 7.6 Hz, 2H), 7.15 (t, *J* = 7.3 Hz, 1H), 6.23 (s,1H), 4.13 (s, 2H), 2.47 (s, 3H); **^{13}C NMR** (101 MHz, CD_3OD) δ 194.5, 165.1, 164.9, 144.9, 138.9, 131.2, 129.6, 127.0, 113.7, 110.9, 110.5, 27.2, 18.2; **HRMS (ESI)** *m/z*: $[M+H]^+$ calculated for $C_{15}H_{13}O_3S^+$ 275.0736, found 275.0737; **IR** (thin film): 3076, 2242, 1584, 1480, 1430, 1330, 1256, 1025, 988, 844, 736, 687, 634, 560, 504 cm^{-1}.

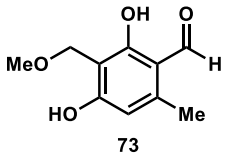

2,4-dihydroxy-3-(methoxymethyl)-6-methylbenzaldehyde (73)
The title compound was synthesized according to the general procedure for *ortho*-quinone methide conjugate addition reactions using methanol (1 mL) as both the solvent and nucleophile. Purification on silica gel (gradient elution 1% to 75% EtOAc in hexanes) afforded 16 mg (73% yield) of **73** as a colorless oil. **^{1}H NMR** (400 MHz, CD_3OD) δ 10.07 (s, 1H), 6.27 (s, 1H), 4.53 (s, 2H), 3.35 (s, 3H), 2.51 (s, 3H); **^{13}C NMR** (151 MHz, CD_3OD) δ 194.6, 166.2, 166.1, 146.3, 113.7, 111.2, 110.1, 63.1, 58.1, 18.3; **HRMS (ESI)** *m/z*: $[M+H]^+$ calculated for $C_{10}H_{11}O_4^+$ 197.0808, found 197.0802; **IR** (thin film): 2924, 1622, 1428, 1245, 1123 cm^{-1}.

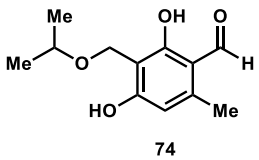

2,4-dihydroxy-3-(isopropoxymethyl)-6-methylbenzaldehyde (74)
The title compound was synthesized according to the general procedure for *ortho*-quinone methide conjugate addition reactions using isopropanol (1 mL) as both the solvent and nucleophile. Purification on silica gel (gradient elution 1% to 75% EtOAc in hexanes) afforded 15 mg (61% yield) of **74** as a colorless oil. **^{1}H NMR** (599 MHz, CD_3OD) δ 10.05 (s, 1H), 6.25 (s, 1H), 4.58 (s, 2H), 3.74 (hept, *J* = 6.1 Hz, 1H), 2.49 (s, 3H), 1.18 (d, *J* = 6.1 Hz, 6H); **^{13}C NMR** (151 MHz, CD_3OD) δ 194.6, 166.1, 166.0, 146.0, 113.7, 111.3, 110.6, 72.6, 59.4, 22.4, 18.3; **HRMS (ESI)** *m/z*: $[M+H]^+$ calculated for $C_{12}H_{15}O_4^+$ 225.1121, found 225.1106; **IR** (thin film): 3219, 2925, 1621, 1489, 1229, 1119 cm^{-1}.

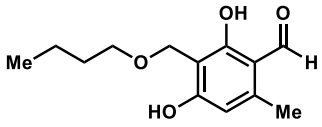

75

2,4-dihydroxy-3-(*n*-butoxymethyl)-6-methylbenzaldehyde (75)
The title compound was synthesized according to the general procedure for *ortho*-quinone methide conjugate addition reactions using isopropanol (1 mL) as both the solvent and nucleophile. Purification on silica gel (gradient elution 1% to 75% EtOAc in hexanes) afforded 12 mg (47% yield) of **75** as a colorless solid. **^{1}H NMR** (599 MHz, CD_3OD) δ 10.06 (s, 1H), 6.26 (s, 1H), 4.56 (s, 2H), 3.50 (t, *J* = 6.6 Hz, 2H), 2.49 (s, 3H), 1.55 (dt, *J* = 14.5, 6.7 Hz, 2H), 1.36 (h, *J* = 7.4 Hz, 2H), 0.90 (t, *J* = 7.4 Hz, 3H); **^{13}C NMR** (151 MHz, CD_3OD) δ 194.7, 166.1, 166.0, 146.1, 113.7, 111.2, 110.4, 71.1, 61.5, 32.7, 20.3, 18.3, 14.2; **HRMS (ESI)** *m/z*: $[M+H]^+$ calculated for $C_{13}H_{17}O_4^+$ 239.1278, found 239.1222; **IR** (thin film): 2913, 1618, 1435, 1302, 1016, 951, 697 cm^{-1}.

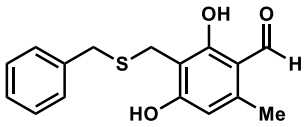

76

3-((benzylthio)methyl)-2,4-dihydroxy-6-methylbenzaldehyde (76)
The title compound was synthesized according to the general procedure for *ortho*-quinone methide conjugate addition reactions using benzylmercaptan (26 µL, 0.22 mmol) as the nucleophile. Purification on silica gel (gradient elution 1% to 75% EtOAc in hexanes) afforded 31 mg (97% yield) of **76** as an off-white solid. **^{1}H NMR** (599 MHz, CD_3OD) δ 10.03 (s, 1H), 7.32 (d, *J* = 7.1 Hz, 2H), 7.24 (t, *J* = 7.6 Hz, 2H), 7.17 (t, *J* = 7.3 Hz, 1H), 6.24 (s, 1H), 3.78 (s, 2H), 3.69 (s, 2H), 2.48 (s, 3H); **^{13}C NMR** (151 MHz, CD_3OD) δ 194.5, 165.0, 165.0, 144.5, 140.5, 129.9, 129.2, 127.6, 113.7, 112.3, 111.2, 37.7, 24.0, 18.1; **HRMS (ESI)** *m/z*: $[M+H]^+$ calculated for $C_{16}H_{15}O_3S^+$ 289.0893, found 289.0887; **IR** (thin film): 3083, 1606, 1429, 1288, 1255, 1102, 699 cm^{-1}.

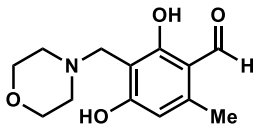

77

2,4-dihydroxy-6-methyl-3-(morpholinomethyl)benzaldehyde (77)
The title compound was synthesized according to the general procedure for *ortho*-quinone methide conjugate addition reactions using morpholine (19 µL, 0.22 mmol) as the nucleophile. Purification on silica

gel (gradient elution 1% to 75% EtOAc in hexanes) afforded 18 mg (65% yield) of **77** as a white solid. **^{1}H NMR** (599 MHz, CD_3OD) δ 10.00 (s, 1H), 6.18 (s, 1H), 3.84 (s, 2H), 3.75 (m, 4H), 2.70 (m, 4H), 2.47 (s, 3H); ^{13}C NMR (151 MHz, CD_3OD) δ 193.9, 169.4, 165.5, 145.5, 113.0, 112.8, 105.8, 67.3, 53.8, 53.2, 18.3; **HRMS (ESI)** *m/z*: $[M+H]^+$ calculated for $C_{13}H_{16}NO_4^+$ 252.1230, found 252.1279; **IR** (thin film): 2850, 1620, 1483, 1363, 1293, 1269, 1243, 1114, 997, 861, 626 cm^{-1}.

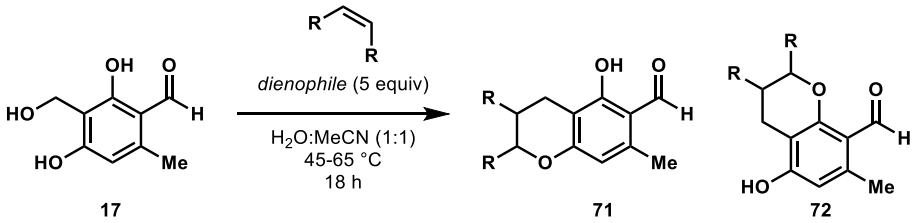

17 71 72

Supplementary Figure S20. Inverse electron-demand Diels-Alder reactions with benzylic alcohol, **17**.

General procedure for Diels-Alder reactions: Benzylic alcohol **17** (20 mg, 0.110 mmol, 1.0 equiv) was added to an oven-dried 1 dram vial equipped with a stir bar and dissolved in 1 mL of 1:1 H_2O:MeCN. Dienophile (5 equiv) was then added to the vial and the reaction heated at 45-65 °C for 18 h. The solvent and excess dienophile were removed under reduced pressure. Purification on silica gel afforded the cycloadduct products.

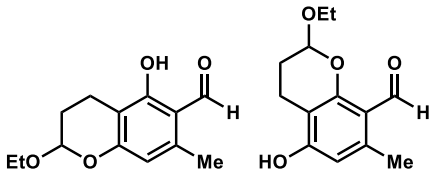

78 79

2-ethoxy-5-hydroxy-7-methylchromane-6-carbaldehyde (78) and 2-ethoxy-5-hydroxy-7-methylchromane-8-carbaldehyde (79)

The title compounds were synthesized according to the general procedure for *ortho*-quinone methide Diels-Alder reactions using ethyl vinyl ether (53 µL, 0.549 mmol) as the dienophile and heating at 45 °C. The reaction gave a 2:1 ratio of **78** and **79**, respectively (as judged by the ^{1}H NMR spectrum of the unpurified reaction mixture). Purification on silica gel (gradient elution 1% to 75% EtOAc in hexanes) afforded 16 mg (61% yield) of **78** and 8 mg (30% yield) of **79** as colorless oils.

Data for **78**: **^{1}H NMR** (599 MHz, $CDCl_3$) δ 12.68 (s, 1H), 10.07 (s, 1H), 6.21 (s, 1H), 5.26 (s, 1H), 3.87 (dq, *J* = 14.3, 7.1 Hz, 1H), 3.65 (dq, *J* = 14.3, 7.1 Hz, 1H), 2.73 – 2.62 (m, 2H), 2.49 (s, 3H), 2.06 (dq, *J* = 13.3, 4.7 Hz, 1H), 1.94 – 1.84 (m, 1H), 1.20 (t, *J* = 7.1 Hz, 3H); **^{13}C NMR** (151 MHz, $CDCl_3$) δ 193.1, 163.2, 159.5, 141.0, 112.9, 111.4, 108.5, 97.8, 64.2, 25.7, 18.0, 15.1, 13.9; **HRMS (ESI)** *m/z*: $[M+H]^+$ calculated for $C_{13}H_{15}O_4^+$ 237.1121, found 237.1084; **IR** (thin film): 2928, 1622, 1579, 1483, 1325, 1281, 1242, 1217, 1132, 1099, 1046, 967, 934, 850 cm^{-1}.

Data for **79**: **^{1}H NMR** (599 MHz, CD_3OD) δ 10.38 (s, 1H), 6.27 (s, 1H), 5.38 (s, 1H), 3.88 (dt, *J* = 14.3, 7.2 Hz, 1H), 3.76 – 3.64 (m, 1H), 2.65 (dd, *J* = 10.1, 6.0 Hz, 2H), 2.47 (s, 3H), 2.08 – 2.02 (m, 1H), 1.99 – 1.93 (m, 1H), 1.21 (t, *J* = 7.1 Hz, 3H); **^{13}C NMR** (151 MHz, CD_3OD) δ 191.9, 162.2, 159.6, 142.7, 116.9, 111.7, 109.0, 98.8, 65.3, 26.6, 22.2, 15.6, 15.5; **HRMS (ESI)** *m/z*: $[M+H]^+$ calculated for $C_{13}H_{15}O_4^+$ 237.1121, found 237.1073; **IR** (thin film): 2924, 1626, 1493, 1327, 1282, 1243, 1100, 1049, 935, 851 cm^{-1}.

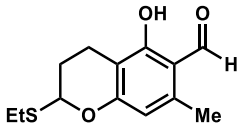

80

2-(ethylthio)-5-hydroxy-7-meth-ylchromane-8-carbaldehyde (80)

The title compounds were synthesized according to the general procedure for *ortho*-quinone methide Diels-Alder reactions using ethyl vinyl sulfide (56 µL, 0.549 mmol) as the dienophile and heating at 45 °C. The reaction gave a 4:1 ratio of **80** and **81**, respectively (as judged by the ^{1}H NMR spectrum of the unpurified reaction mixture). Purification on silica gel (gradient elution 1% to 75% EtOAc in hexanes) afforded 19 mg (70% yield) of **80**. **^{1}H NMR** (599 MHz, CD_3OD) δ 10.10 (s, 1H), 6.23 (s, 1H), 5.64 (t, *J* = 4.0 Hz, 1H), 2.80 (dq, *J* = 13.0, 7.4 Hz, 1H), 2.75 – 2.66 (m, 2H), 2.63 (ddd, *J* = 16.8, 10.2, 6.2 Hz, 1H), 2.21 (dddd, *J* = 14.0, 10.2, 6.3, 3.8 Hz, 1H), 2.11 (ddt, *J* = 14.3, 6.2, 4.4 Hz, 1H); **^{13}C NMR** (151 MHz, CD_3OD) δ 195.1, 164.3, 161.1, 142.8, 114.2, 112.8, 109.1, 82.5, 27.4, 25.7, 18.0, 16.8, 15.6; **HRMS (ESI)** *m/z*: $[M+H]^+$ calculated for $C_{13}H_{15}O_3S^+$ 253.0893, found 253.0844; **IR** (thin film): 2926, 1624, 1578, 1481, 1419, 1372, 1321, 1279, 1239, 1116, 853 cm^{-1}.

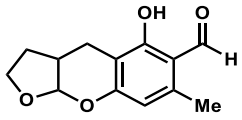

82

5-hydroxy-7-methyl-2,3,3a,9a-tetrahydro-4H-furo[2,3-b]chromene-6-carbaldehyde (82) and 5-hydroxy-7-methyl-2,3,3a,9a-tetrahydro-4H-furo[2,3-b]chromene-8-carbaldehyde (83)

The title compounds were synthesized according to the general procedure for *ortho*-quinone methide Diels-Alder reactions using 2,3-dihydrofuran (42 µL, 0.549 mmol) as the dienophile and heating at 45 °C. The reaction gave a 4:1 ratio of **82** and **83**, respectively (as judged by the ^{1}H NMR spectrum of the unpurified reaction mixture). Purification on silica gel (gradient elution 1% to 75% EtOAc in hexanes) afforded 18 mg (70% yield) of **82** as a white solid. **^{1}H NMR** (599 MHz, $CDCl_3$) δ 12.73 (s, 1H), 10.06 (s, 1H), 6.23 (s, 1H), 5.59 (d, *J* = 3.9 Hz, 1H), 4.18 – 4.11 (m, 1H), 4.02 (q, *J* = 8.4 Hz, 1H), 2.94 (d, *J* = 17.3 Hz, 1H), 2.79 (dd, *J* = 17.3, 6.3 Hz, 1H), 2.75 – 2.65 (m, 1H), 2.49 (s, 3H), 2.08 (td, *J* = 11.6, 10.5, 5.4 Hz, 1H), 1.69 (p, *J* = 9.7 Hz, 1H); **^{13}C NMR** (151 MHz, $CDCl_3$) δ 193.0, 163.8, 160.1, 141.6, 113.0, 111.2, 104.6, 101.0, 68.5, 36.3, 27.5, 18.4, 18.0; **HRMS (ESI)** *m/z*: $[M+H]^+$ calculated for $C_{13}H_{13}O_4^+$ 235.0965, found 235.0976; **IR** (thin film): 2897, 1620, 1483, 1423, 1374, 1319, 1280, 1240, 1140, 1106, 1051, 931, 833, 547 cm^{-1}.

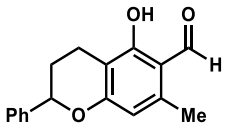

84

5-hydroxy-7-methyl-2-phenylchromane-6-carbaldehyde (84)

The title compound was synthesized according to the general procedure for *ortho*-quinone methide Diels-Alder reactions using styrene (63 µL, 0.549 mmol) as the dienophile and heating at 65 °C. The reaction gave a 1:3 ratio of **84** and **85**, respectively (as judged by the ^{1}H NMR spectrum of the unpurified reaction mixture). Purification on silica gel (gradient elution 1% to 75% EtOAc in hexanes) afforded 6 mg (33% yield) of **84** as a colorless oil. **^{1}H NMR** (599 MHz, $CDCl_3$) δ 12.78 (s, 1H), 10.08 (s, 1H), 7.45 – 7.29 (m, 5H), 6.30 (s, 1H), 5.09 (dd, *J* = 10.2, 2.1 Hz, 1H), 2.82 (dt, *J* = 16.8, 4.3 Hz, 1H), 2.69 (ddd, *J* = 17.0, 11.0, 6.1 Hz, 1H), 2.51 (s, 3H), 2.27 (ddt, *J* = 13.4, 5.7, 2.8 Hz, 1H), 2.03 (ddt, *J* = 21.0, 10.7, 5.5 Hz, 1H); **^{13}C NMR** (151

MHz, $CDCl_3$) δ 193.0, 163.7, 162.3, 141.1, 140.6, 128.6, 128.1, 125.9, 112.7, 111.4, 107.9, 78.5, 28.8, 18.2, 18.0. **HRMS (ESI)** *m/z*: $[M+H]^+$ calculated for $C_{17}H_{15}O_3^+$ 269.1172, found 269.1186; **IR** (thin film): 3433, 2923, 1624, 1514, 1373, 1280, 1238, 1132, 1025, 819 cm^{-1}.

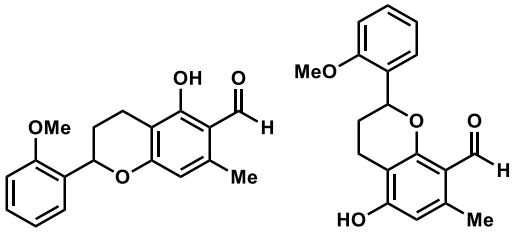

86 87

5-hydroxy-2-(2-methoxyphenyl)-7-methylchromane-6-carbaldehyde (86) and 5-hydroxy-2-(2-methoxyphenyl)-7-methylchromane-8-carbaldehyde (87)

The title compounds were synthesized according to the general procedure for *ortho*-quinone methide Diels-Alder reactions using 2-methoxystyrene (74 µL, 0.549 mmol) as the dienophile and heating at 65 °C. The reaction gave a 1:3 ratio of **86** and **87**, respectively (as judged by the ^{1}H NMR spectrum of the unpurified reaction mixture). Purification on silica gel (gradient elution 1% to 75% EtOAc in hexanes) afforded 16 mg (39% yield) of **86** and 6 mg (13% yield) of **87** as white solids.

Data for **86**: **^{1}H NMR** (599 MHz, $CDCl_3$) δ 12.78 (s, 1H), 10.08 (s, 1H), 7.40 (d, *J* = 7.4 Hz, 1H), 7.30 (t, *J* = 7.7 Hz, 1H), 7.00 (t, *J* = 7.4 Hz, 1H), 6.92 (d, *J* = 8.2 Hz, 1H), 6.30 (s, 1H), 5.47 (d, *J* = 9.5 Hz, 1H), 3.86 (s, 3H), 2.77 (d, *J* = 16.8 Hz, 1H), 2.70 (ddd, *J* = 16.8, 10.8, 6.0 Hz, 1H), 2.51 (s, 3H), 2.33 – 2.21 (m, 1H), 1.89 (dh, *J* = 15.5, 5.6 Hz, 1H); **^{13}C NMR** (151 MHz, $CDCl_3$) δ 192.9, 163.7, 162.8, 155.8, 140.9, 129.1, 128.8, 126.2, 120.7, 112.6, 111.4, 110.4, 108.2, 73.3, 55.4, 27.4, 18.3, 18.0; **HRMS (ESI)** *m/z*: $[M+H]^+$ calculated for $C_{18}H_{17}O_4^+$ 299.1278, found 299.1279; **IR** (thin film): 2923, 1642, 1576, 1492, 1436, 1340, 1303, 1240, 1016, 952, 824, 750 cm^{-1}.

Data for **87**: **^{1}H NMR** (599 MHz, CD_3OD) δ 10.37 (s, 1H), 7.42 (d, *J* = 7.5 Hz, 1H), 7.30 (t, *J* = 7.7 Hz, 1H), 7.02 (d, *J* = 8.2 Hz, 1H), 6.99 (t, *J* = 7.5 Hz, 1H), 6.25 (s, 1H), 5.41 (d, *J* = 9.8 Hz, 1H), 3.87 (s, 3H), 2.81 – 2.61 (m, 2H), 2.47 (s, 3H), 2.33 – 2.23 (m, 1H), 1.87 (dh, *J* = 16.5, 6.0 Hz, 1H); **^{13}C NMR** (151 MHz, CD_3OD) δ 192.0, 163.1, 162.9, 157.4, 142.8, 130.7, 129.9, 126.9, 121.7, 116.6, 111.6, 111.4, 108.7, 74.6, 55.9, 28.7, 22.3, 20.3; **HRMS (ESI)** *m/z*: $[M+H]^+$ calculated for $C_{18}H_{17}O_4^+$ 299.1278, found 299.1276; **IR** (thin film): 2927, 1625, 1494, 1373, 1281, 1238, 1136 cm^{-1}.

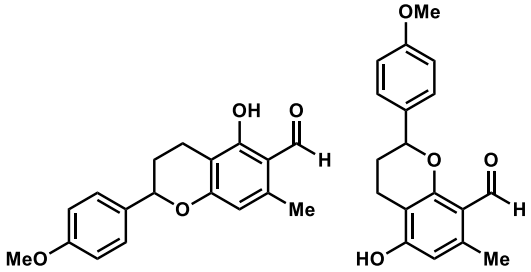

88 89

5-hydroxy-2-(4-methoxyphenyl)-7-methylchromane-6-carbaldehyde (88) and 5-hydroxy-2-(4-methoxyphenyl)-7-methylchromane-8-carbaldehyde (89)

The title compounds were synthesized according to the general procedure for *ortho*-quinone methide Diels-Alder reactions using 4-methoxystyrene (73 µL, 0.549 mmol) as the dienophile and heating at 65 °C. The reaction gave a 1:4 ratio of **88** and **89**, respectively (as judged by the ^{1}H NMR spectrum of the unpurified reaction mixture). Purification on silica gel (gradient elution 1% to 75% EtOAc in hexanes) afforded 18 mg (44% yield) of **88** and 5 mg (12% yield) of **89** as white solids.

Data for **88**: **^{1}H NMR** (599 MHz, $CDCl_3$) δ 12.77 (s, 1H), 10.07 (s, 1H), 7.32 (d, *J* = 8.5 Hz, 2H), 6.93 (d, *J* = 8.6 Hz, 2H), 6.27 (s, 1H), 5.03 (dd, *J* = 10.5, 2.4 Hz, 1H), 3.82 (s, 3H), 2.84 (ddd, *J* = 16.9, 5.6, 3.1 Hz, 1H), 2.67 (ddd, *J* = 17.1, 11.3, 6.1 Hz, 1H), 2.49 (s, 3H), 2.23 (ddd, *J* = 11.1, 5.9, 2.9 Hz, 1H), 2.09 – 1.94 (m, 1H); **^{13}C NMR** (151 MHz, $CDCl_3$) δ 192.9, 163.7, 162.4, 159.5, 141.0, 132.7, 127.4, 114.0, 112.7, 111.4, 107.9, 78.3, 55.3, 28.6, 18.4, 18.0; **HRMS (ESI)** *m/z*: $[M+H]^+$ calculated for $C_{18}H_{17}O_4^+$ 299.1278, found 299.1268; **IR** (thin film): 2924, 1578, 1496, 1422, 1291, 1239, 1086, 757, 695 cm^{-1}.

Data for **89**: **^{1}H NMR** (599 MHz, $((CD_3)_2SO)$ δ 10.46 (s, 1H), 10.30 (s, 1H), 7.36 (d, *J* = 8.4 Hz, 2H), 6.94 (d, *J* = 8.5 Hz, 2H), 6.26 (s, 1H), 5.09 (d, *J* = 10.0 Hz, 1H), 3.74 (s, 3H), 2.68 – 2.54 (m, 2H), 2.38 (s, 3H), 2.17 (d, *J* = 13.4 Hz, 1H), 1.98 – 1.86 (m, 1H); **^{13}C NMR** (151 MHz, $((CD_3)_2SO)$ δ 189.0, 160.6, 160.6, 158.9, 140.1, 133.0, 127.3, 114.9, 113.9, 110.2, 107.1, 76.9, 55.1, 27.8, 21.6, 18.9; **HRMS (ESI)** *m/z*: $[M+H]^+$ calculated for $C_{18}H_{17}O_4^+$ 299.1278, found 299.1268; **IR** (thin film): 2925, 1619, 1570, 1427, 1293, 1247, 1120, 729 cm^{-1}.

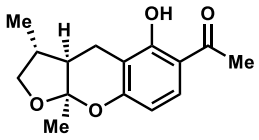

xx (-)-xyloketal D

(-)-xyloketal D (15)

Enantiomerically pure xyloketal D was prepared through the inverse electron-demand Diels-Alder reaction of enzymatically prepared benzylic alcohol **60** and dienophile **93**. Benzylic alcohol **60** (35 mg, 0.192 mmol, 1.0 equiv) was added to an oven-dried 1 dram vial equipped with a stir bar and dissolved in MeCN (2 mL). Dienophile **93** (49 µL, 0.384 mmol, 2.0 equiv) was then added to the vial and the reaction heated at 75 °C for 18 hours until starting material was completely consumed as determined by UPLC-DAD analysis. The reaction was concentrated to remove solvent and excess dienophile. The reaction gave a 2:1 mixture of diastereomers (as judged by ^{1}H NMR and UPLC-DAD analysis of the unpurified reaction). Purification on silica gel (gradient elution 1% to 5% EtOAc in hexanes) afforded 23 mg (46% yield) of (-)-xyloketal D. Reaction analysis by UPLC-DAD with product standard curve showed full conversion of starting material after 18 hours and 66% yield of (-)-xyloketal D when the reaction was performed in benzene and heated at 80 °C. All spectroscopic data for the compound matched previously reported literature values.

Data for **15**: **^{1}H NMR** (599 MHz, $CDCl_3$) δ13.11 (s, 1H), 7.52 (d, *J* = 8.9 Hz, 1H), 6.36 (d, *J* = 8.9 Hz, 1H), 4.20 (t, *J* = 8.4 Hz, 1H), 3.56 (t, *J* = 8.6 Hz, 1H), 2.96 (d, *J* = 17.8 Hz, 1H), 2.72 (dd, *J* = 17.9, 6.5 Hz, 1H), 2.54 (s, 3H), 2.14 – 2.03 (m, 1H), 1.98 (dd, *J* = 11.3, 6.5 Hz, 1H), 1.53 (s, 3H), 1.08 (d, *J* = 6.5 Hz, 3H); **^{13}C NMR** (151 MHz, $CDCl_3$) δ 202.7, 162.9, 159.5, 130.0, 113.1, 108.8, 108.3, 106.1, 77.2, 77.0, 76.8, 74.3, 46.9, 35.1, 26.1, 22.7, 18.0, 15.8; **HRMS (ESI)** *m/z*: $[M+H]^+$ calculated for $C_{18}H_{17}O_4^+$ 299.1278, found 299.1268; **$[\alpha]^{23}_D$** = -73.50° (c. 0.100, $CHCl_3$).

Part VI. Substrate and product calibration curves

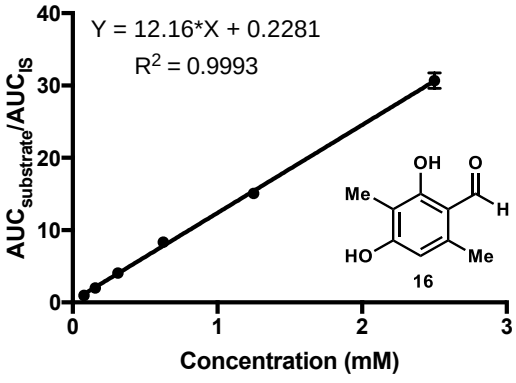

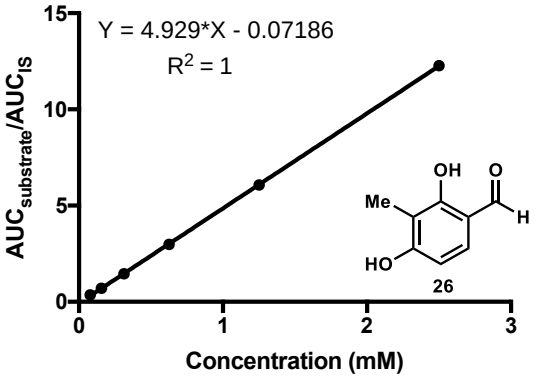

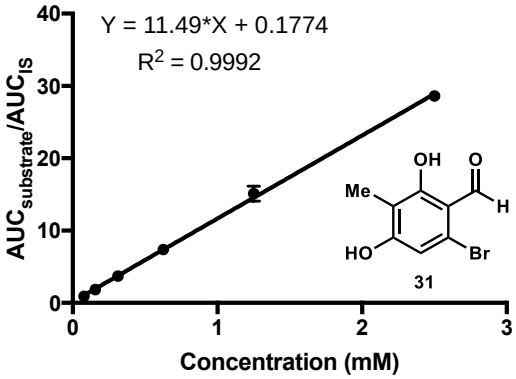
Y = 11.49*X + 0.1774
R2 = 0.9992
AUCsubstrate/AUCIS
Concentration (mM)
31

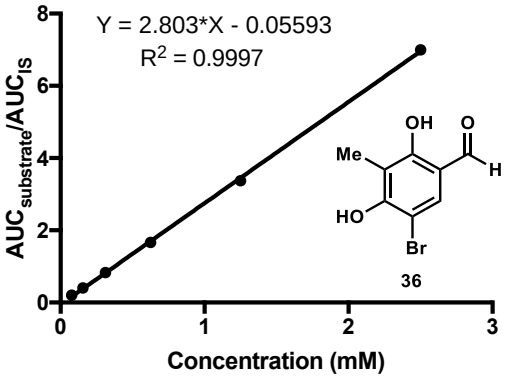
Y = 2.803*X - 0.05593
R2 = 0.9997
AUCsubstrate/AUCIS
Concentration (mM)
36

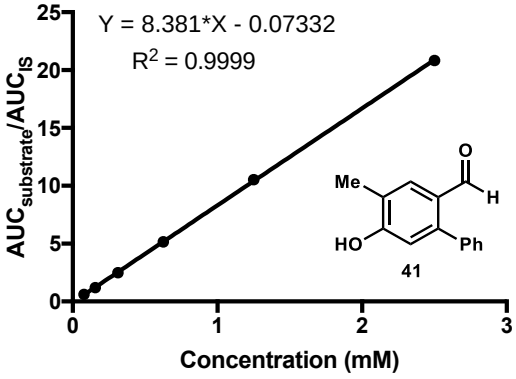
Y = 8.381*X - 0.07332
R2 = 0.9999
AUCsubstrate/AUCIS
Concentration (mM)
41

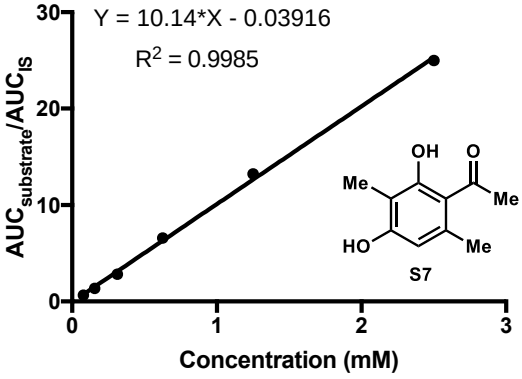
Y = 10.14*X - 0.03916
R2 = 0.9985
AUCsubstrate/AUCIS
Concentration (mM)
S7

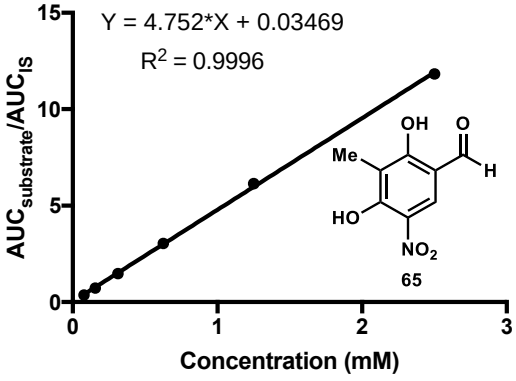
Y = 4.752*X + 0.03469
R2 = 0.9996
AUCsubstrate/AUCIS
Concentration (mM)
65

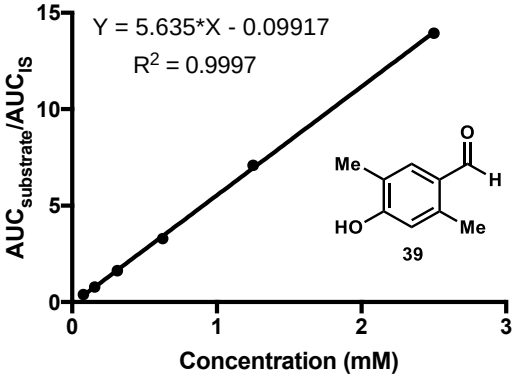
Y = 5.635*X - 0.09917
R2 = 0.9997
AUCsubstrate/AUCIS
Concentration (mM)
39

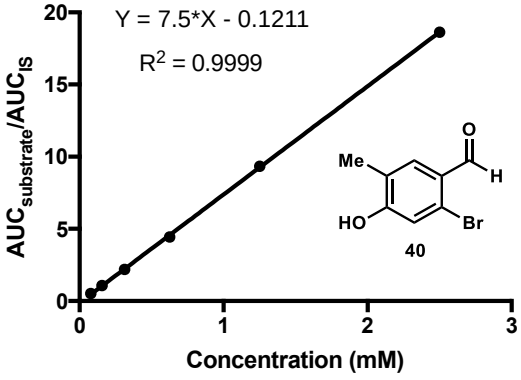
Y = 7.5*X - 0.1211
R2 = 0.9999
AUCsubstrate/AUCIS
Concentration (mM)
40

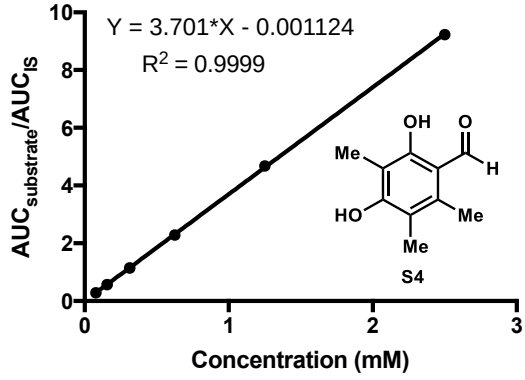
Y = 3.701*X - 0.001124
R2 = 0.9999
AUCsubstrate/AUCIS
Concentration (mM)
S4

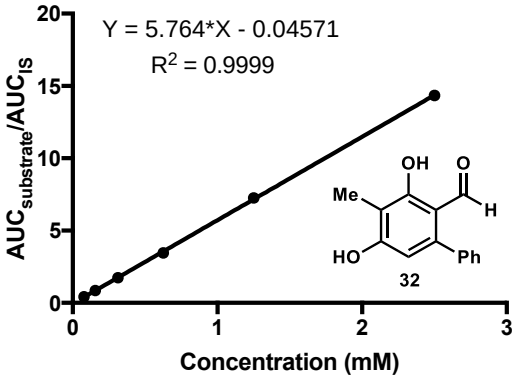
Y = 5.764*X - 0.04571
R2 = 0.9999
AUCsubstrate/AUCIS
Concentration (mM)
32

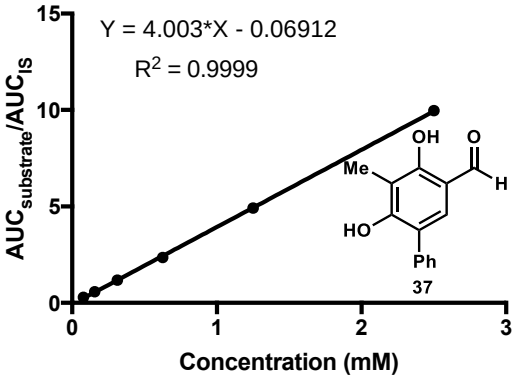
Y = 4.003*X - 0.06912
R2 = 0.9999
AUCsubstrate/AUCIS
Concentration (mM)
37

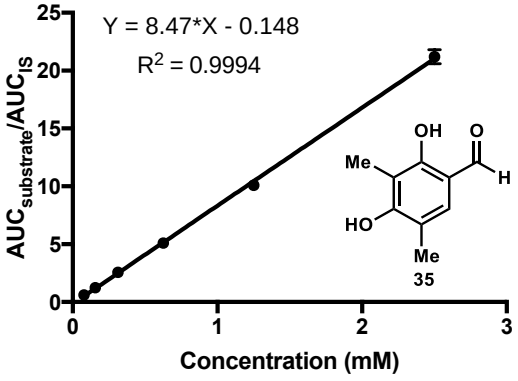
Y = 8.47*X - 0.148
R2 = 0.9994
AUCsubstrate/AUCIS
Concentration (mM)
35

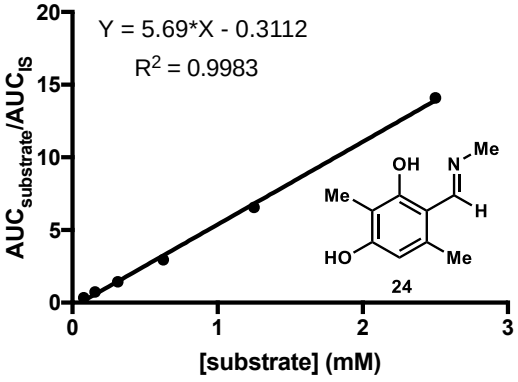
Y = 5.69*X - 0.3112
R2 = 0.9983
AUCsubstrate/AUCIS
[substrate] (mM)
24

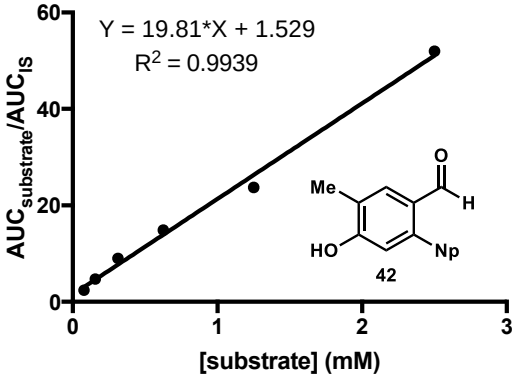
Y = 19.81*X + 1.529
R2 = 0.9939
AUCsubstrate/AUCIS
[substrate] (mM)
42

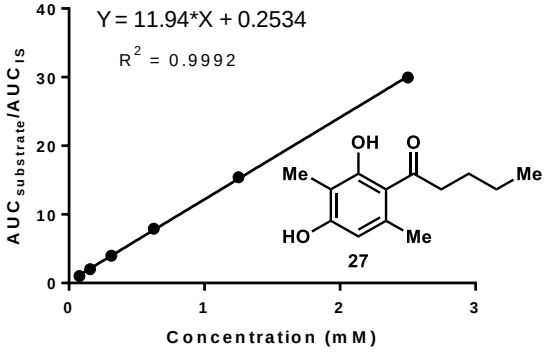
Y = 11.94*X + 0.2534
R2 = 0.9992
AUCsubstrate/AUCIS
Concentration (mM)
27

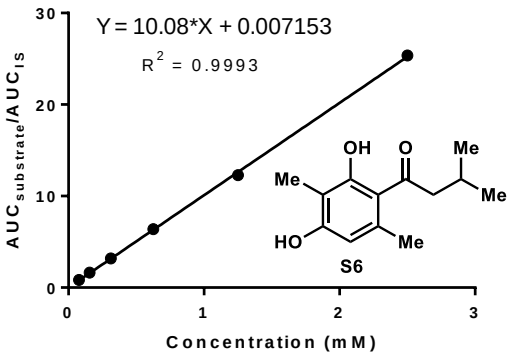
Y = 10.08*X + 0.007153
R2 = 0.9993
AUCsubstrate/AUCIS
Concentration (mM)
S6

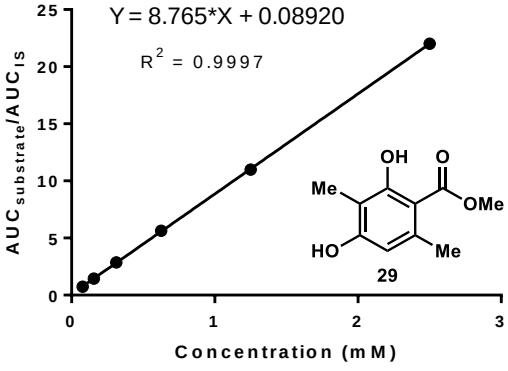
Y = 8.765*X + 0.08920
R2 = 0.9997
AUCsubstrate/AUCIS
Concentration (mM)
29

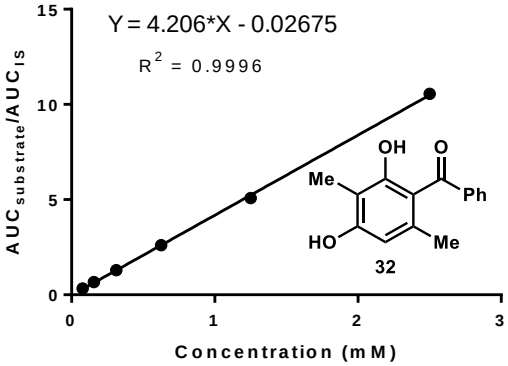
Y = 4.206*X - 0.02675
R2 = 0.9996
AUCsubstrate/AUCIS
Concentration (mM)
OH
O
Me
Ph
HO
Me
32

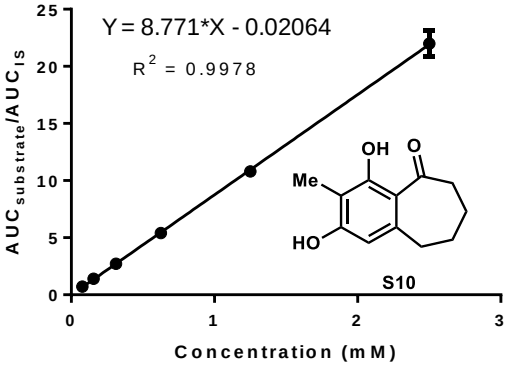
Y = 8.771*X - 0.02064
R2 = 0.9978
AUCsubstrate/AUCIS
Concentration (mM)
OH
O
Me
HO
S10

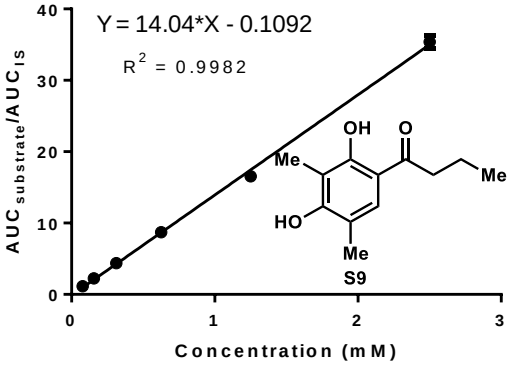
Y = 14.04*X - 0.1092
R2 = 0.9982
AUCsubstrate/AUCIS
Concentration (mM)
OH
O
Me
Me
HO
Me
S9

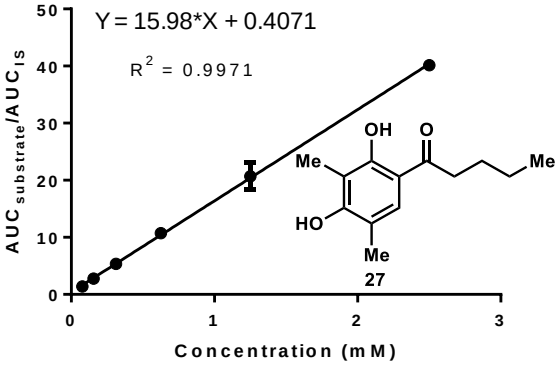
Y = 15.98*X + 0.4071
R2 = 0.9971
AUCsubstrate/AUCIS
Concentration (mM)
OH
O
Me
Me
HO
Me
27

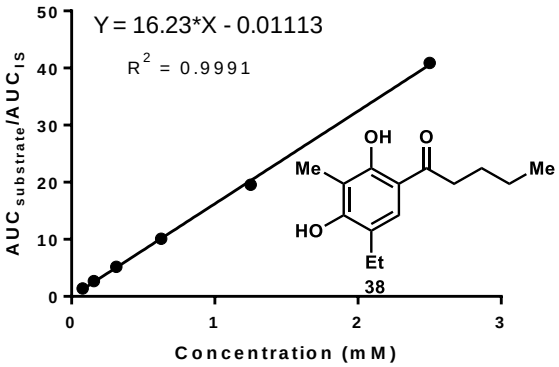
Y = 16.23*X - 0.01113
R2 = 0.9991
AUCsubstrate/AUCIS
Concentration (mM)
OH
O
Me
Me
HO
Et
38

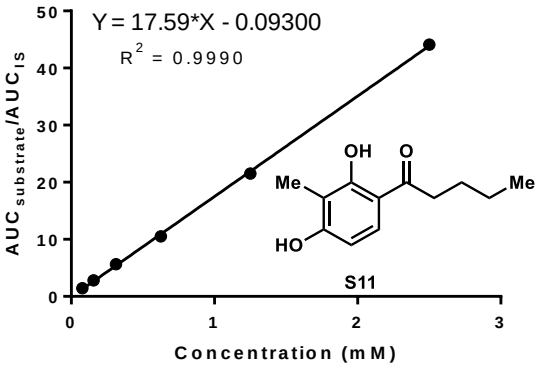
Y = 17.59*X - 0.09300
R2 = 0.9990
AUCsubstrate/AUCIS
Concentration (mM)
OH
O
Me
Me
HO
S11

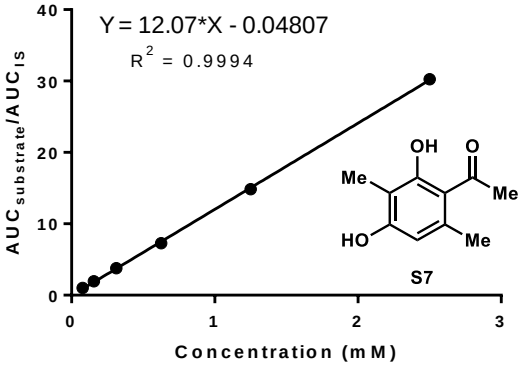
Y = 12.07*X - 0.04807
R2 = 0.9994
AUCsubstrate/AUCIS
Concentration (mM)
OH
O
Me
Me
HO
Me
S7

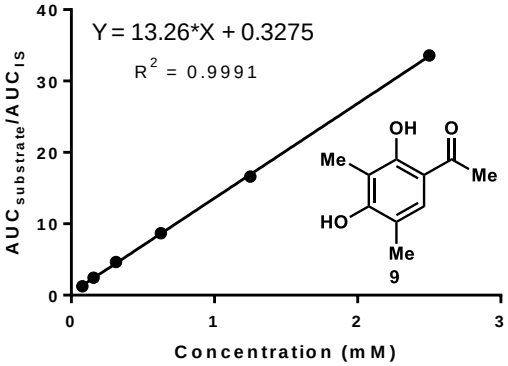
Y = 13.26*X + 0.3275
R2 = 0.9991
AUCsubstrate/AUCIS
Concentration (mM)
OH
O
Me
Me
HO
Me
9

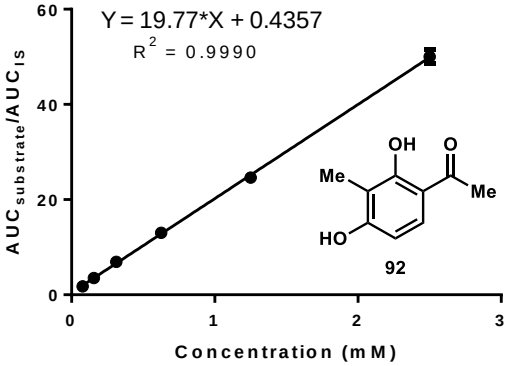
Y = 19.77*X + 0.4357
R2 = 0.9990
AUCsubstrate/AUCIS
Concentration (mM)
OH
O
Me
Me
HO
92

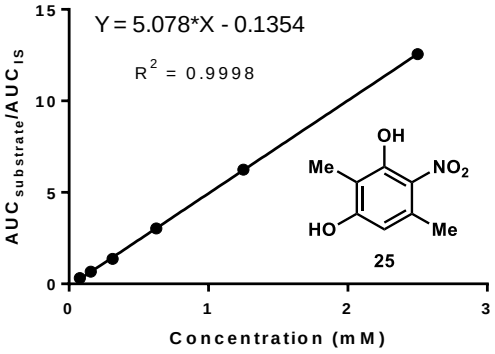
Y = 5.078*X - 0.1354
R2 = 0.9998
AUCsubstrate/AUCIS
Concentration (mM)
OH
Me
NO2
HO
Me
25

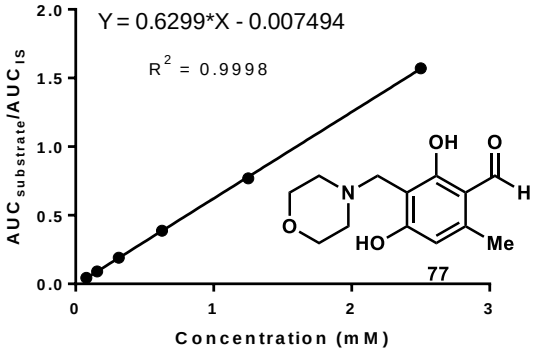
Y = 0.6299*X - 0.007494
R2 = 0.9998
AUCsubstrate/AUCIS
Concentration (mM)
OH
O
N
O
H
HO
Me
77

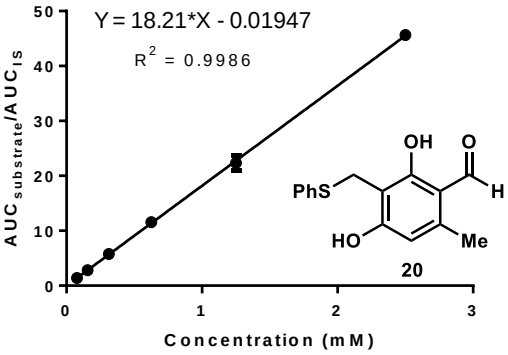
Y = 18.21*X - 0.01947
R2 = 0.9986
AUCsubstrate/AUCIS
Concentration (mM)
OH
O
PhS
H
HO
Me
20

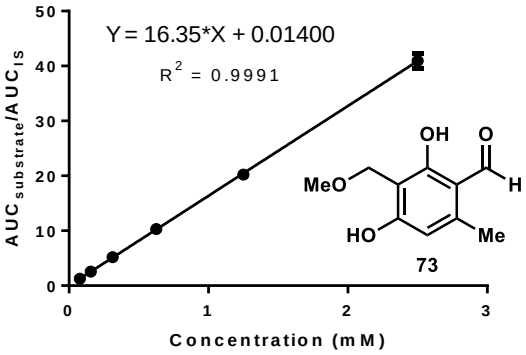
Y = 16.35*X + 0.01400
R2 = 0.9991
AUCsubstrate/AUCIS
Concentration (mM)
OH
O
MeO
H
HO
Me
73

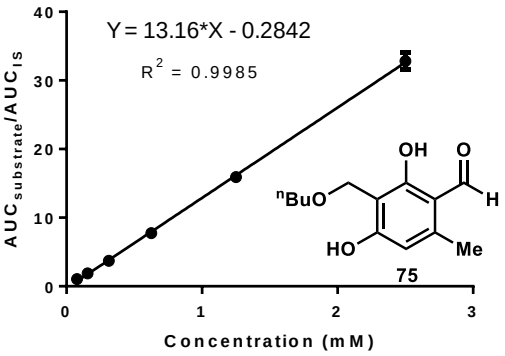
Y = 13.16*X - 0.2842
R2 = 0.9985
AUCsubstrate/AUCIS
Concentration (mM)
OH
O
nBuO
H
HO
Me
75

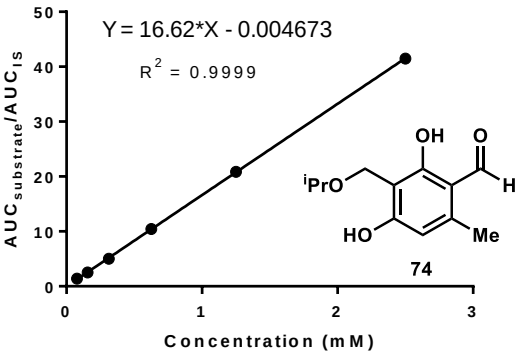
Y = 16.62*X - 0.004673
R2 = 0.9999
AUCsubstrate/AUCIS
Concentration (mM)
OH
O
iPrO
H
HO
Me
74

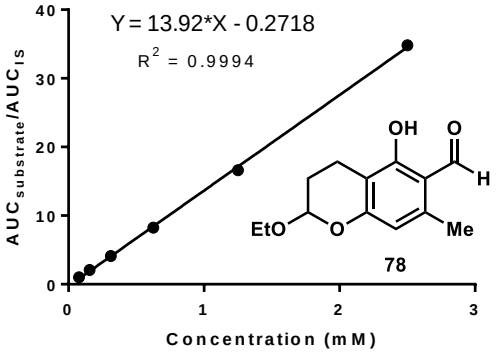
Y = 13.92*X - 0.2718
R2 = 0.9994
AUCsubstrate/AUCIS
Concentration (mM)
OH
O
H
EtO
O
Me
78

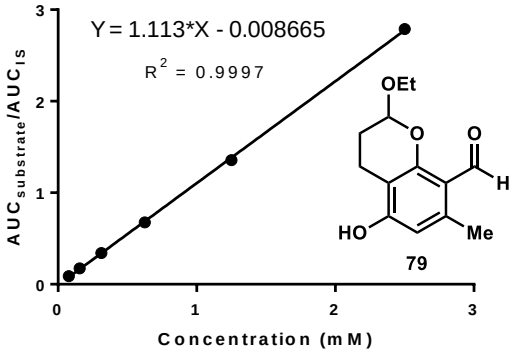
Y = 1.113*X - 0.008665
R2 = 0.9997
AUCsubstrate/AUCIS
Concentration (mM)
OEt
O
O
H
HO
Me
79

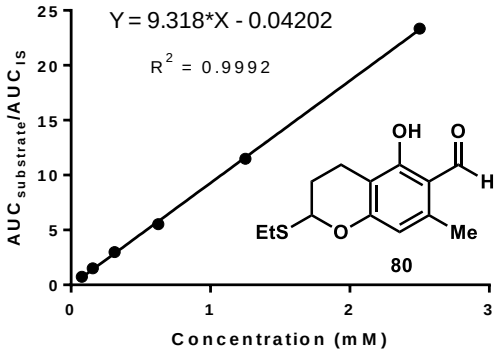
Y = 9.318*X - 0.04202
R2 = 0.9992
AUCsubstrate/AUCIS
Concentration (mM)
OH
O
H
EtS
O
Me
80

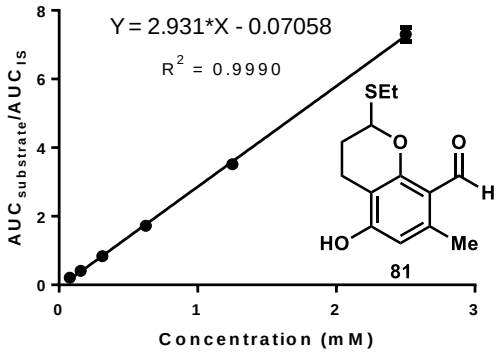
Y = 2.931*X - 0.07058
R2 = 0.9990
AUCsubstrate/AUCIS
Concentration (mM)
SEt
O
O
H
HO
Me
81

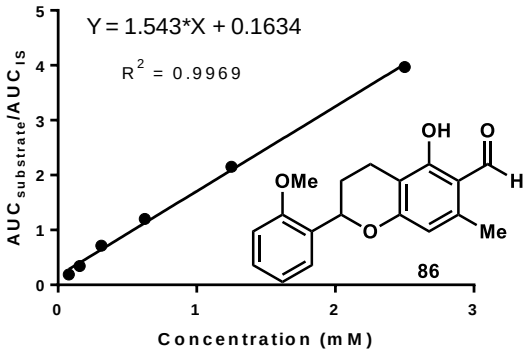
Y = 1.543*X + 0.1634
R2 = 0.9969
AUCsubstrate/AUCIS
Concentration (mM)
OH
O
H
OMe
O
Me
86

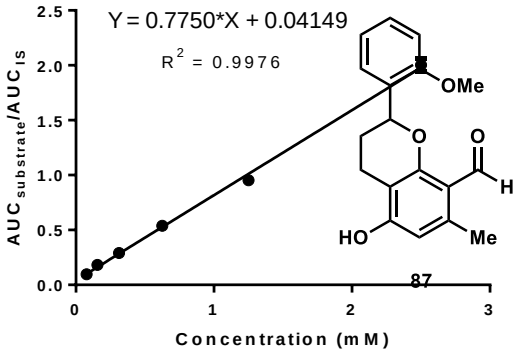
Y = 0.7750*X + 0.04149
R2 = 0.9976
AUCsubstrate/AUCIS
Concentration (mM)
OMe
O
O
H
HO
Me
87

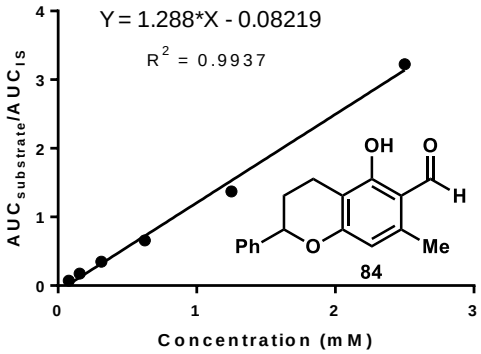
Y = 1.288*X - 0.08219
R2 = 0.9937
AUCsubstrate/AUCIS
Concentration (mM)
OH
O
H
Ph
O
Me
84

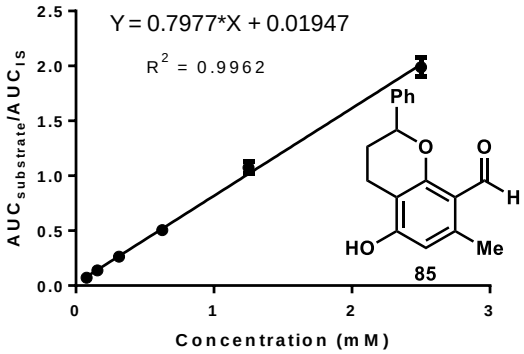
Y = 0.7977*X + 0.01947
R2 = 0.9962
AUCsubstrate/AUCIS
Concentration (mM)
Ph
O
O
H
HO
Me
85

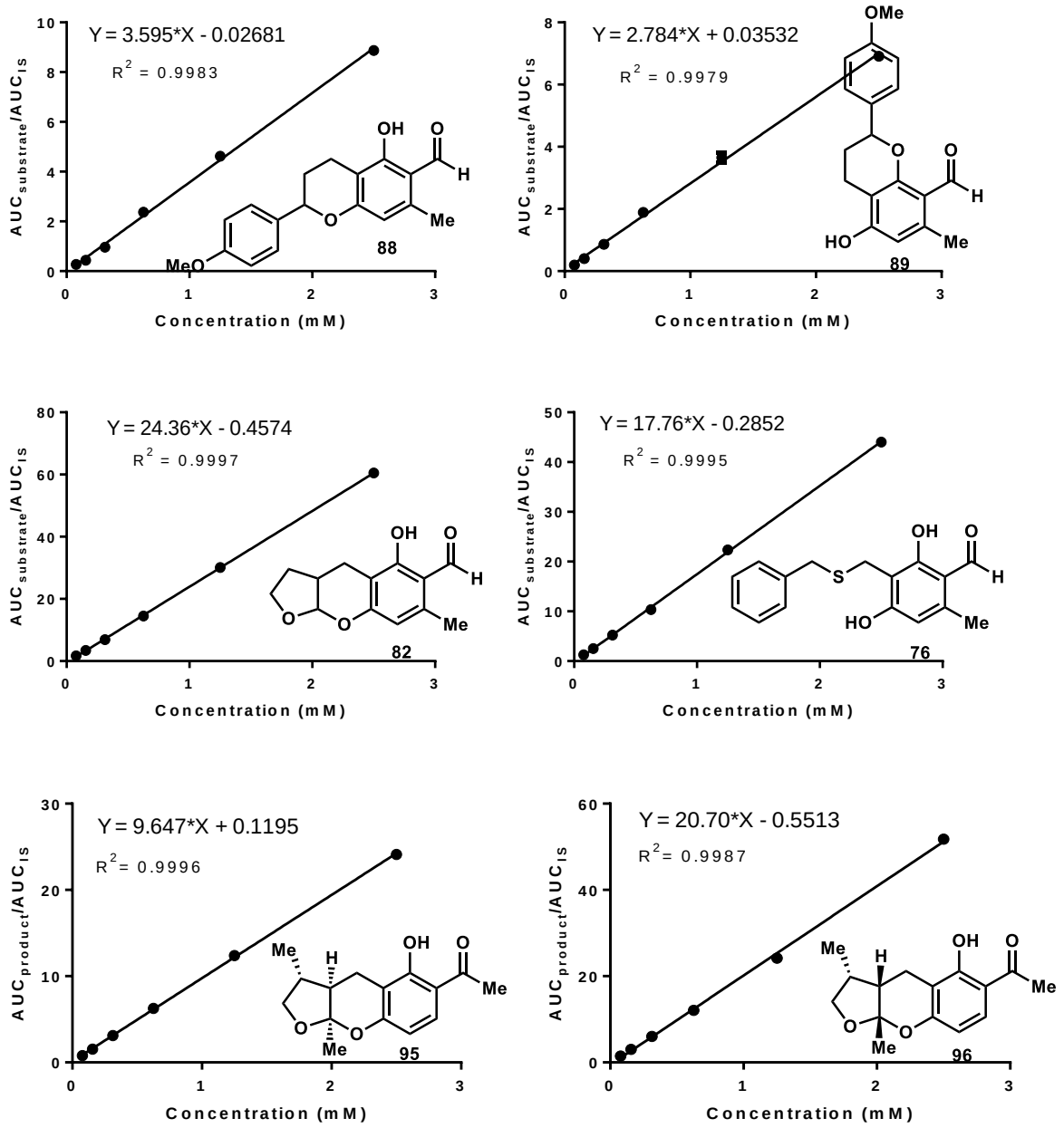

Part VII. UPLC traces of CitB-catalyzed biocatalytic reactions

Supplementary Figure S21. Benzylic hydroxylation of **16** by CitB. PDA traces of enzymatic reaction and control reaction.

With CitB

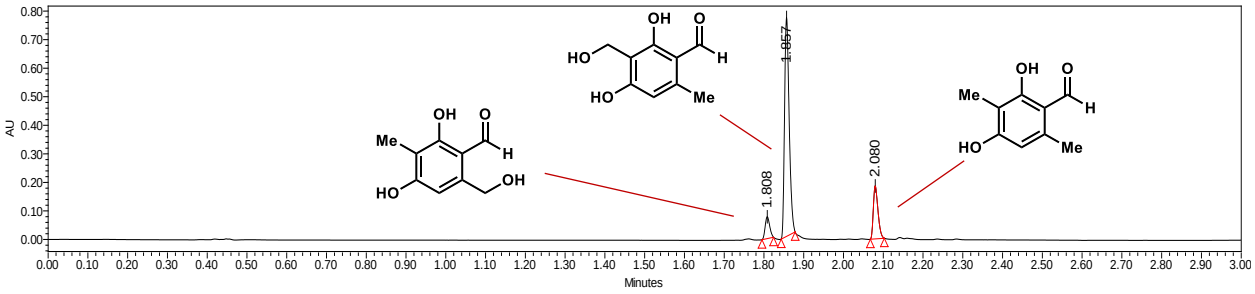

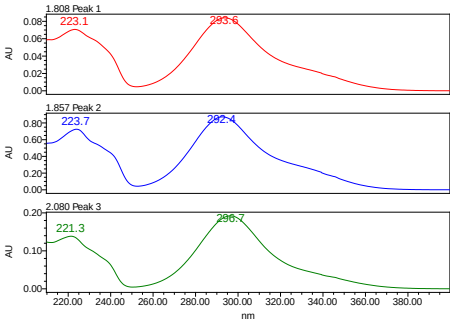

	Retention Time	Area	% Area	Height
1	1.808	60277	7.28	76765
2	1.857	617301	74.60	767275
3	2.080	149848	18.11	185817

No enzyme control

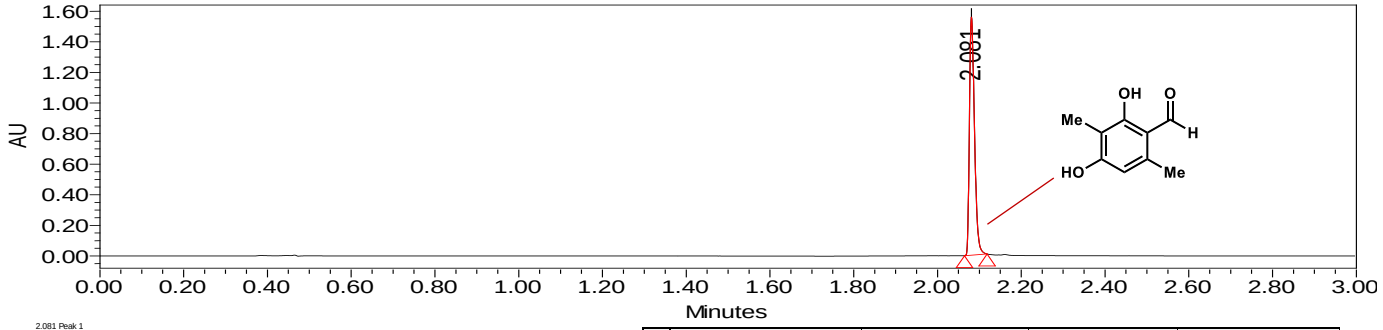

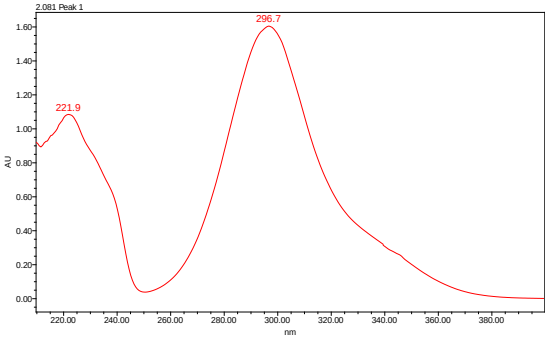

	Retention Time	Area	% Area	Height
1	2.081	1311812	100.00	1557555

Supplementary Figure S22. Benzylic hydroxylation of **26** by CitB. PDA traces of enzymatic reaction and control reaction.

With CitB

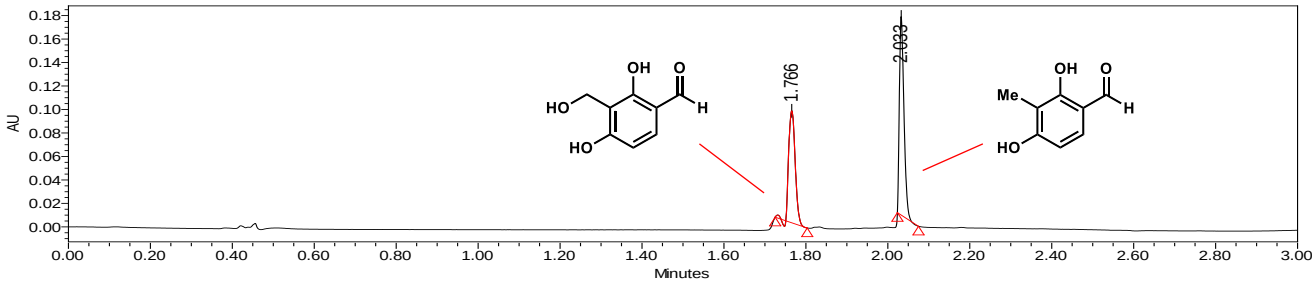

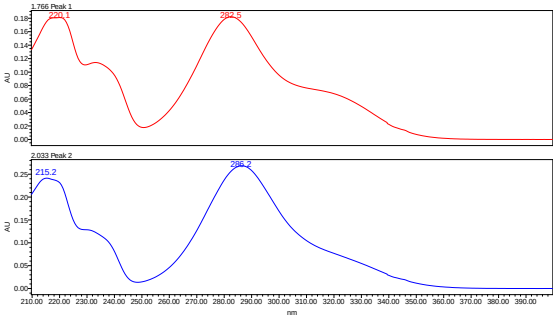

	Retention Time	Area	% Area	Height
1	1.766	106501	41.09	96087
2	2.033	152671	58.91	179576

No Enzyme Control

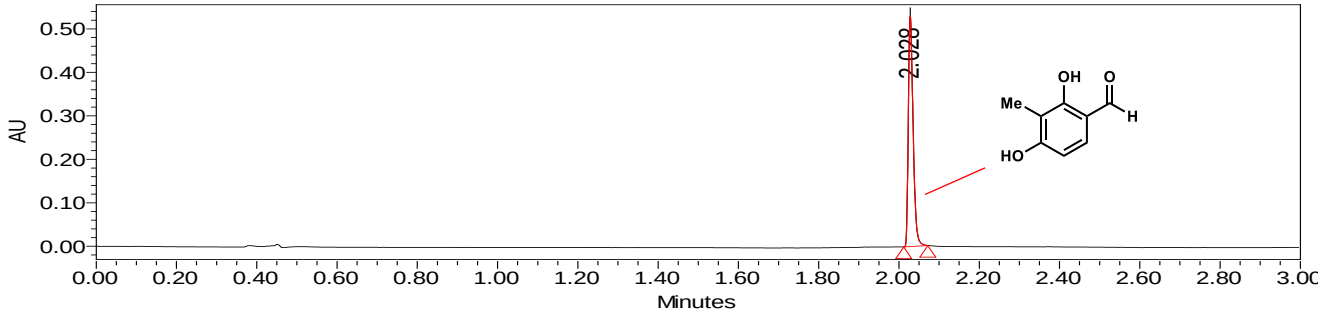

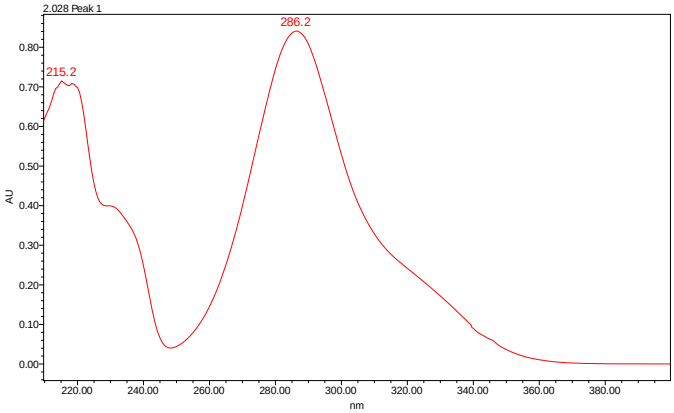

	Retention Time	Area	% Area	Height
1	2.028	440126	100.00	529701

Supplementary Figure S23. Benzylic hydroxylation of **31** by CitB. PDA traces of enzymatic reaction and control reaction.

With CitB

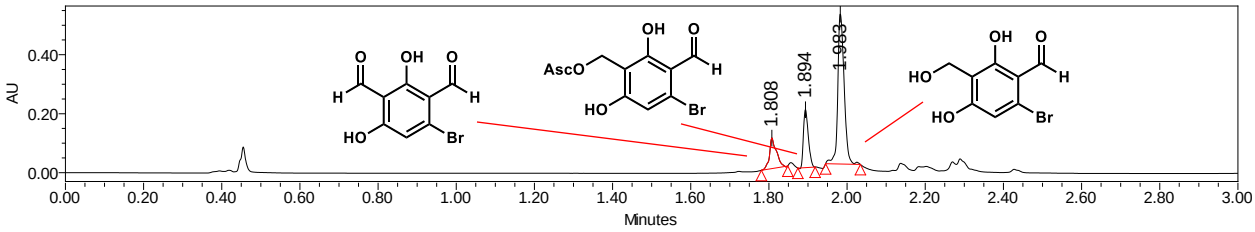

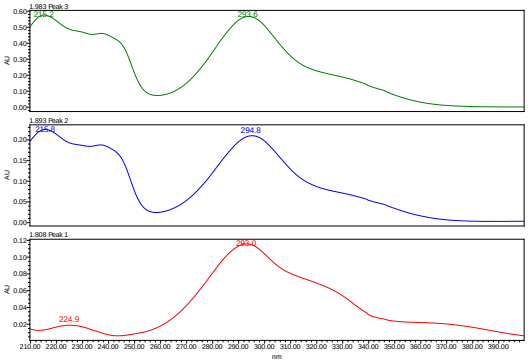

	Retention Time	Area	% Area	Height
1	1.808	128097	14.58	103791
2	1.894	171465	19.52	197059
3	1.983	579028	65.90	508932

No Enzyme Control

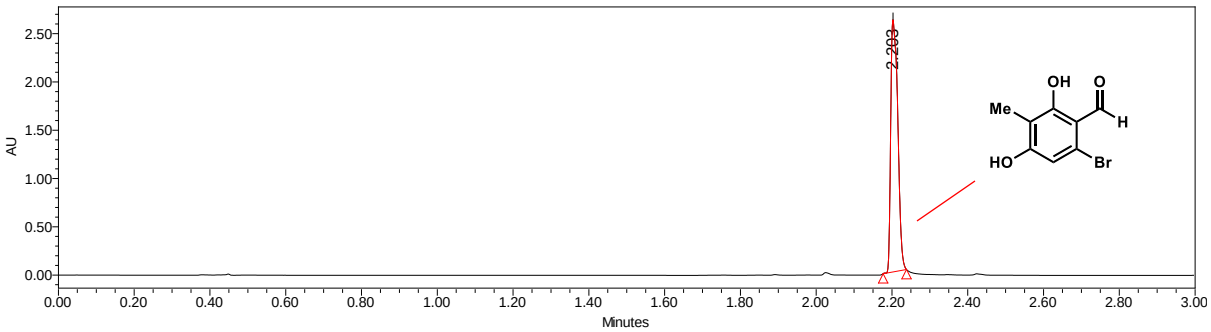

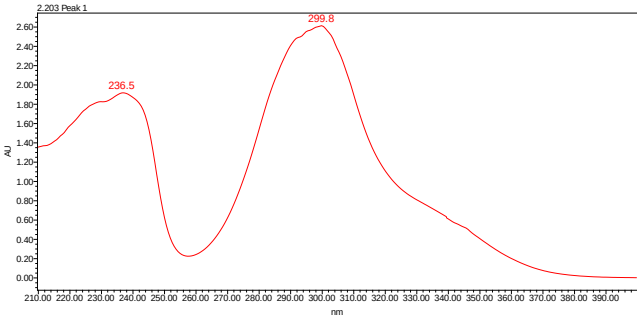

	Retention Time	Area	% Area
1	2.203	3364169	100.00

Supplementary Figure S24. Benzylic hydroxylation of **32** by CitB. PDA traces of enzymatic reaction and control reaction.

With CitB

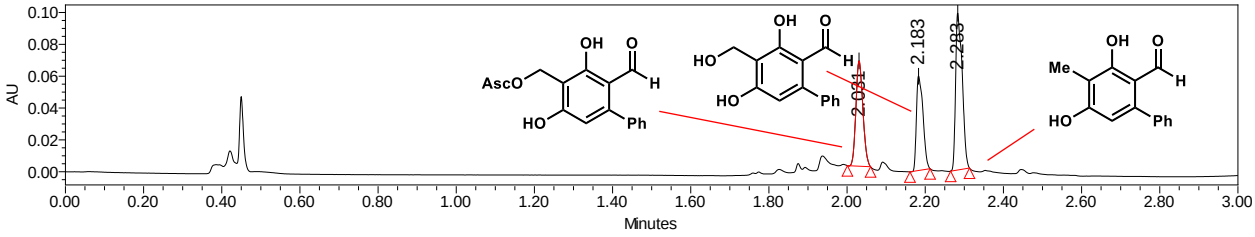

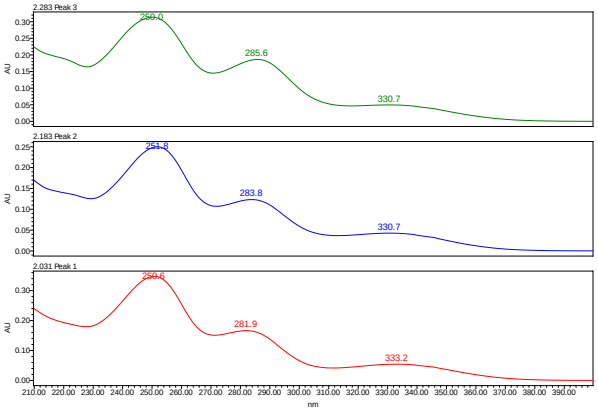

	Retention Time	Area	% Area	Height
1	2.031	81644	30.74	66110
2	2.183	69007	25.98	59416
3	2.283	114961	43.28	98454

No Enzyme Control

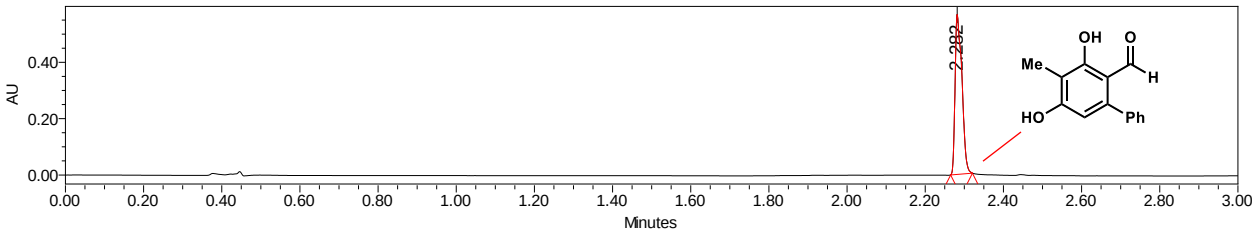

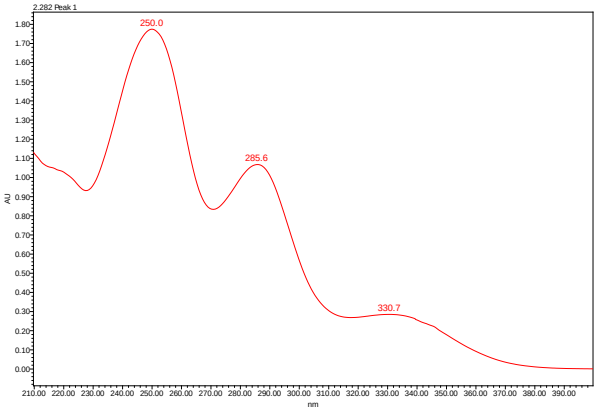

	Retention Time	Area	% Area	Height
1	2.282	688212	100.00	567732

Supplementary Figure S25. Benzylic hydroxylation of **S4** by CitB. PDA traces of enzymatic reaction and control reaction.

With CitB

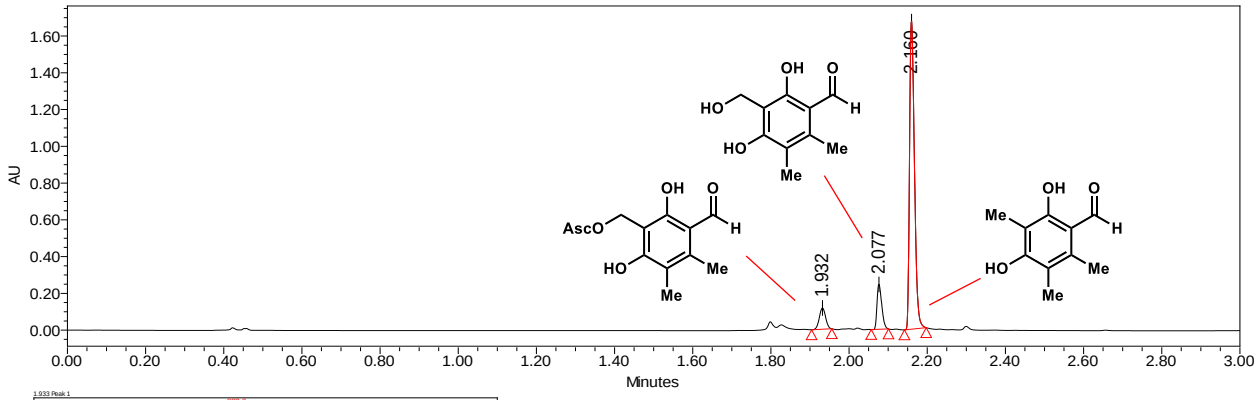

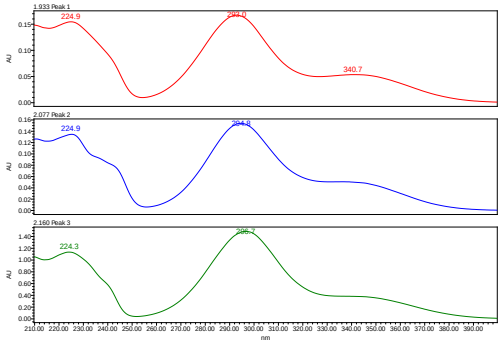

	Retention Time	Area	% Area	Height
1	1.933	162421	10.45	145194
2	2.077	117134	7.53	142594
3	2.160	1275214	82.02	1447841

No Enzyme Control

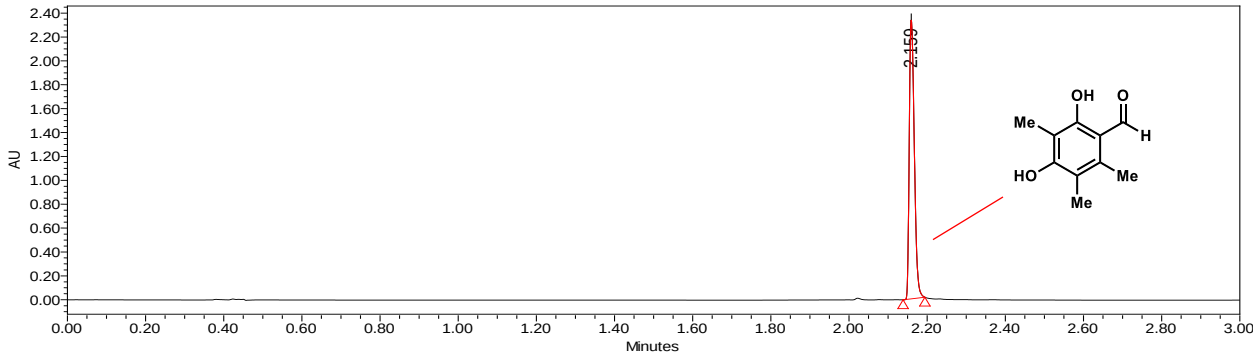

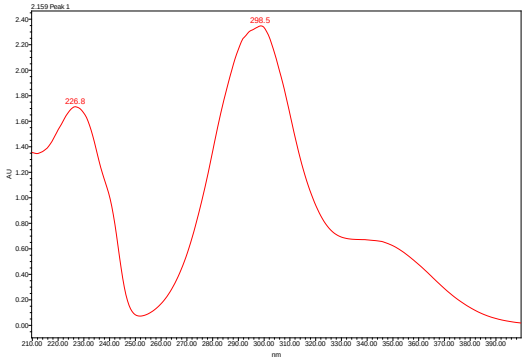

	Retention Time	Area	% Area	Height
1	2.159	2103425	100.00	2334654

Supplementary Figure S26. Benzylic hydroxylation of **35** by CitB. PDA traces of enzymatic reaction and control reaction.

With CitB

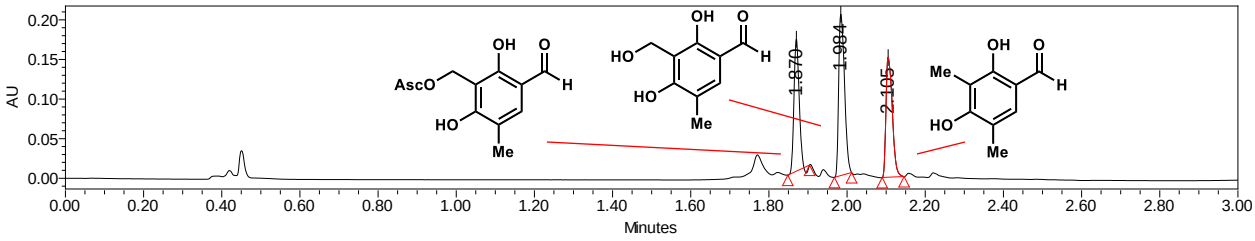

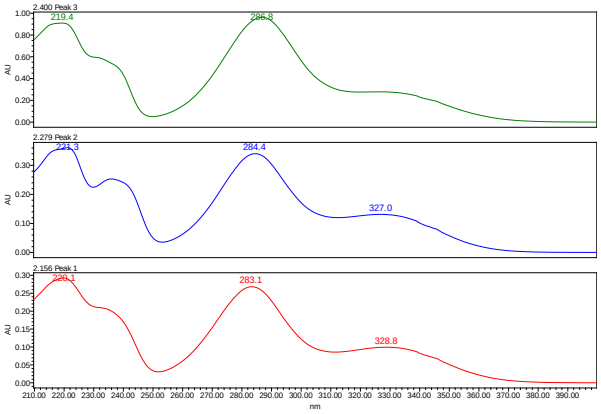

	Retention Time	Area	% Area	Height
1	2.156	88057	16.11	122058
2	2.279	104200	19.07	171834
3	2.400	354268	64.82	564898

No Enzyme Control

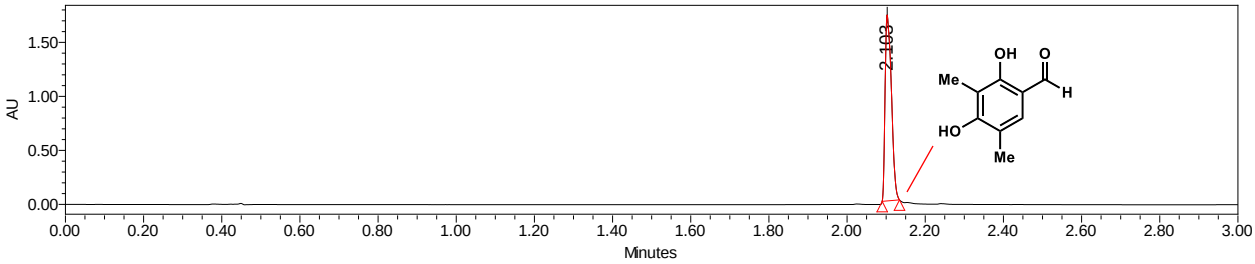

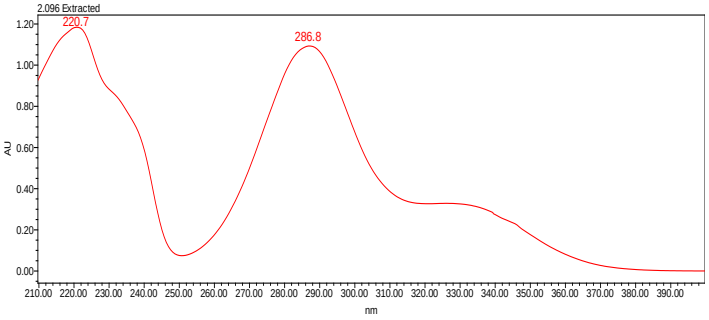

	Retention Time	Area	% Area
1	2.103	1934409	100.00

Supplementary Figure S27. Benzylic hydroxylation of **36** by CitB. PDA traces of enzymatic reaction and control reaction.

With CitB

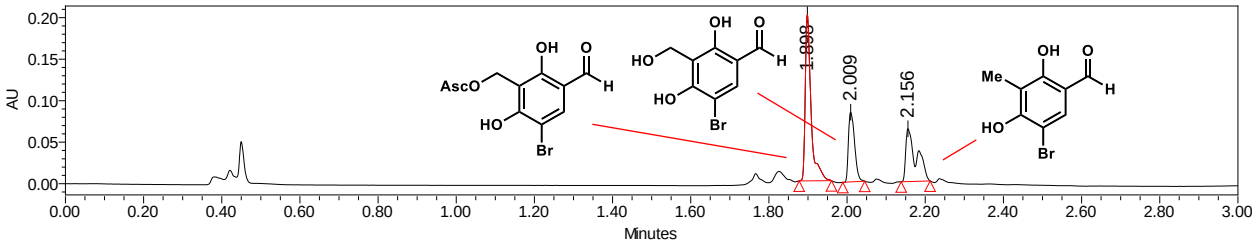

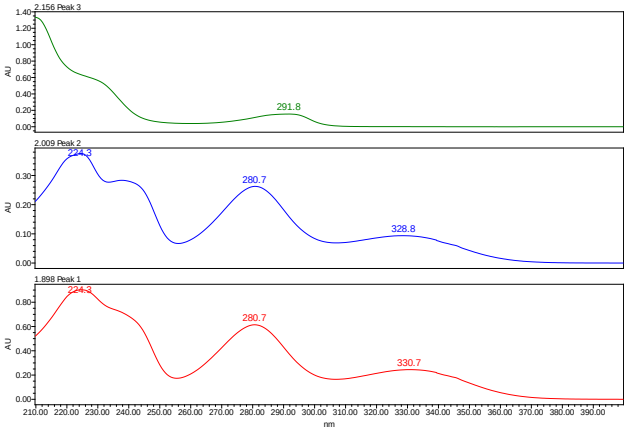

	Retention Time	Area	% Area	Height
1	1.898	206718	49.42	200189
2	2.009	92301	22.07	84095
3	2.156	119266	28.51	63782

No Enzyme Control

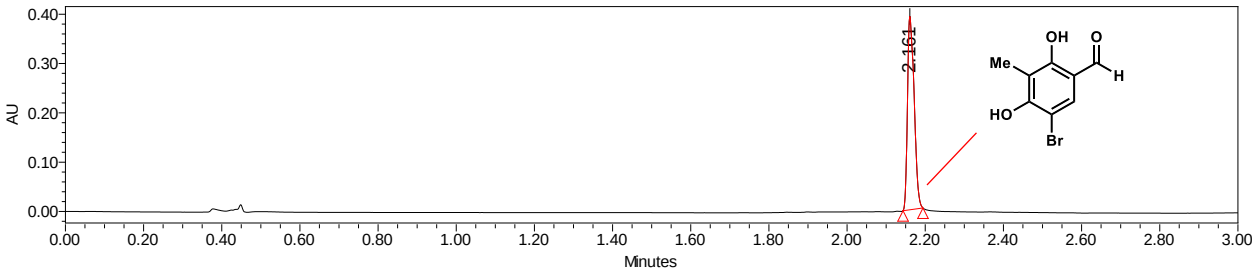

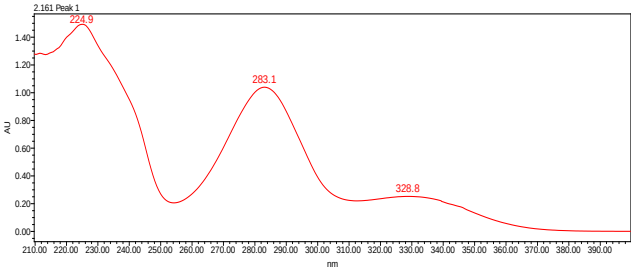

	Retention Time	Area	% Area
1	2.161	462518	100.00

Supplementary Figure S28. Benzylic hydroxylation of **65** by CitB. PDA traces of enzymatic reaction and control reaction.

With CitB

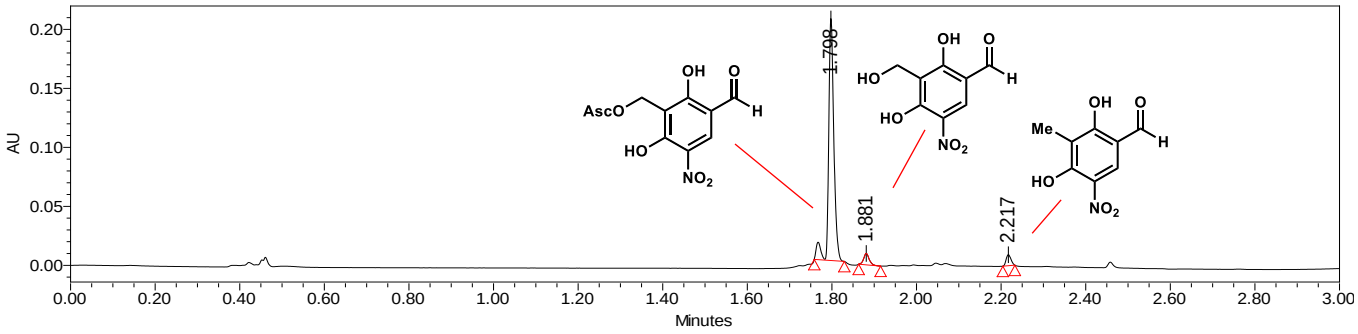

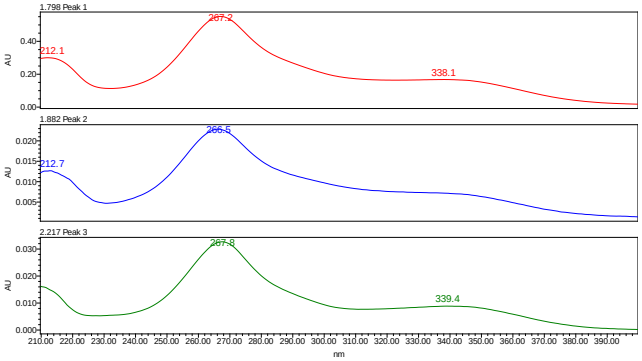

	Retention Time	Area	% Area	Height
1	1.798	178212	91.61	205348
2	1.881	8876	4.56	9736
3	2.217	7446	3.83	9399

No Enzyme Control

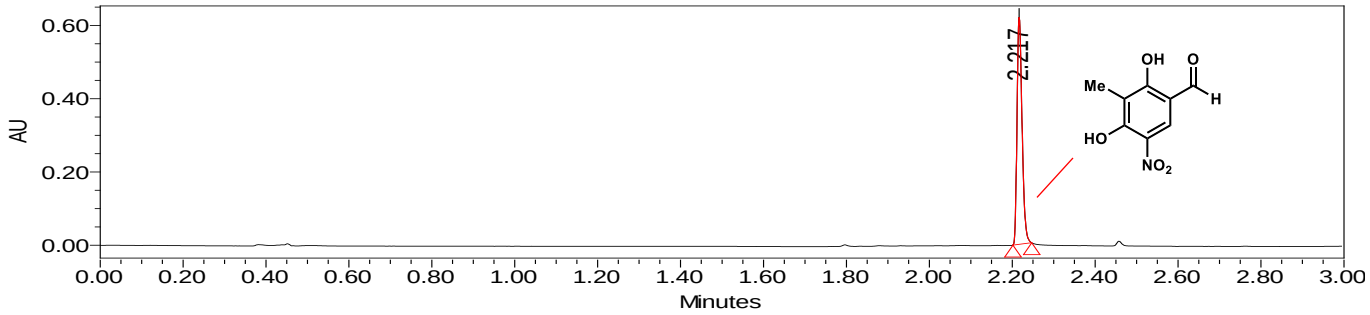

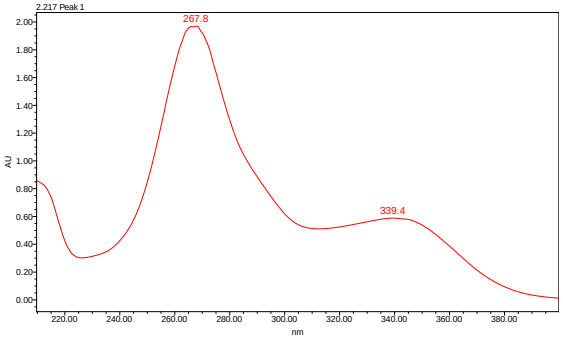

	Retention Time	Area	% Area	Height
1	2.217	523699	100.00	619137

Supplementary Figure S29. Benzylic hydroxylation of **37** by CitB. PDA traces of enzymatic reaction and control reaction.

With CitB

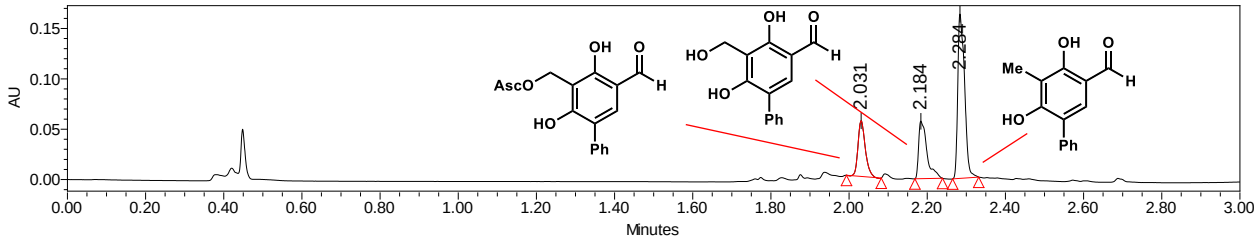

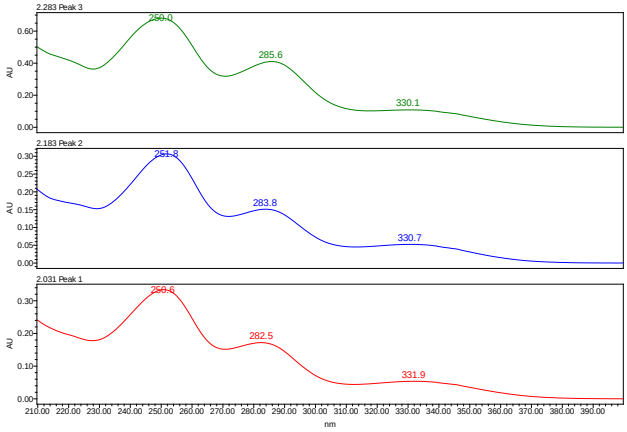

	Retention Time	Area	% Area	Height
1	2.031	72174	20.42	55343
2	2.184	84576	23.93	57187
3	2.284	196618	55.64	163569

No Enzyme Control

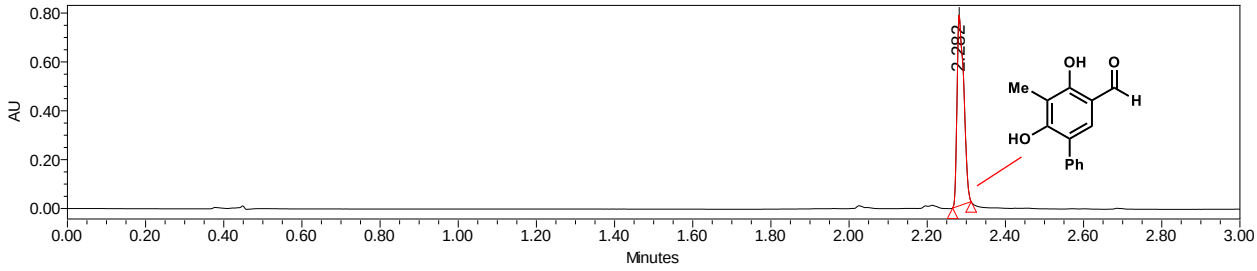

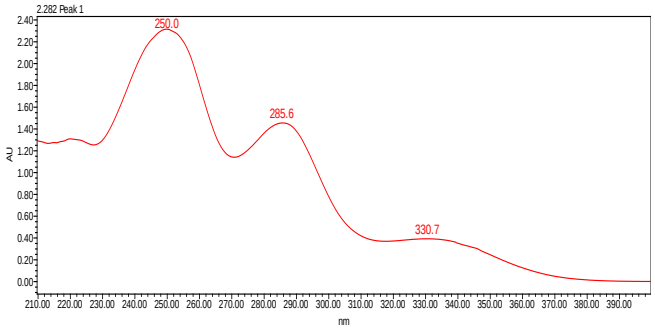

	Retention Time	Area	% Area
1	2.282	935160	100.00

Supplementary Figure S30. Benzylic hydroxylation of **39** by CitB. PDA traces of enzymatic reaction and control reaction.

With CitB

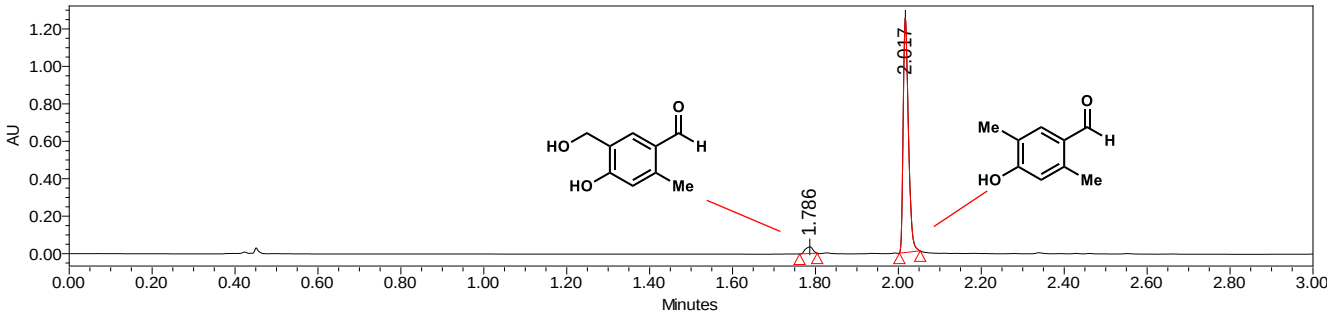

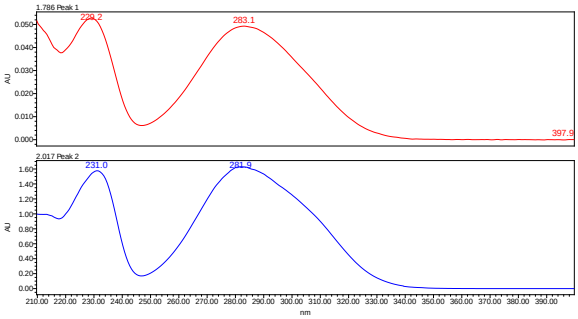

	Retention Time	Area	% Area	Height
1	1.786	48006	4.14	37151
2	2.017	1111944	95.86	1254418

No Enzyme Control

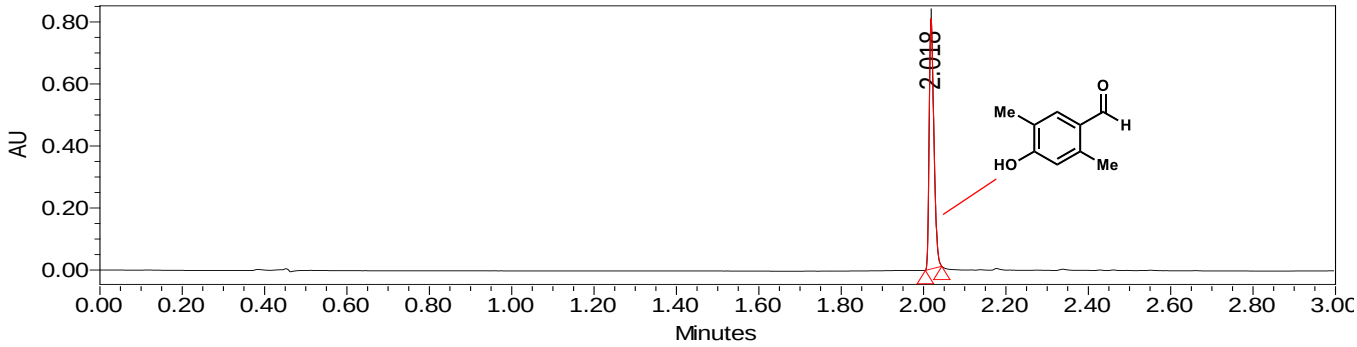

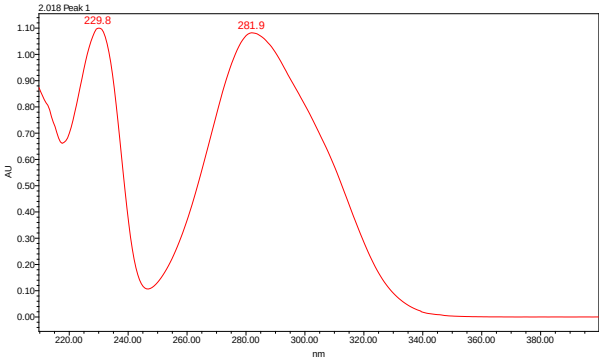

	Retention Time	Area	% Area	Height
1	2.018	641158	100.00	807200

Supplementary Figure S31. Benzylic hydroxylation of **40** by CitB. PDA traces of enzymatic reaction and control reaction.

With CitB

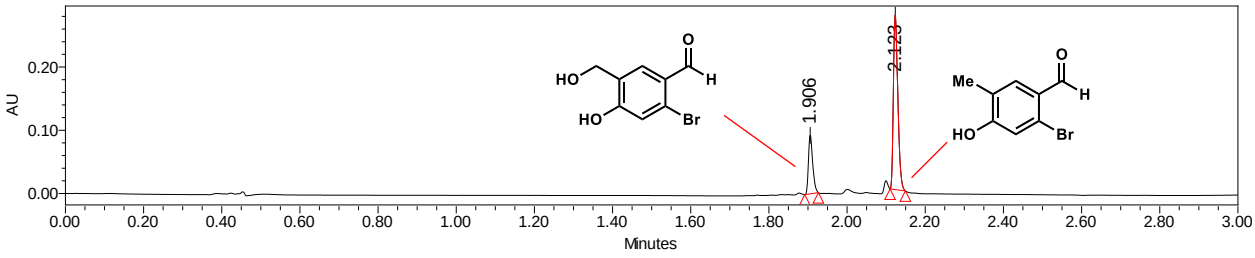

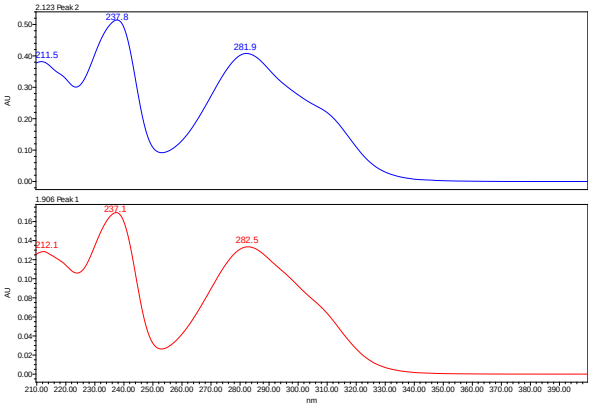

	Retention Time	Area	% Area	Height
1	1.906	70147	24.27	92506
2	2.123	218853	75.73	275931

No Enzyme Control

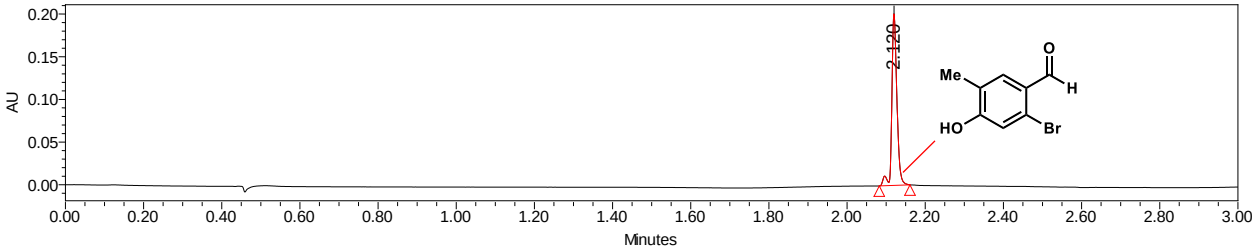

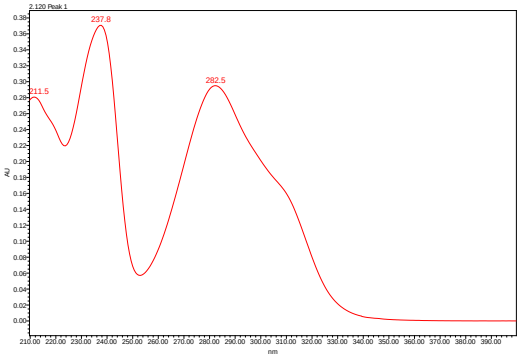

	Retention Time	Area	% Area	Height
1	2.120	181187	100.00	201068

Supplementary Figure S32. Benzylic hydroxylation of **41** by CitB. PDA traces of enzymatic reaction and control reaction.

With CitB

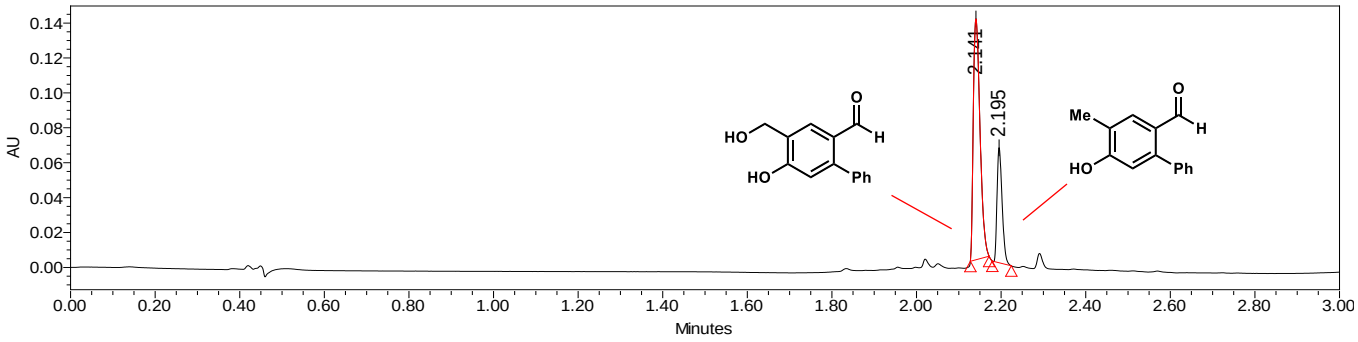

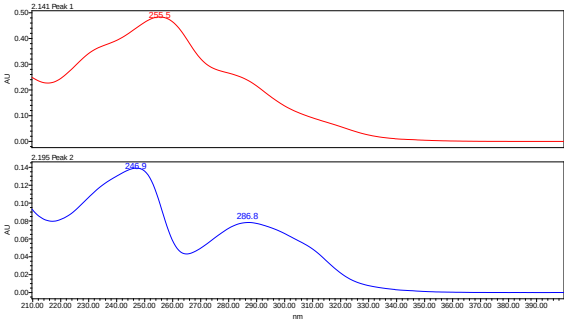

	Retention Time	Area	% Area	Height
1	2.141	155984	73.88	139978
2	2.195	55158	26.12	66133

No enzyme control

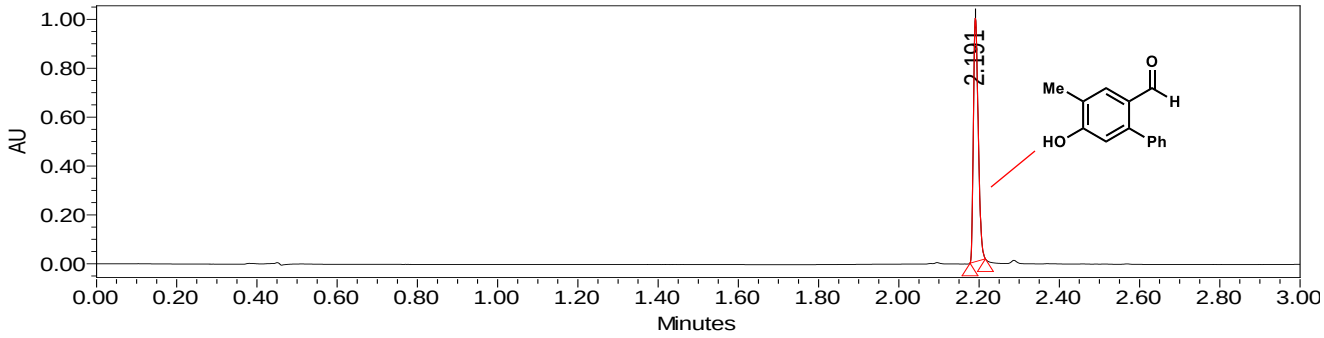

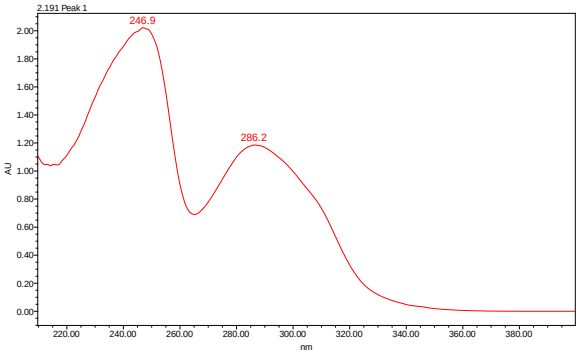

	Retention Time	Area	% Area	Height
1	2.191	836389	100.00	995849

Supplementary Figure S33. Benzylic hydroxylation of **42** by CitB. PDA traces of enzymatic reaction and control reaction.

With CitB

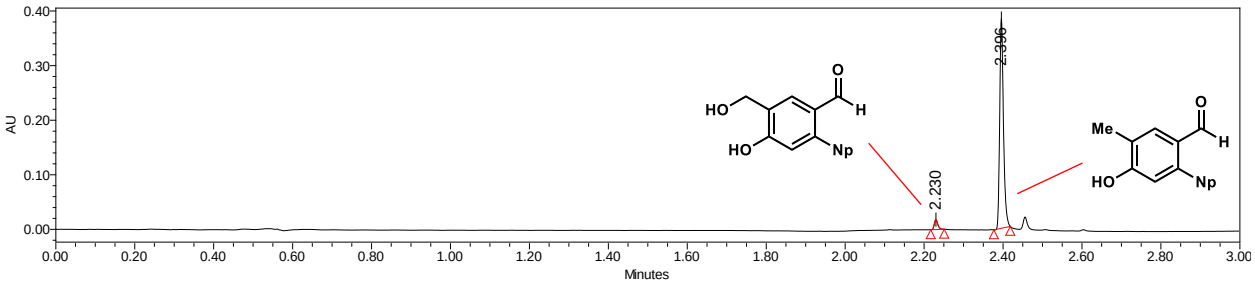

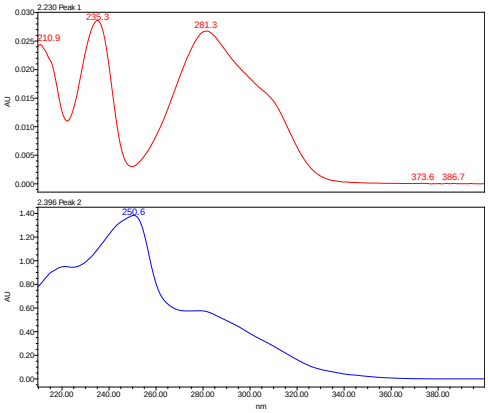

	Retention Time	Area	% Area	Height
1	2.230	11489	4.33	18425
2	2.396	253676	95.67	383695

No Enzyme Control

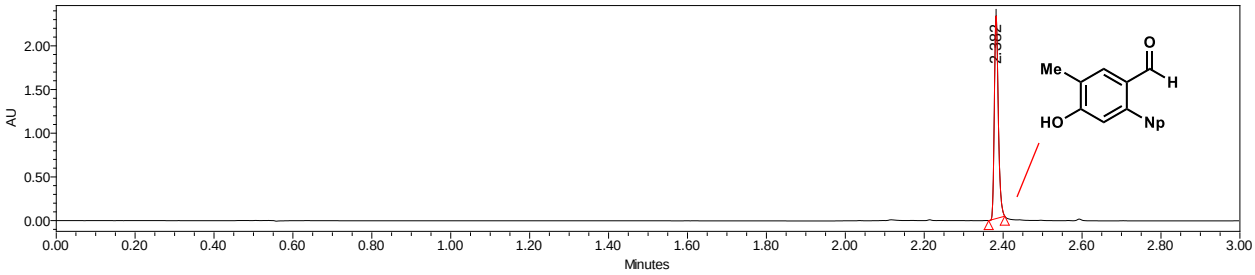

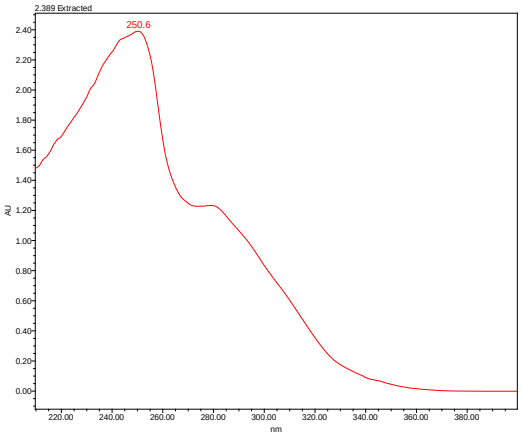

	Retention Time	Area	% Area	Height
1	2.382	1630305	100.00	2323928

Supplementary Figure S34. Benzylic hydroxylation of **S7** by CitB. PDA traces of enzymatic reaction and control reaction.

With CitB

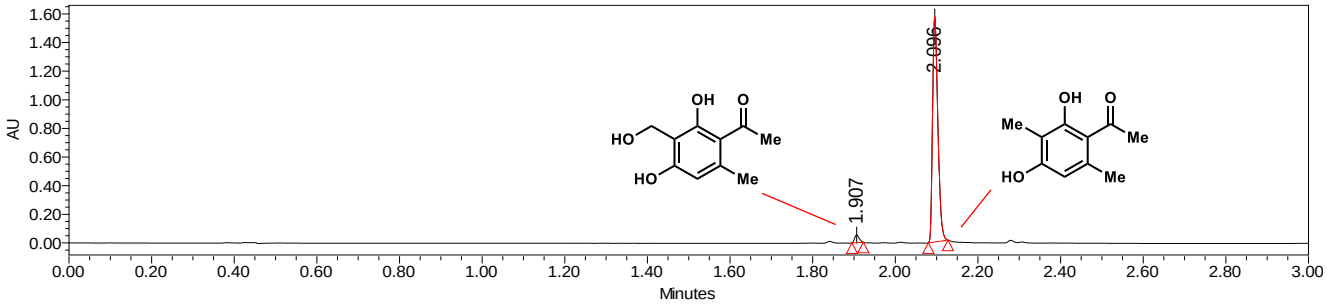

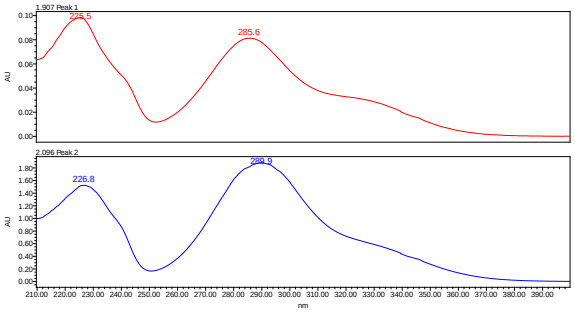

	Retention Time	Area	% Area	Height
1	1.907	41893	2.89	54401
2	2.096	1405932	97.11	1575505

No Enzyme Control

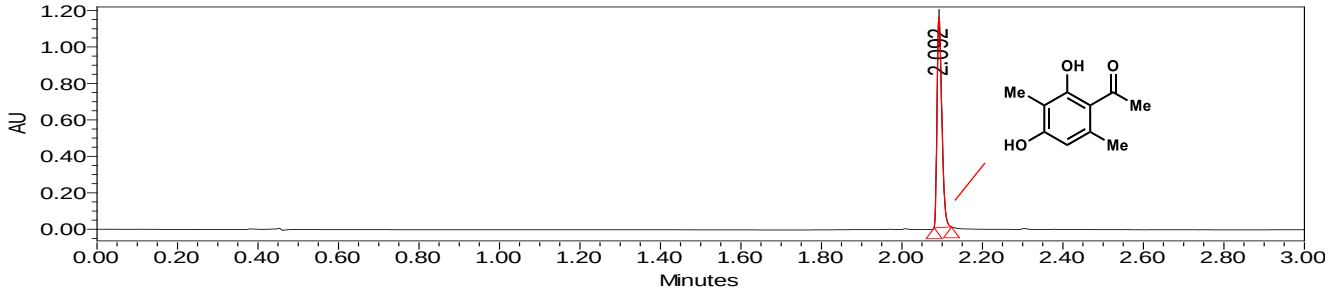

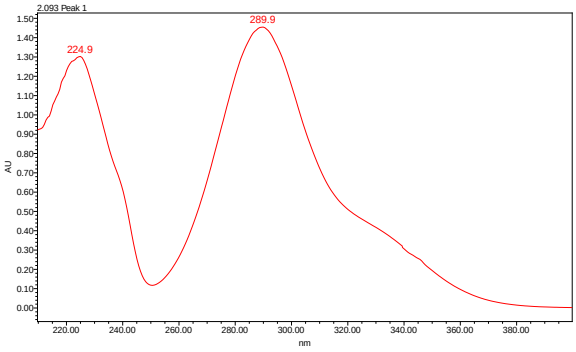

	Retention Time	Area	% Area	Height
1	2.092	956958	100.00	1153000

Supplementary Figure S35. Benzylic hydroxylation of **34** by CitB. PDA traces of enzymatic reaction and control reaction.

With CitB

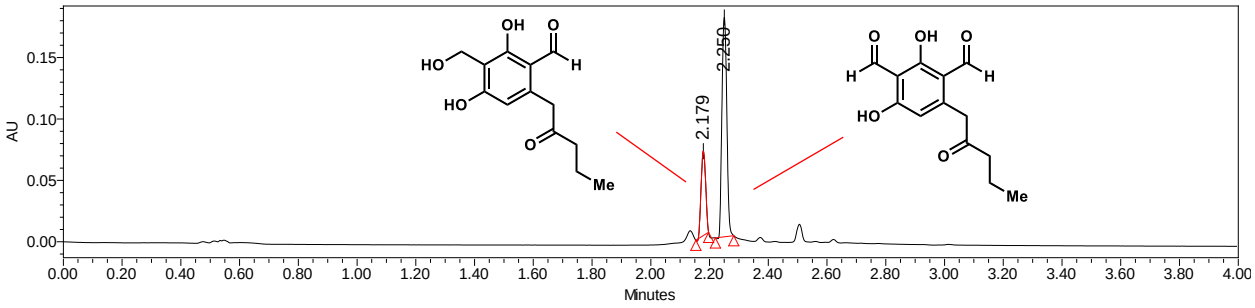

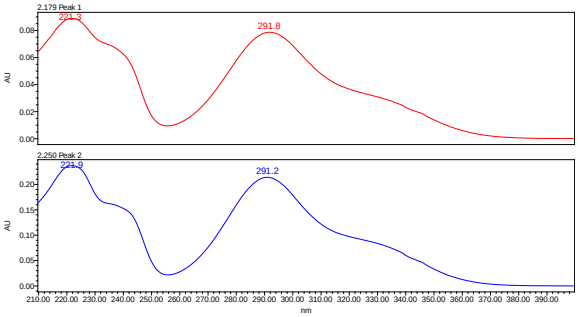

	Retention Time	Area	% Area	Height
1	2.179	74913	26.66	68811
2	2.250	206069	73.34	178596

No Enzyme Control

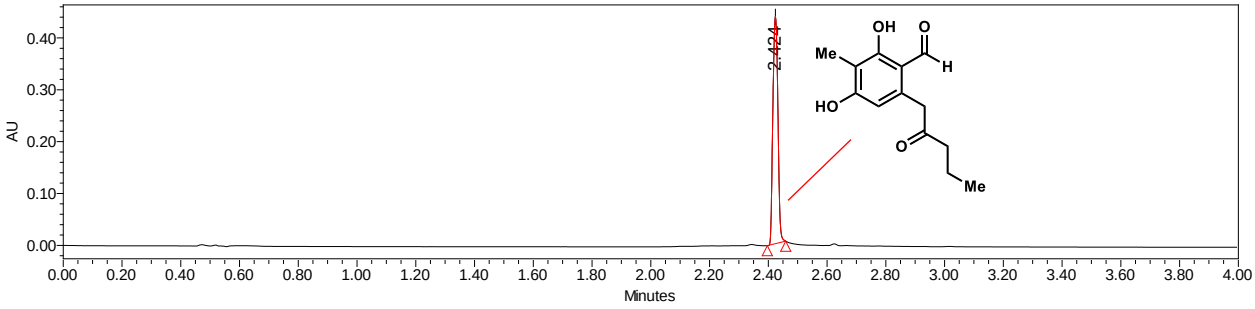

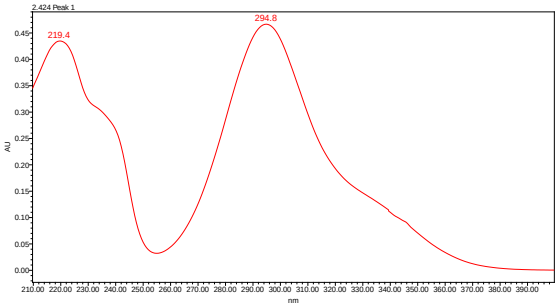

	Retention Time	Area	% Area	Height
1	2.424	519715	100.00	438090

Supplementary Figure S36. Benzylic hydroxylation of **25** by CitB. PDA traces of enzymatic reaction and control reaction.

With CitB

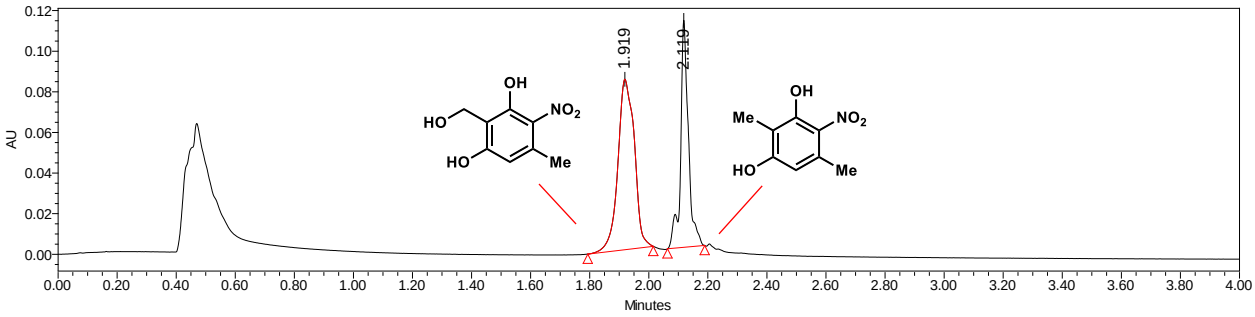

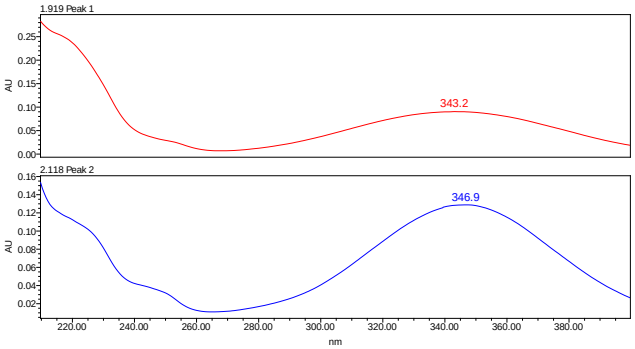

	Retention Time	Area	% Area	Height
1	1.919	325393	61.26	83942
2	2.119	205798	38.74	111809

No Enzyme Control

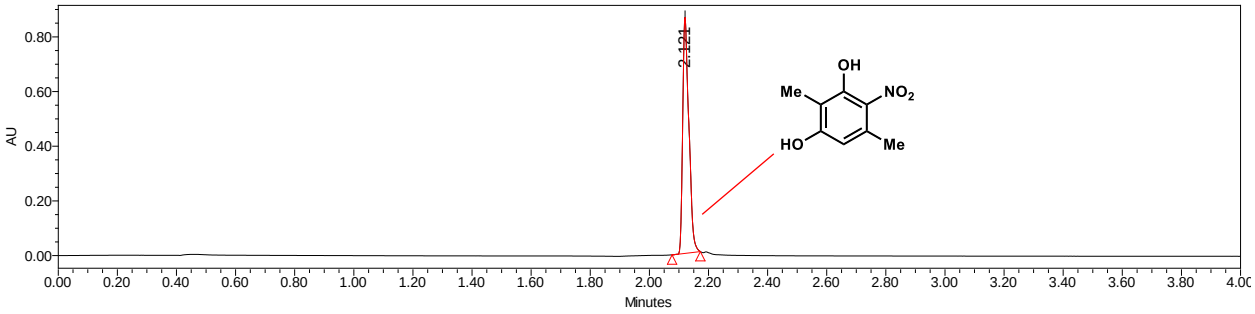

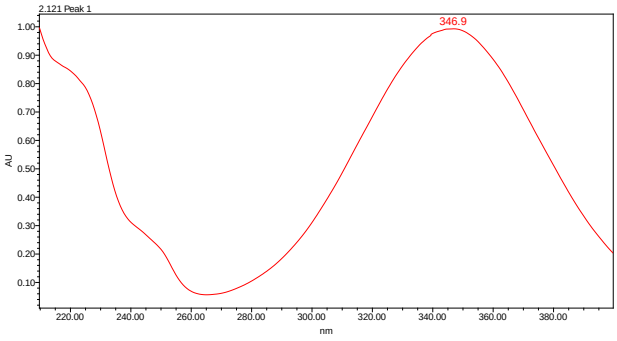

	Retention Time	Area	% Area	Height
1	2.121	1250924	100.00	863894

Supplementary Figure S37. Benzylic hydroxylation of **24** by CitB. LC/MS traces of enzymatic reaction and control reaction.

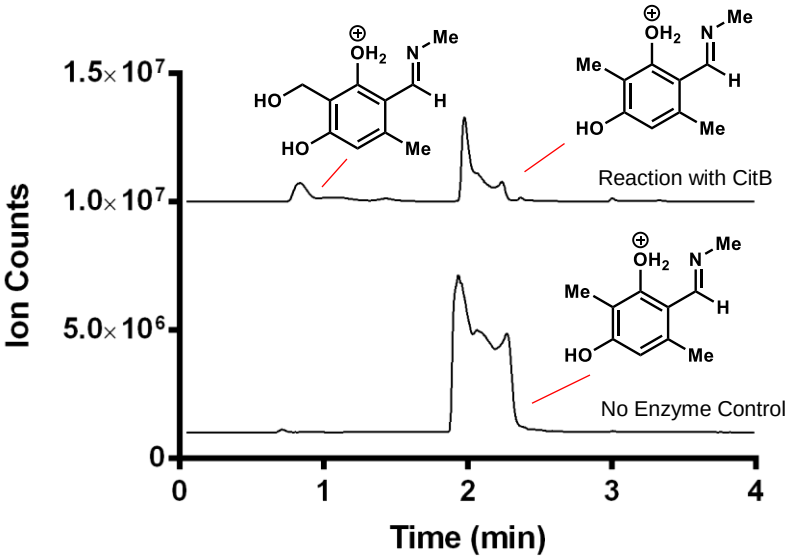

Part VIII. UPLC traces of ClaD-catalyzed biocatalytic reactions

Supplementary Figure S38. Benzylic hydroxylation of **17** by ClaD. PDA traces of enzymatic reaction and control reaction.

With ClaD

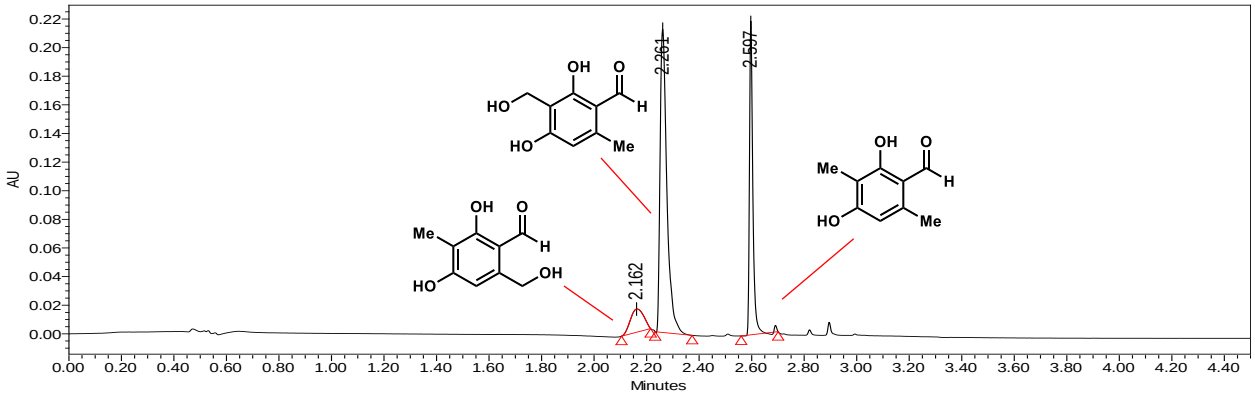

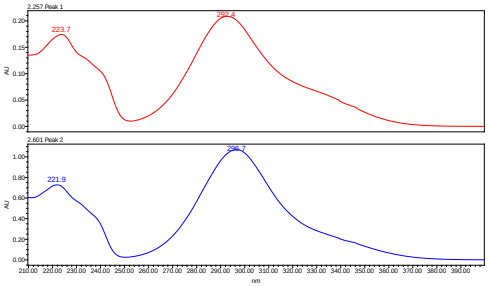

	Retention Time	Area	% Area	Height
1	2.257	372059	27.82	183479
2	2.601	965233	72.18	1038145

No Enzyme Control

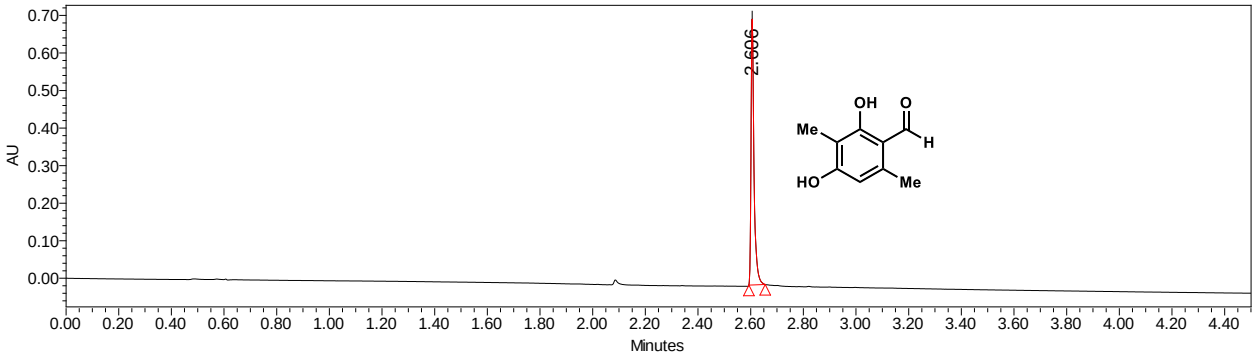

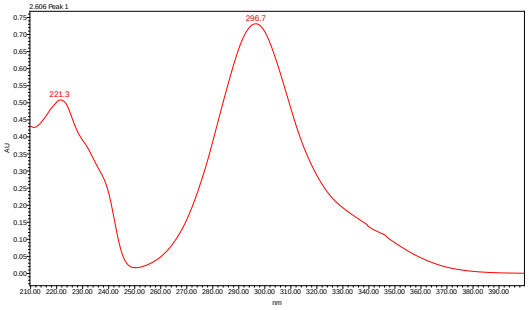

	Retention Time	Area	% Area	Height
1	2.606	552559	100.00	707838

Supplementary Figure S39. Benzylic hydroxylation of **27** by ClaD. PDA traces of enzymatic reaction and control reaction.

With ClaD

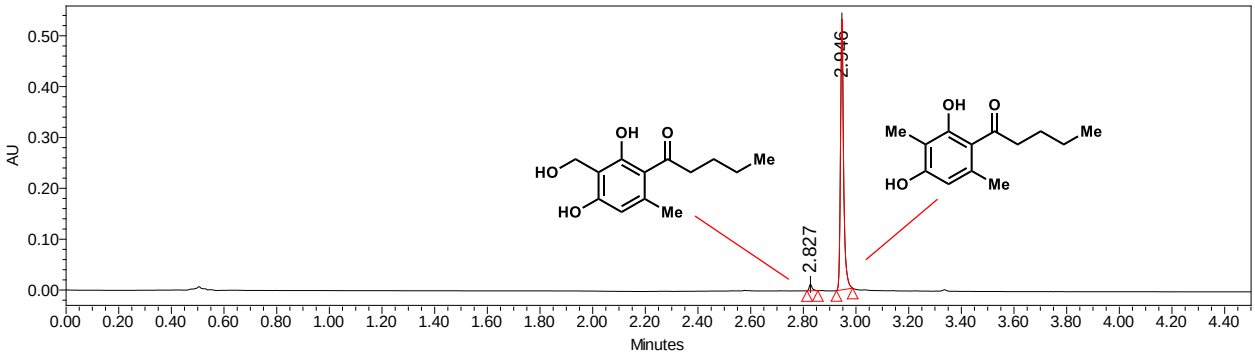

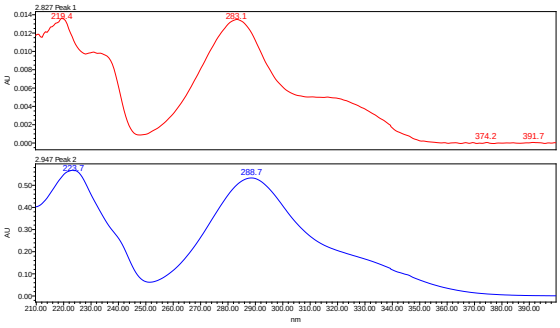

	Retention Time	Area	% Area	Height
1	2.827	10070	2.26	12630
2	2.946	435438	97.74	531349

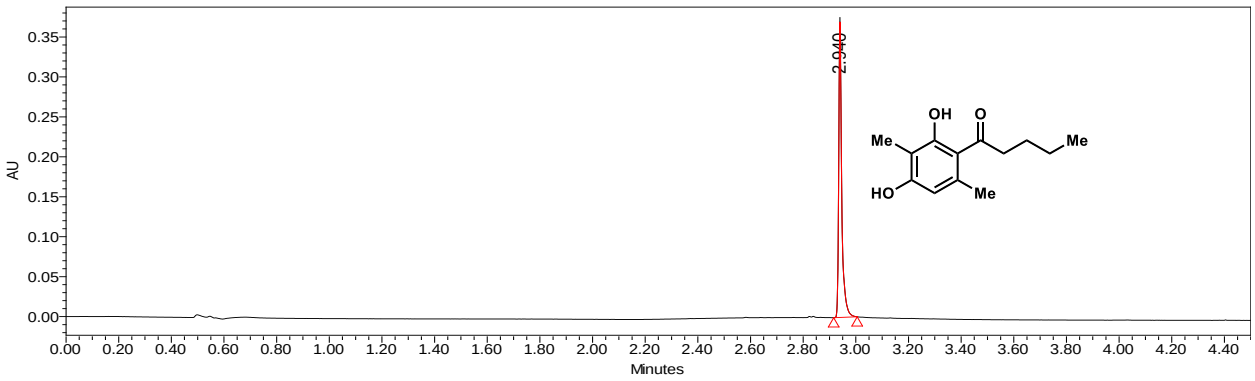

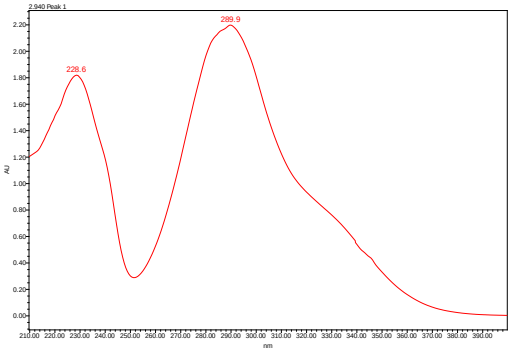

	Retention Time	Area	% Area	Height
1	2.940	298836	100.00	370517

Supplementary Figure S40. Benzylic hydroxylation of **S6** by ClaD. PDA traces of enzymatic reaction and control reaction.

With ClaD

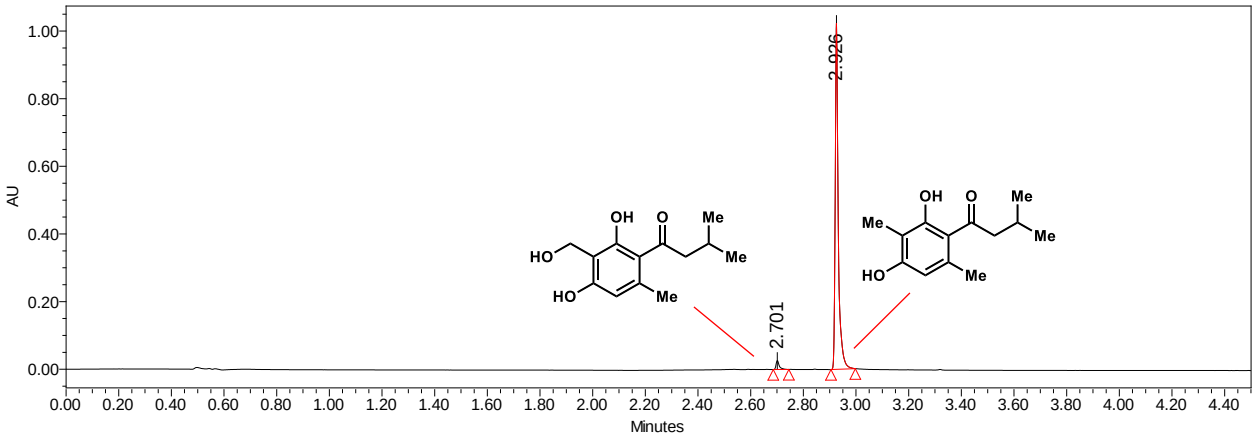

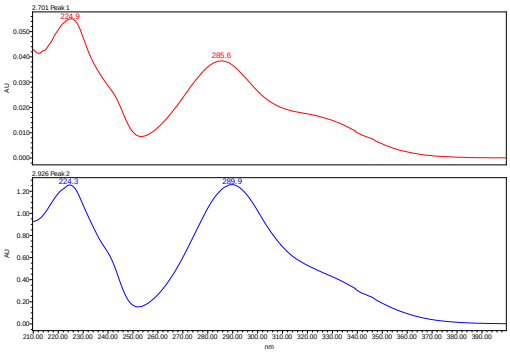

	Retention Time	Area	% Area	Height
1	2.701	22569	2.65	26526
2	2.926	828224	97.35	1022478

No Enzyme Control

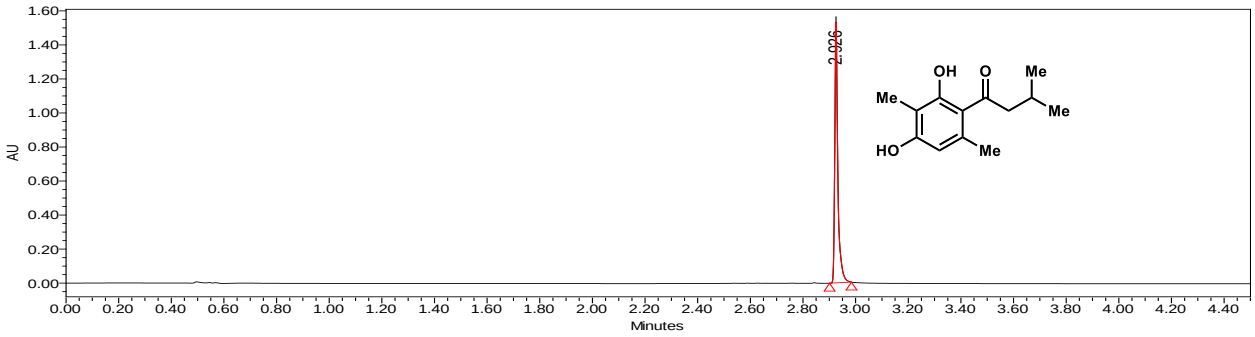

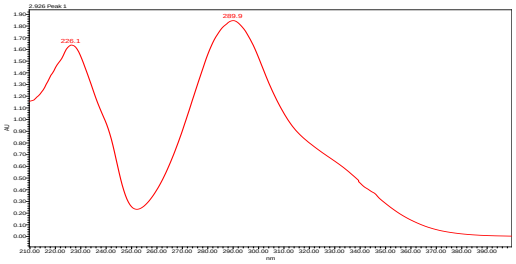

	Retention Time	Area	% Area	Height
1	2.926	1241096	100.00	1532691

Supplementary Figure S41. Benzylic hydroxylation of **32** by ClaD. PDA traces of enzymatic reaction and control reaction.

With ClaD

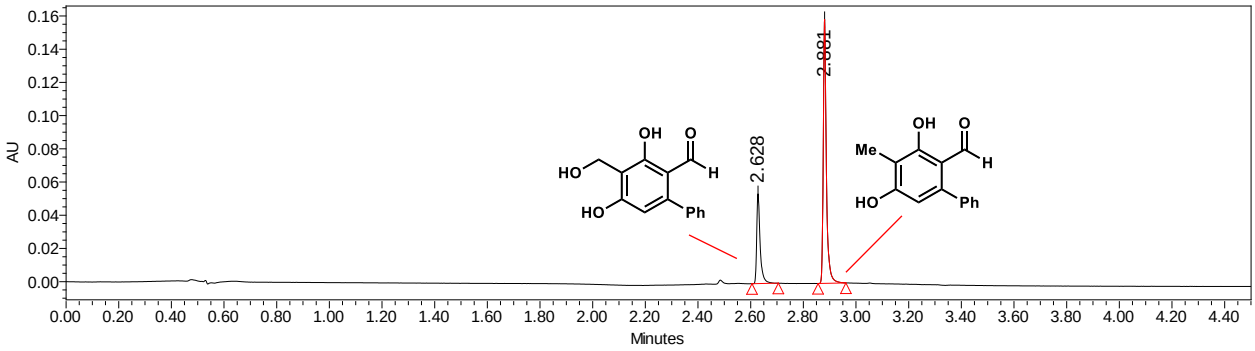

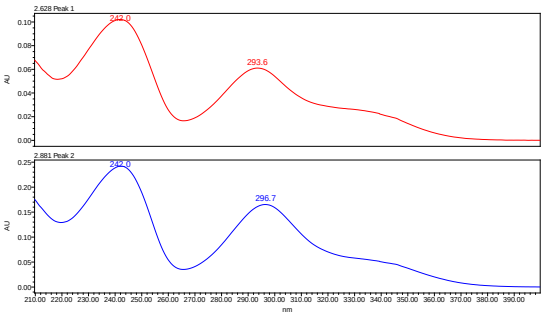

	Retention Time	Area	% Area	Height
1	2.628	49270	27.38	54215
2	2.881	130673	72.62	158993

No Enzyme Control

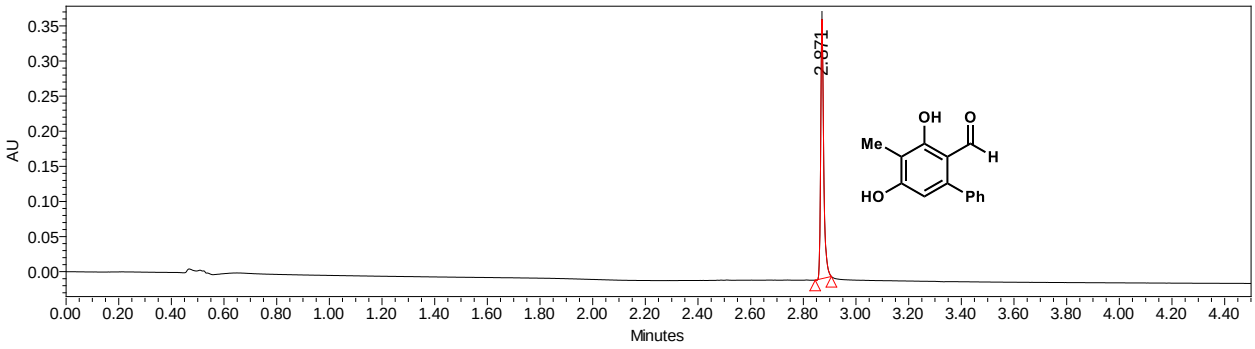

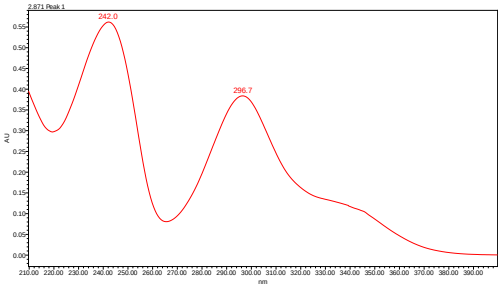

	Retention Time	Area	% Area	Height
1	2.871	292001	100.00	369040

Supplementary Figure S42. Benzylic hydroxylation of **31** by ClaD. PDA traces of enzymatic reaction and control reaction.

With ClaD

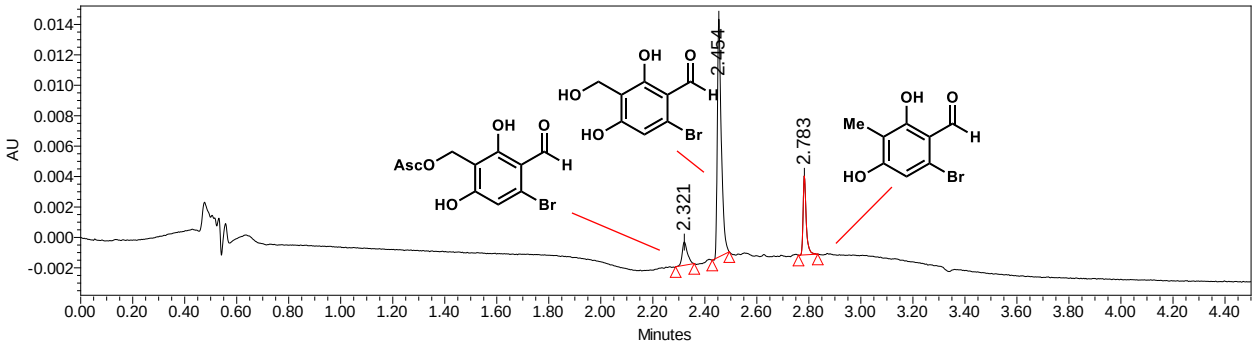

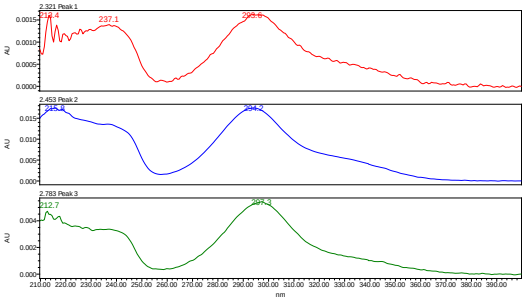

	Retention Time	Area	% Area	Height
1	2.321	2148	9.27	1533
2	2.454	16733	72.18	15666
3	2.783	4302	18.56	5206

No Enzyme Control

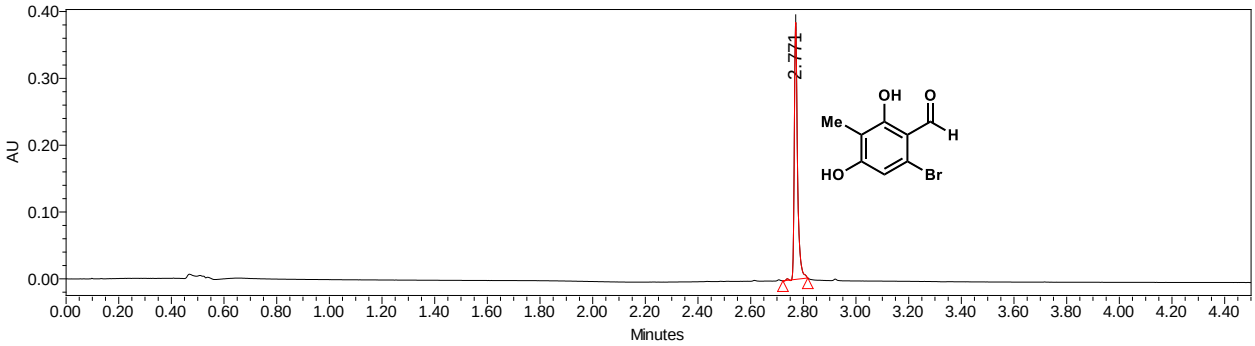

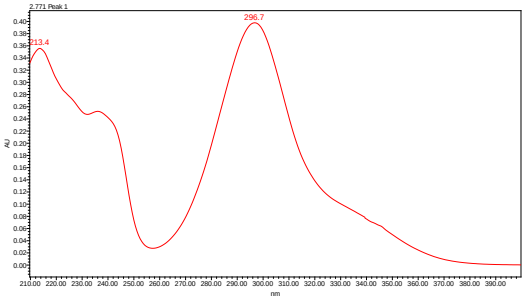

	Retention Time	Area	% Area	Height
1	2.771	324677	100.00	384271

Supplementary Figure S43. Benzylic hydroxylation of **29** by ClaD. PDA traces of enzymatic reaction and control reaction.

With ClaD

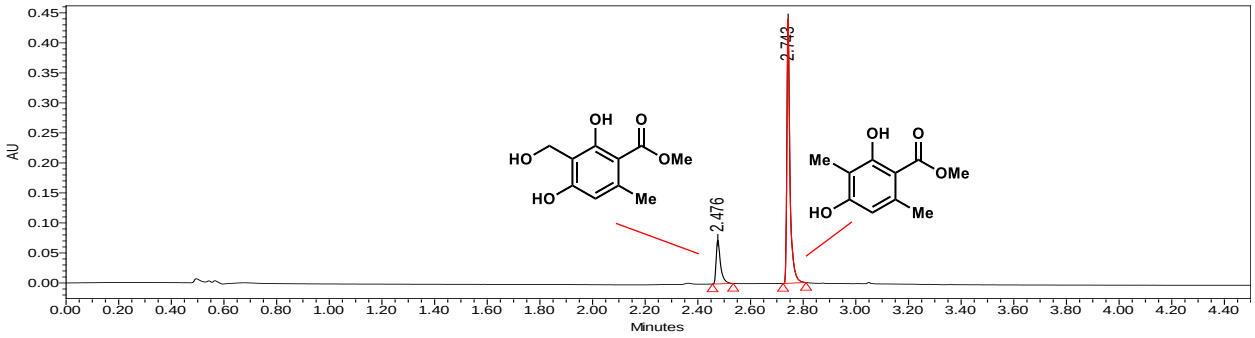

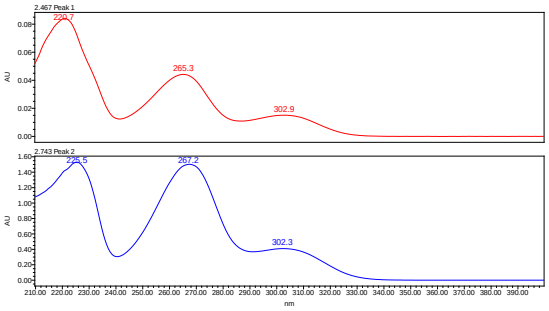

	Retention Time	Area	% Area	Height
1	2.476	84170	18.80	72961
2	2.743	363593	81.20	440078

No Enzyme Control

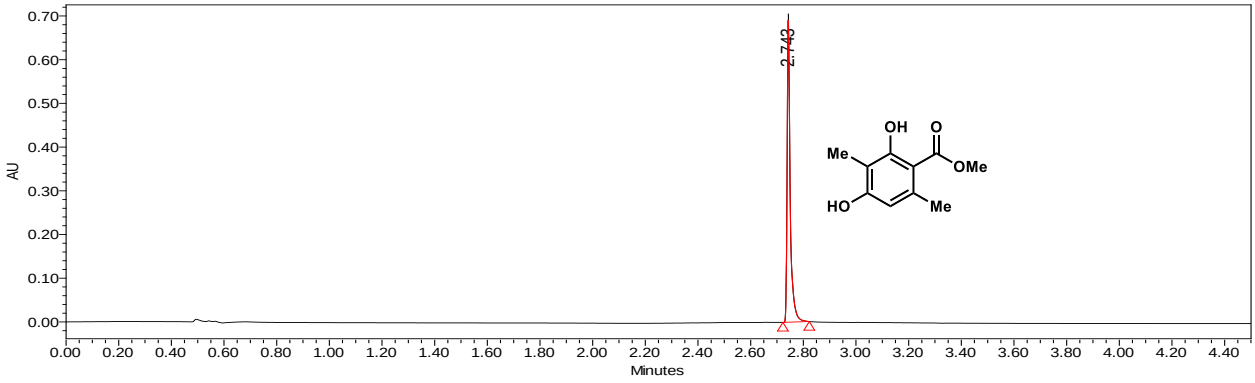

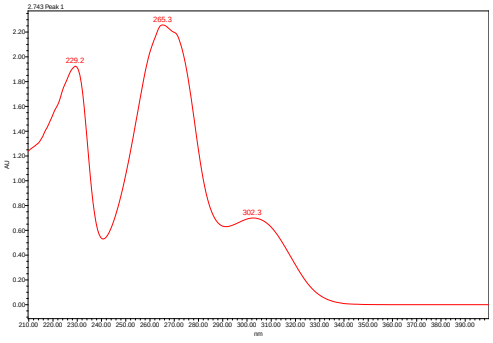

	Retention Time	Area	% Area	Height
1	2.743	568850	100.00	692384

Supplementary Figure S44. Benzylic hydroxylation of **9** by ClaD. PDA traces of enzymatic reaction and control reaction.

With ClaD

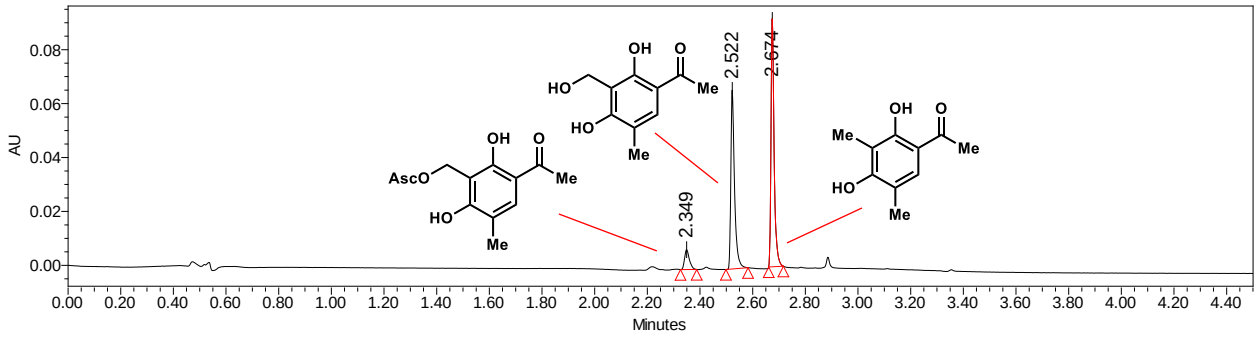

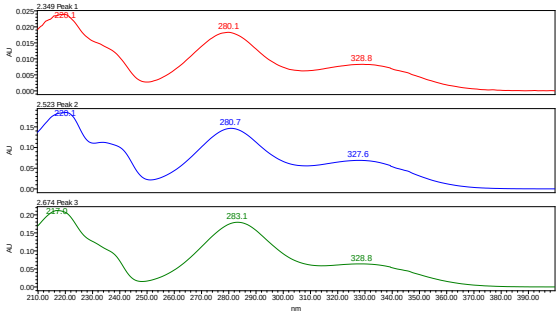

	Retention Time	Area	% Area	Height
1	2.349	9326	6.25	7385
2	2.522	64221	43.04	66319
3	2.674	75678	50.71	92174

No Enzyme Control

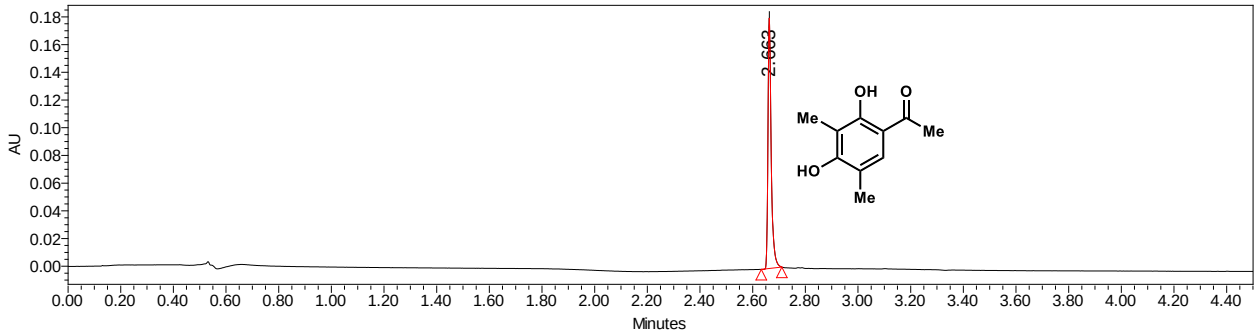

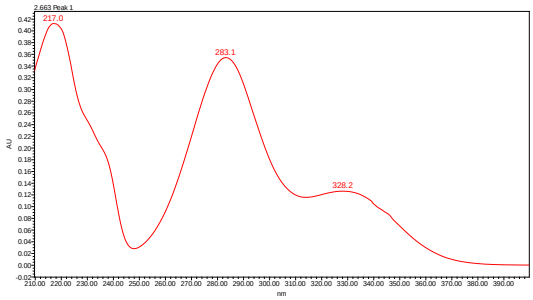

	Retention Time	Area	% Area	Height
1	2.663	155114	100.00	180974

Supplementary Figure S45. Benzylic hydroxylation of **37** by ClaD. PDA traces of enzymatic reaction and control reaction.

With ClaD

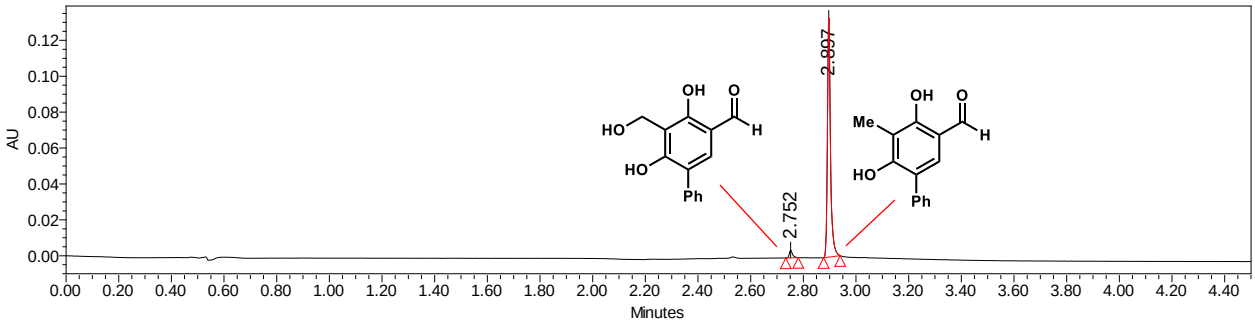

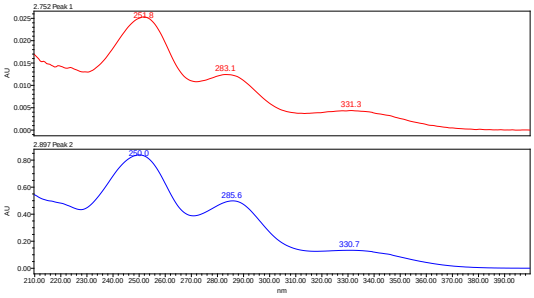

	Retention Time	Area	% Area	Height
1	2.752	3621	3.26	4362
2	2.897	107598	96.74	133020

No Enzyme Control

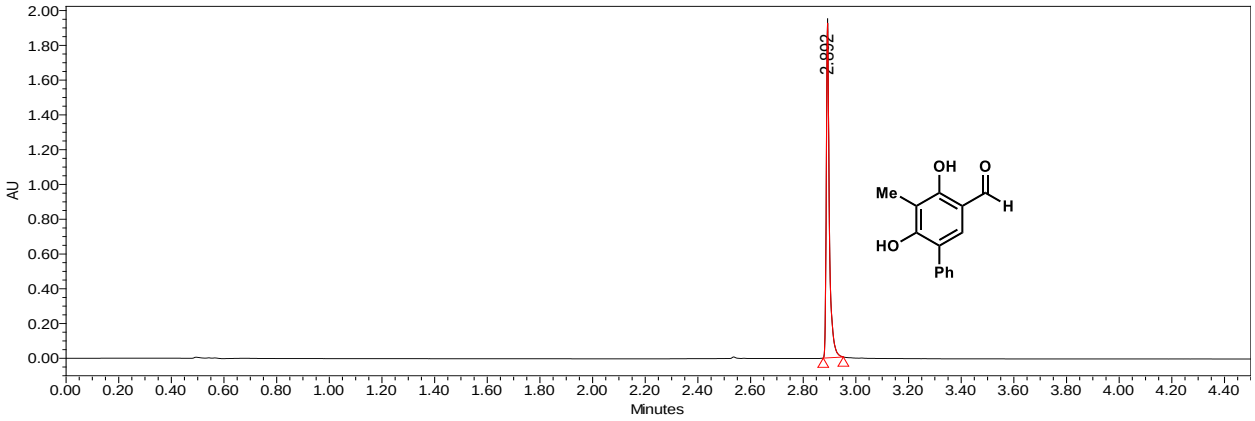

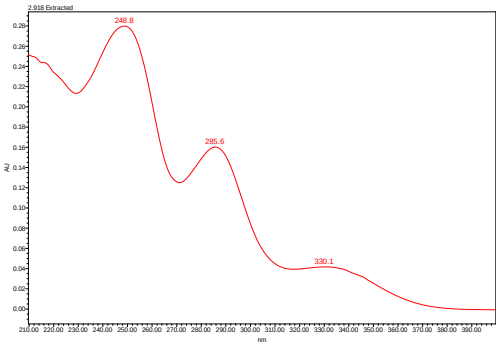

	Retention Time	Area	% Area	Height
1	2.892	96616	100.00	127279

Supplementary Figure S46. Benzylic hydroxylation of **36** by ClaD. PDA traces of enzymatic reaction and control reaction.

With ClaD

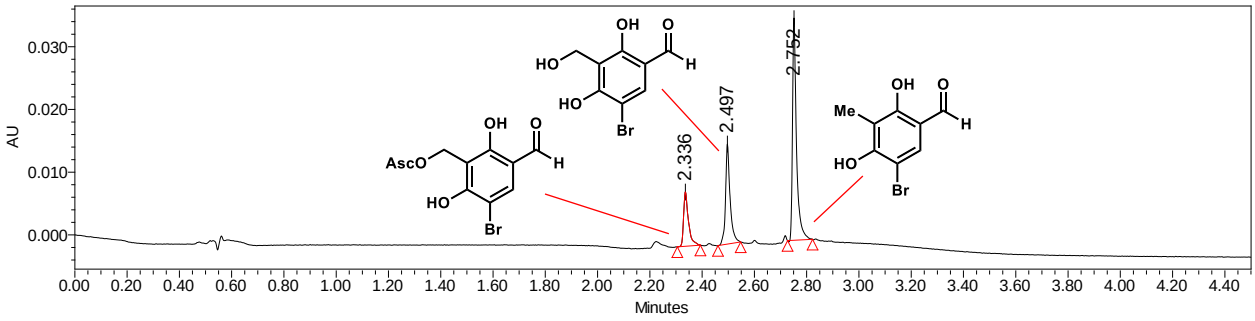

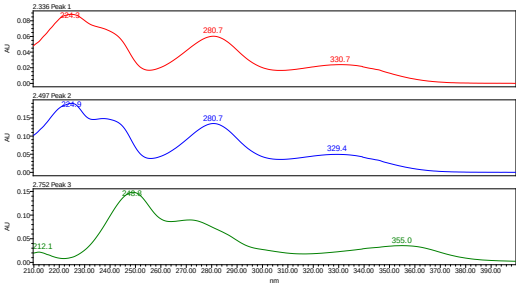

	Retention Time	Area	% Area	Height
1	2.336	11217	16.48	8670
2	2.497	19302	28.36	15961
3	2.752	37533	55.15	35440

No Enzyme Control

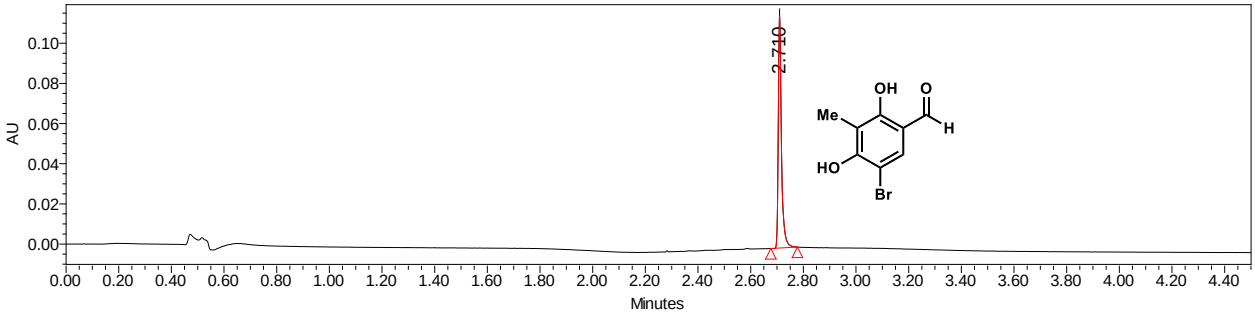

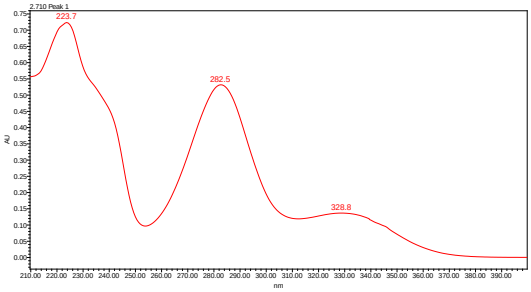

	Retention Time	Area	% Area	Height
1	2.710	97130	100.00	115426

Supplementary Figure S47. Benzylic hydroxylation of **25** by ClaD. PDA traces of enzymatic reaction and control reaction.

With ClaD

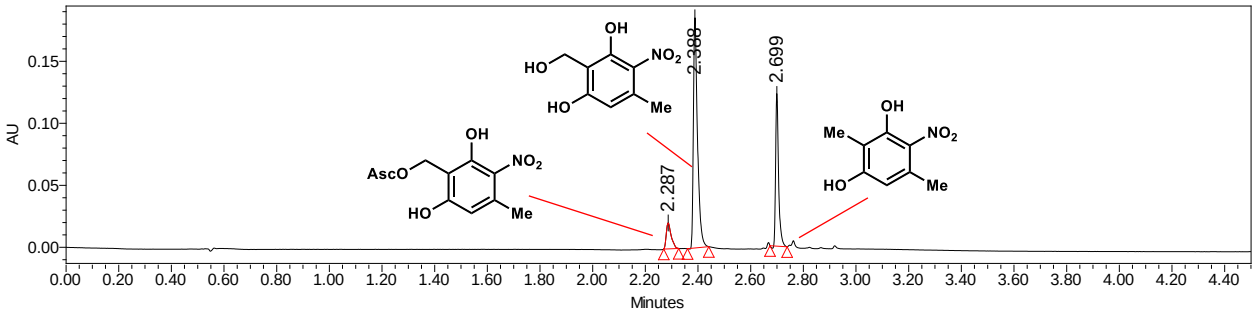

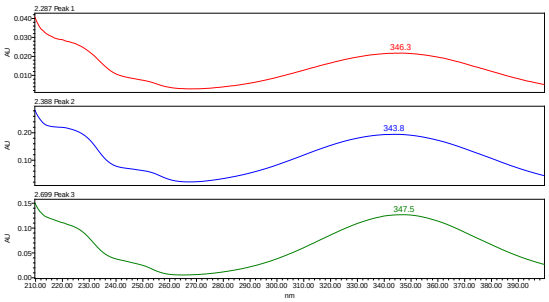

	Retention Time	Area	% Area	Height
1	2.287	27135	8.36	20949
2	2.388	200637	61.84	185589
3	2.699	96692	29.80	122972

No Enzyme Control

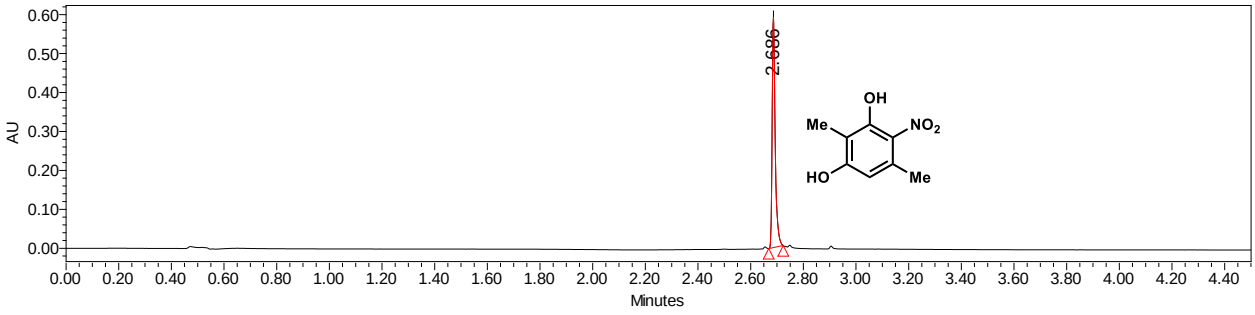

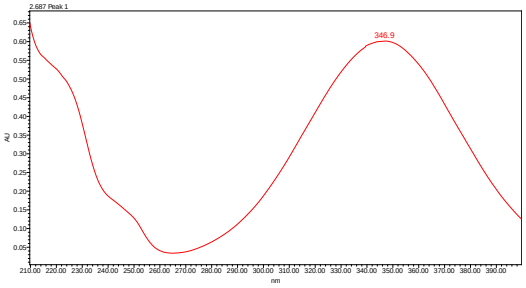

	Retention Time	Area	% Area	Height
1	2.686	475366	100.00	592606

Supplementary Figure S48. Benzylic hydroxylation of **32** by ClaD. PDA traces of enzymatic reaction and control reaction.

With ClaD

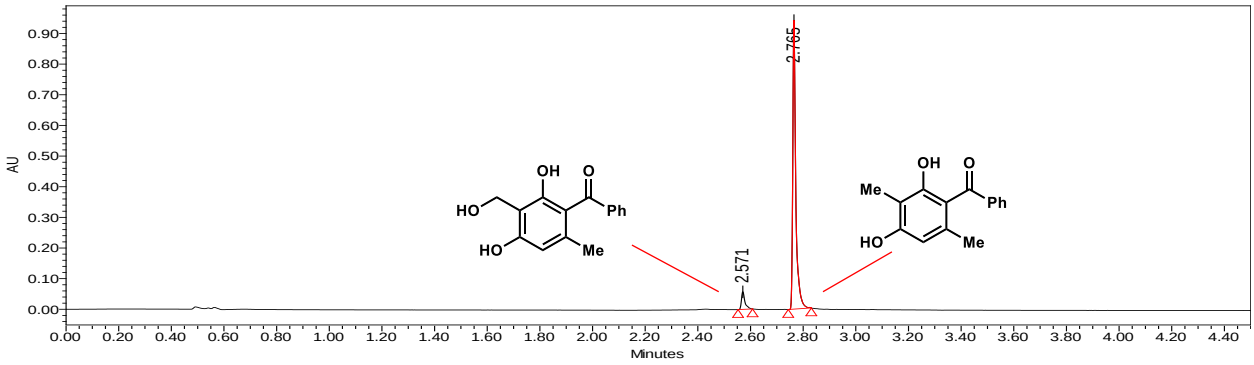

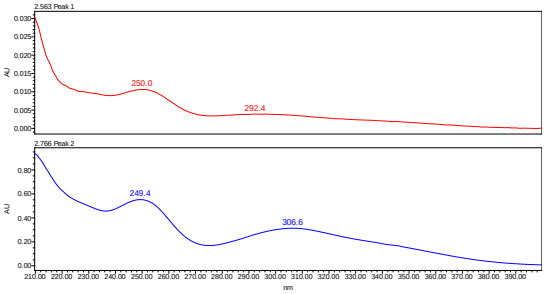

	Retention Time	Area	% Area	Height
1	2.571	52992	6.57	57801
2	2.765	754098	93.43	941895

No Enzyme Control

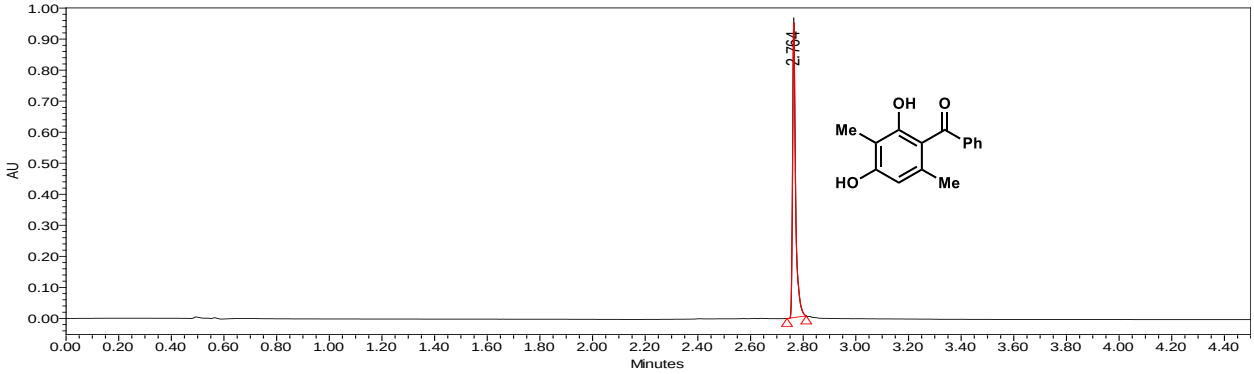

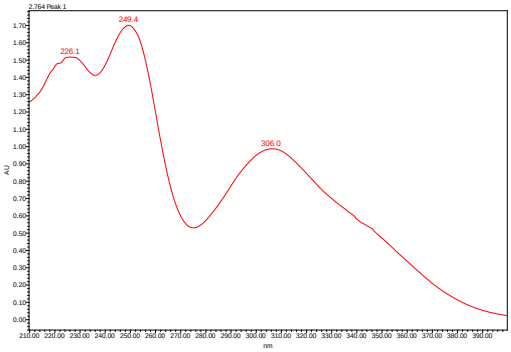

	Retention Time	Area	% Area	Height
1	2.764	764260	100.00	949653

Supplementary Figure S49. Benzylic hydroxylation of **S10** by ClaD. PDA traces of enzymatic reaction and control reaction.

With ClaD

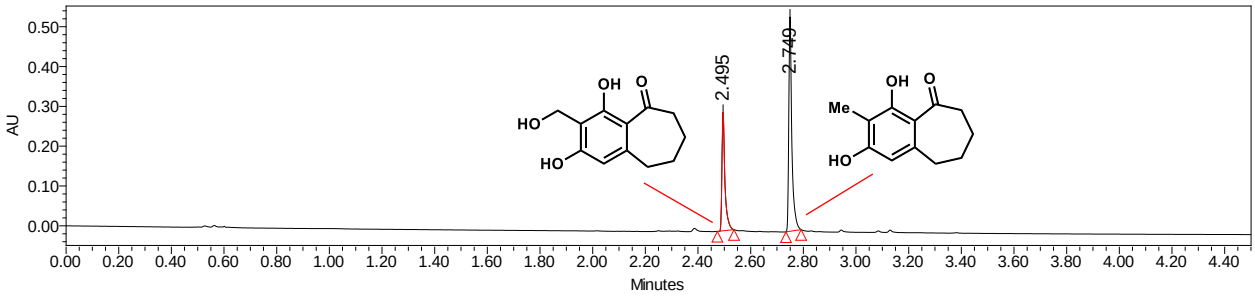

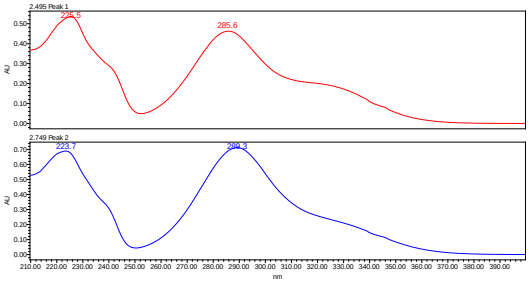

	Retention Time	Area	% Area	Height
1	2.495	234136	35.21	297866
2	2.749	430771	64.79	538897

No Enzyme Control

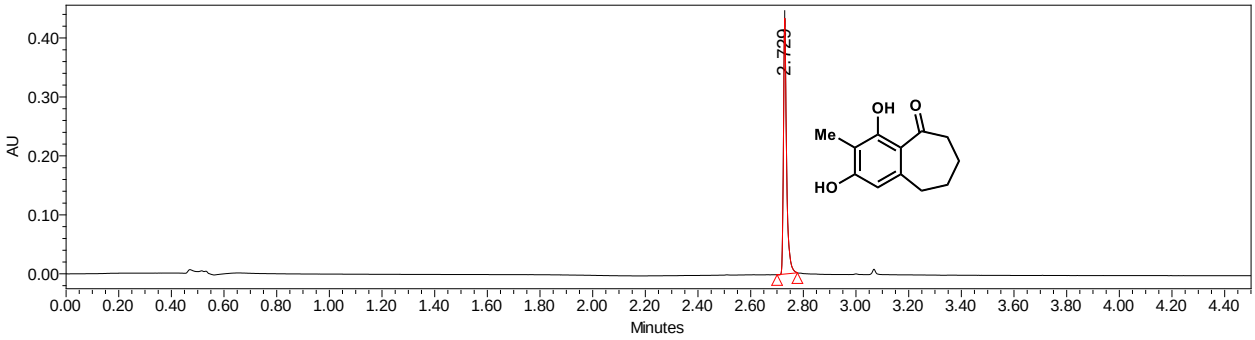

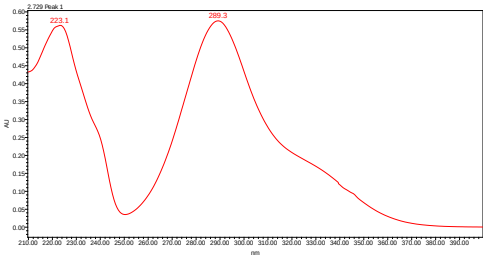

	Retention Time	Area	% Area	Height
1	2.729	354920	100.00	434150

Supplementary Figure S50. Benzylic hydroxylation of **26** by ClaD. PDA traces of enzymatic reaction and control reaction.

With ClaD

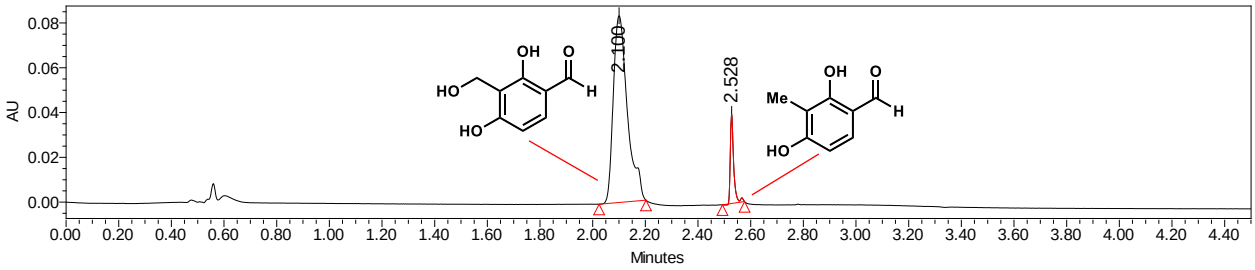

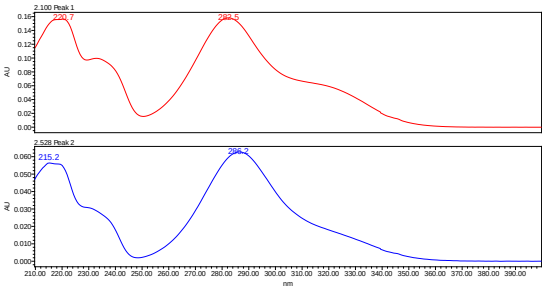

	Retention Time	Area	% Area	Height
1	2.100	311160	89.76	83400
2	2.528	35513	10.24	39781

No Enzyme Control

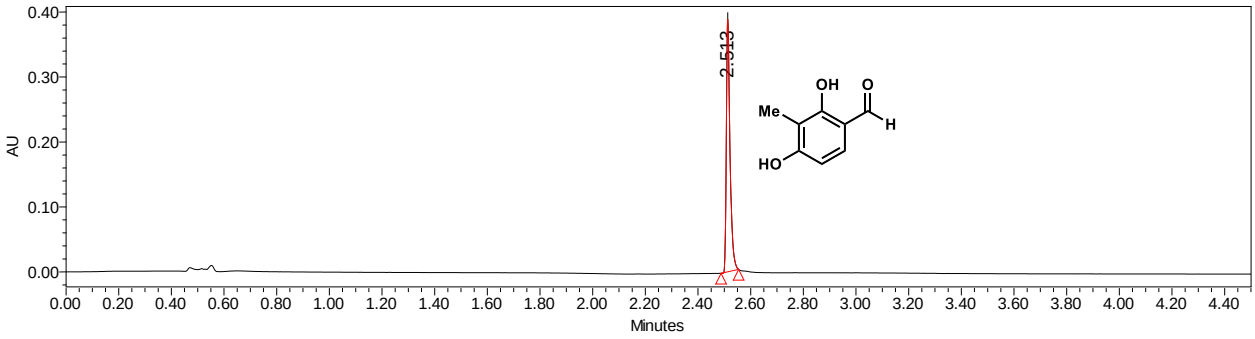

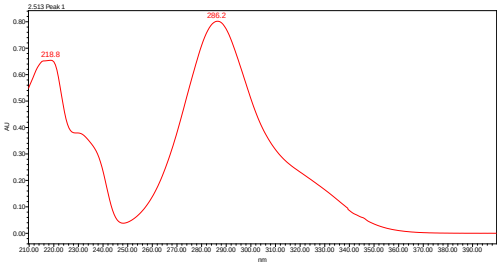

	Retention Time	Area	% Area	Height
1	2.513	374802	100.00	389926

Supplementary Figure S51. Benzylic hydroxylation of **40** by ClaD. PDA traces of enzymatic reaction and control reaction.

With ClaD

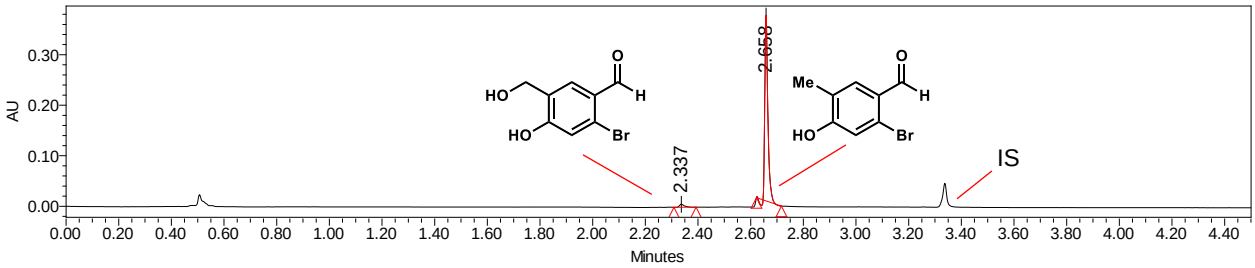

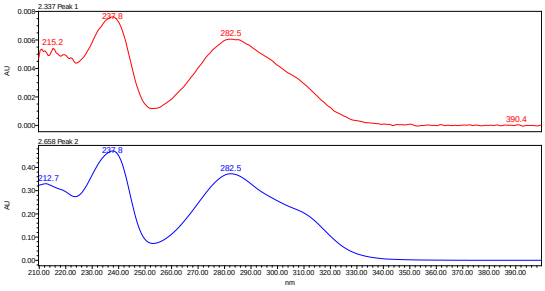

	Retention Time	Area	% Area	Height
1	2.337	7645	2.40	5967
2	2.658	310583	97.60	366569

No Enzyme Control

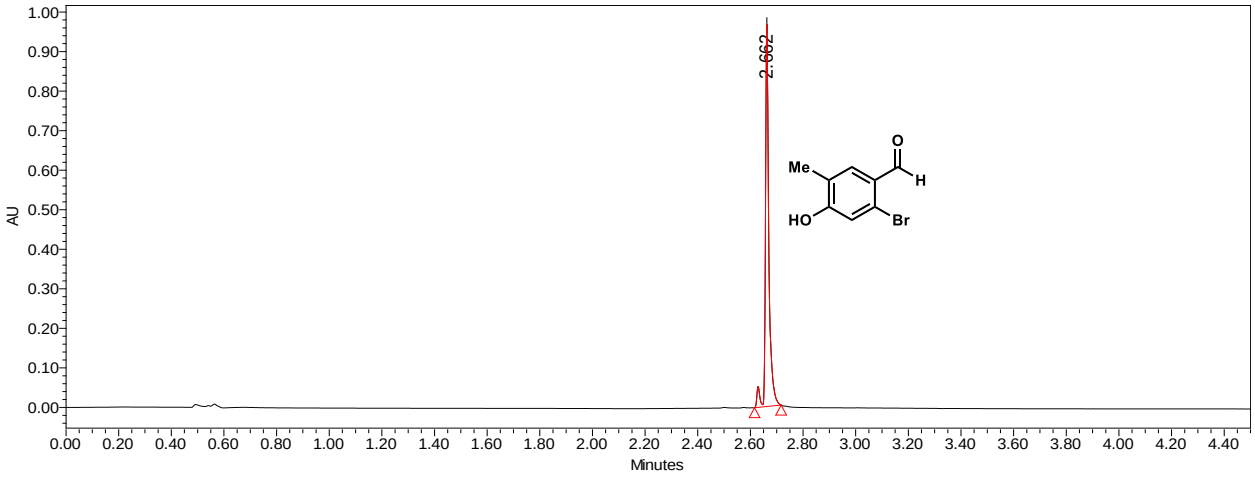

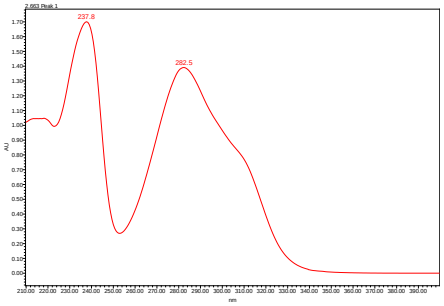

	Retention Time	Area	% Area	Height
1	2.662	880367	100.00	965611

Supplementary Figure S52. Benzylic hydroxylation of **41** by ClaD. PDA traces of enzymatic reaction and control reaction.

With ClaD

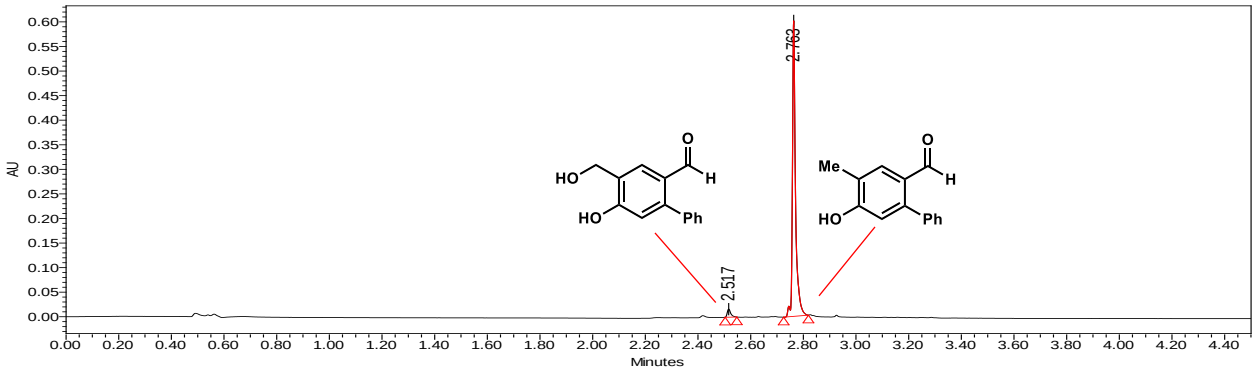

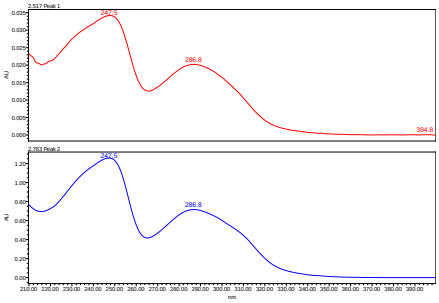

	Retention Time	Area	% Area	Height
1	2.517	15034	2.97	16459
2	2.763	491458	97.03	601297

No Enzyme Control

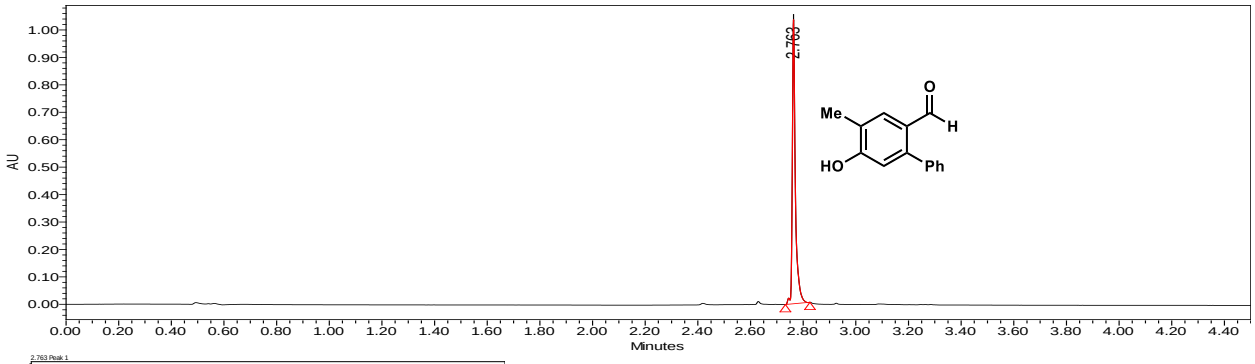

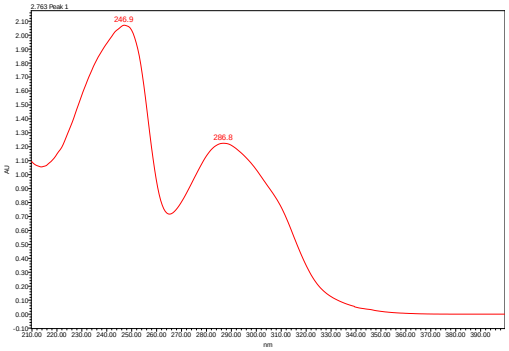

	Retention Time	Area	% Area	Height
1	2.763	832443	100.00	1034833

Supplementary Figure S53. Benzylic hydroxylation of **42** by ClaD. PDA traces of enzymatic reaction and control reaction.

With ClaD

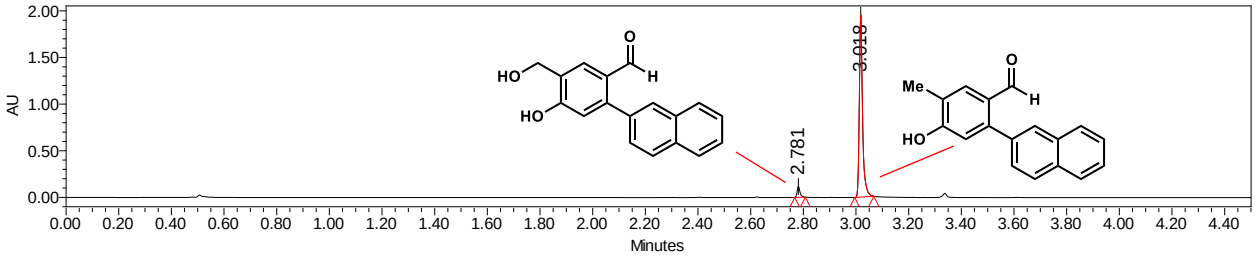

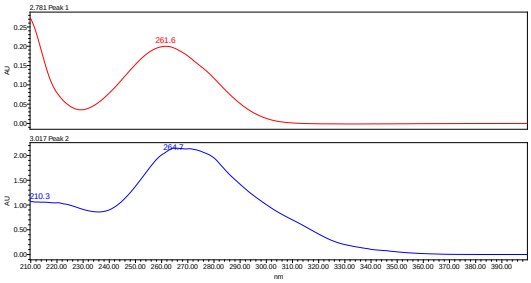

	Retention Time	Area	% Area	Height
1	2.781	87888	5.00	117285
2	3.018	1668633	95.00	1956582

No Enzyme Control

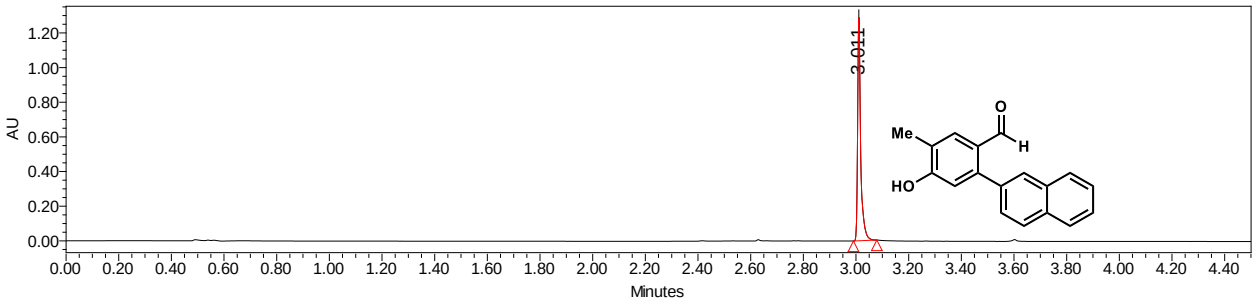

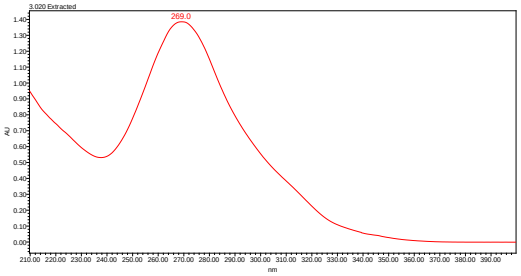

	Retention Time	Area	% Area	Height
1	3.011	1033281	100.00	1288141

Supplementary Figure S54. Benzylic hydroxylation of **S9** by ClaD. PDA traces of enzymatic reaction and control reaction.

With ClaD

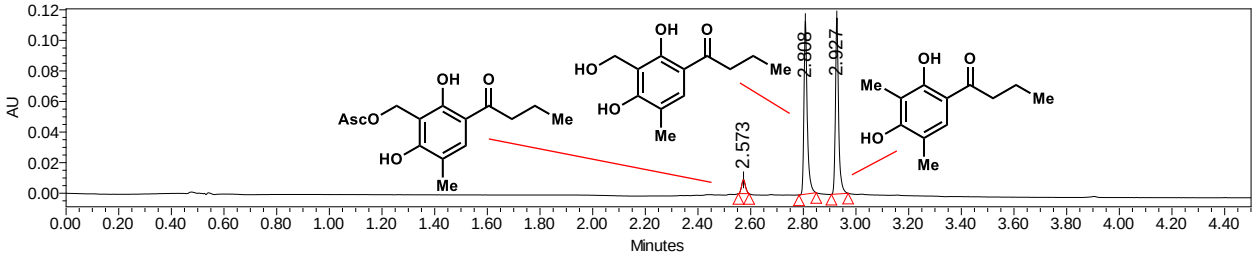

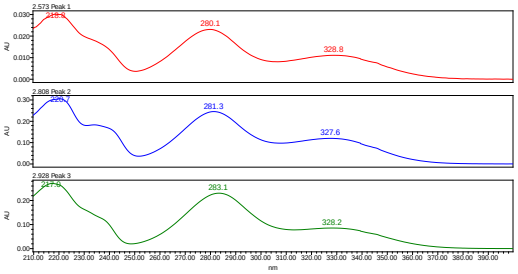

	Retention Time	Area	% Area	Height
1	2.573	9363	4.62	9119
2	2.808	97837	48.29	113182
3	2.927	95393	47.09	115398

No Enzyme Control

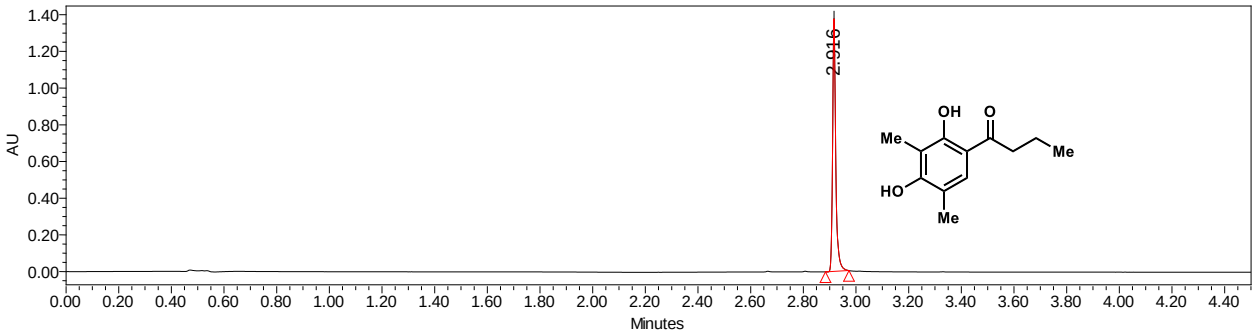

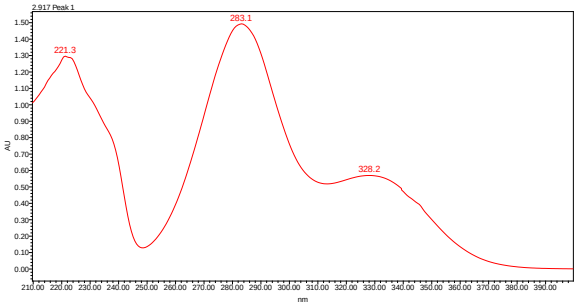

	Retention Time	Area	% Area	Height
1	2.916	1139767	100.00	1378357

Supplementary Figure S55. Benzylic hydroxylation of **27** by ClaD. PDA traces of enzymatic reaction and control reaction.

With ClaD

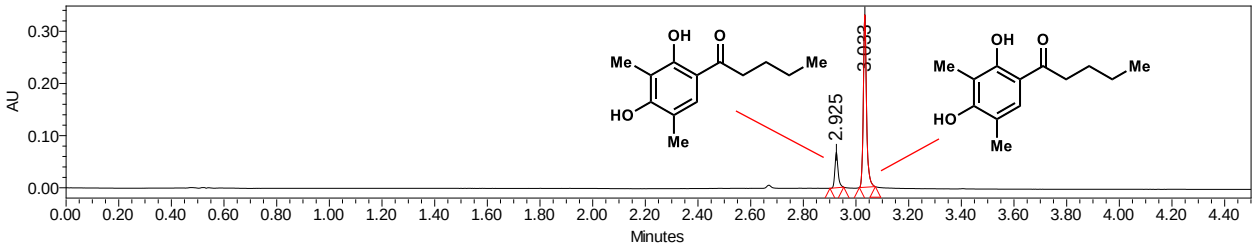

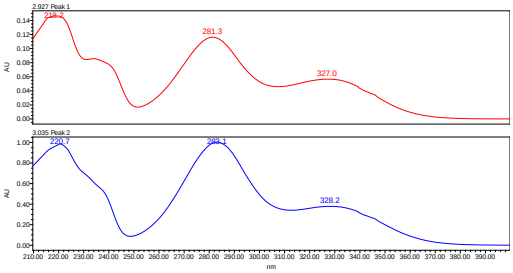

	Retention Time	Area	% Area	Height
1	2.927	39775	12.60	48177
2	3.035	275823	87.40	338915

No Enzyme Control

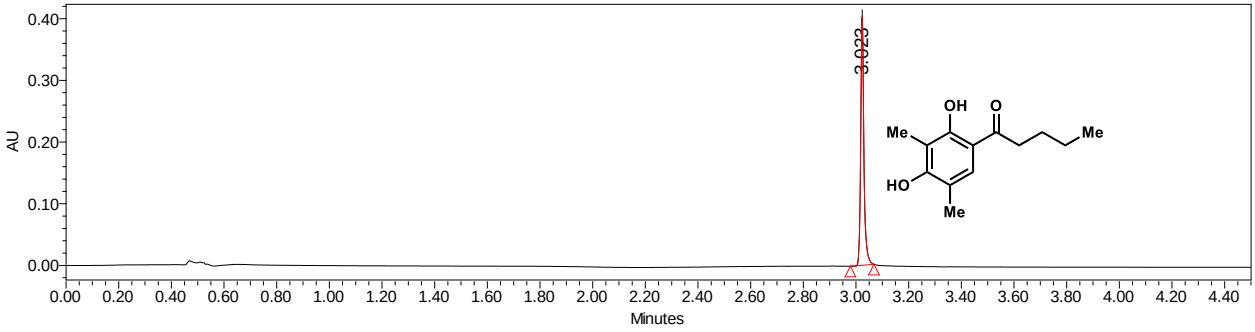

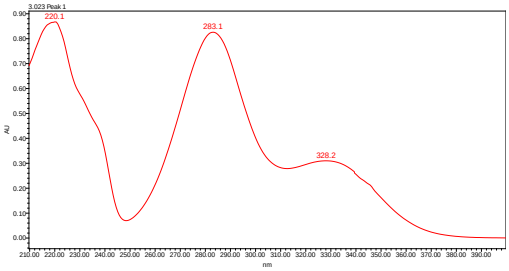

	Retention Time	Area	% Area	Height
1	3.023	339980	100.00	402647

Supplementary Figure S56. Benzylic hydroxylation of **38** by ClaD. PDA traces of enzymatic reaction and control reaction.

With ClaD

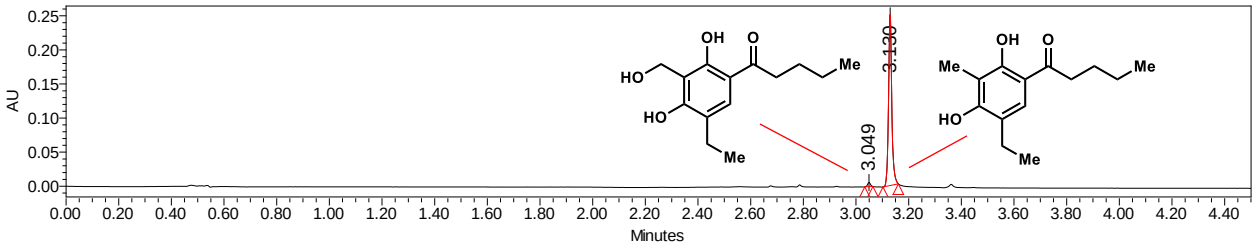

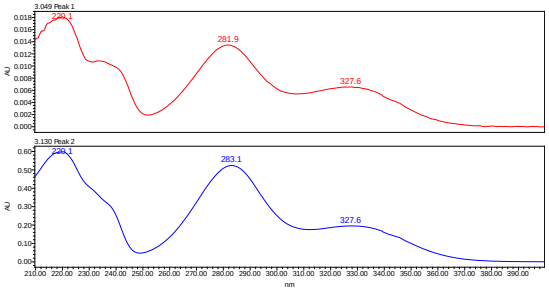

	Retention Time	Area	% Area	Height
1	3.049	4714	2.15	6257
2	3.130	215026	97.85	251237

No Enzyme Control

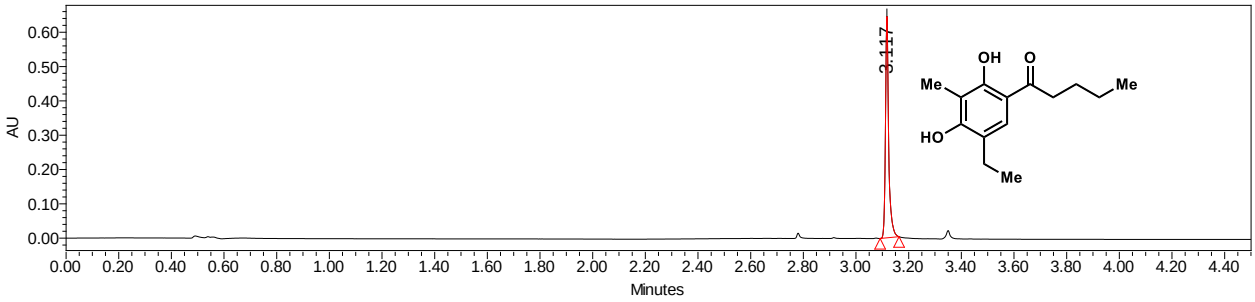

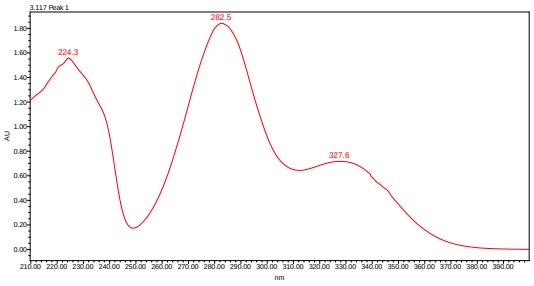

	Retention Time	Area	% Area	Height
1	3.117	543126	100.00	645051

Supplementary Figure S57. Benzylic hydroxylation of **S11** by ClaD. PDA traces of enzymatic reaction and control reaction.

With ClaD

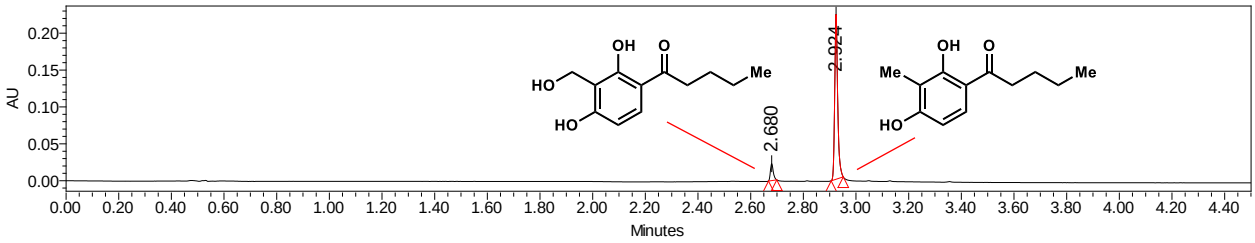

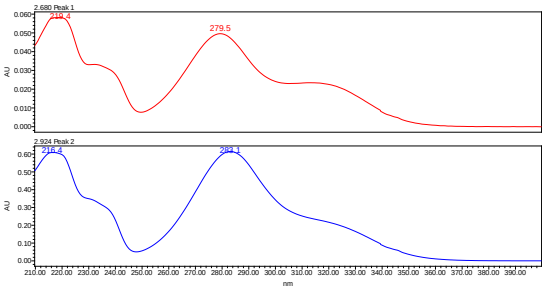

	Retention Time	Area	% Area	Height
1	2.680	17449	9.10	23001
2	2.924	174322	90.90	223470

No Enzyme Control

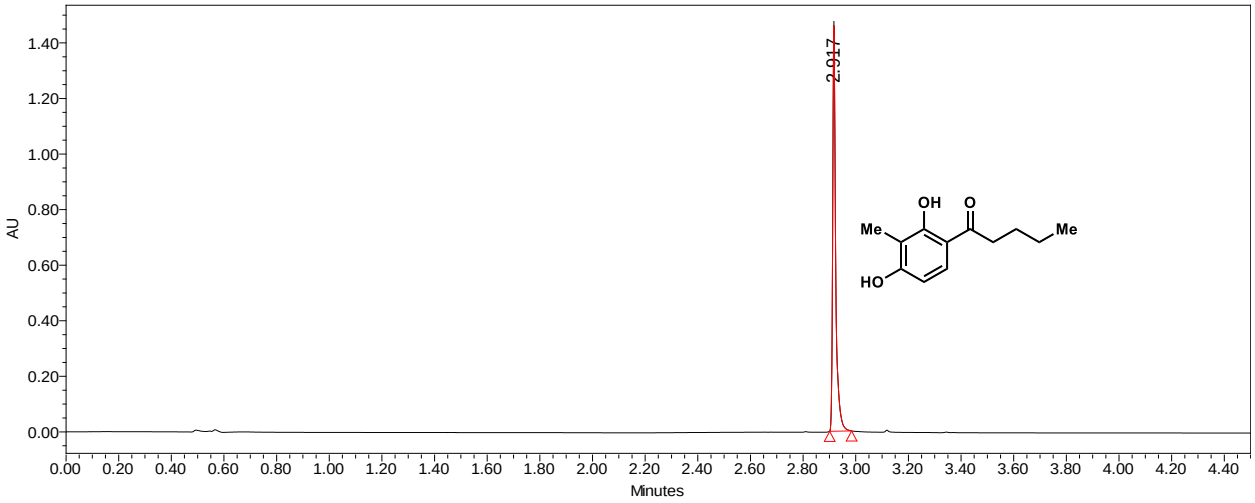

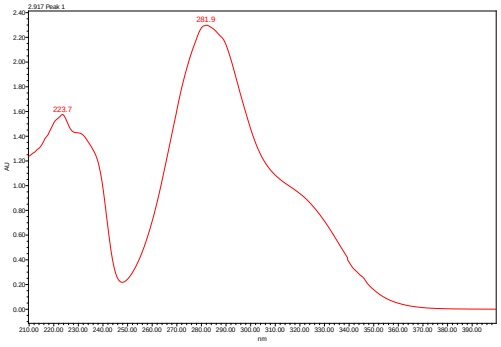

	Retention Time	Area	% Area	Height
1	2.917	1167633	100.00	1462896

Supplementary Figure S58. Benzylic hydroxylation of **S7** by ClaD. PDA traces of enzymatic reaction and control reaction.

With ClaD

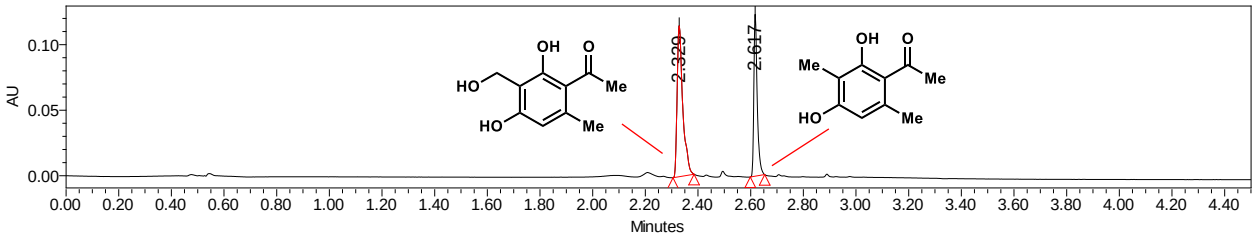

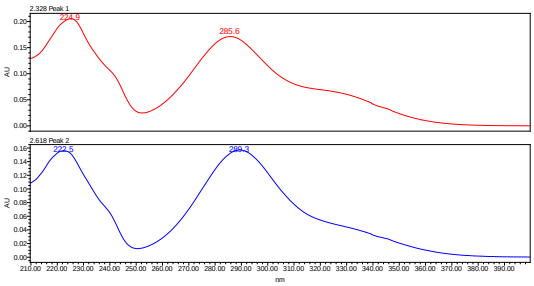

	Retention Time	Area	% Area	Height
1	2.329	171376	61.01	115246
2	2.617	109536	38.99	123736

No Enzyme Control

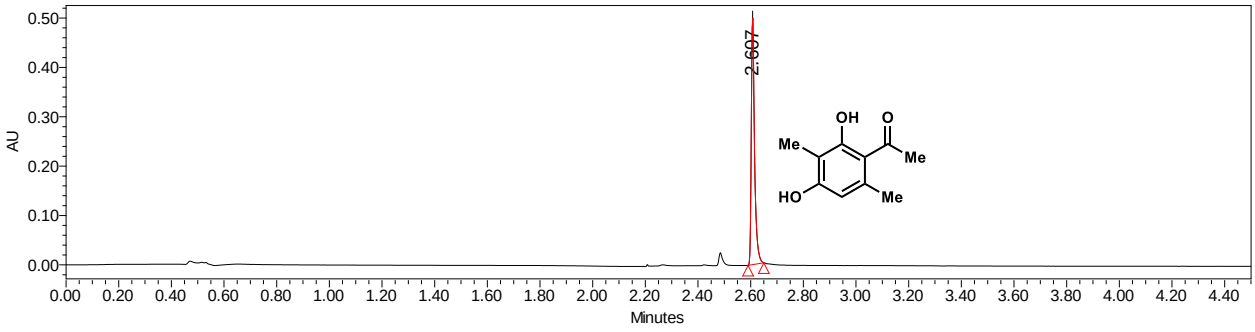

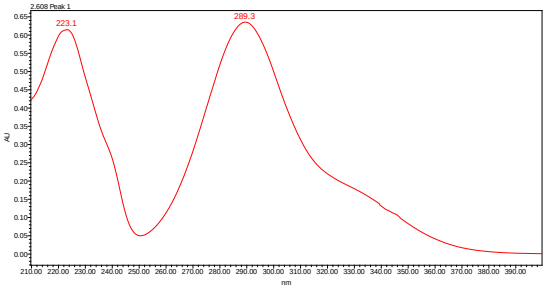

	Retention Time	Area	% Area	Height
1	2.607	428890	100.00	499813

Supplementary Figure S59. Benzylic hydroxylation of **92** by ClaD. PDA traces of enzymatic reaction and control reaction.

With ClaD

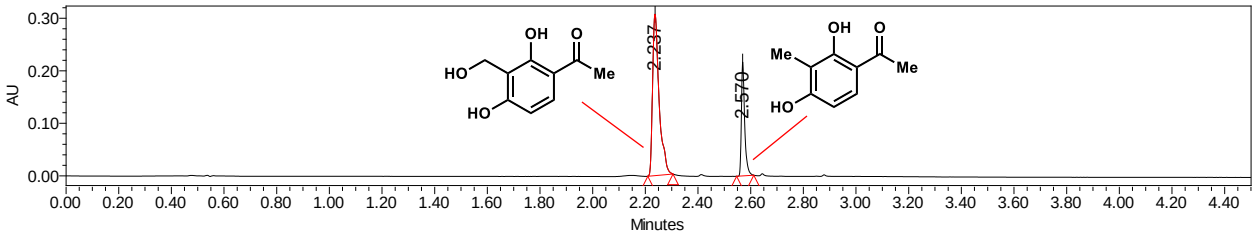

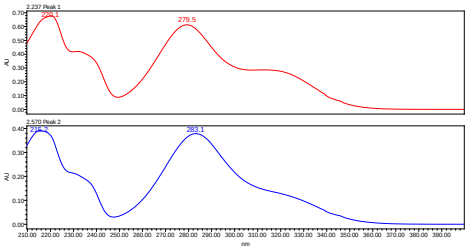

	Retention Time	Area	% Area	Height
1	2.237	531242	73.92	307152
2	2.570	187452	26.08	217040

No Enzyme Control

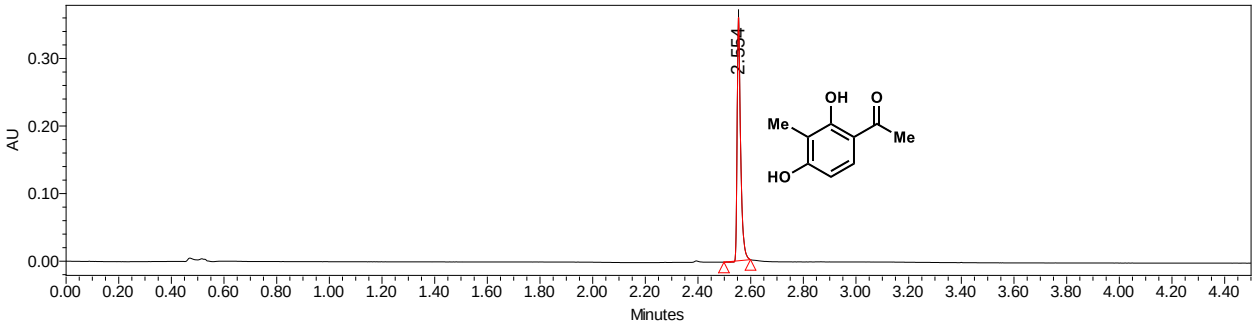

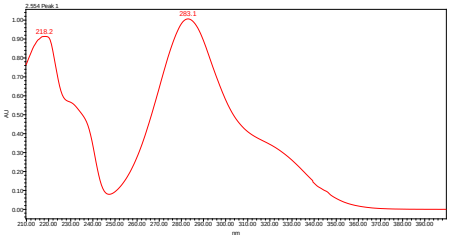

	Retention Time	Area	% Area	Height
1	2.554	329611	100.00	360497

Supplementary Figure S60. Benzylic hydroxylation of **33** by ClaD. PDA traces of enzymatic reaction and control reaction.

With ClaD

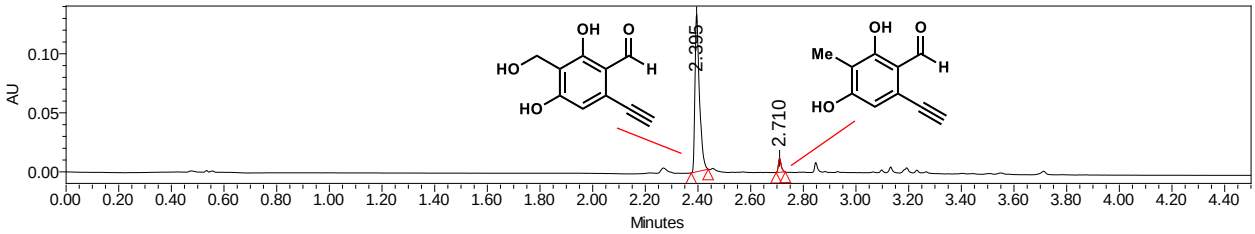

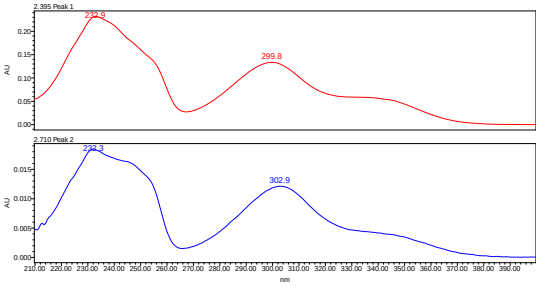

	Retention Time	Area	% Area	Height
1	2.395	156338	95.35	132623
2	2.710	7617	4.65	10921

No Enzyme Control

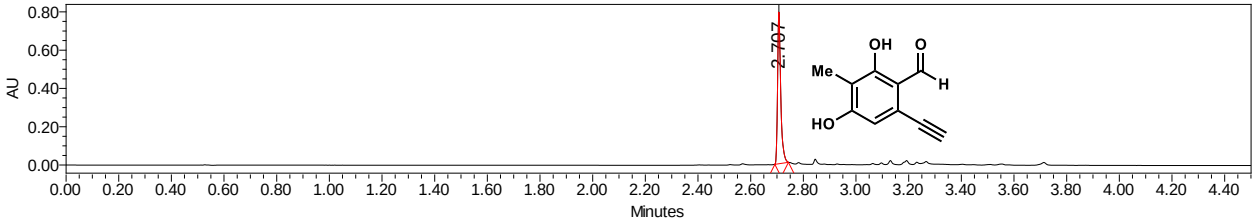

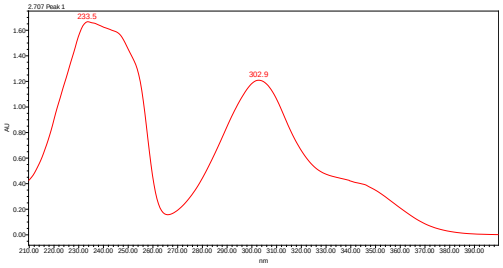

	Retention Time	Area	% Area	Height
1	2.707	658162	100.00	794410

Supplementary Figure S61. Benzylic hydroxylation of **35** by ClaD. PDA traces of enzymatic reaction and control reaction.

With ClaD

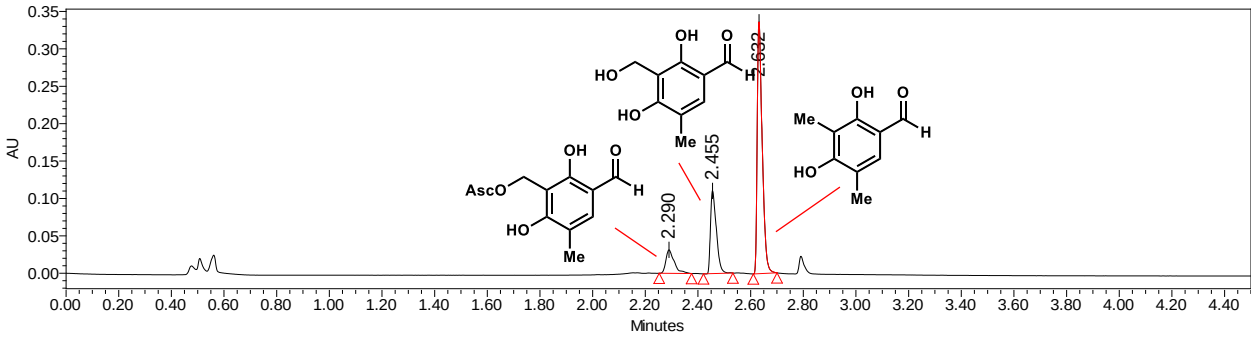

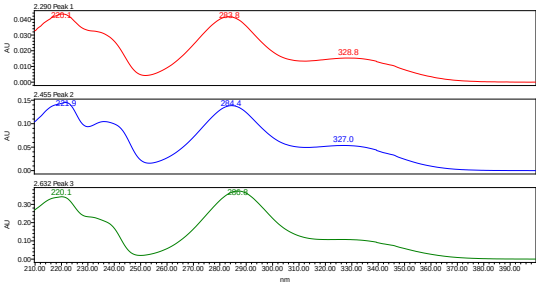

	Retention Time	Area	% Area	Height
1	2.290	69105	10.09	31515
2	2.455	170675	24.92	110968
3	2.632	445078	64.99	336764

No Enzyme Control

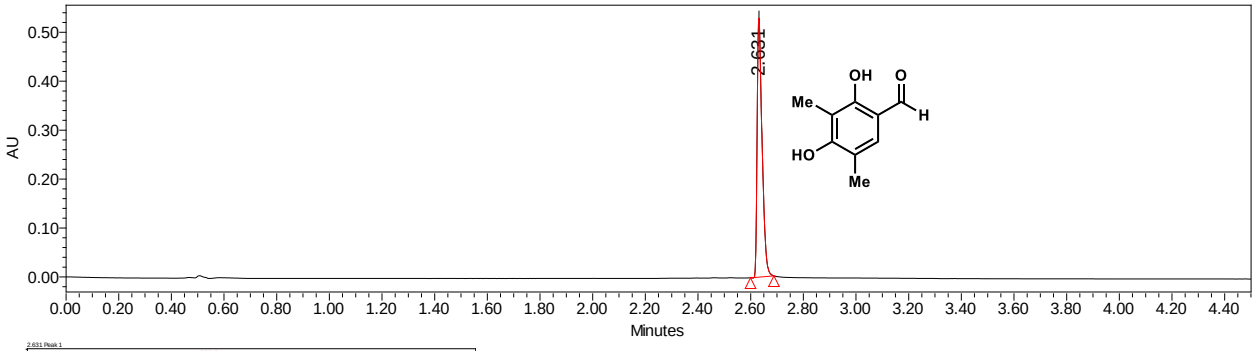

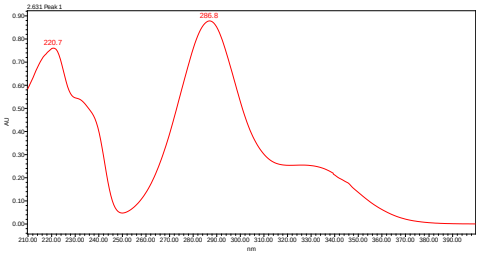

	Retention Time	Area	% Area	Height
1	2.631	693251	100.00	530045

Supplementary Figure S62. Benzylic hydroxylation of **34** by ClaD. PDA traces of enzymatic reaction and control reaction.

With ClaD

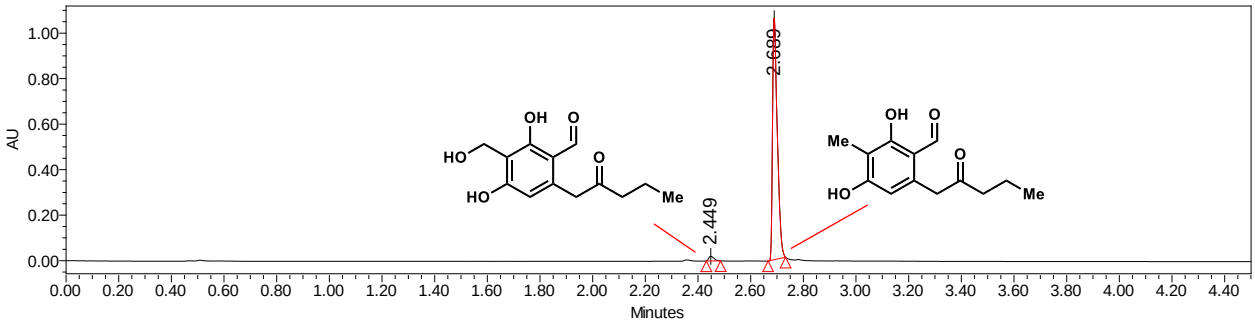

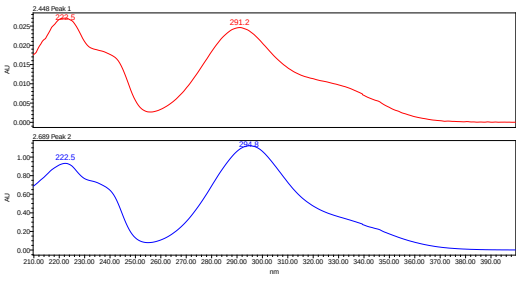

	Retention Time	Area	% Area	Height
1	2.449	28624	2.10	20551
2	2.689	1331934	97.90	1061826

No Enzyme Control

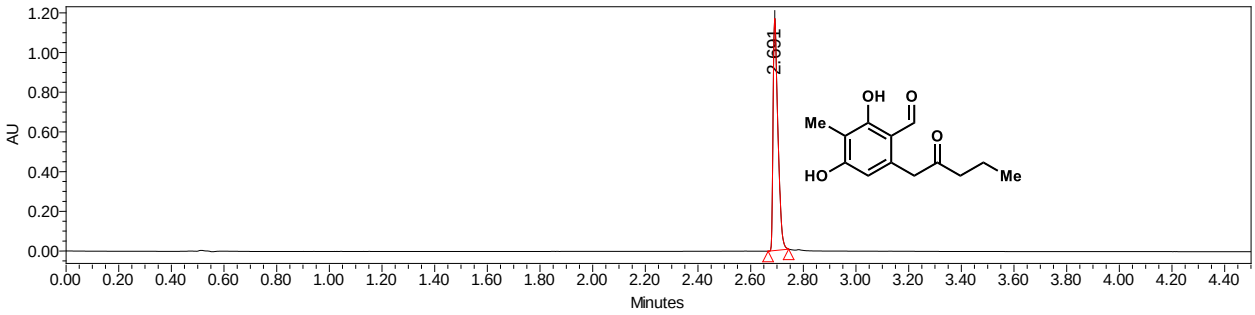

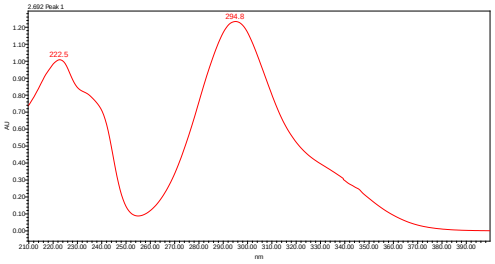

	Retention Time	Area	% Area	Height
1	2.691	1488761	100.00	1169965

Supplementary Figure S63. Characterization of ascorbate adduct from reaction of **36** with ClaD. PDA traces of enzymatic reaction and isolated ascorbate product.

Reaction with ClaD

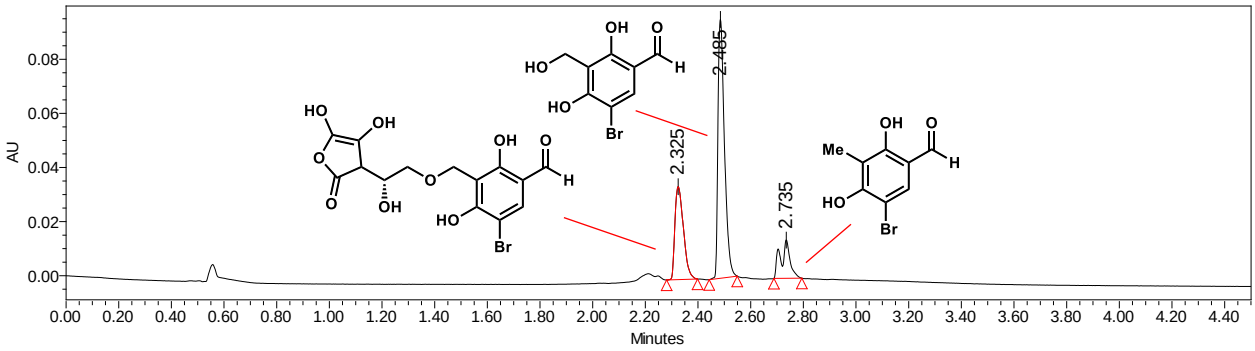

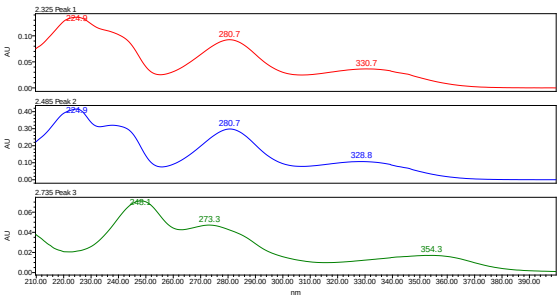

	Retention Time	Area	% Area	Height
1	2.325	77133	27.84	34356
2	2.485	164615	59.42	95691
3	2.735	35309	12.74	14164

Isolated adduct

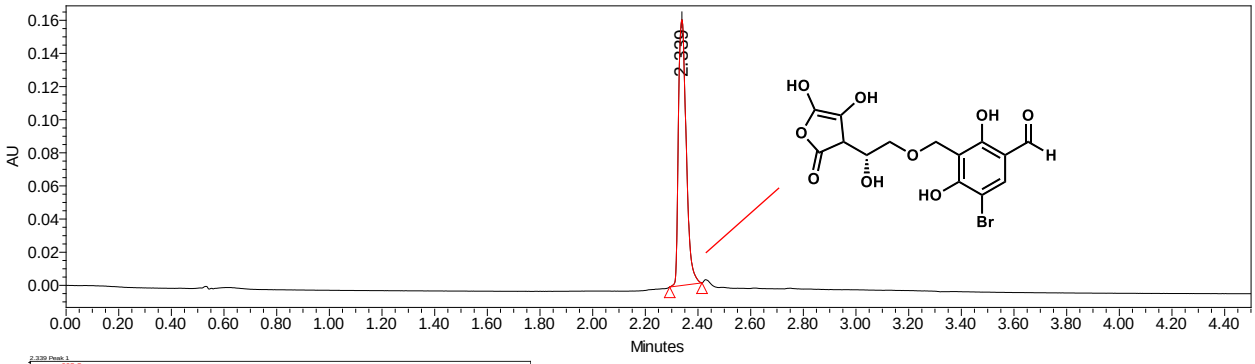

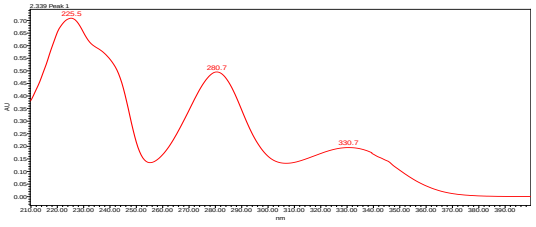

	Retention Time	Area	% Area	Height
1	2.339	328663	100.00	161313

Characterization data for ascorbate adduct S17 (NMR spectra can be found on page S147):
^{1}H NMR (599 MHz, $(CD_3)_2SO$) δ 11.37 (s, 1H), 9.75 (s, 1H), 7.86 (s, 1H), 4.52 (s, 1H), 4.31-4.27 (m, 1H), 4.18 (dd, *J* = 9.4, 6.2 Hz, 1H), 3.92 (dd, *J* = 9.4, 4.1 Hz, 1H), 3.20 (d, *J* = 15.2 Hz, 1H), 2.98 (d, *J* = 15.2 Hz, 1H); **^{13}C NMR** (151 MHz, $(CD_3)_2SO$) δ 173.4, 160.7, 136.3, 116.2, 112.1, 107.5, 102.3, 87.7, 79.3, 75.3, 74.2, 61.5 28.8, 24.9; **HRMS (ESI)** *m/z*: $[M+H]^+$ calculated for $C_{14}H_{14}O_9Br^+$ 404.9816, found 404.9819; **IR** (thin film): 3391, 2256, 1653, 1048, 1023, 993, 824, 762, 609 cm^{-1}.

Part IX. UPLC traces for CitB or ClaD benzylic functionalization cascade reactions

Supplementary Figure S64. Generation of **20** by in situ functionalization of benzylic alcohol **17**. PDA traces of enzymatic reaction analyzed at 300 nm.

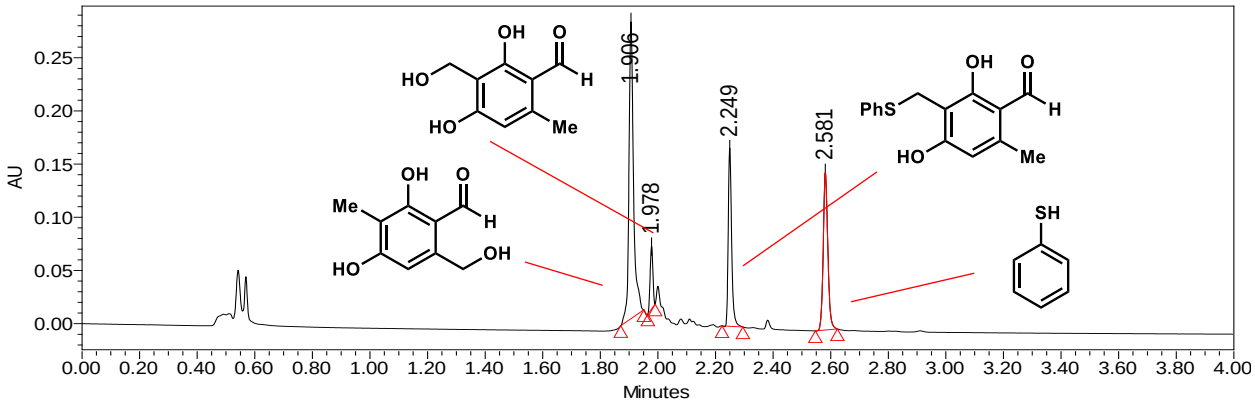

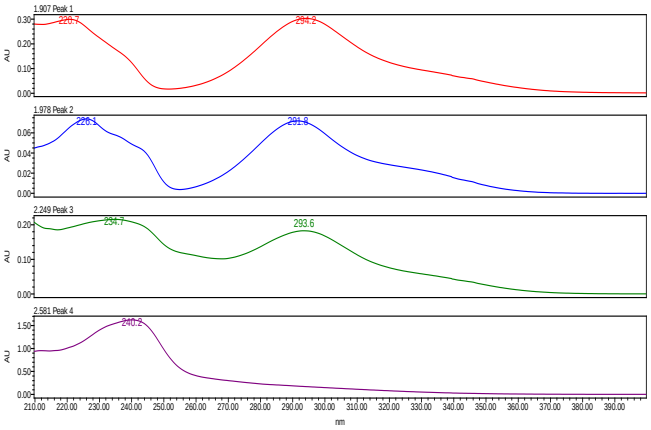

	Retention Time	Area	% Area	Height
1	1.906	309186	47.62	279592
2	1.978	39410	6.07	59128
3	2.249	136155	20.97	167599
4	2.581	164504	25.34	148190

Product Standard

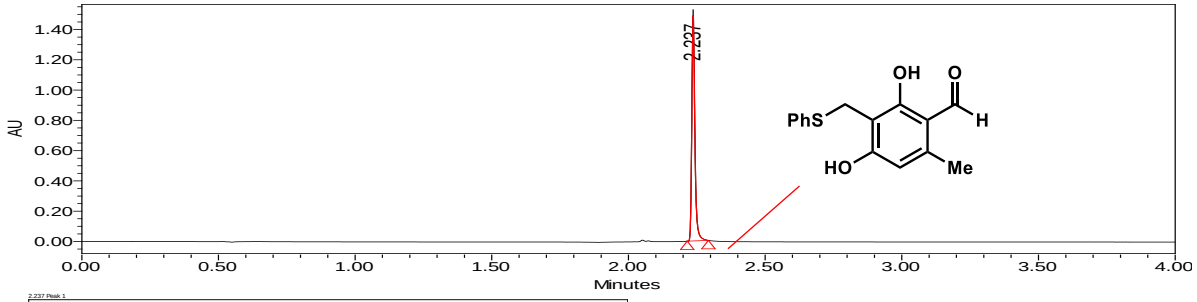

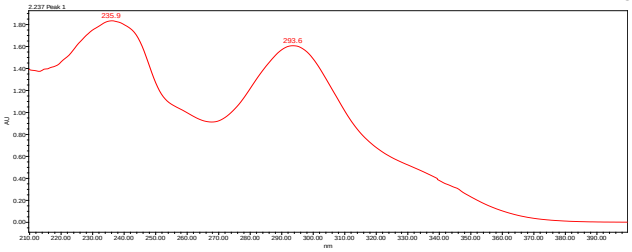

	Retention Time	Area	% Area	Height
1	2.237	1179174	100.00	1486508

Supplementary Figure S65 Generation of **74** by in situ functionalization of benzylic alcohol **17**. PDA traces of enzymatic reaction analyzed at 300 nm.

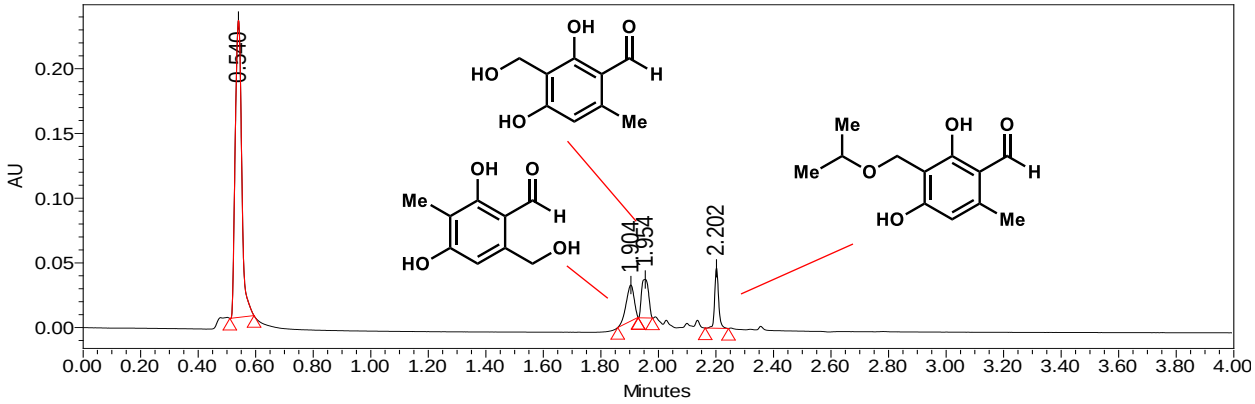

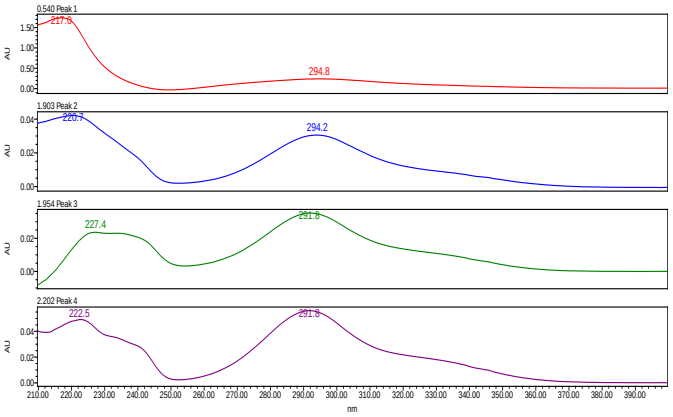

	Retention Time	Area	% Area	Height
1	0.540	358000	70.88	229495
2	1.904	53153	10.52	27838
3	1.954	50460	9.99	29724
4	2.202	43458	8.60	46409

Product Standard

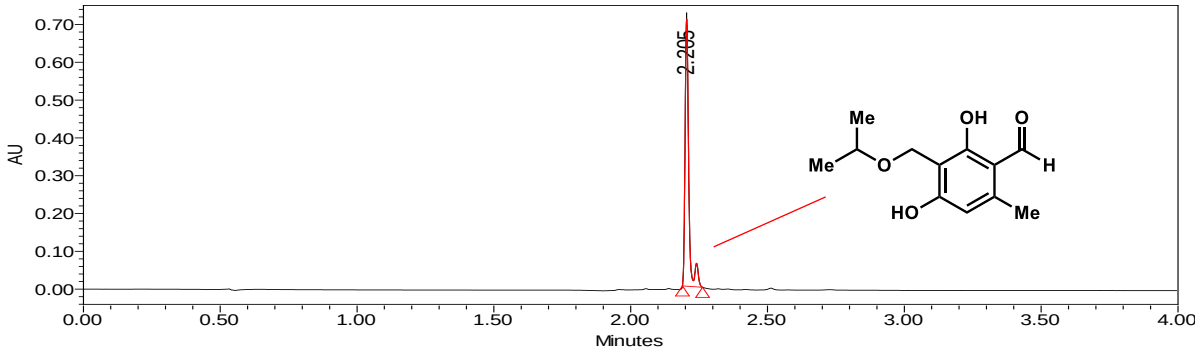

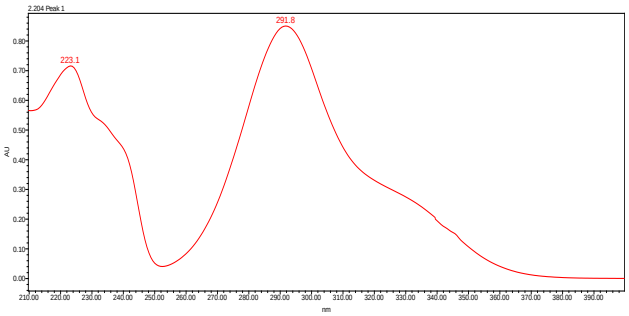

	Retention Time	Area	% Area	Height
1	2.205	663414	100.00	707988

Supplementary Figure S66. Generation of **73** by in situ functionalization of benzylic alcohol **17**. PDA traces of enzymatic reaction analyzed at 300 nm.

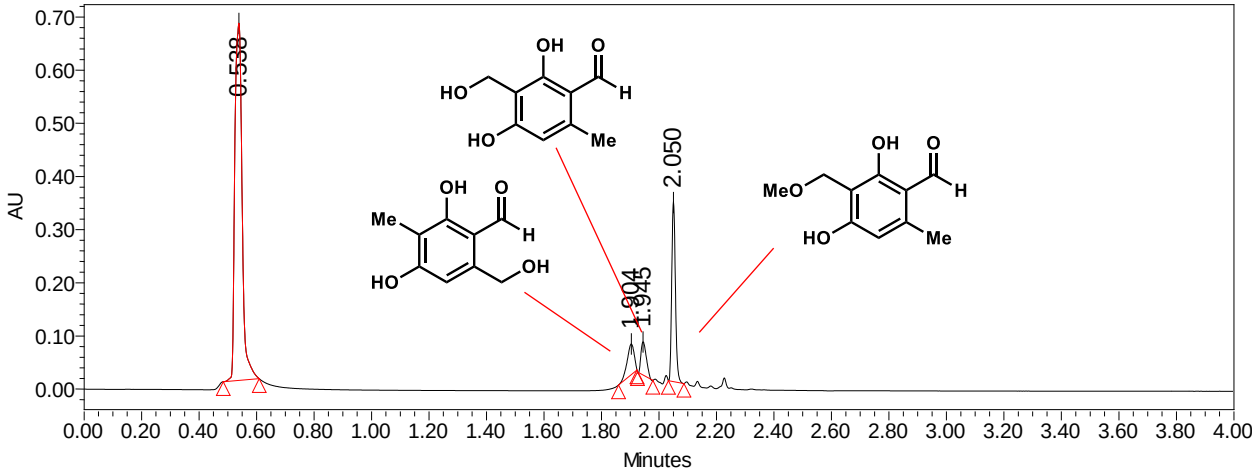

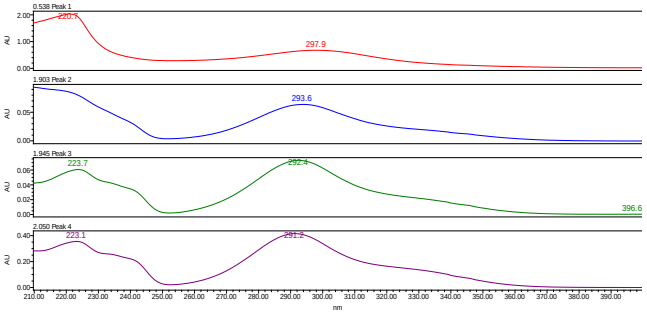

	Retention Time	Area	% Area	Height
1	0.538	1178917	71.01	671933
2	1.904	97978	5.90	57828
3	1.945	82146	4.95	62552
4	2.050	301185	18.14	338785

Product Standard

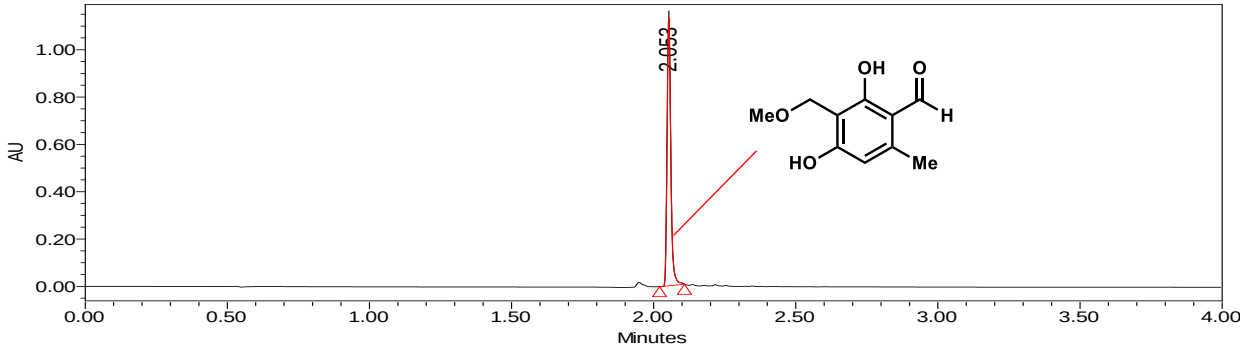

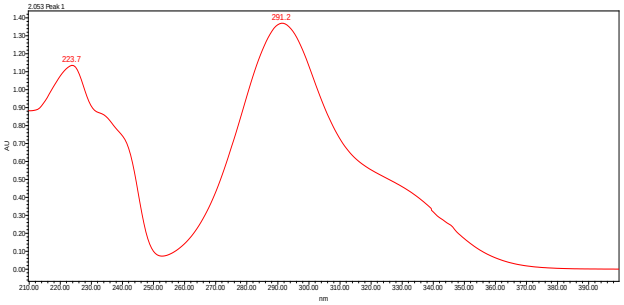

	Retention Time	Area	% Area	Height
1	2.053	1038651	100.00	1131436

Supplementary Figure S67. Generation of **75** by in situ functionalization of benzylic alcohol **17**. PDA traces of enzymatic reaction analyzed at 300 nm.

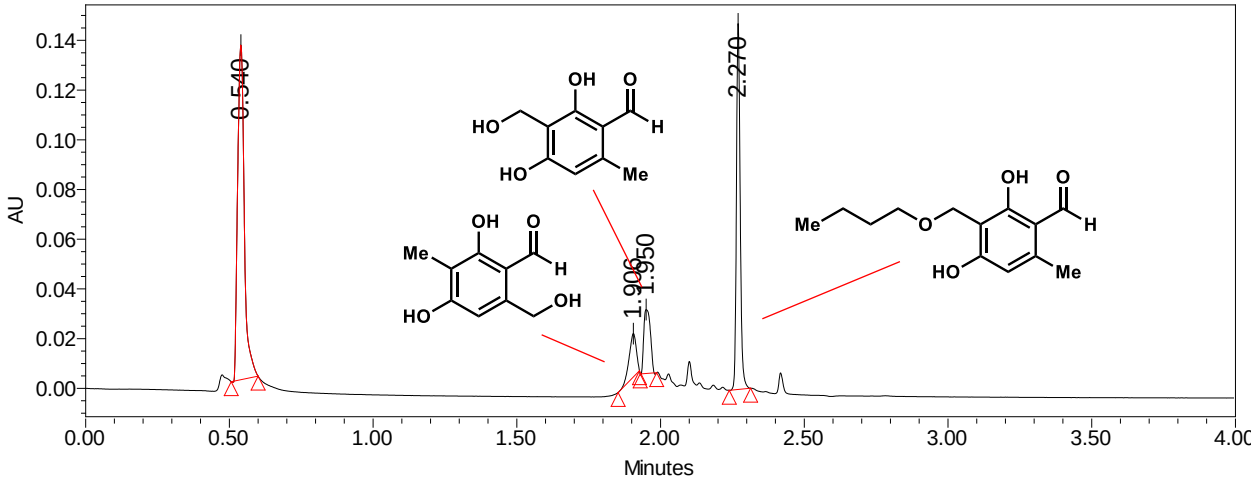

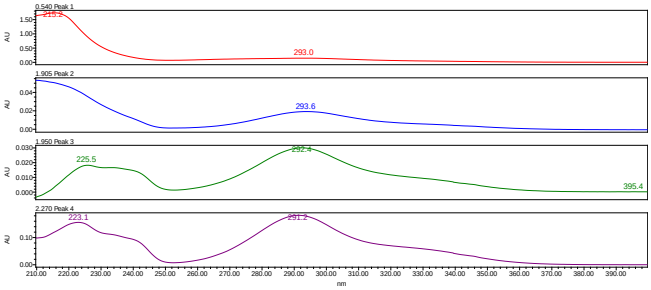

	Retention Time	Area	% Area	Height
1	0.540	217704	51.57	134654
2	1.906	30105	7.13	17480
3	1.950	41174	9.75	25714
4	2.270	133156	31.54	147141

Product Standard

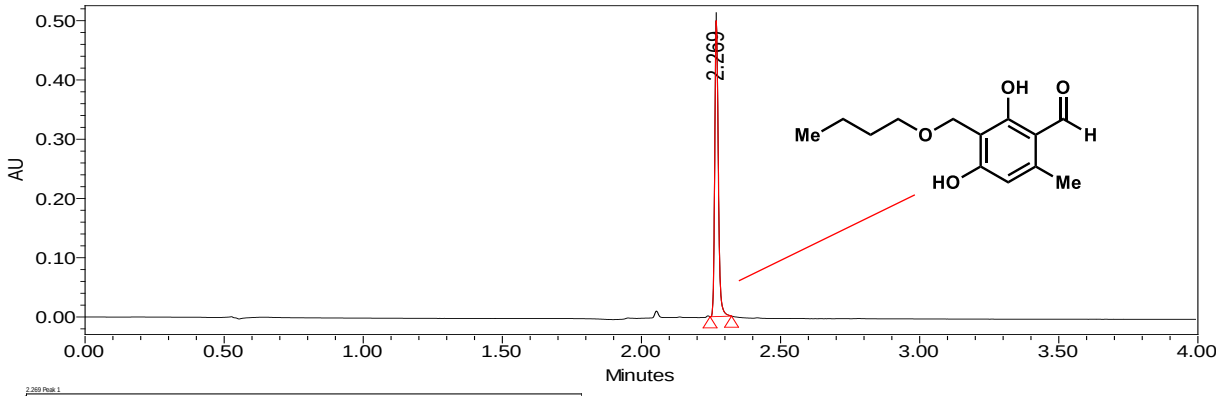

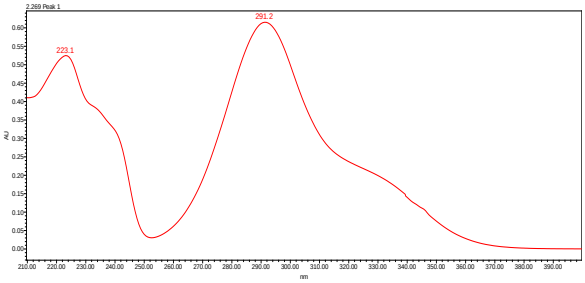

	Retention Time	Area	% Area	Height
1	2.269	445637	100.00	499328

Supplementary Figure S68. Generation of **77** by in situ functionalization of benzylic alcohol **17**. PDA traces of enzymatic reaction analyzed at 300 nm.

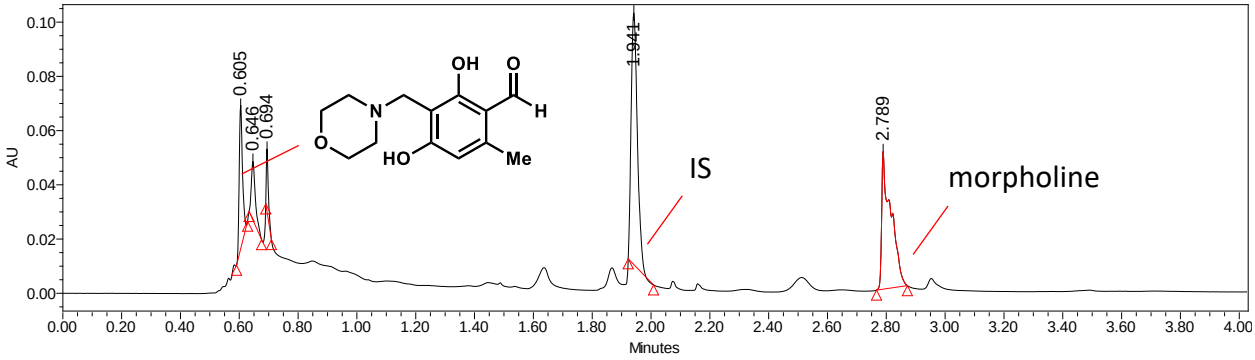

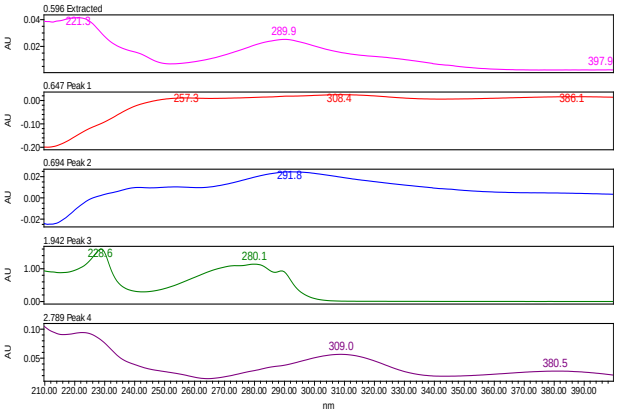

	Retention Time	Area	% Area	Height
1	0.605	37602	10.48	50739
2	0.646	27255	7.60	24885
3	0.694	22399	6.24	34536
4	1.941	163933	45.70	100322
5	2.789	107496	29.97	49217

Product Standard (300 nm)

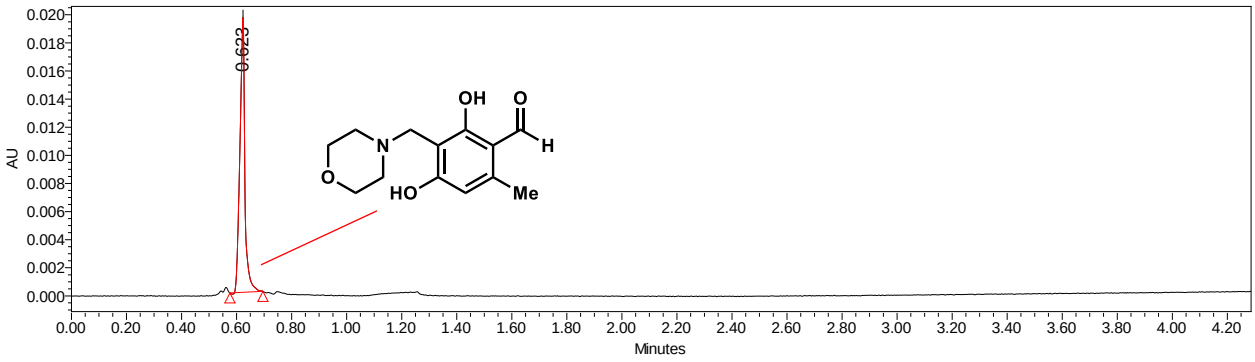

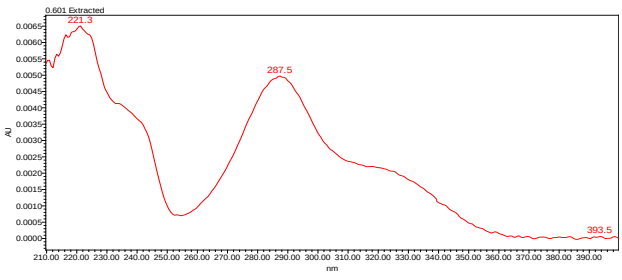

	Retention Time	Area	% Area	Height
1	0.623	24886	100.00	19617

Supplementary Figure S69. Generation of **78** and **79** by in situ functionalization of benzylic alcohol **17**. PDA traces of enzymatic reaction analyzed at 300 nm.

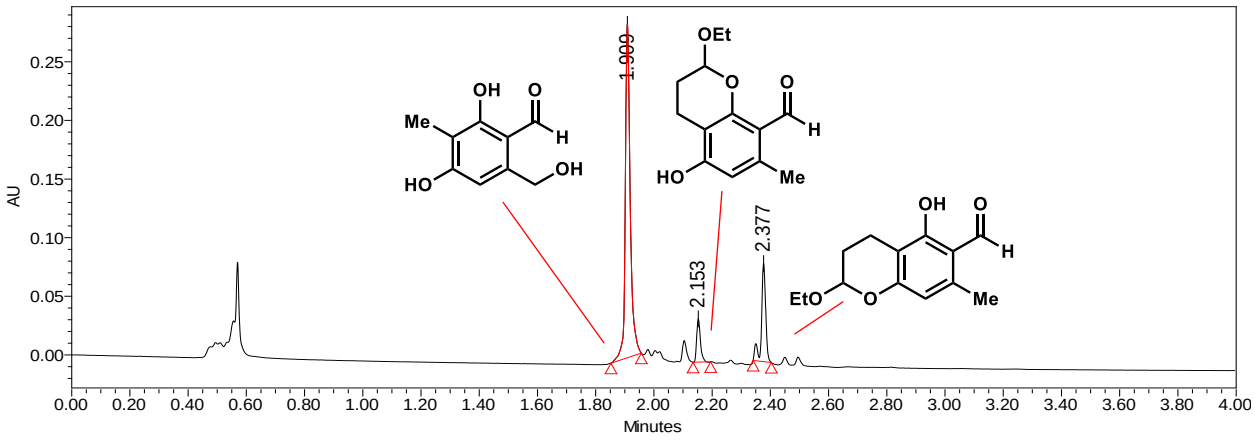

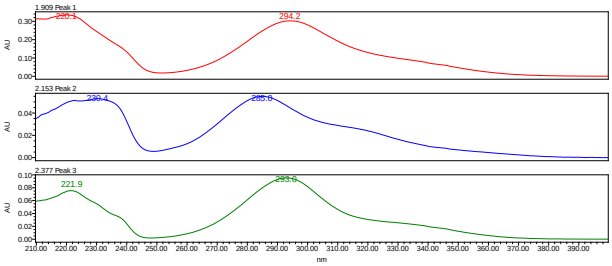

	Retention Time	Area	% Area	Height
1	1.909	337063	73.92	284770
2	2.153	33190	7.28	36905
3	2.377	85721	18.80	83776

Product Standard A (300 nm)

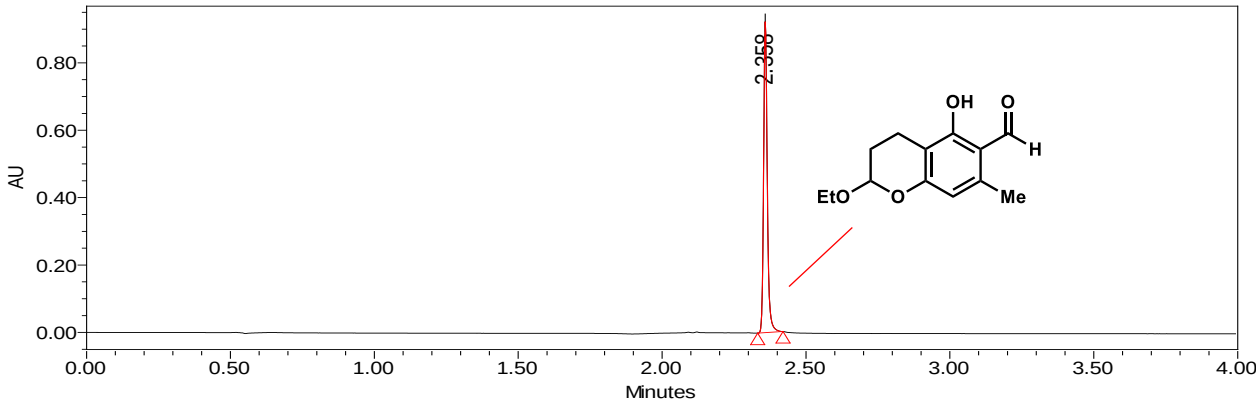

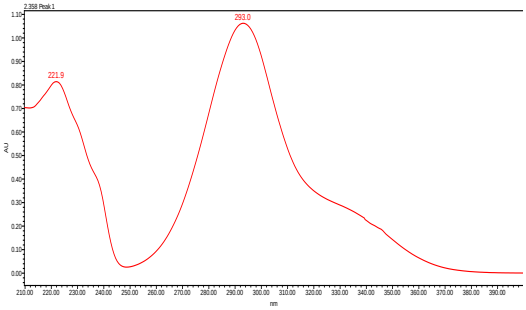

	Retention Time	Area	% Area	Height
1	2.358	623683	100.00	736773

Product Standard B (300 nm)

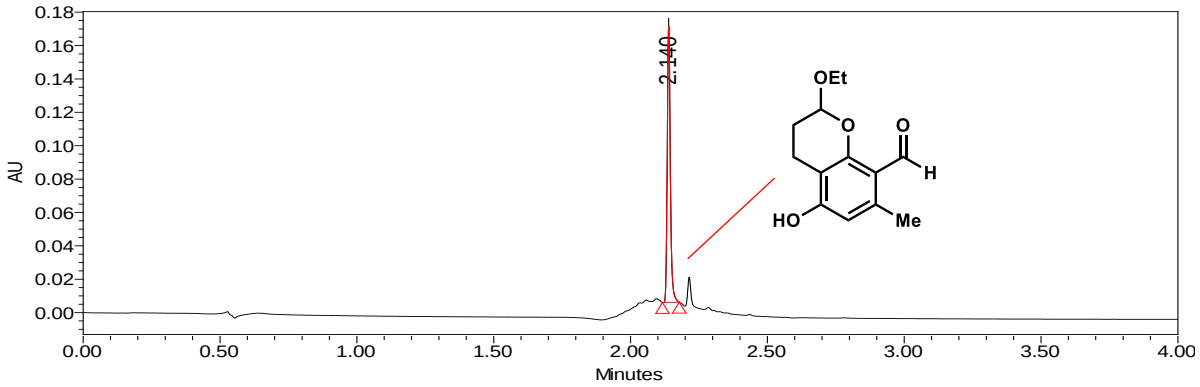

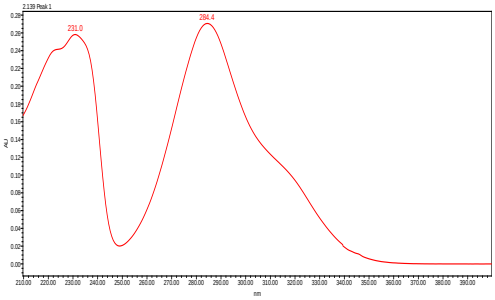

	Retention Time	Area	% Area	Height
1	2.140	129934	100.00	165772

Supplementary Figure S70. Generation of **80** and **81** by in situ functionalization of benzylic alcohol **17**. PDA traces of enzymatic reaction analyzed at 300 nm.

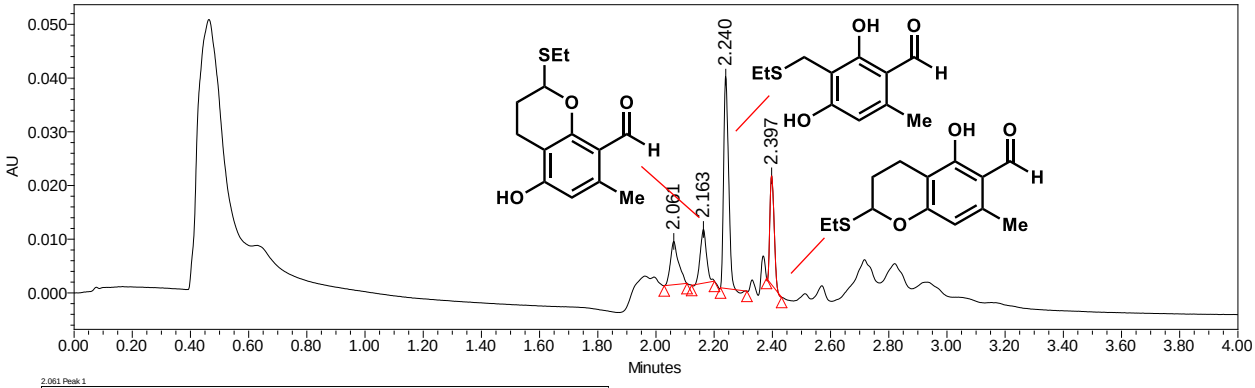

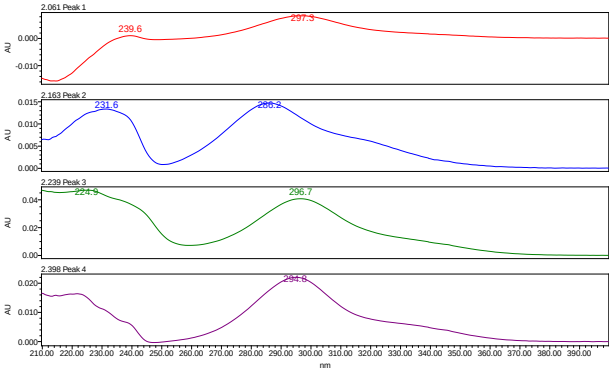

	Retention Time	Area	% Area	Height
1	2.061	15479	15.72	8080
2	2.163	15048	15.28	10019
3	2.240	47127	47.86	39579
4	2.397	20805	21.13	20289

Product Standard A at (300 nm)

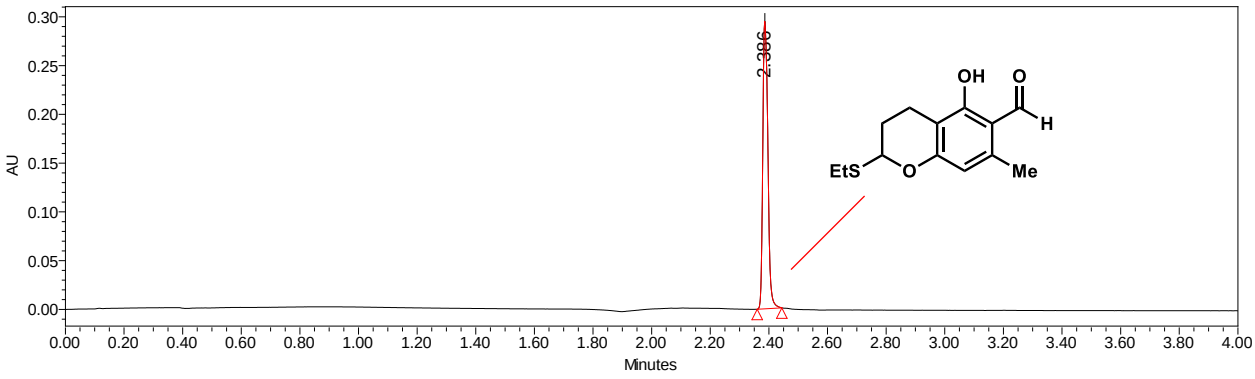

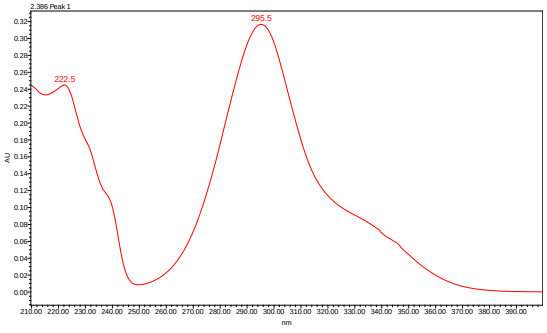

	Retention Time	Area	% Area	Height
1	2.386	354591	100.00	294946

Product Standard B (280 nm)

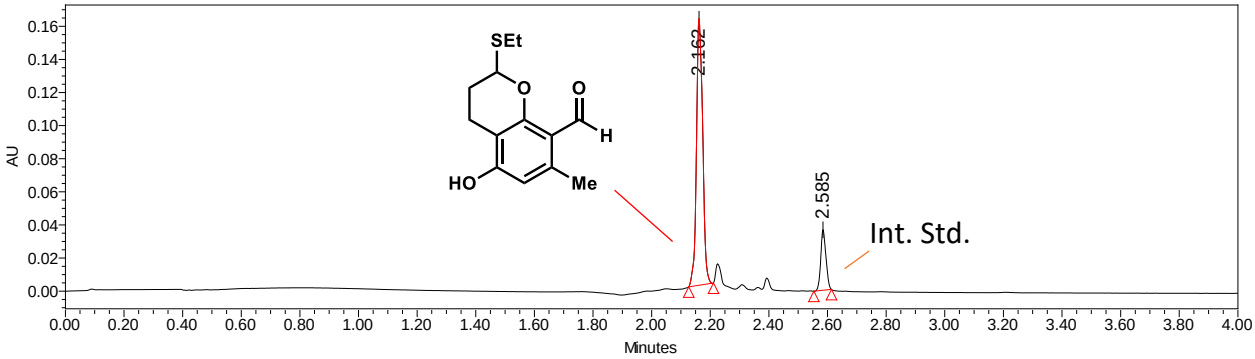

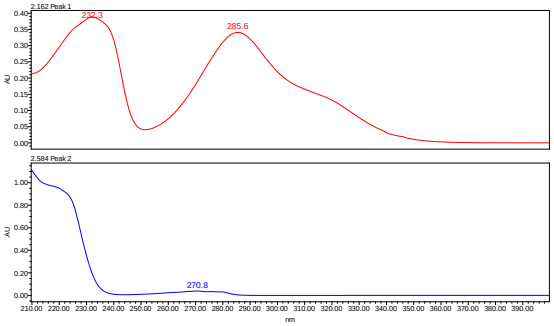

	Retention Time	Area	% Area	Height
1	2.162	237852	84.14	160927
2	2.585	44841	15.86	36598

Supplementary Figure S71. Generation of **82** and **83** by in situ functionalization of benzylic alcohol **17**. PDA traces of enzymatic reaction analyzed at 300 nm.

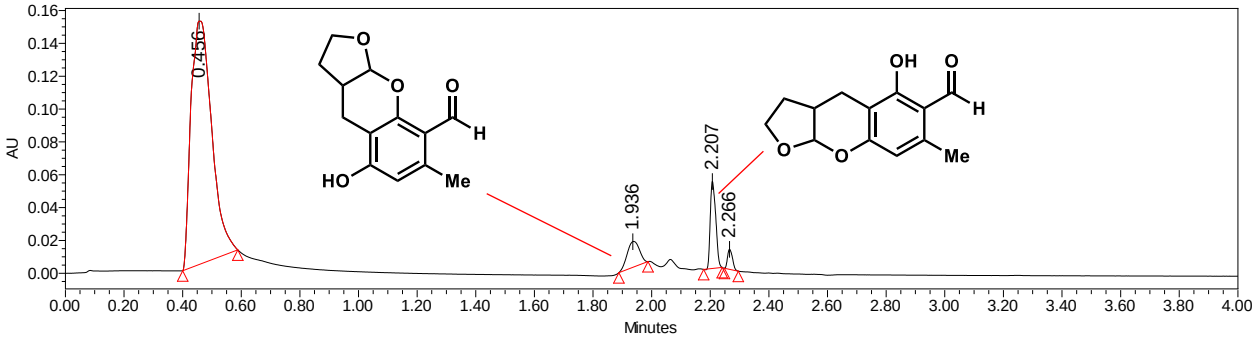

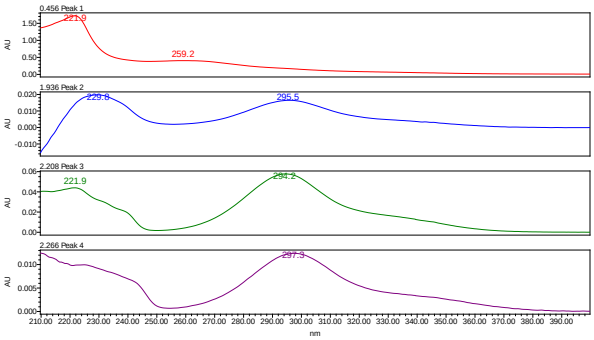

	Retention Time	Area	% Area	Height
1	0.456	727787	84.98	148137
2	1.936	45573	5.32	15630
3	2.207	68820	8.04	53066
4	2.266	14250	1.66	12202

Product Standard A (300 nm)

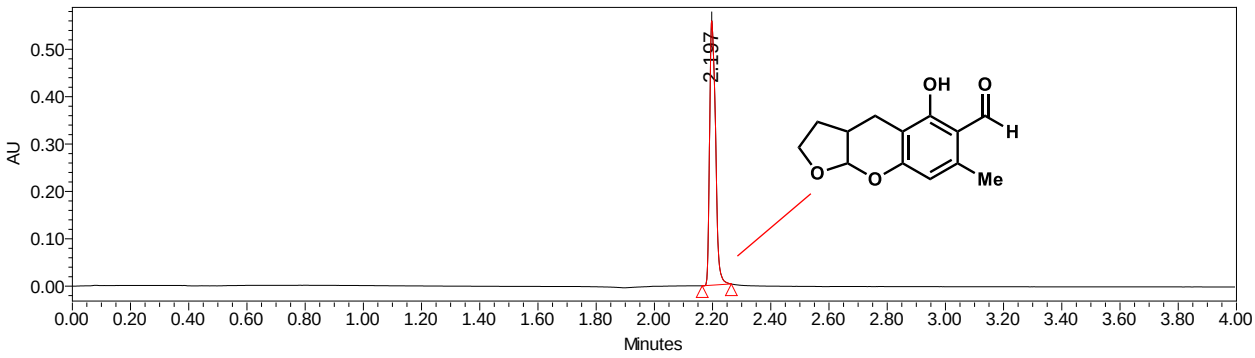

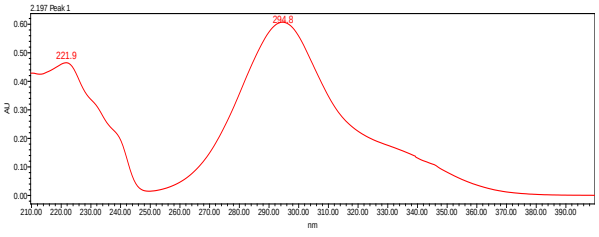

	Retention Time	Area	% Area	Height
1	2.197	786523	100.00	559085

Supplementary Figure S72. Synthesis of (-)-xyloketal D (**15**) and the diastereomer of (-)-xyloketal D **95** by in situ functionalization of benzylic alcohol **60**. PDA traces of enzymatic reaction analyzed at 300 nm.

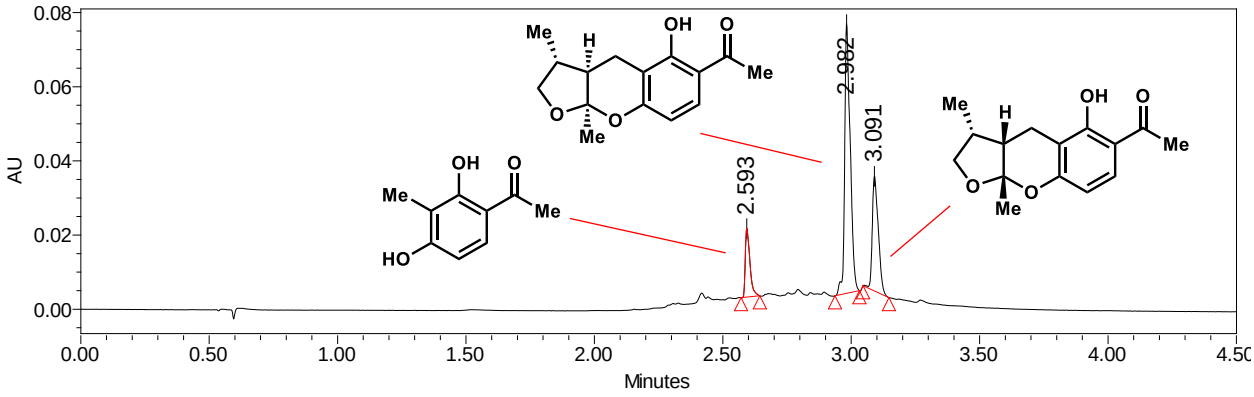

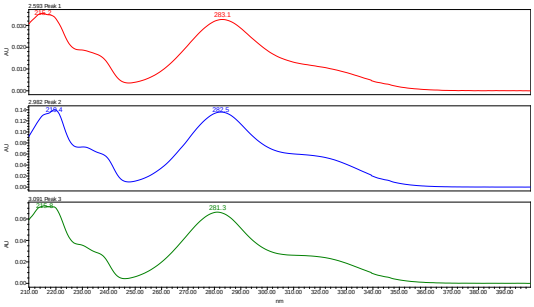

	Retention Time	Area	% Area	Height
1	2.594	15629	11.31	12596
2	2.982	81309	58.82	57927
3	3.091	41299	29.88	25902

Product standard: (-)-xyloketal D

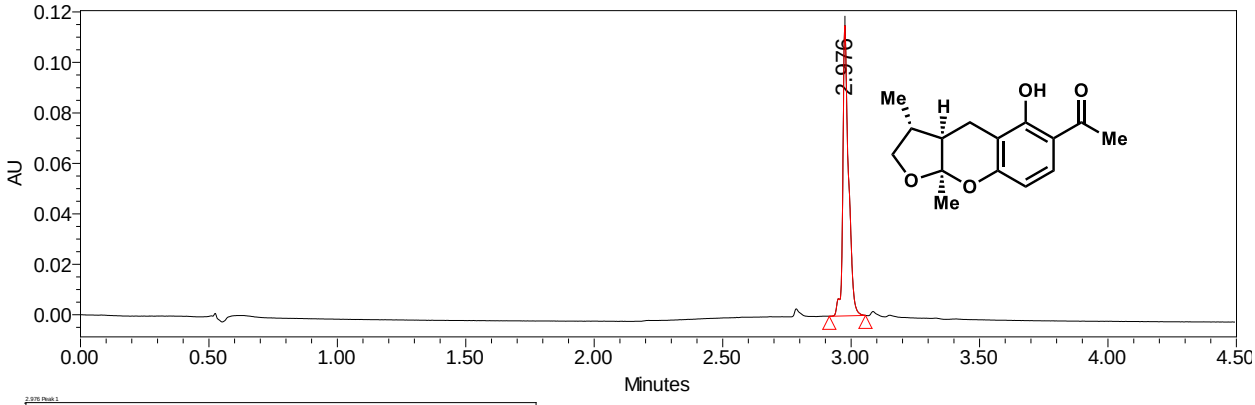

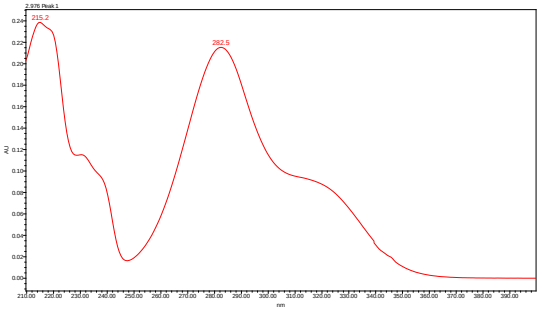

	Retention Time	Area	% Area	Height
1	2.976	177894	100.00	115101

Product standard: diastereomer of (-)-xyloketal D

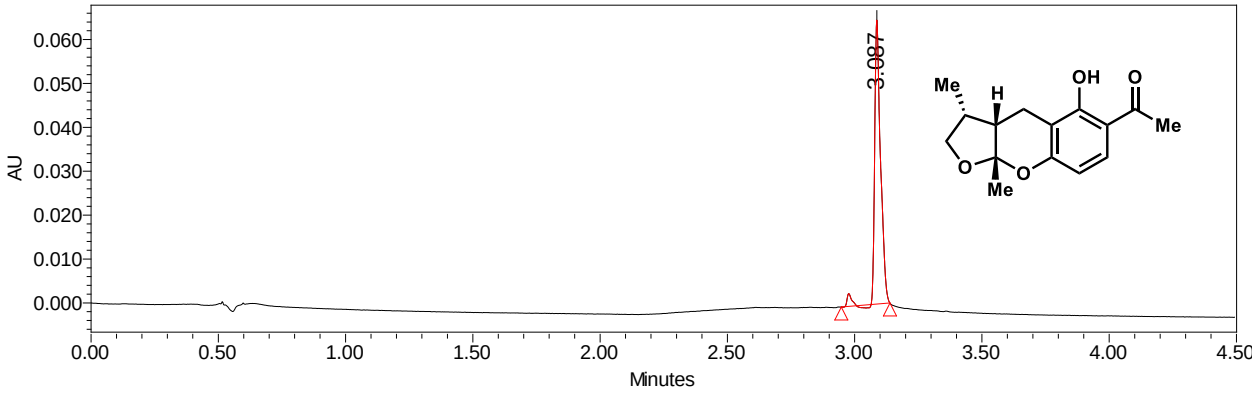

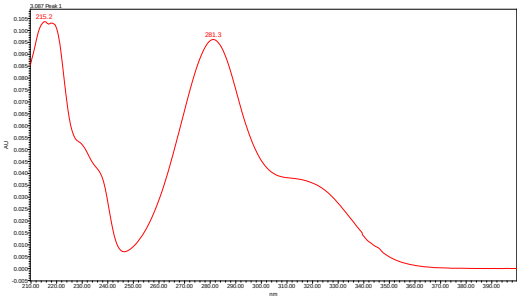

	Retention Time	Area	% Area	Height
1	3.087	108813	100.00	64723

Part X. LC/MS traces for CitB benzylic functionalization cascade reactions

Supplementary Figure S73. Generation of **86** and **87** by in situ functionalization of benzylic alcohol **17**.

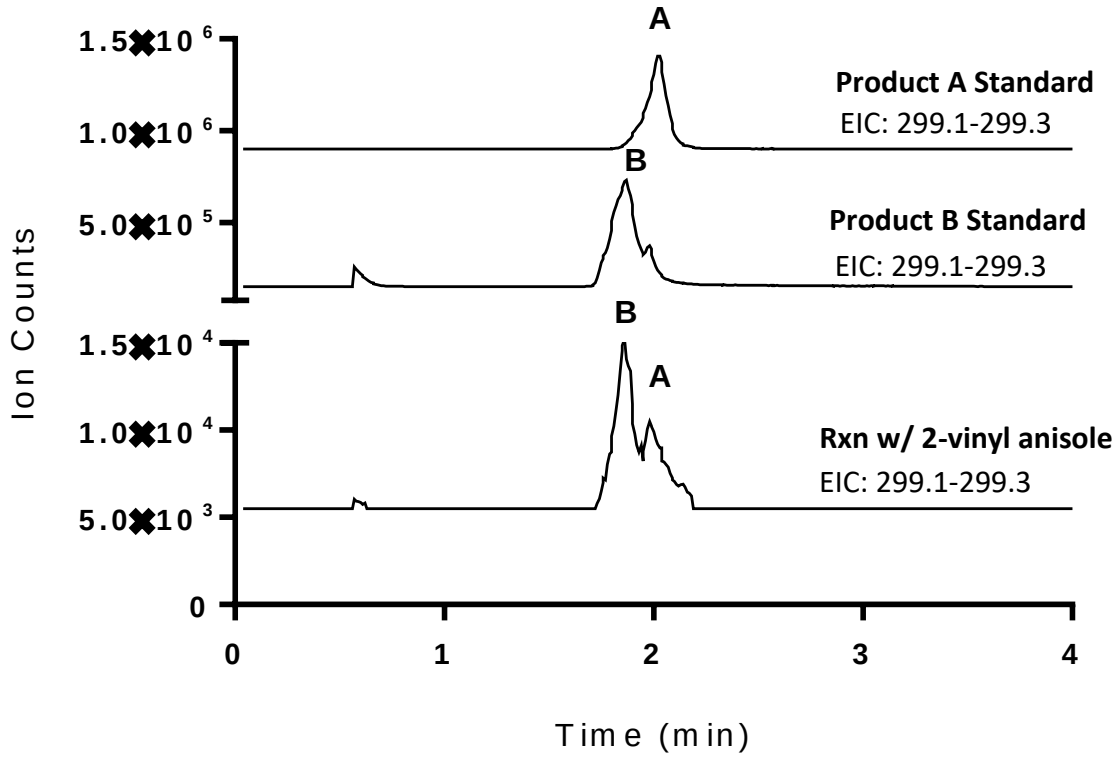

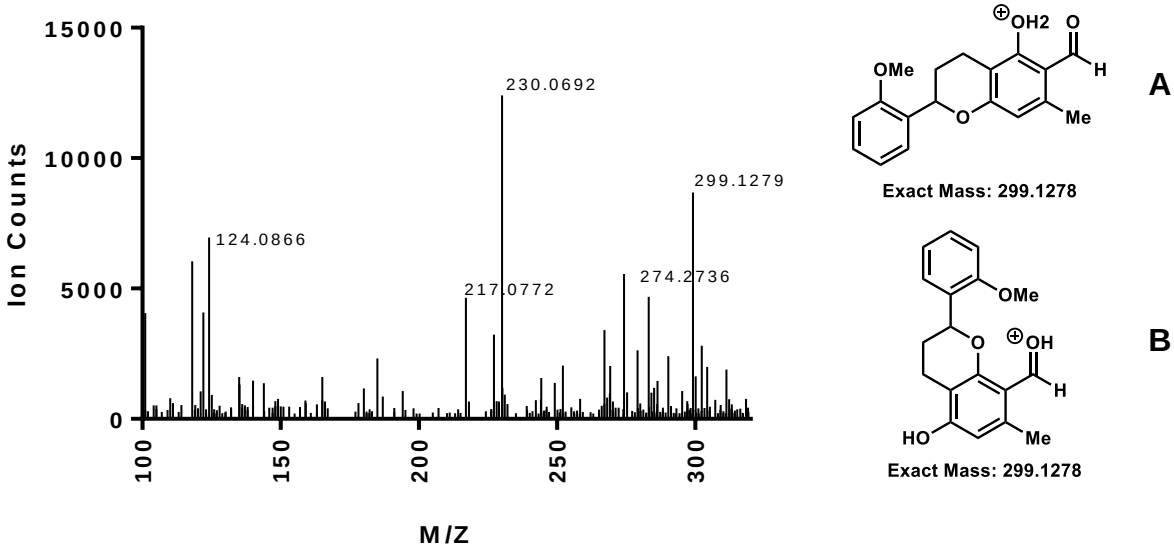

Mass spectrum of reaction with 2-vinylanisole

Supplementary Figure S74. Generation of **84** and **85** by in situ functionalization of benzylic alcohol **17**.

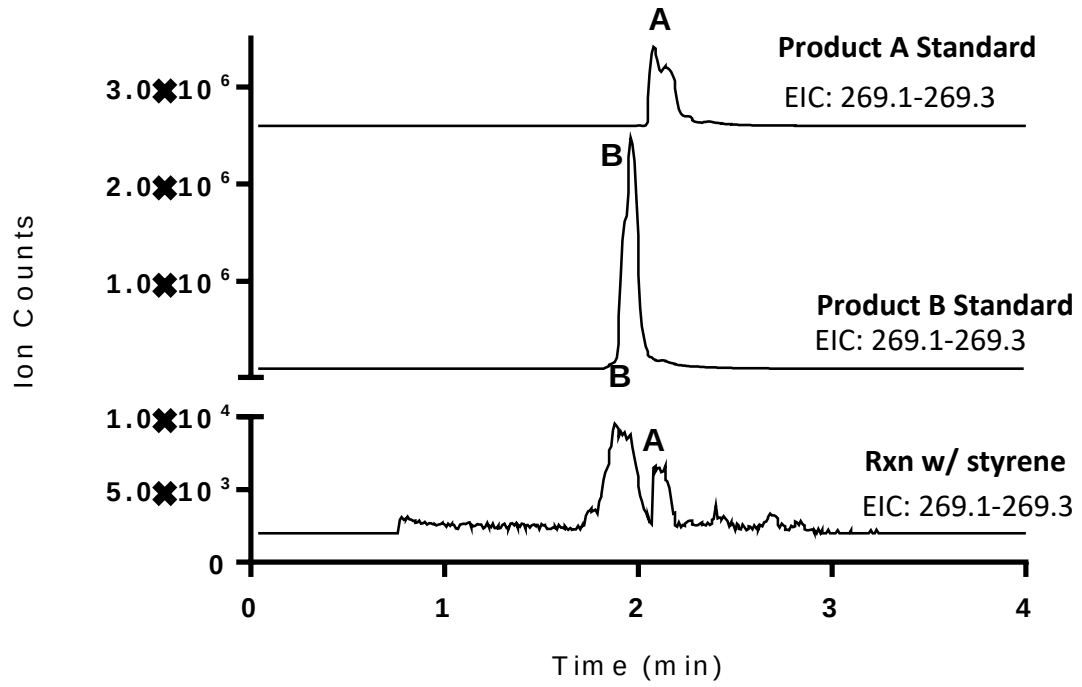

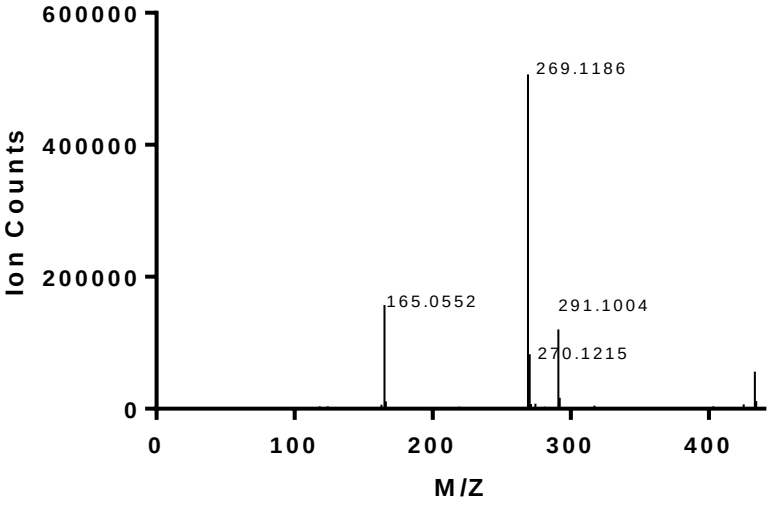

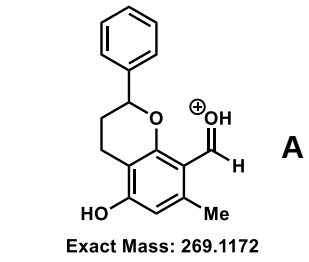

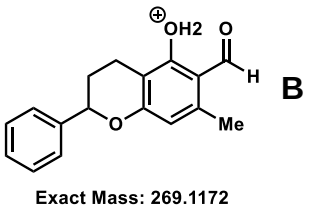

Mass spectrum of reaction with styrene

Supplementary Figure S75. Generation of **88** and **89** by in situ functionalization of benzylic alcohol **17**.

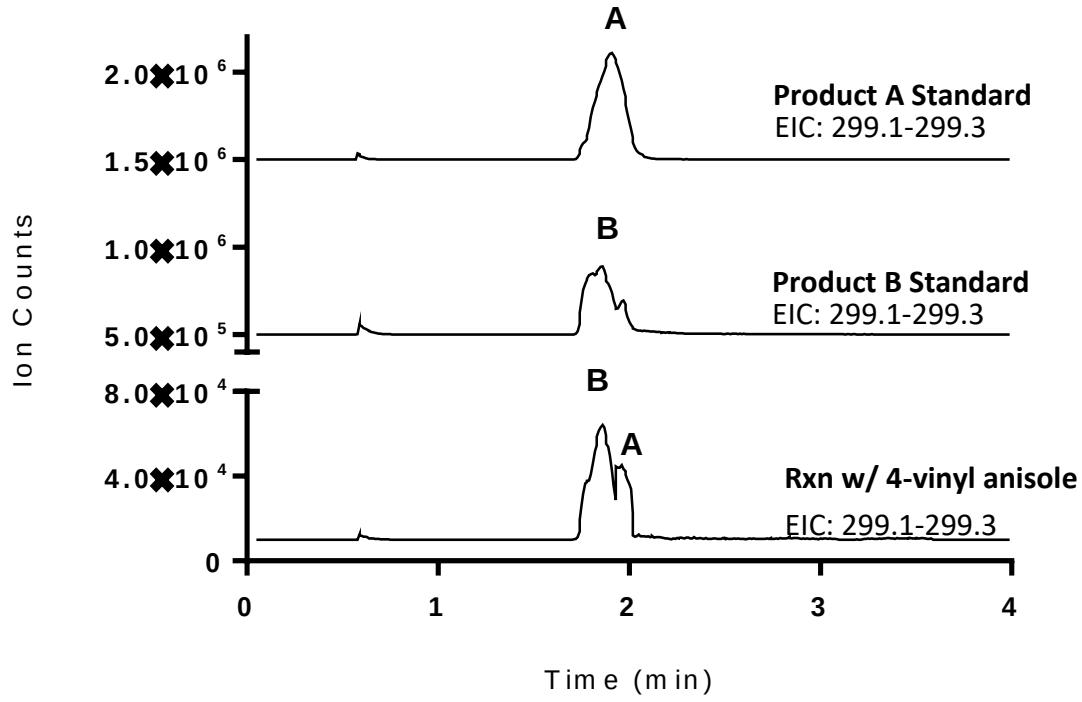

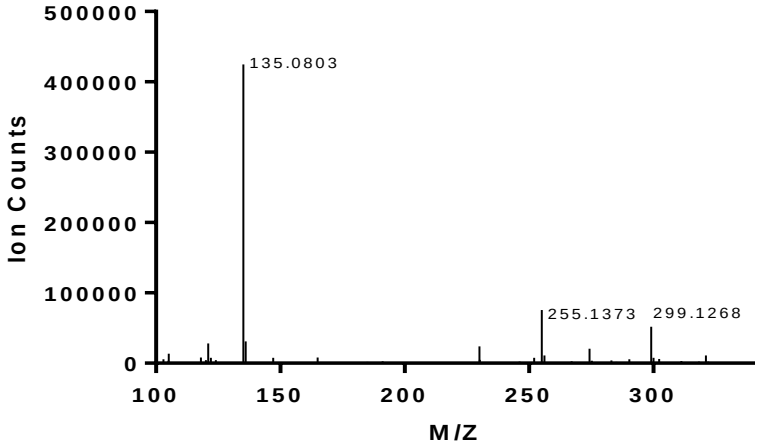

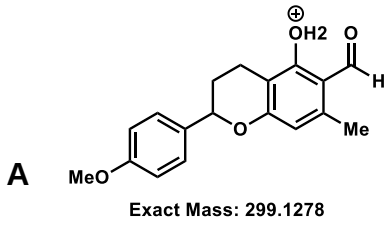

Exact Mass: 299.1278

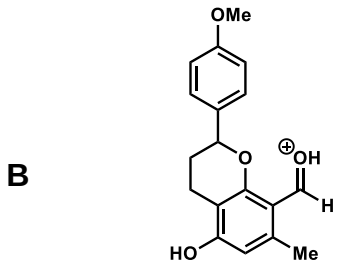

Exact Mass: 299.1278

Mass spectrum of reaction with 4-vinyl anisole

Part XI. LC/MS traces for peptide functionalization reactions

Sequence of peptides used in this study:

Peptide A. Ac-Tyr-βAla-Phe-Ala-Glu-Arg-Arg-Phe-Cys-Pro-Phe-Ala-Glu-Arg-NH_2
Peptide B. Ac-Tyr-βAla-Phe-Ala-Glu-Arg-Arg-Phe-Lys-Pro-Phe-Ala-Glu-Arg-NH_2

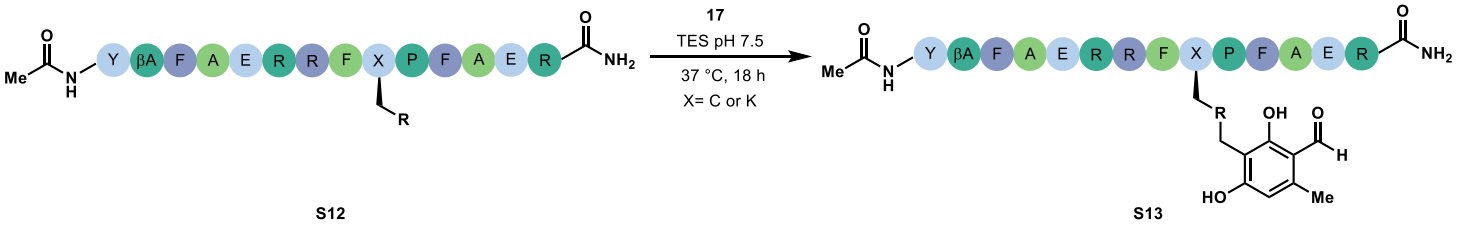

Supplementary Figure S76. Functionalization of peptides with CitB-generated benzylic alcohol, **17**.

Analytical-scale peptide reactions: Each reaction contained 50 mM TES buffer pH 7.5 (2.5 µL of a 1 M solution), 50 µM peptide (1 µL of a 2.5 mM stock in DMSO), 200 µM (4 equiv) benzylic alcohol (**17**, 1 µL of a 10 mM stock in DMSO) and Milli-Q water to a final volume of 50 µL. Reactions were performed (in duplicate) at 37 °C for 18 h before diluting the reaction with Milli-Q water (with 1% v/v formic acid) to a final concentration of 10 µM peptide. Reactions were analyzed by LC/MS using the method described below for peptide analysis. Peptide reactions were quantified by analyzing the extracted ion chromatogram for the area under the curve (AUC) for product/total AUC (product AUC + starting material AUC). All reactions were performed in duplicate and percent conversion determined as an average of those trials.

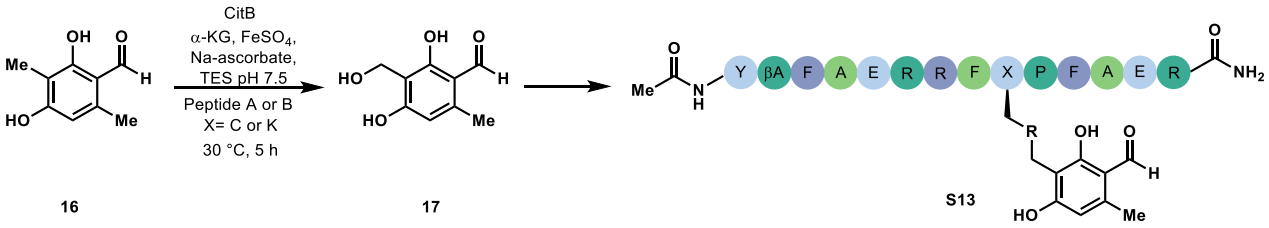

Supplementary Figure S77. One-pot CitB-catalyzed hydroxylation and peptide functionalization.

Procedure for one-pot CitB-catalyzed hydroxylation and peptide functionalization reactions: CitB-catalyzed benzylic functionalization and *in situ* peptide functionalization was performed under the following conditions: 50 µL total reaction volume, 1 µM CitB, 50 mM TES (pH 7.5), 0.2 mM substrate, 0.4 mM α-ketoglutaric acid, 8 mM sodium ascorbate, 0.1 mM ferrous sulfate, 50 µM peptide, and Milli-Q water to obtain a total volume of 50 µL. The reaction was incubated for 5 h at 37°C before the addition of 200 µL 1% (v/v) formic acid in water to quench the reaction. The reactions were then analyzed by LC/MS (Q-TOF) using the method described below for peptide analysis. Peptide reactions were quantified by analyzing the extracted ion chromatogram for the area under the curve (AUC) for product/total AUC (product AUC + starting material AUC). All reactions were performed in duplicate and conversion determined as an average of those trials.

LC-MS analysis of peptide reactions: Peptide reactions were quenched with 1% (v/v) formic acid in ddH_2O before analysis by LC/MS on an Agilent 1290 Series Infinity HPLC with a 6545 Series Quadrupole-Time-of-Flight mass spectrometer. Samples were analyzed on a Phenomenex Aeris 3.6 µm WIDEPORE C4 column (2.1 x 50 mm) under the following conditions: mobile phase (solvent A: ddH_2O + 0.1% trifluoroacetic acid; solvent B: acetonitrile + 0.1% trifluoroacetic acid) gradient elution over 6 min (5% to 100% solvent B).

Peptides and potential product masses

Peptide A: Peptide **90** with ligandable cysteine residue

Ac-Tyr-βAla-Phe-Ala-Glu-Arg-Arg-Phe-Cys-Pro-Phe-Ala-Glu-Arg-NH_2

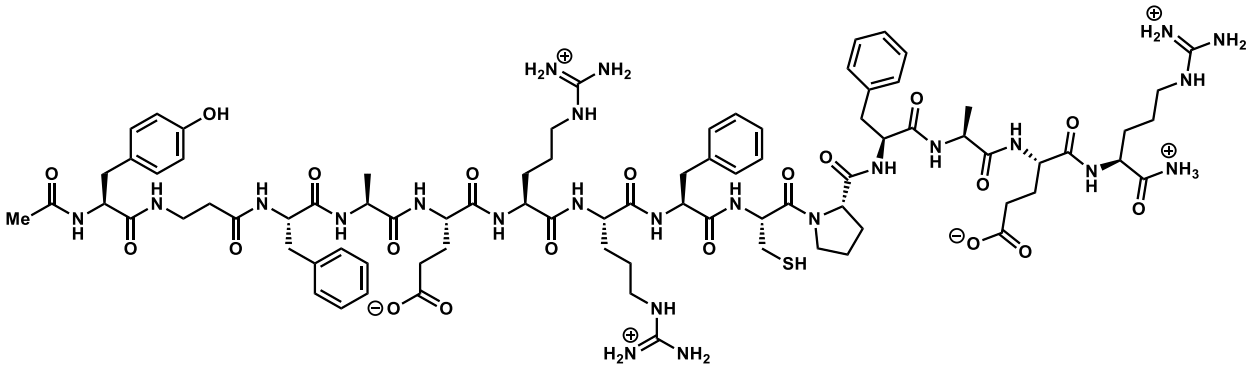

Exact Mass: 1804.8820

Liganded peptide A: Peptide **90** liganded with benzylic alcohol **17**.

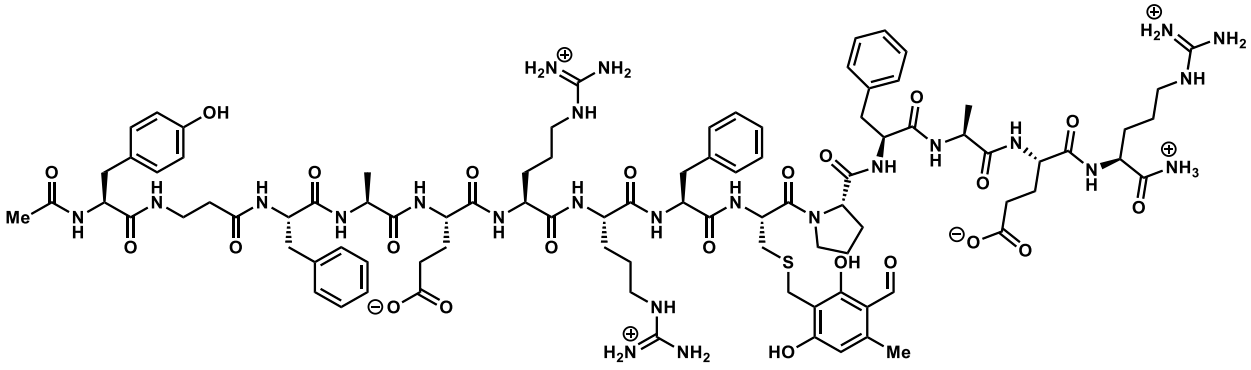

Exact Mass: 1968.9294

Peptide B: Peptide **without** ligandable cysteine residue (**S14**)

Ac-Tyr-βAla-Phe-Ala-Glu-Arg-Arg-Phe-Lys-Pro-Phe-Ala-Glu-Arg-NH_2

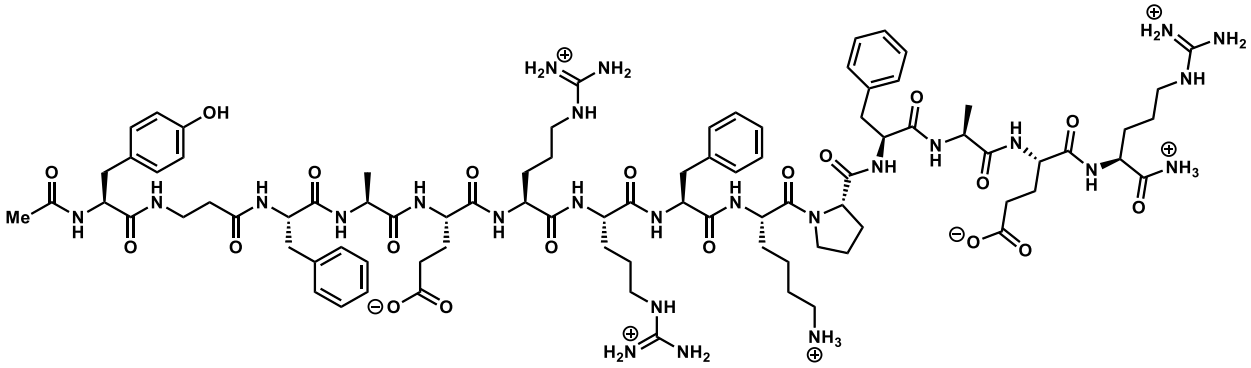

Exact Mass: 1830.9751

Liganded Peptide B (imine condensation): Peptide B liganded (**S15**) with benzylic alcohol **17**.

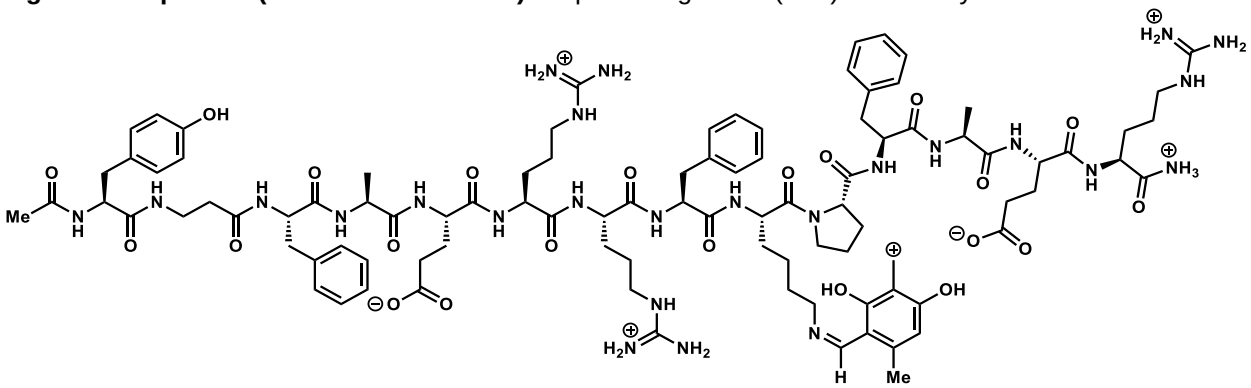

Exact Mass: 1977.0119

Liganded peptide B (*ortho*-quinone methide): Peptide B liganded (**S16**) with benzylic alcohol **17**.

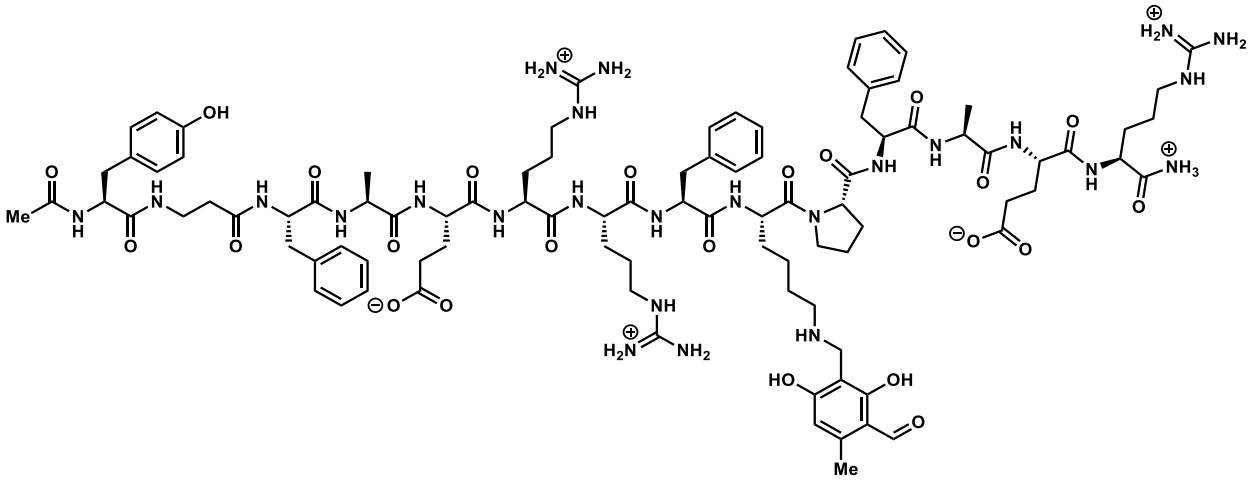

Exact Mass: 1994.0152

Supplementary Table S2. Calculated and observed peptide masses for peptide MS

Peptide	Predicted [M+H] mass	Predicted [(M/2Z)+H] mass	Observed mass (Deconvoluted)
Peptide A	1804.8820	902.4410	1804.870
Peptide A-liganded	1968.9294	984.4647	1968.919
Peptide B	1830.9751	915.4876	1830.860
Peptide B-liganded (imine condensation)	1977.0119	988.5059	Not observed
Peptide B-liganded (*o*-QM addition)	1994.0152	997.0076	Not observed

LC-MS traces for peptide functionalization reactions

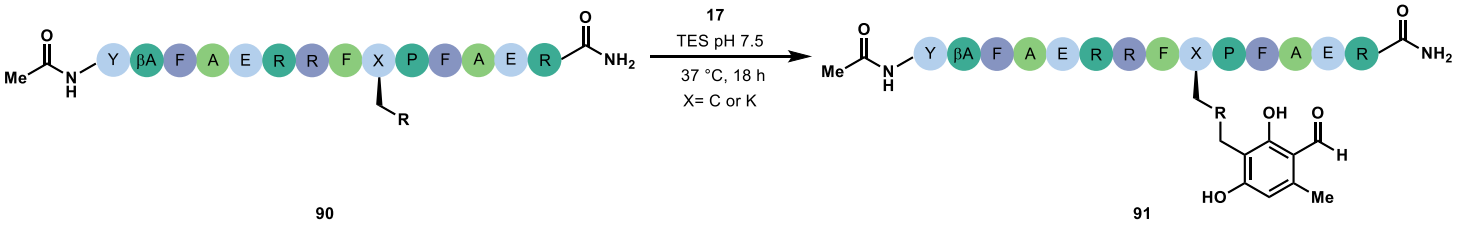

Supplementary Figure S78. Functionalization of Peptide A (**90**) with benzylic alcohol **17**. Extracted ion chromatograms (EICs) for expected product and starting material masses

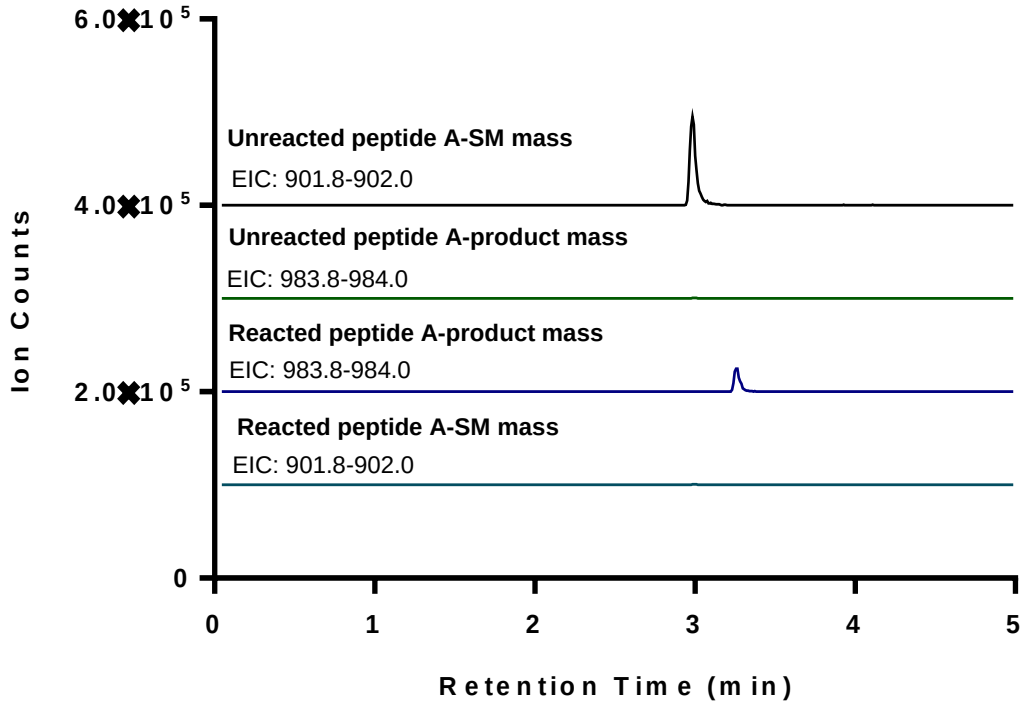

Supplementary Figure S79. Functionalization of Peptide B (**S14**) with benzylic alcohol **17**. Extracted ion chromatograms (EICs) for expected product and starting material masses.

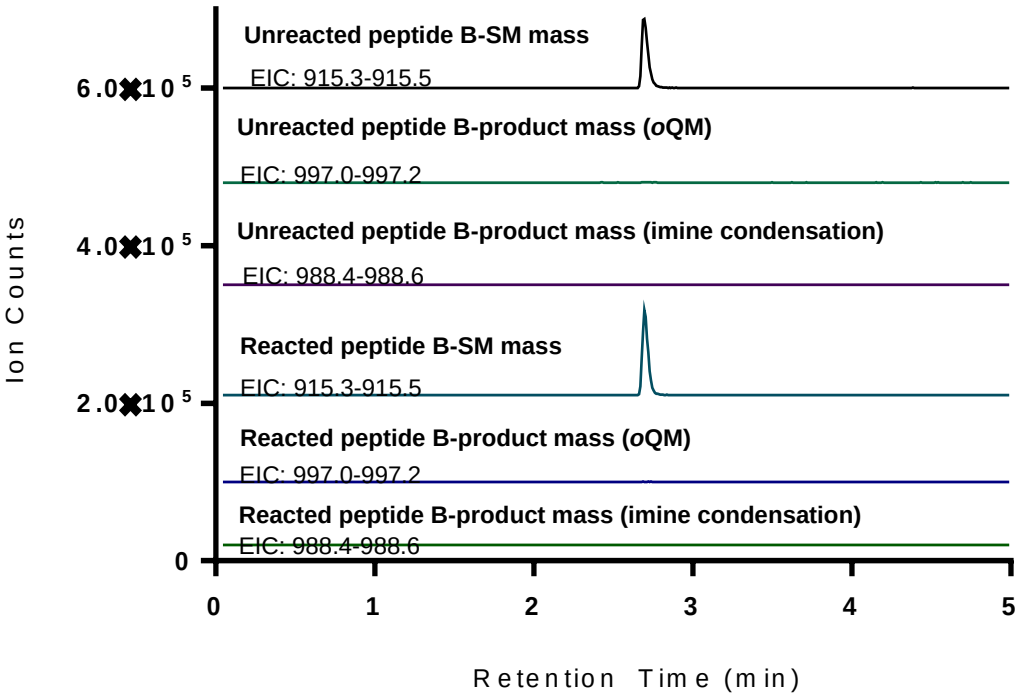

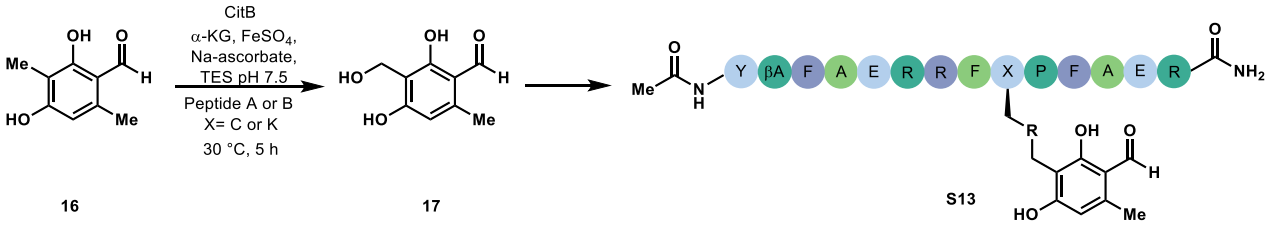

Supplementary Figure S80. *In situ* functionalization of Peptide A (**90**) with CitB-generated benzylic alcohol **17**. Extracted ion chromatograms (EICs) for expected product and starting material masses.

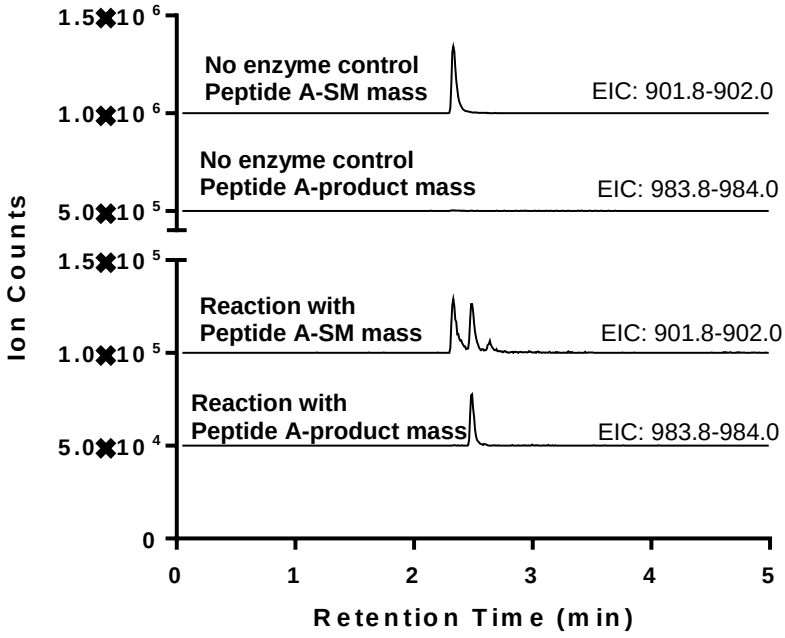

Supplementary Figure S81. *In situ* functionalization of Peptide B (**S14**) with CitB-generated benzylic alcohol **17**. Extracted ion chromatograms (EICs) for expected product and starting material masses.

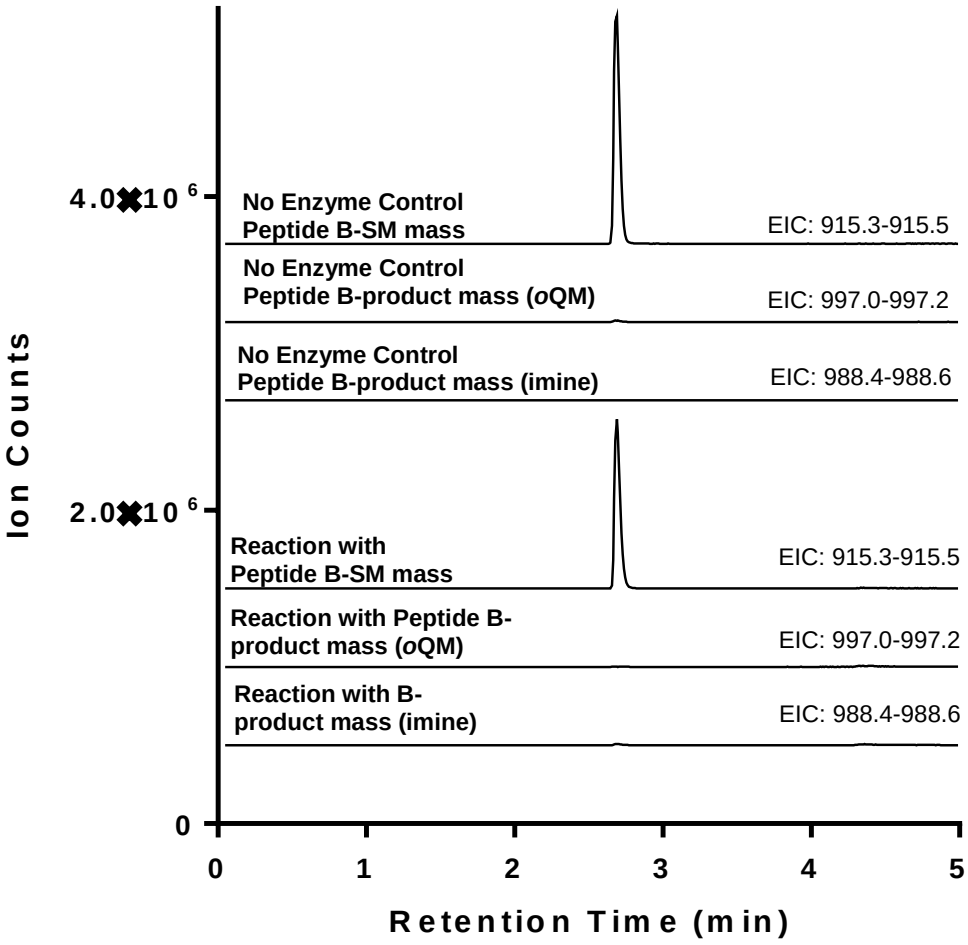

Part XII. ^{1}H and ^{13}C NMR Spectra of Compounds

600 MHz, CD_3OD

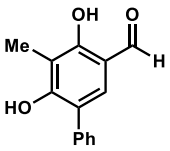

37

150 MHz, CD_3OD

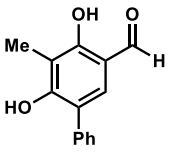

37

600 MHz, CD_3OD

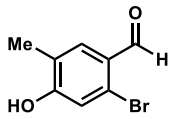

40

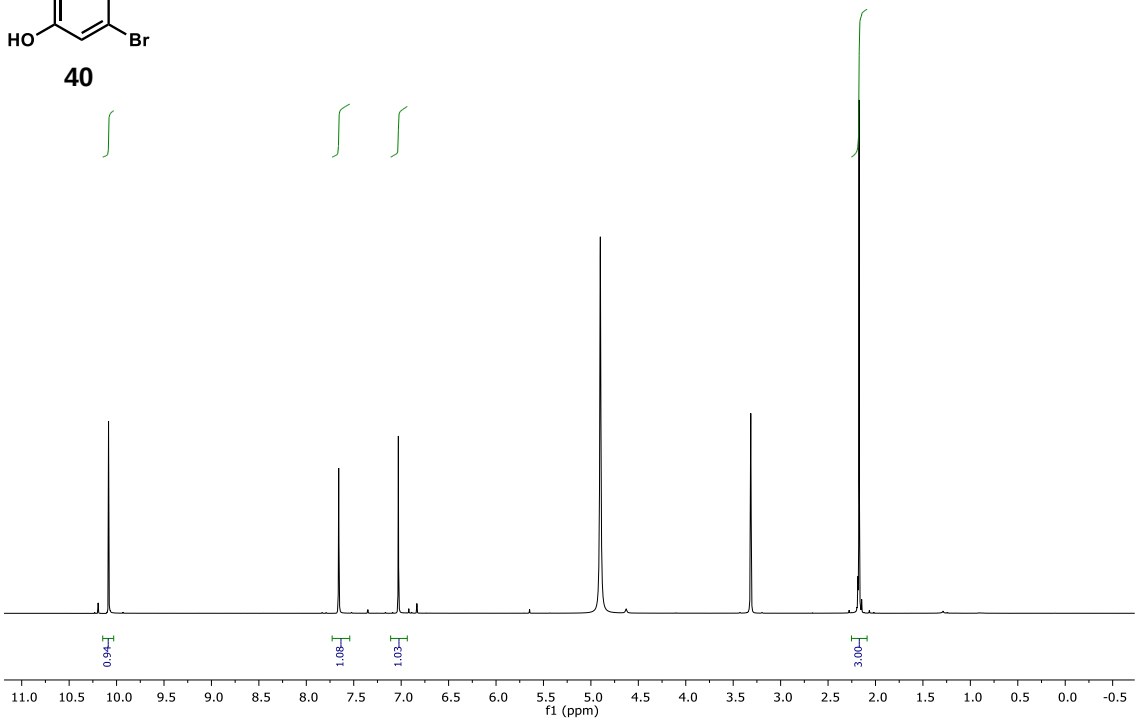

150 MHz, CD_3OD

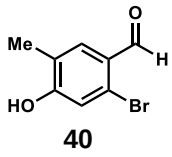

40

600 MHz, CD_3OD

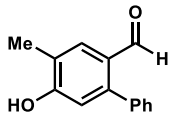

41

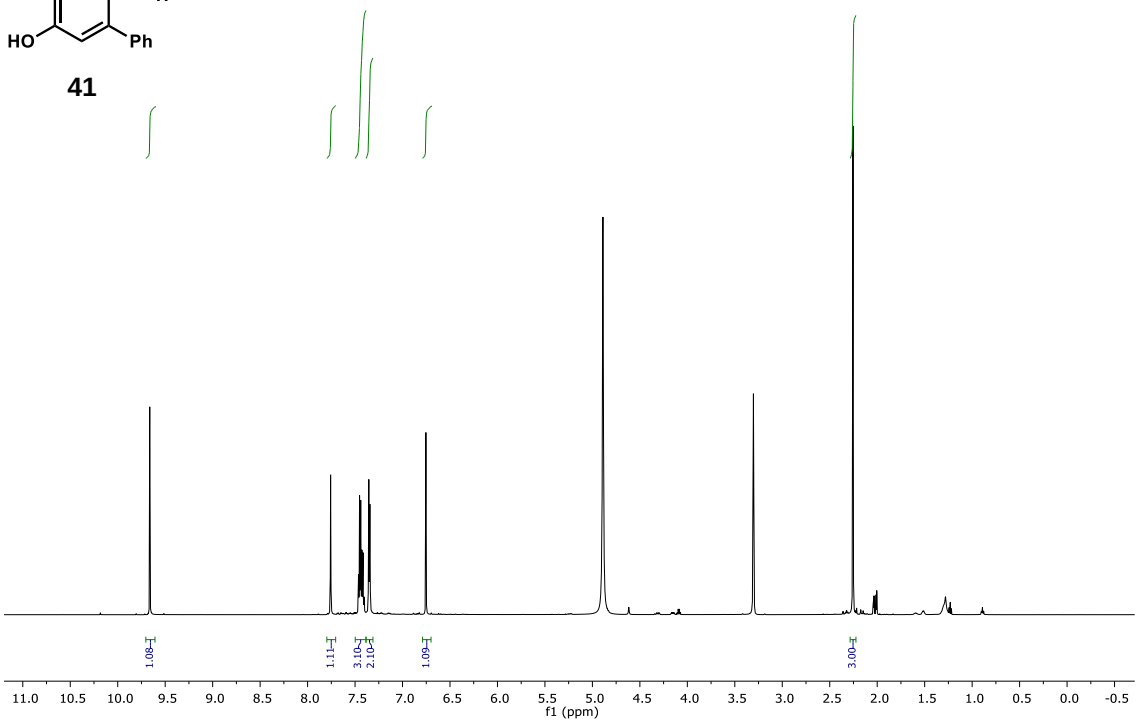

150 MHz, CD_3OD

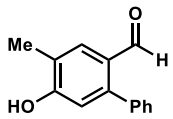

41

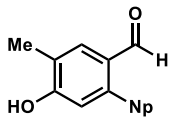

42

600 MHz, CD_3OD

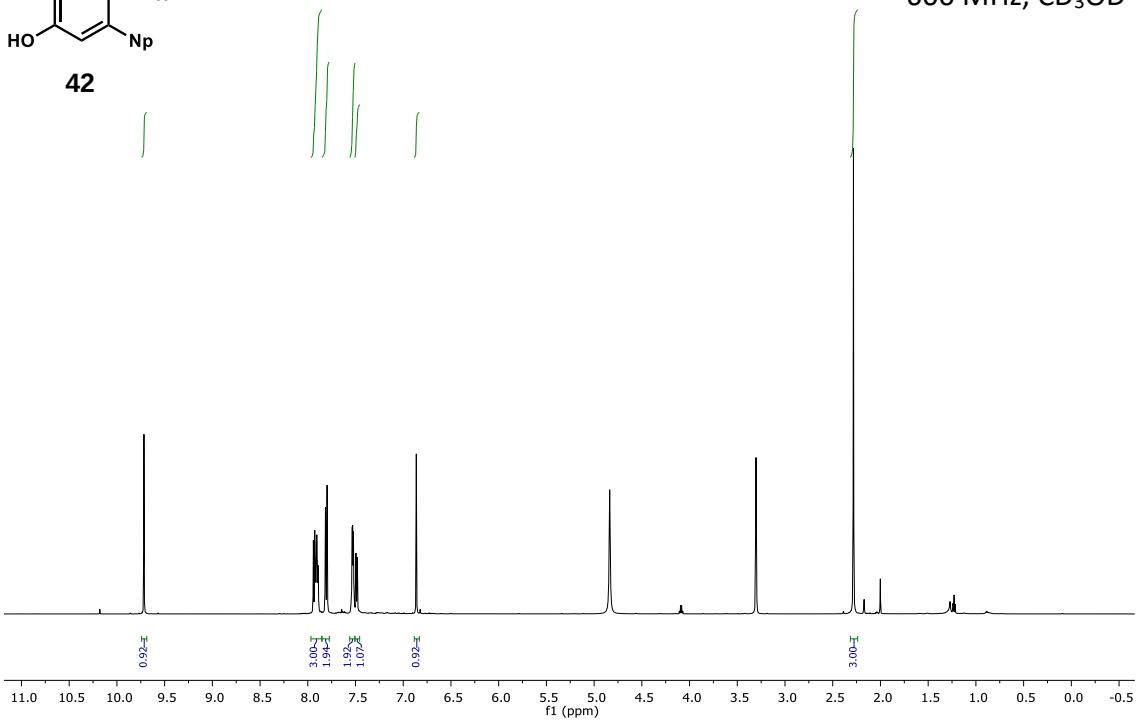

150 MHz, CD_3OD

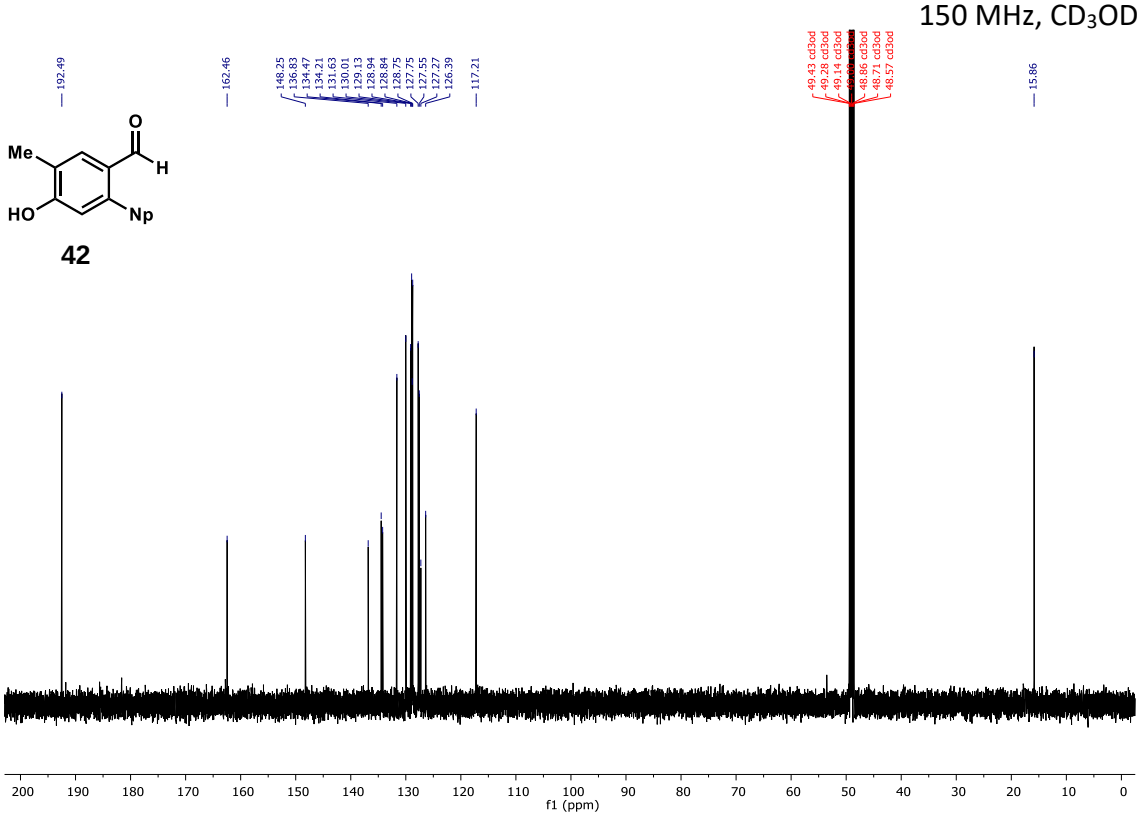

42

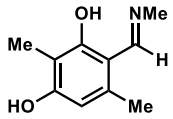

24

600 MHz, $CDCl_3$

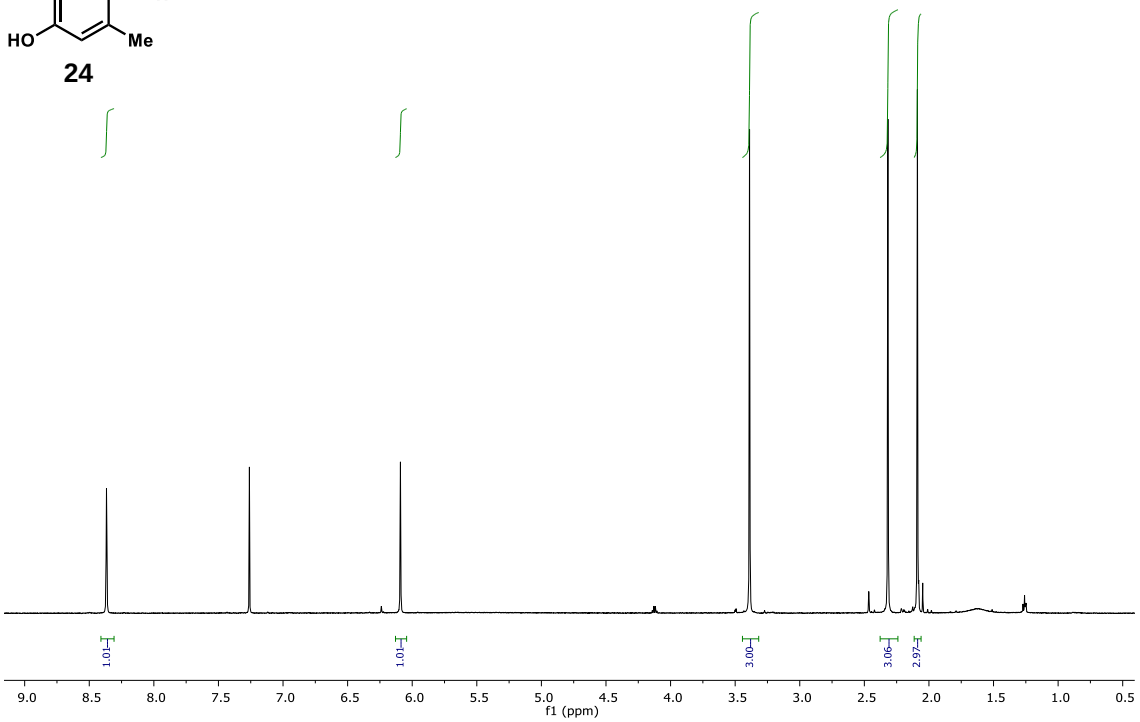

150 MHz, $CDCl_3$

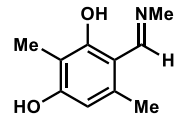

24

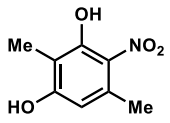

25

600 MHz, CD_3OD

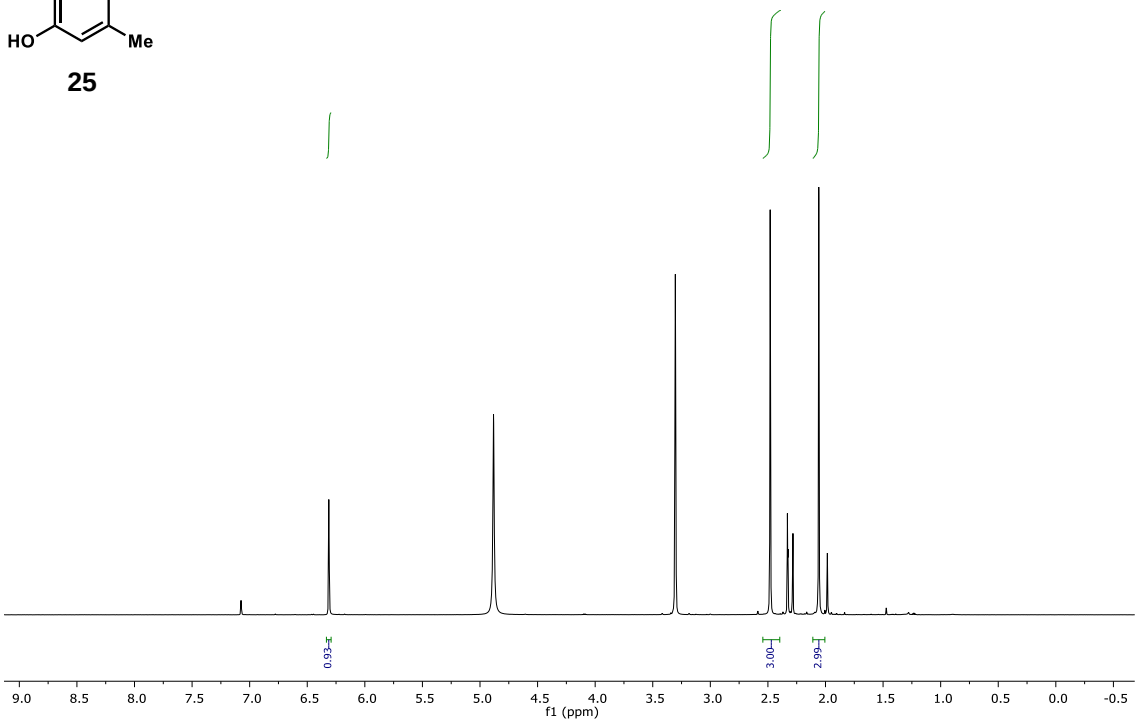

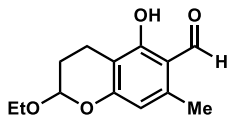

78

600 MHz, $CDCl_3$

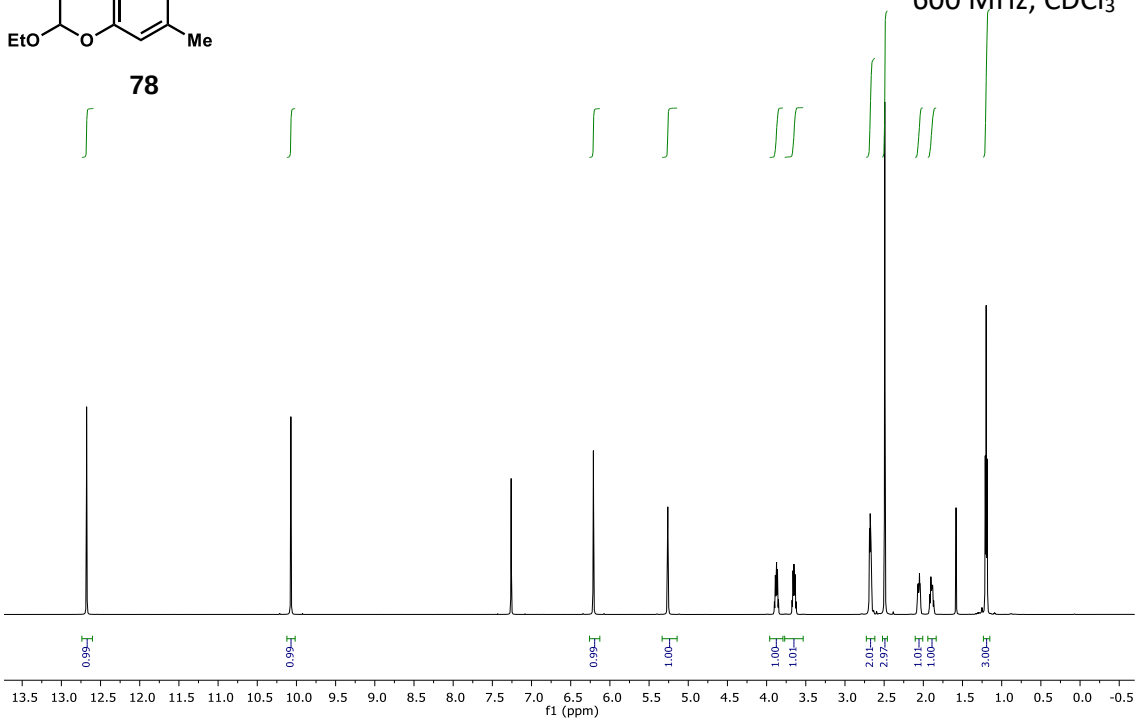

150 MHz, $CDCl_3$

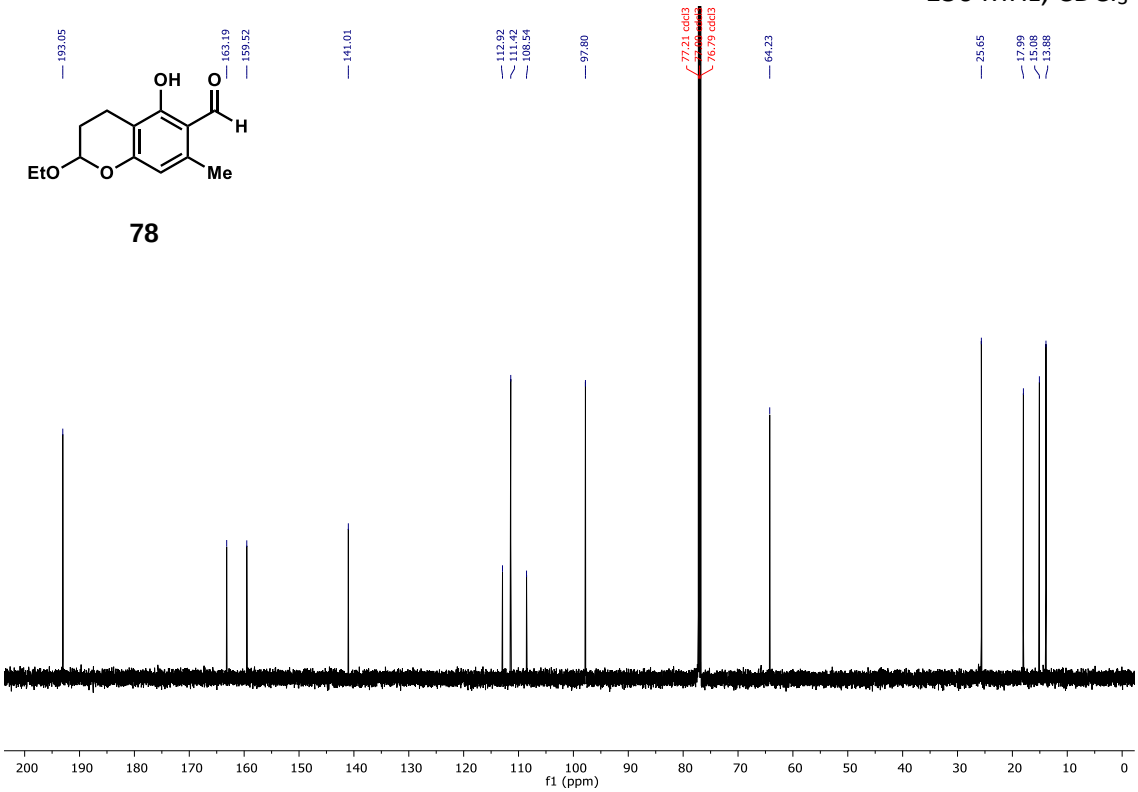

78

600 MHz, $CDCl_3$

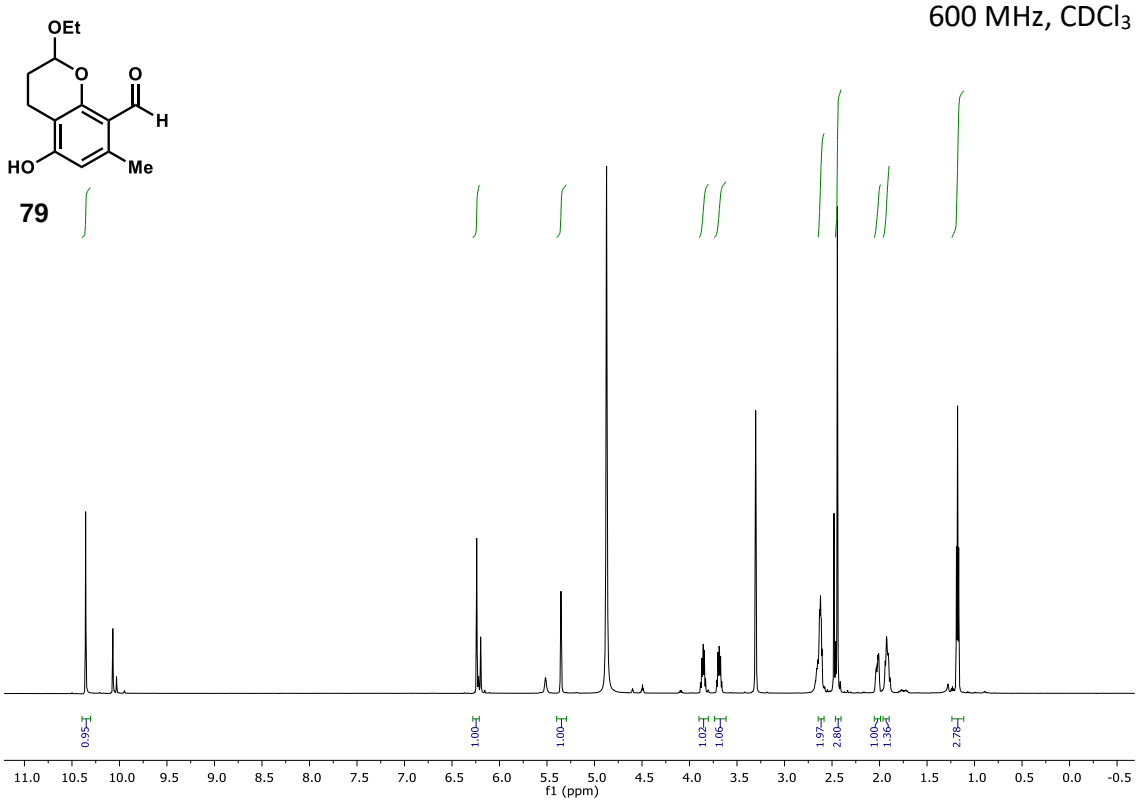

150 MHz, $CDCl_3$

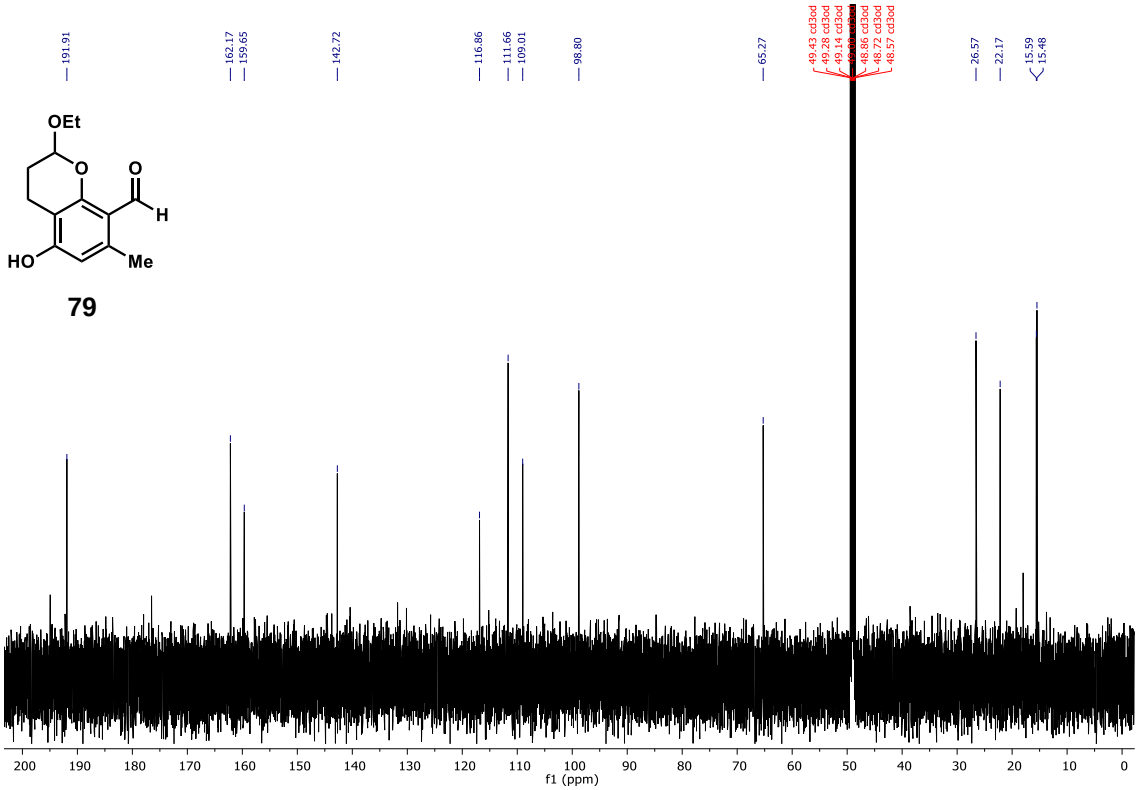

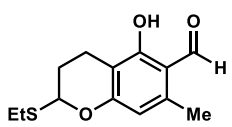

80

600 MHz, CD_3OD

150 MHz, CD_3OD

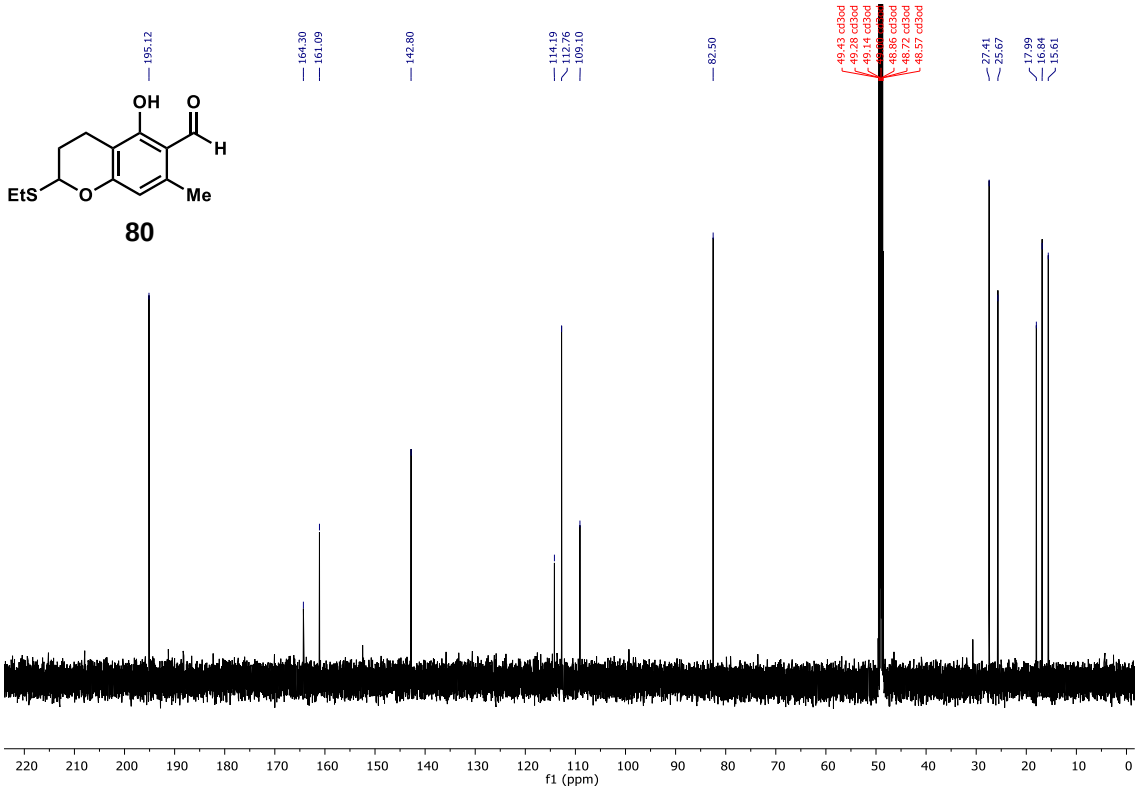

80

600 MHz, $CDCl_3$

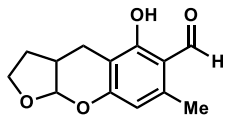

82

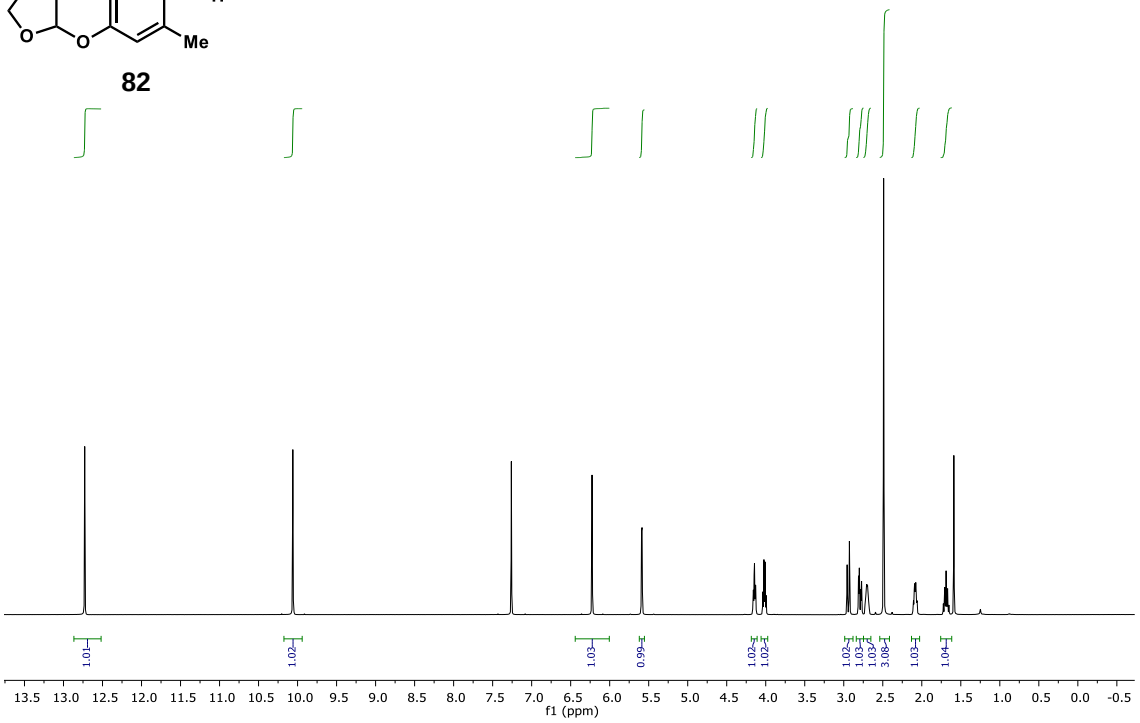

150 MHz, $CDCl_3$

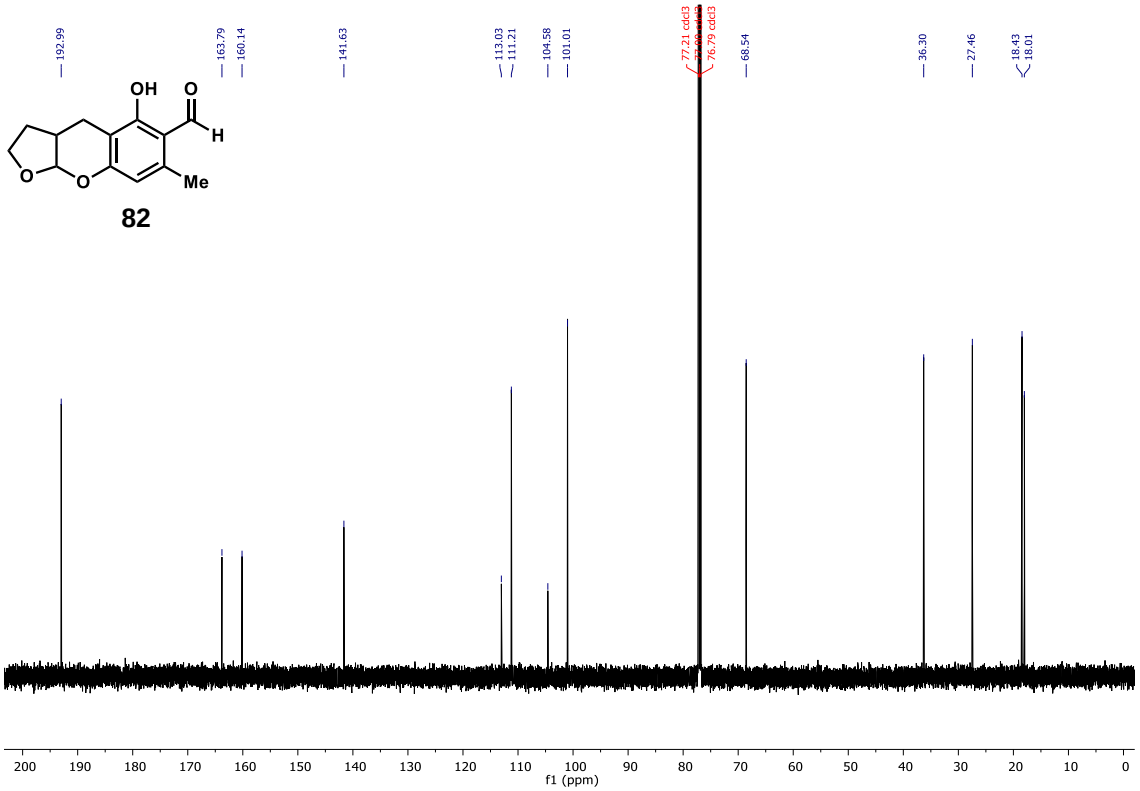

OH
O
H
O
O
Me

82

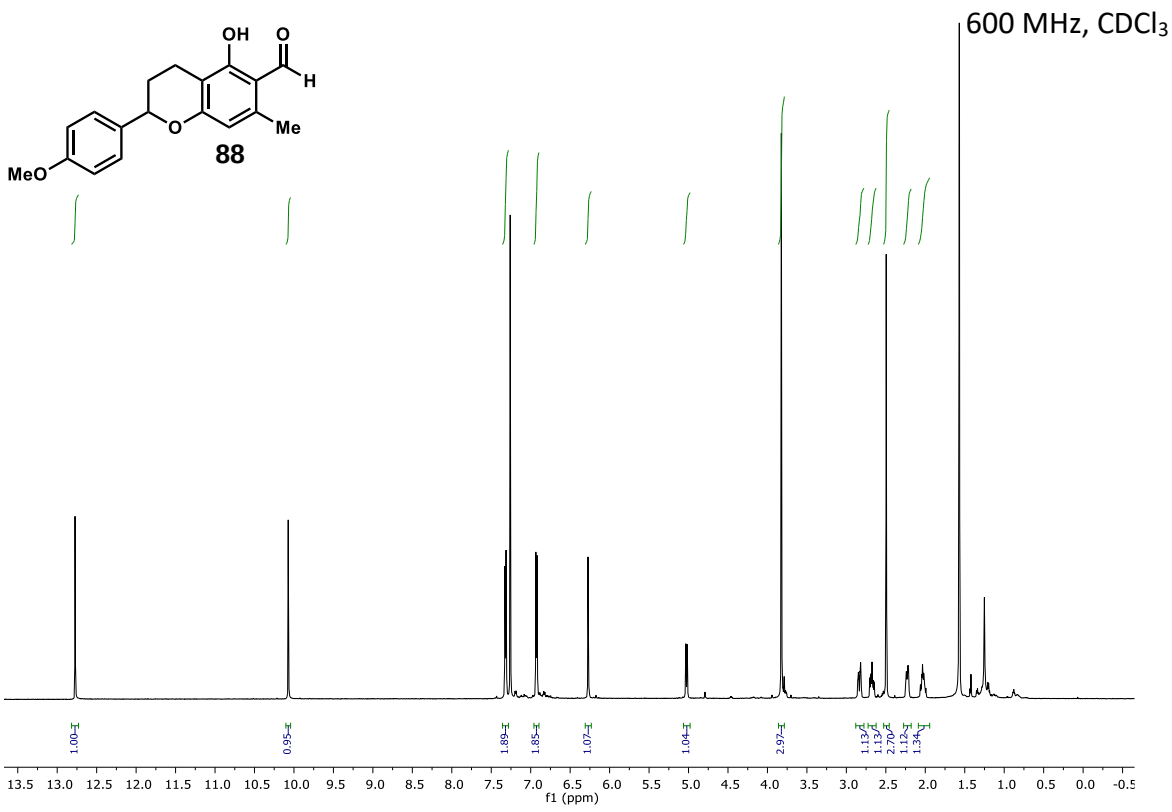
600 MHz, CDCl3
OH
O
H
Me
O
MeO
88
1.00
0.95
1.89
1.85
1.07
1.04
2.97
1.13
1.13
2.70
1.16
1.34
13.5 13.0 12.5 12.0 11.5 11.0 10.5 10.0 9.5 9.0 8.5 8.0 7.5 7.0 6.5 6.0 5.5 5.0 4.5 4.0 3.5 3.0 2.5 2.0 1.5 1.0 0.5 0.0 -0.5
f1 (ppm)

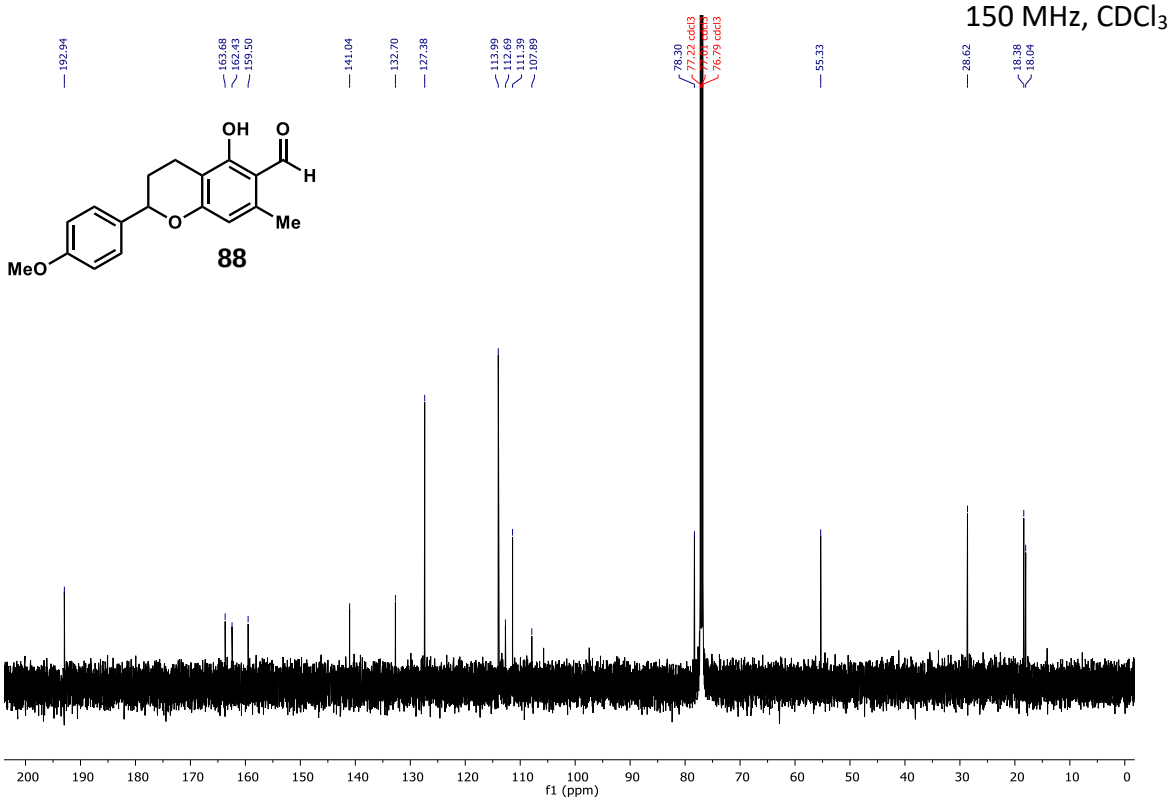
150 MHz, CDCl3
192.94
163.68
162.43
159.50
141.04
132.70
127.38
113.99
112.69
111.39
107.89
78.30
77.22 cdcl3
76.79 cdcl3
55.33
28.62
18.38
18.04
OH
O
H
Me
O
MeO
88
200 190 180 170 160 150 140 130 120 110 100 90 80 70 60 50 40 30 20 10 0
f1 (ppm)

600 MHz, $(CD_3)SO$

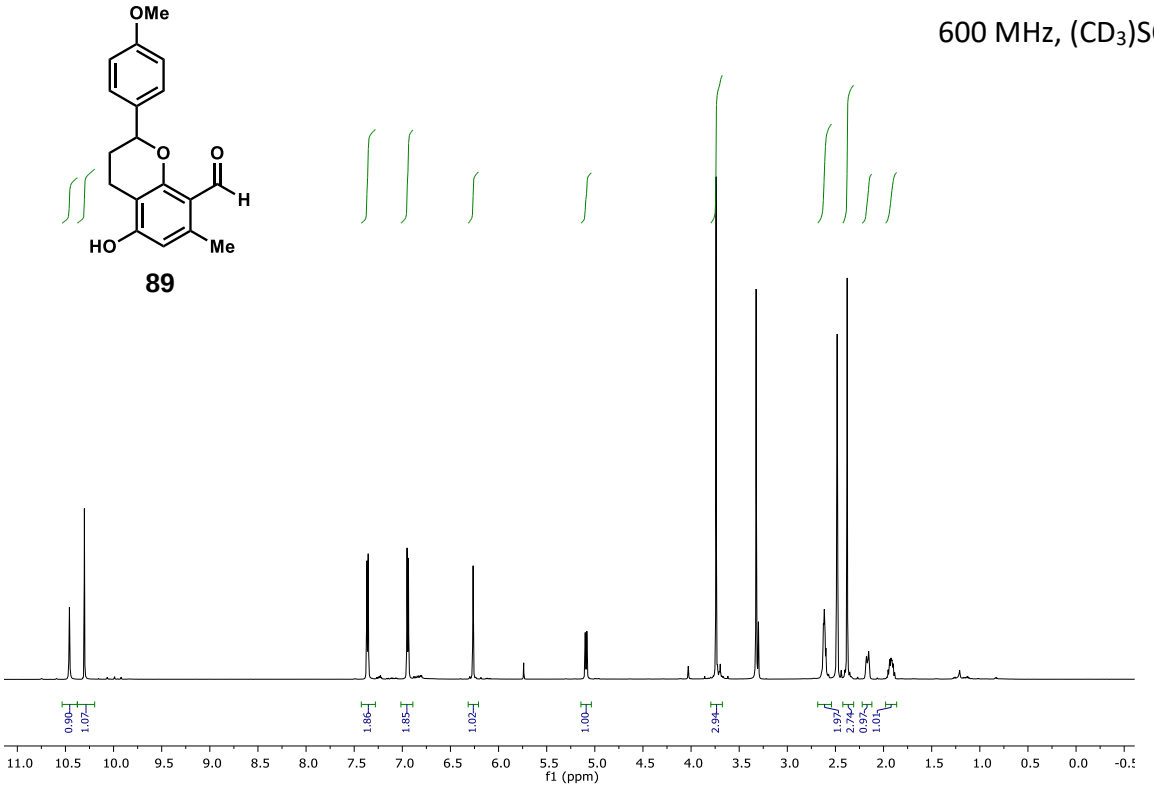

150 MHz, $(CD_3)SO$

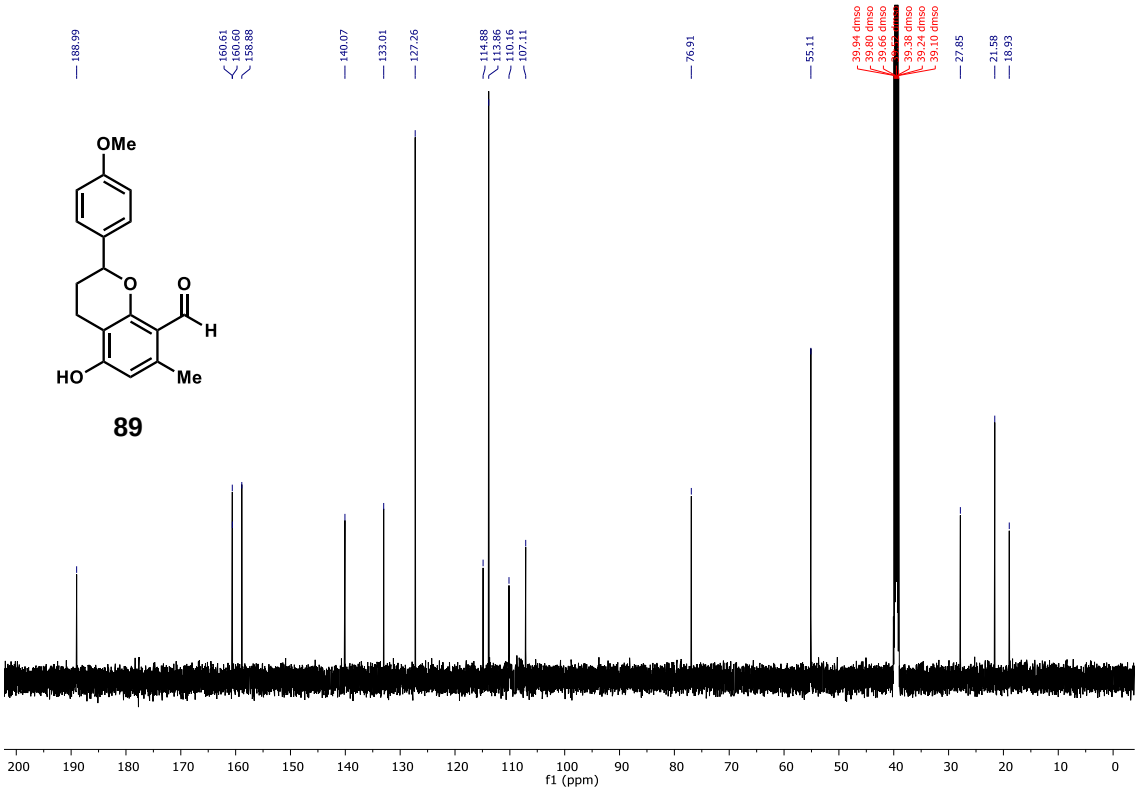

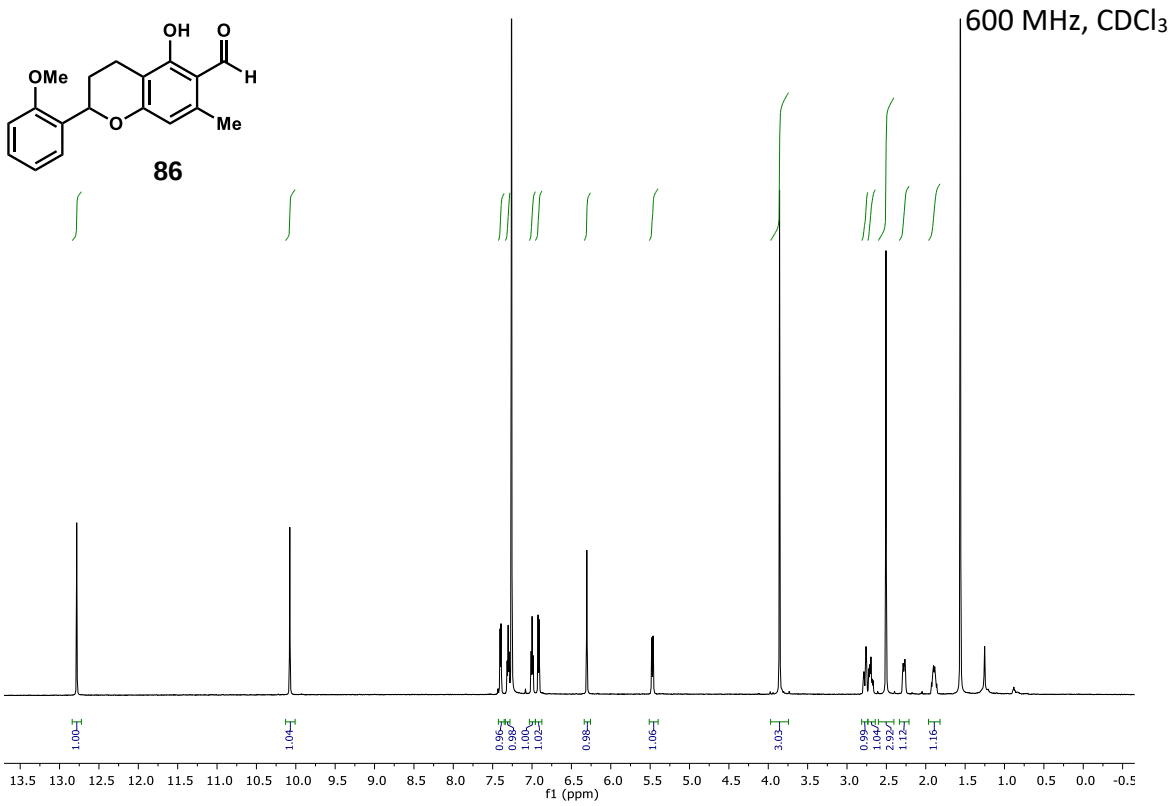
600 MHz, CDCl3
OH
O
H
OMe
Me
O
86
f1 (ppm)

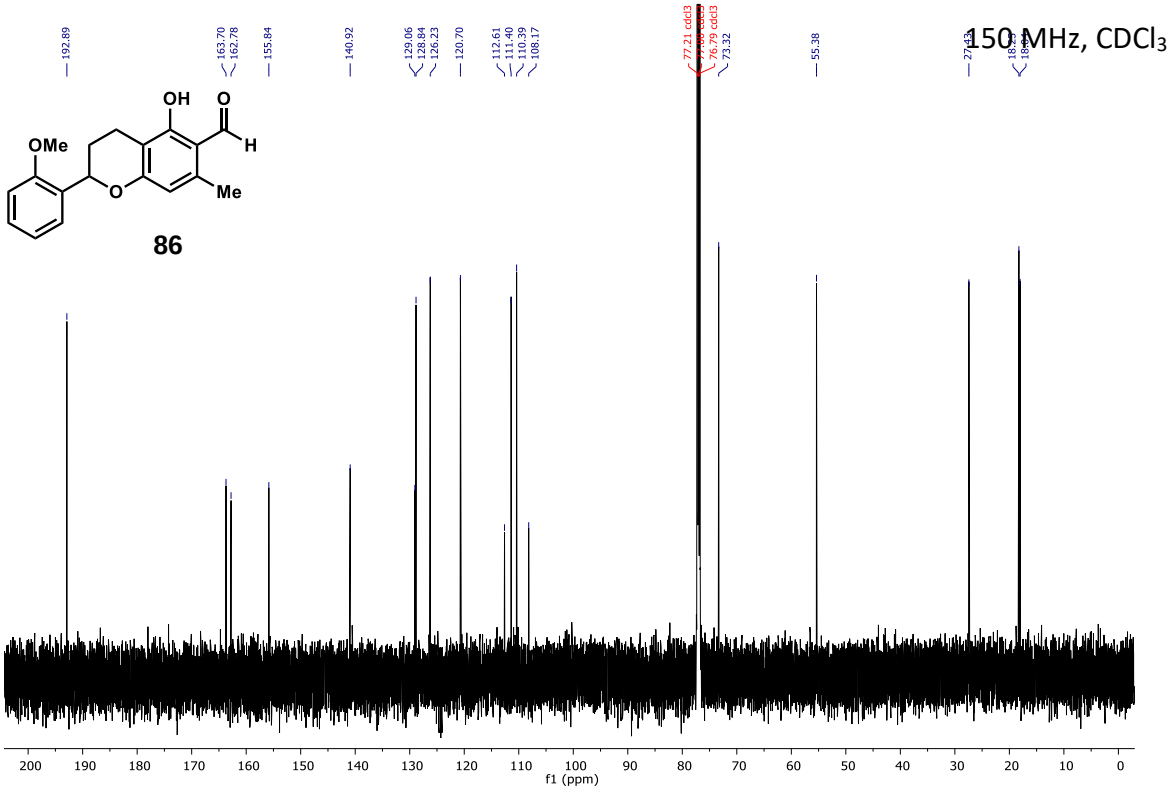
150 MHz, CDCl3
OH
O
H
OMe
Me
O
86
f1 (ppm)

600 MHz, CD_3OD

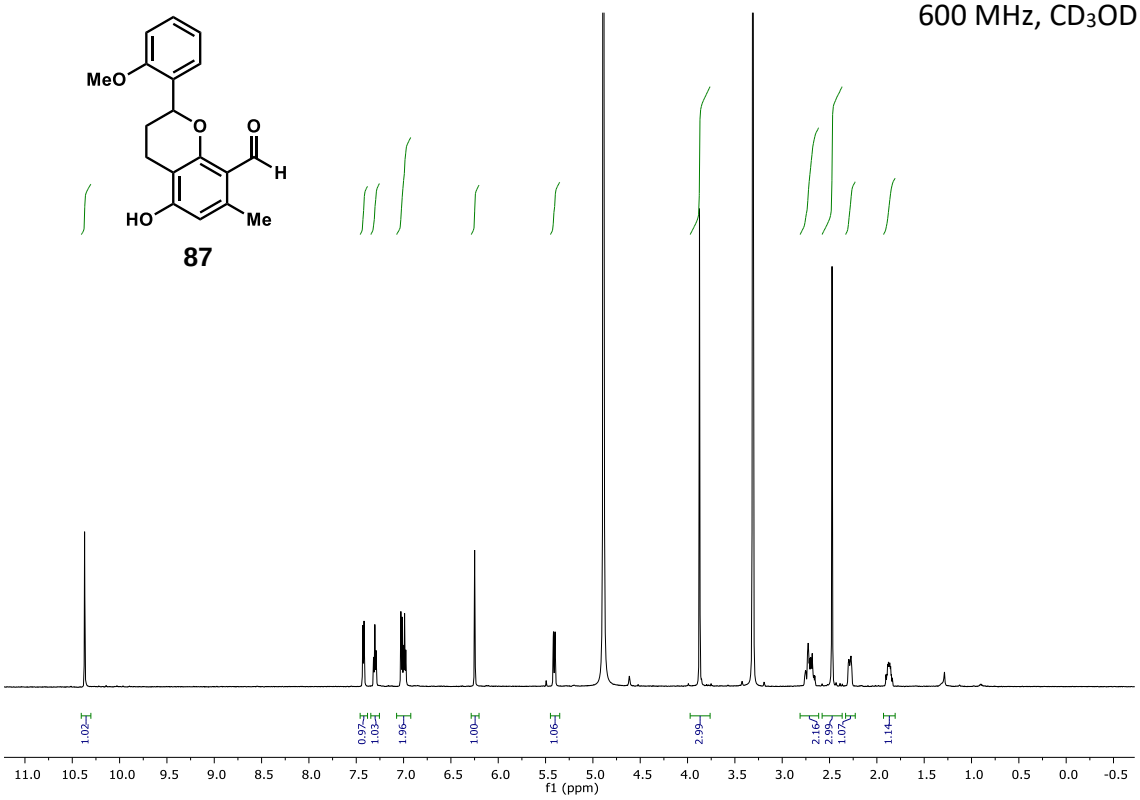

150 MHz, CD_3OD

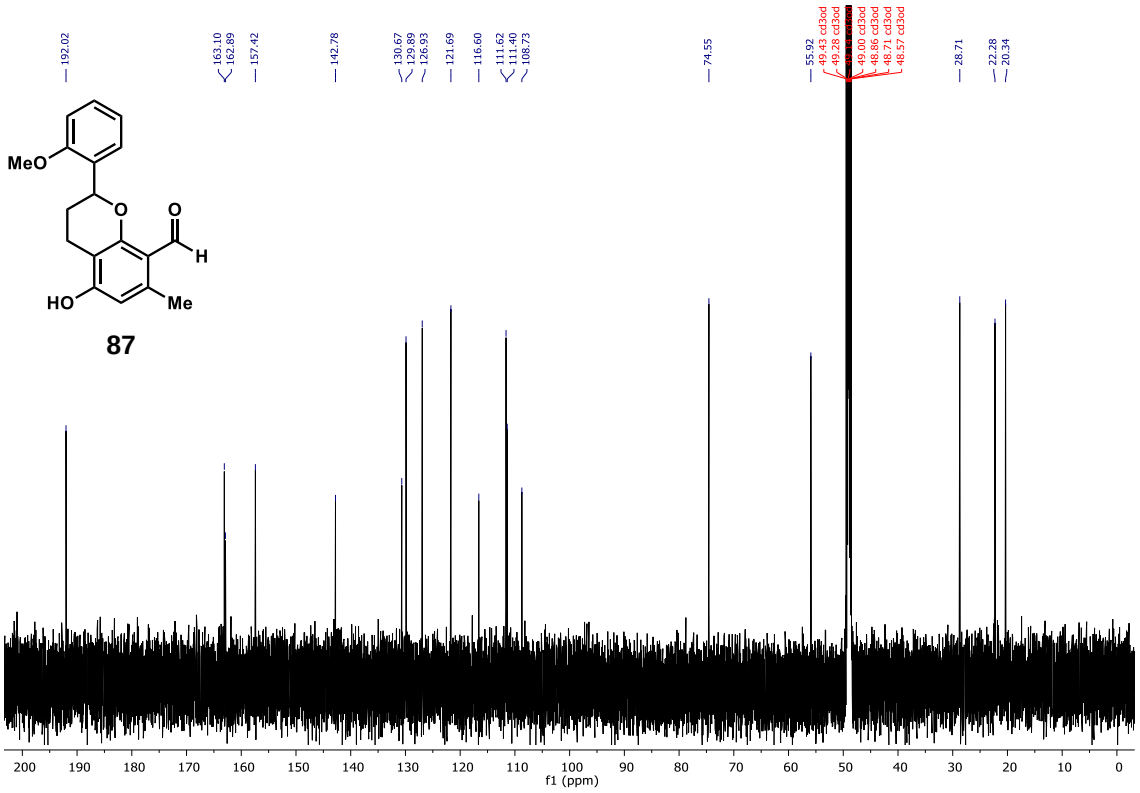

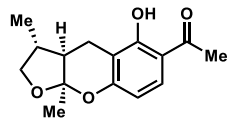

95

600 MHz, $CDCl_3$

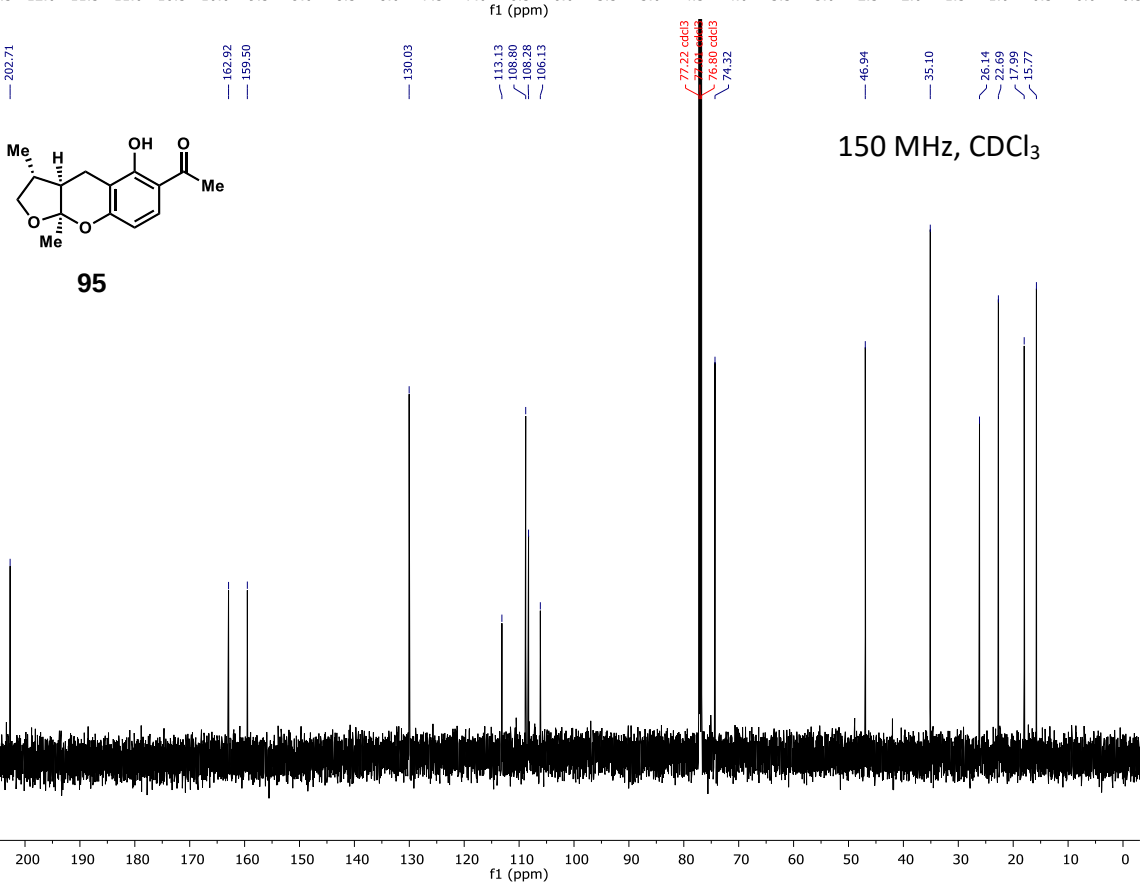

95

150 MHz, $CDCl_3$

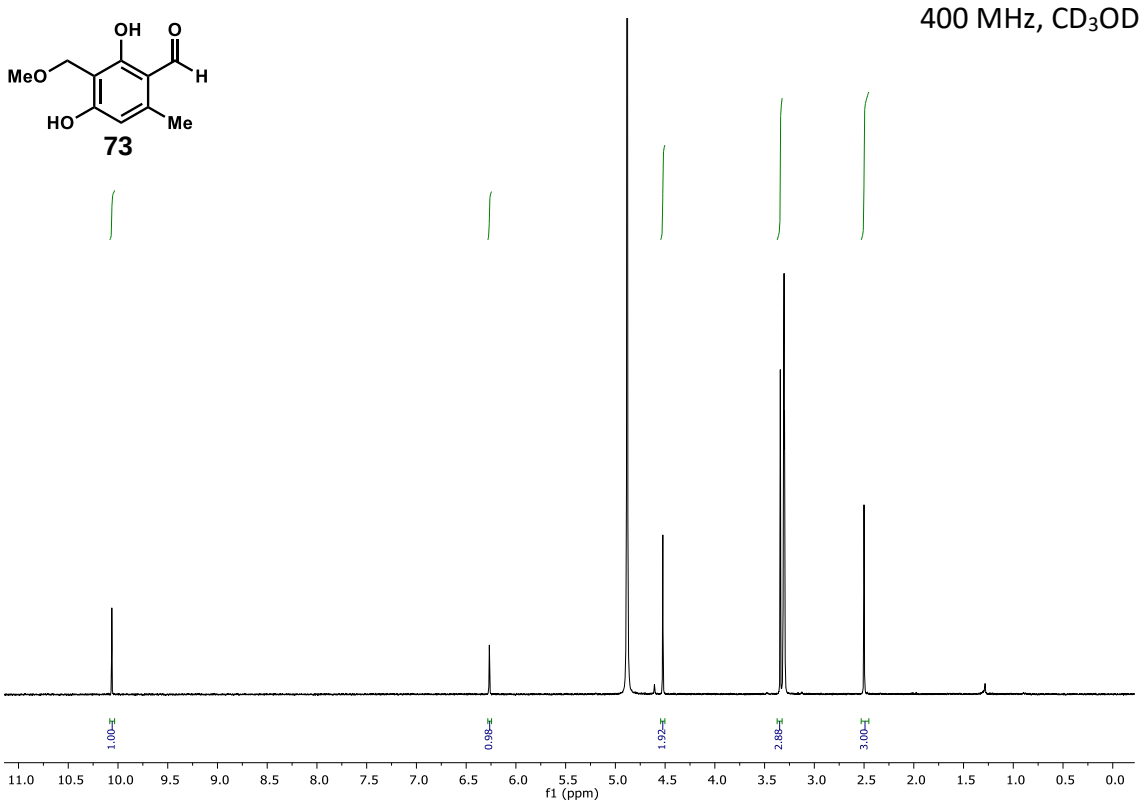
400 MHz, CD3OD
OH
O
MeO
H
HO
Me
73
1.00
0.98
1.92
2.88
3.00
11.0 10.5 10.0 9.5 9.0 8.5 8.0 7.5 7.0 6.5 6.0 5.5 5.0 4.5 4.0 3.5 3.0 2.5 2.0 1.5 1.0 0.5 0.0
f1 (ppm)

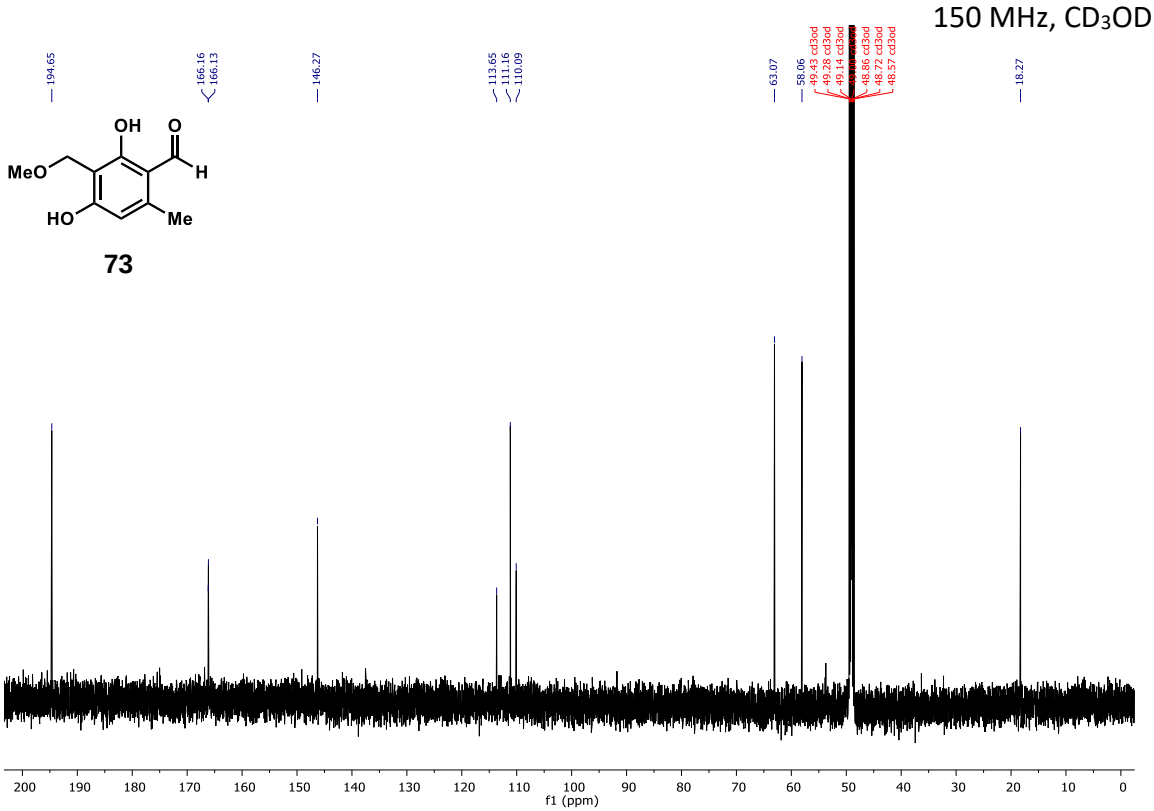
150 MHz, CD3OD
194.65
166.16
166.13
146.27
113.65
111.16
110.09
63.07
58.06
49.43 cd3od
49.28 cd3od
49.14 cd3od
48.86 cd3od
48.72 cd3od
48.57 cd3od
18.27
OH
O
MeO
H
HO
Me
73
200 190 180 170 160 150 140 130 120 110 100 90 80 70 60 50 40 30 20 10 0
f1 (ppm)

600 MHz, CD_3OD

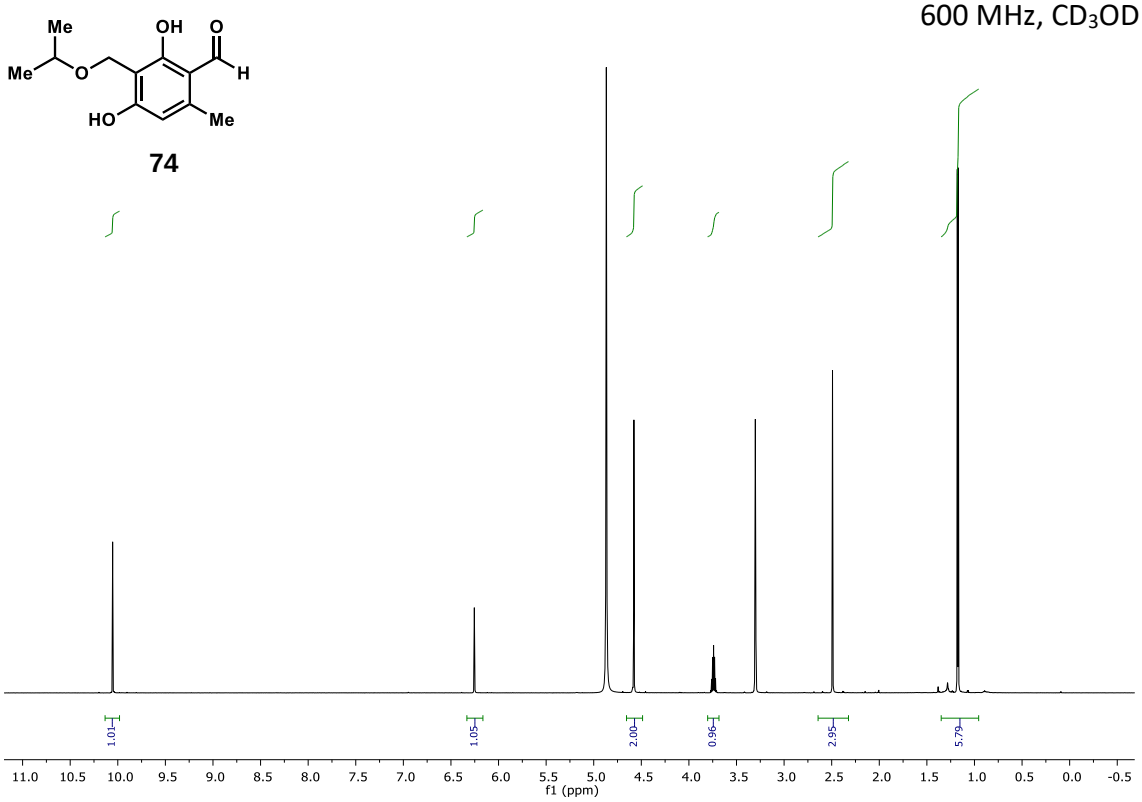

150 MHz, CD_3OD

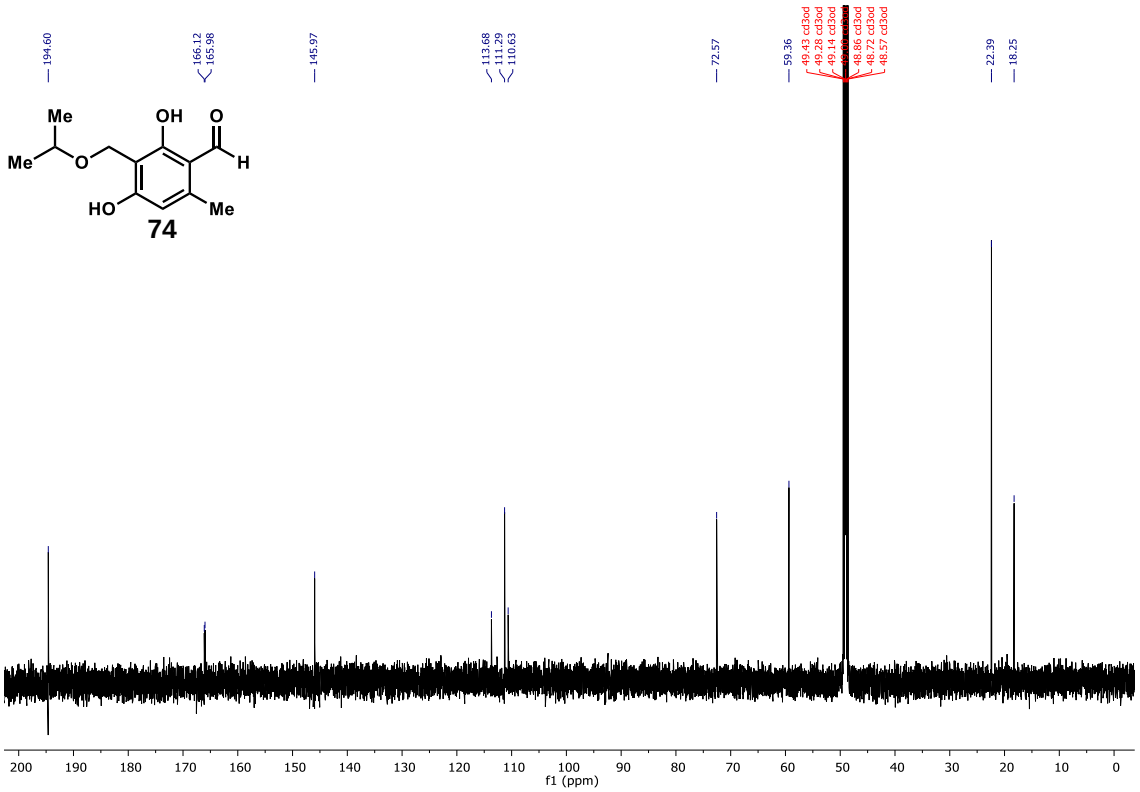

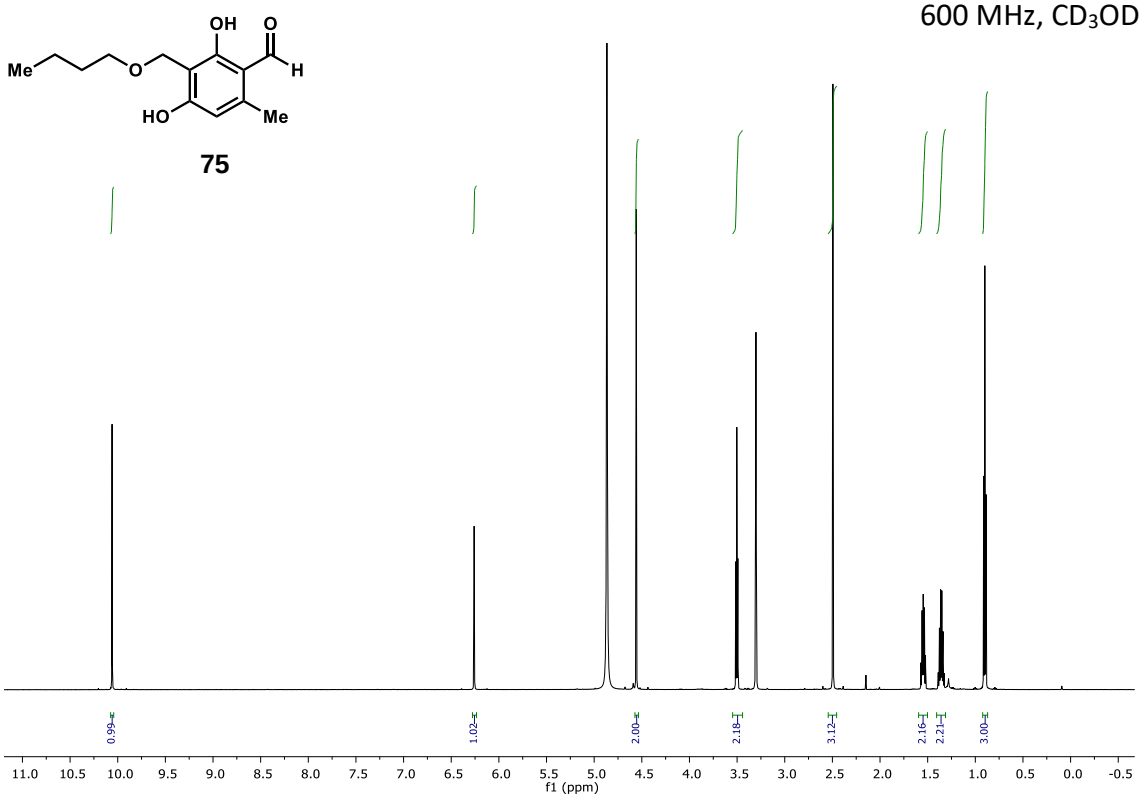
600 MHz, CD3OD
OH
O
Me
O
H
HO
Me
75
0.99
1.02
2.00
2.18
3.12
2.16
2.21
3.00
11.0 10.5 10.0 9.5 9.0 8.5 8.0 7.5 7.0 6.5 6.0 5.5 5.0 4.5 4.0 3.5 3.0 2.5 2.0 1.5 1.0 0.5 0.0 -0.5
f1 (ppm)

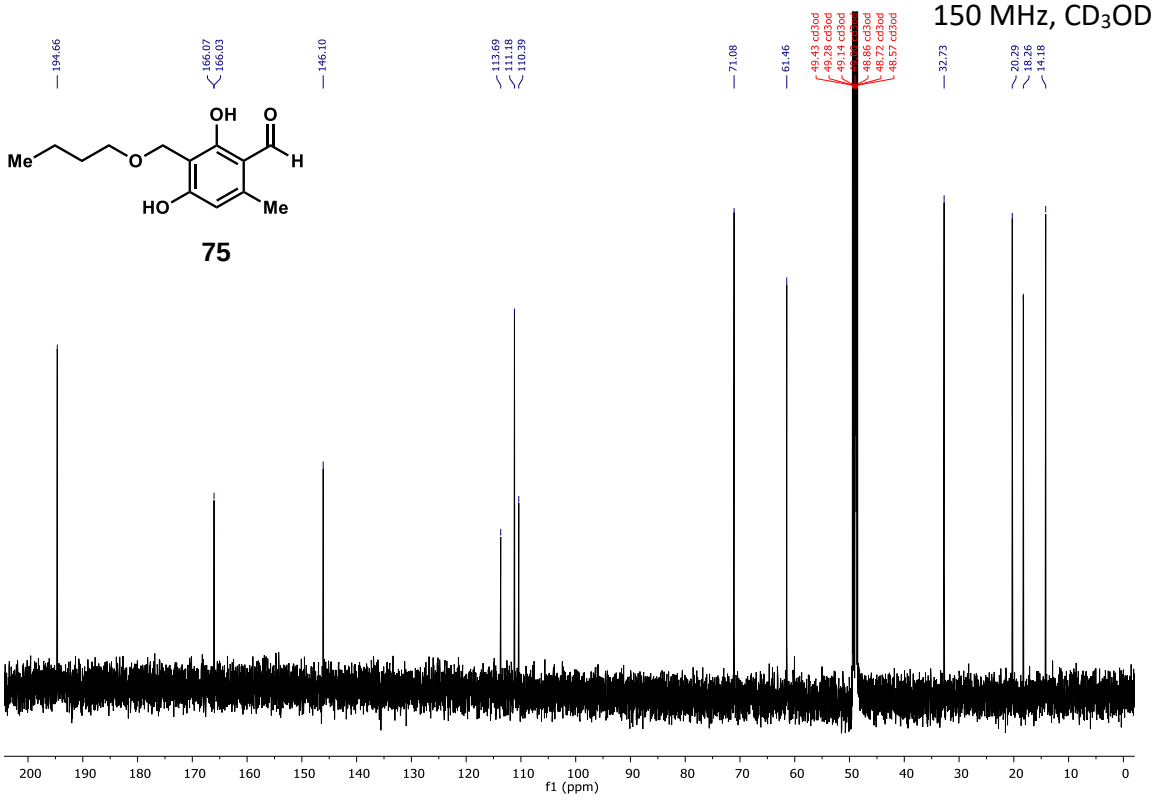
150 MHz, CD3OD
194.66
166.07
166.03
146.10
113.69
111.18
110.39
71.08
61.46
49.43 cd3od
49.28 cd3od
49.14 cd3od
48.86 cd3od
48.72 cd3od
48.57 cd3od
32.73
20.29
18.26
14.18
OH
O
Me
O
H
HO
Me
75
200 190 180 170 160 150 140 130 120 110 100 90 80 70 60 50 40 30 20 10 0
f1 (ppm)

400 MHz, CD_3OD

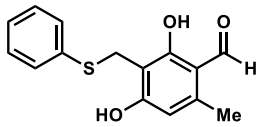

20

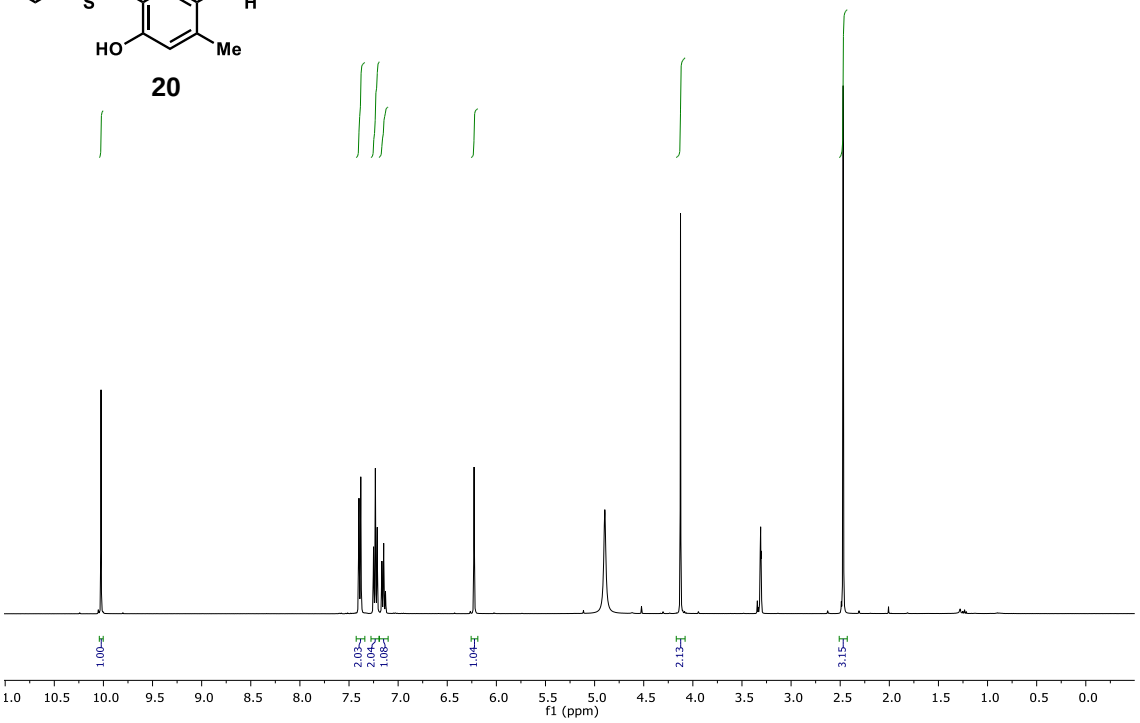

150 MHz, CD_3OD

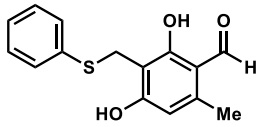

20

600 MHz, CD_3OD

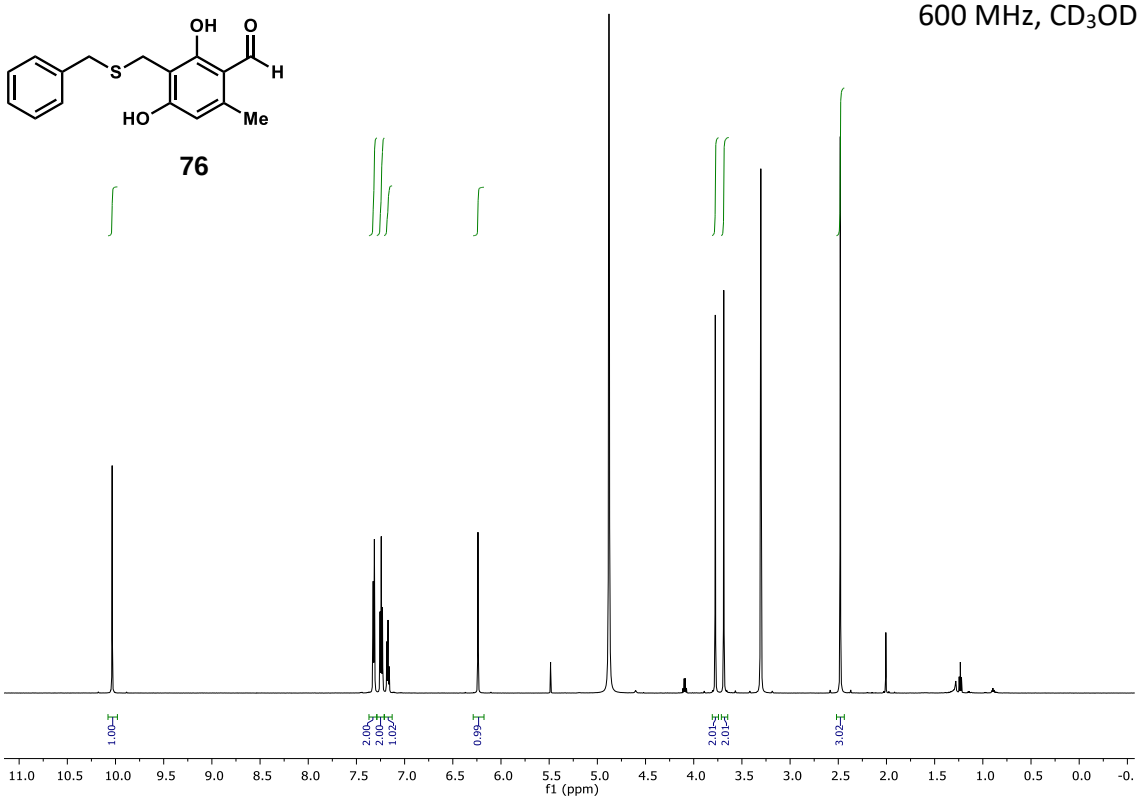

150 MHz, CD_3OD

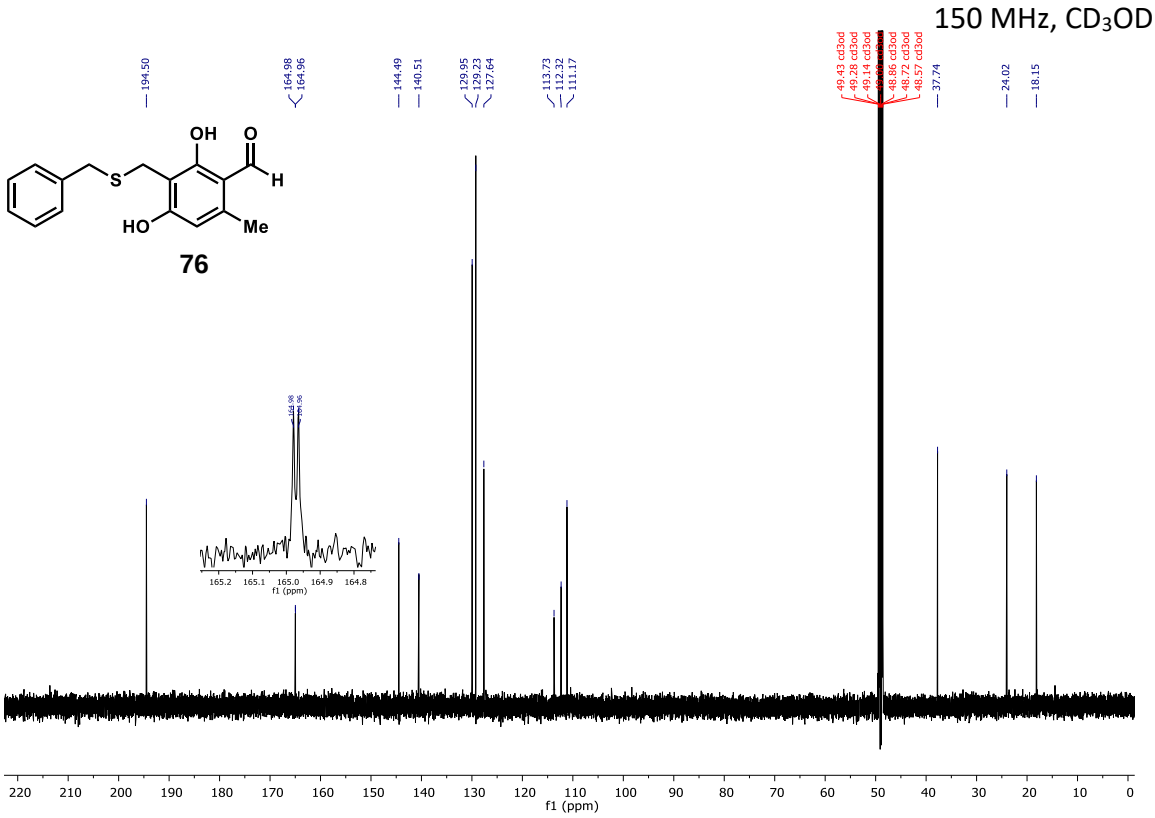

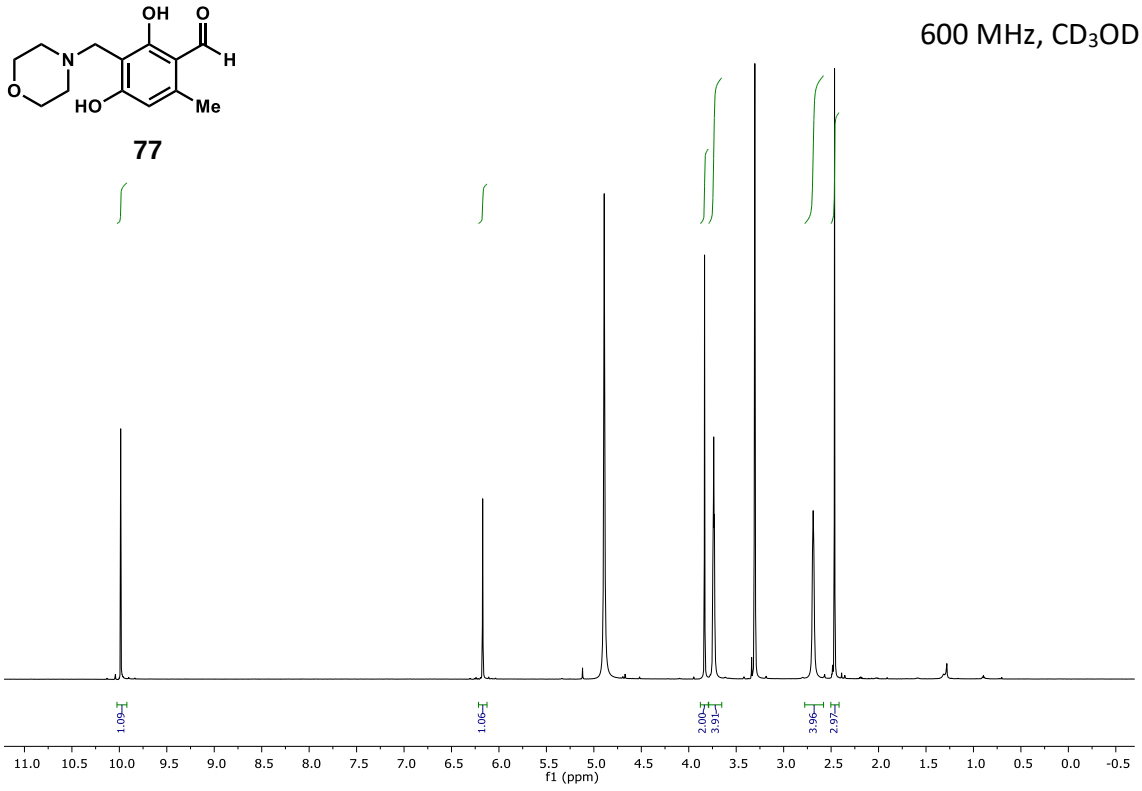
OH
O
H
N
O
HO
Me
77
600 MHz, CD3OD
1.09
1.06
2.00
3.91
3.96
2.97
11.0 10.5 10.0 9.5 9.0 8.5 8.0 7.5 7.0 6.5 6.0 5.5 5.0 4.5 4.0 3.5 3.0 2.5 2.0 1.5 1.0 0.5 0.0 -0.5
f1 (ppm)

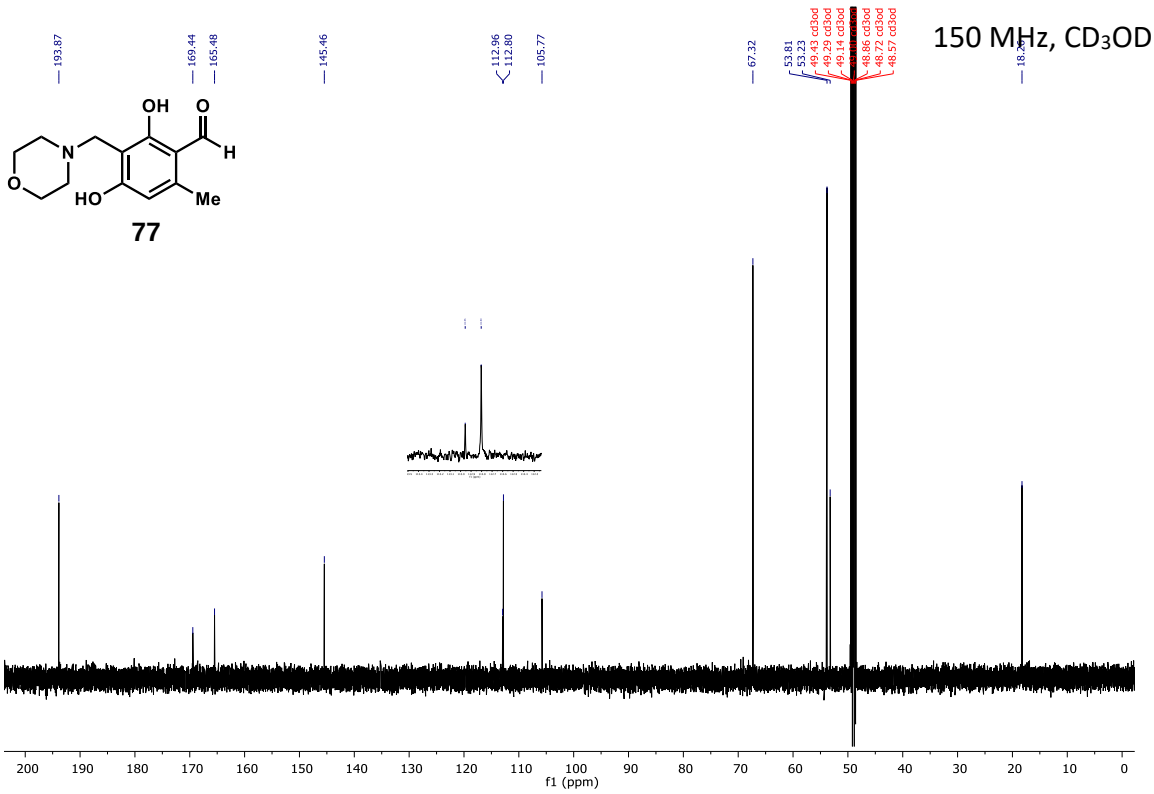
193.87
169.44
165.48
145.46
112.96
112.80
105.77
67.32
53.81
53.23
49.43 cd3od
49.29 cd3od
49.14 cd3od
48.86 cd3od
48.72 cd3od
48.57 cd3od
18.26
OH
O
H
N
O
HO
Me
77
150 MHz, CD3OD
200 190 180 170 160 150 140 130 120 110 100 90 80 70 60 50 40 30 20 10 0
f1 (ppm)

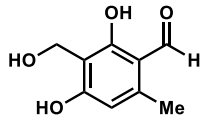

17

400 MHz, CD_3OD

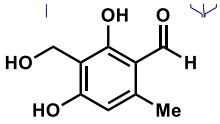

17

150 MHz, CD_3OD

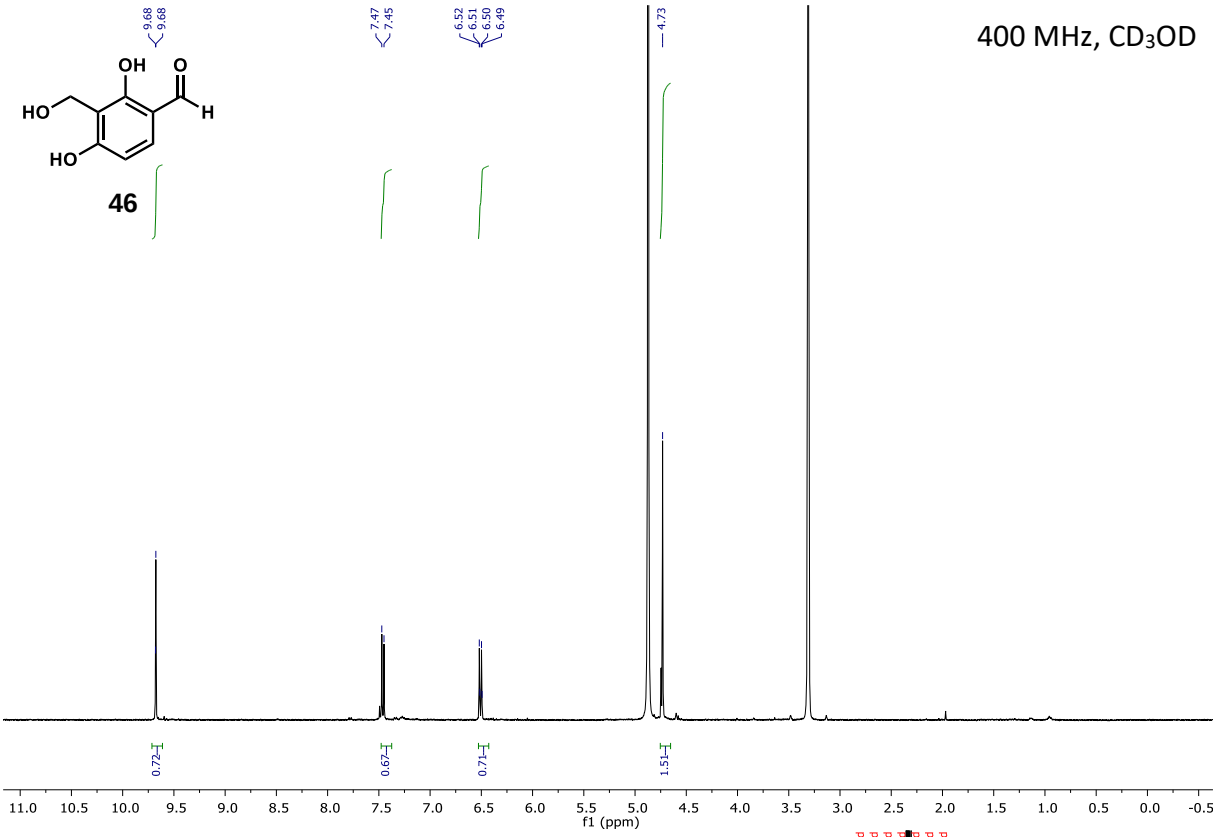
400 MHz, CD3OD
9.68
9.68
7.47
7.45
6.52
6.51
6.50
6.49
4.73
OH
O
HO
H
HO
46
0.72
0.67
0.71
1.51
11.0 10.5 10.0 9.5 9.0 8.5 8.0 7.5 7.0 6.5 6.0 5.5 5.0 4.5 4.0 3.5 3.0 2.5 2.0 1.5 1.0 0.5 0.0 -0.5
f1 (ppm)

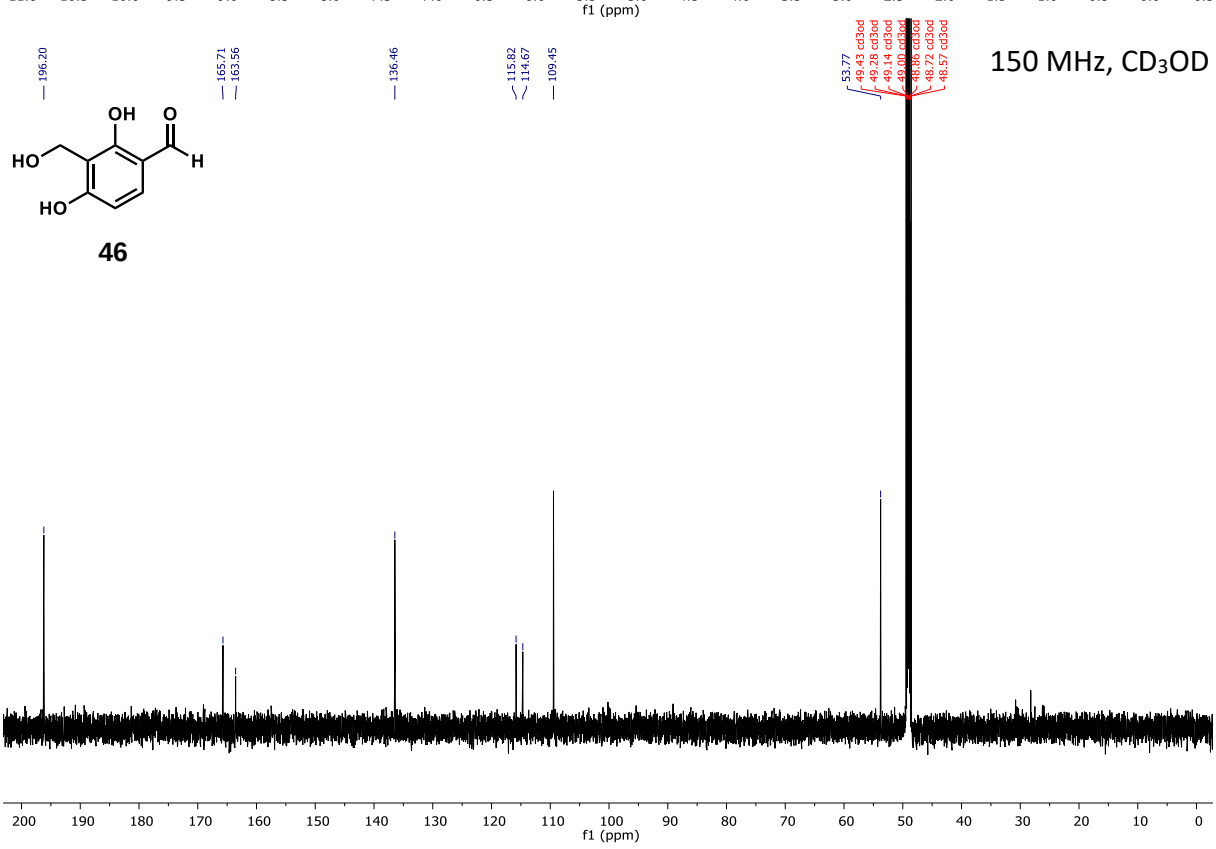
150 MHz, CD3OD
196.20
165.71
163.56
136.46
115.82
114.67
109.45
53.77
49.43 cd3od
49.28 cd3od
49.14 cd3od
49.00 cd3od
48.86 cd3od
48.72 cd3od
48.57 cd3od
OH
O
HO
H
HO
46
200 190 180 170 160 150 140 130 120 110 100 90 80 70 60 50 40 30 20 10 0
f1 (ppm)

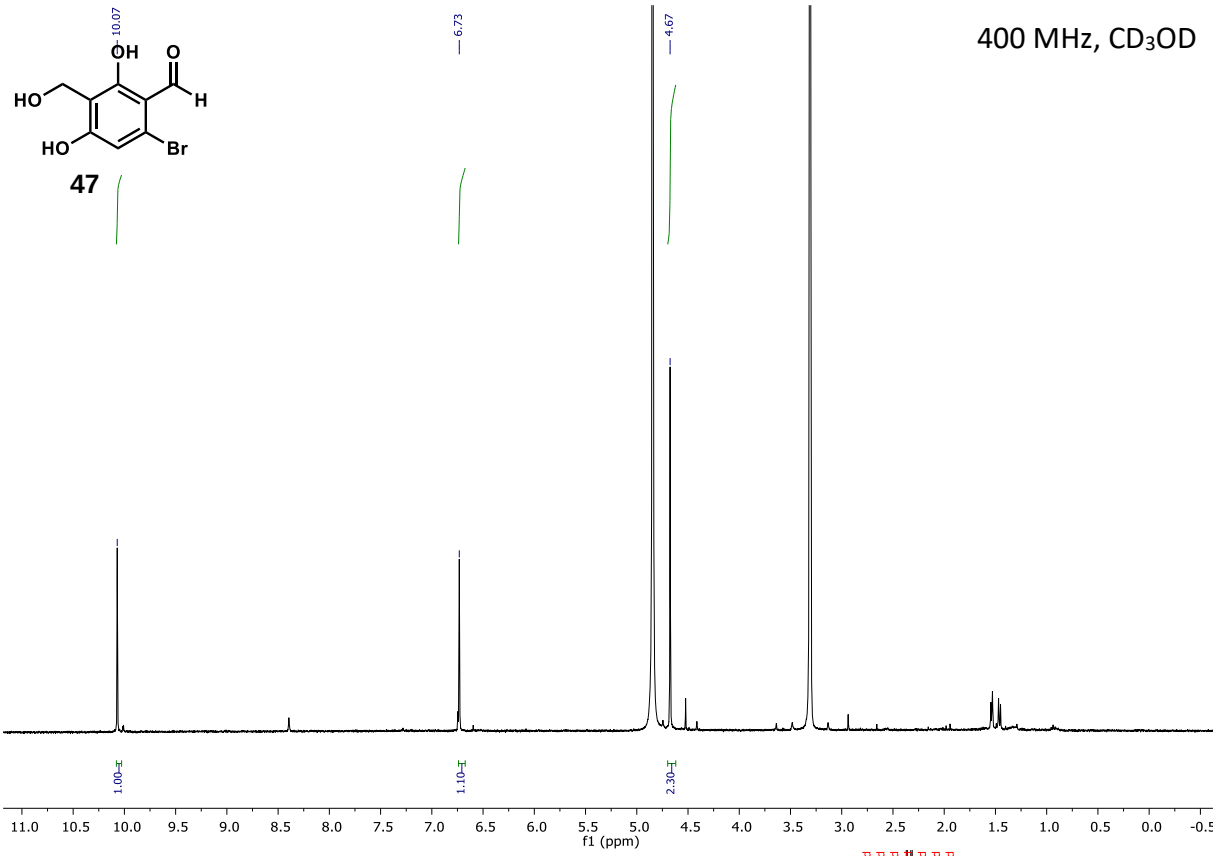
400 MHz, CD3OD
10.07
6.73
4.67
OH
O
HO
H
HO
Br
47
1.00
1.10
2.30
11.0 10.5 10.0 9.5 9.0 8.5 8.0 7.5 7.0 6.5 6.0 5.5 5.0 4.5 4.0 3.5 3.0 2.5 2.0 1.5 1.0 0.5 0.0 -0.5
f1 (ppm)

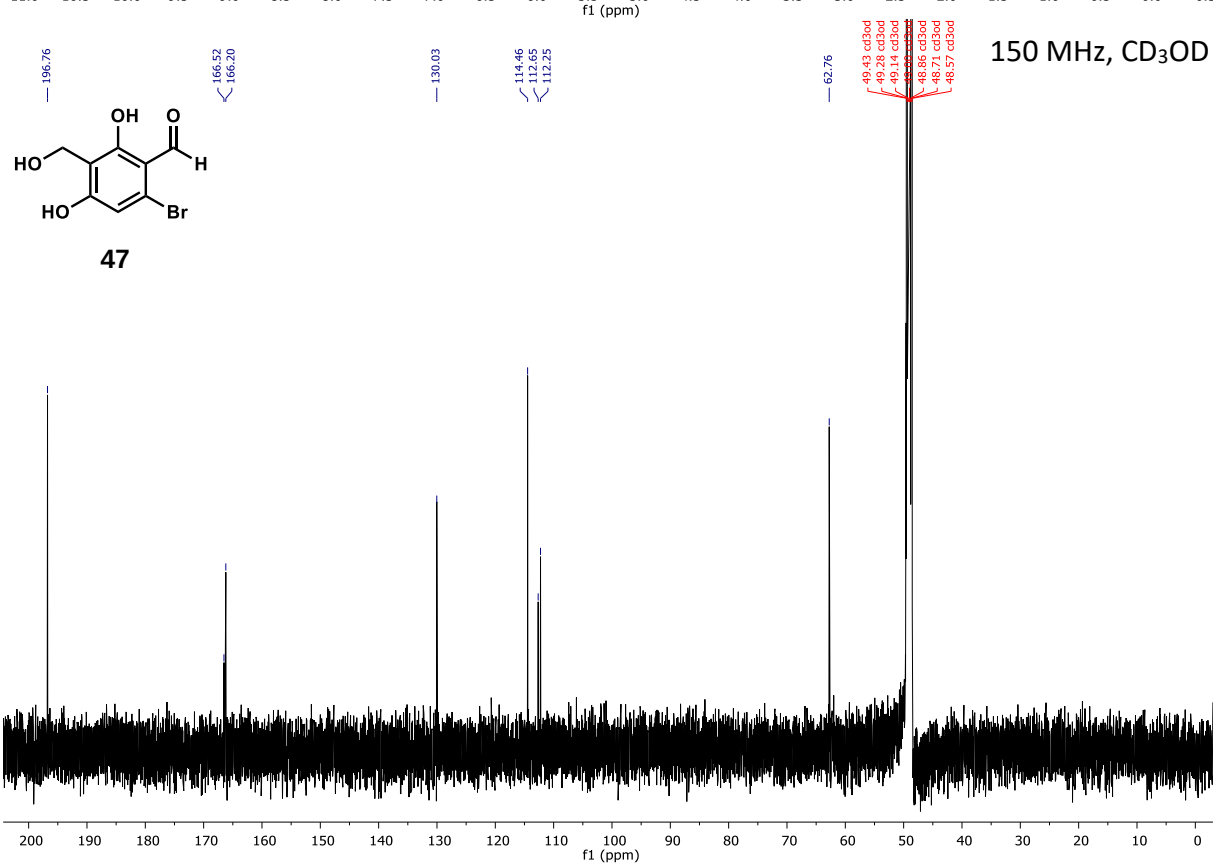
150 MHz, CD3OD
196.76
166.52
166.20
130.03
114.46
112.65
112.25
62.76
49.43 cd3od
49.28 cd3od
49.14 cd3od
48.86 cd3od
48.71 cd3od
48.57 cd3od
OH
O
HO
H
HO
Br
47
200 190 180 170 160 150 140 130 120 110 100 90 80 70 60 50 40 30 20 10 0
f1 (ppm)

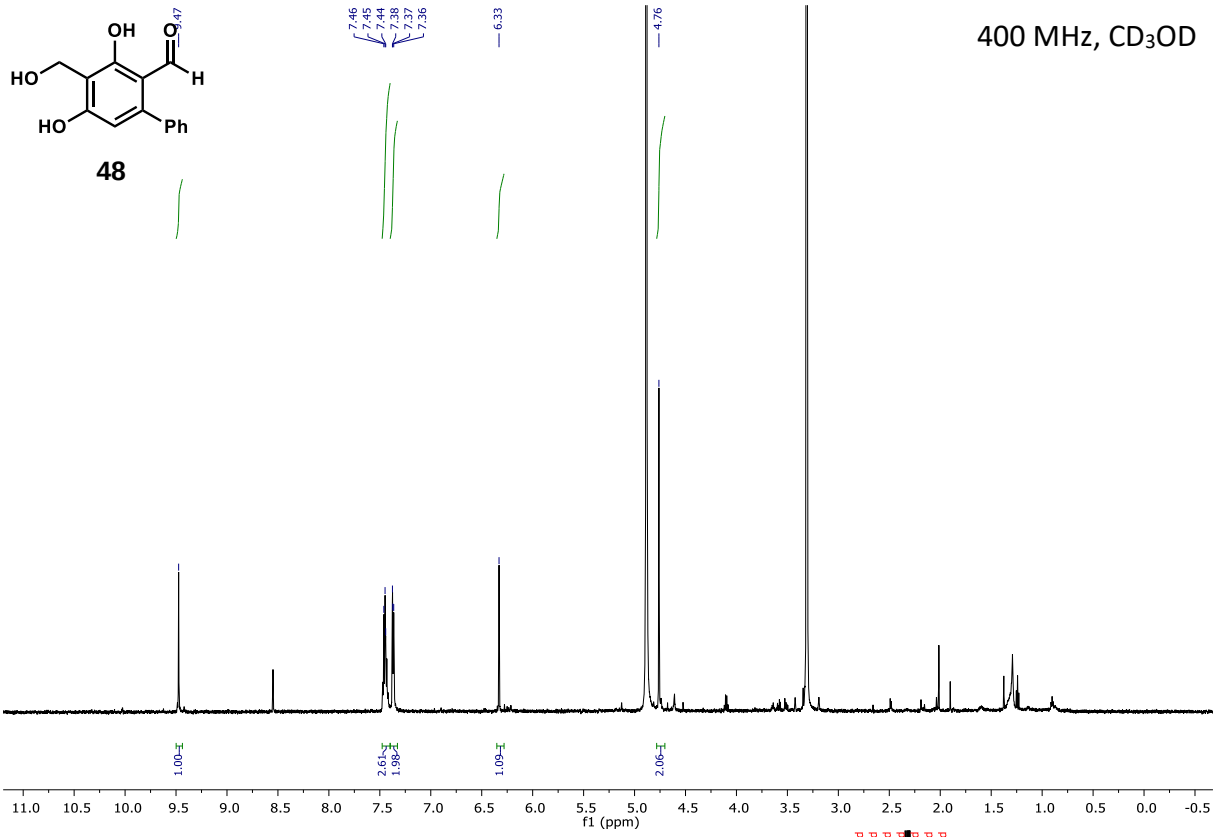
OH
O
HO
H
HO
Ph
48
400 MHz, CD3OD
9.47
7.46
7.45
7.44
7.38
7.37
7.36
6.33
4.76
1.00
2.61
1.98
1.09
2.06
f1 (ppm)

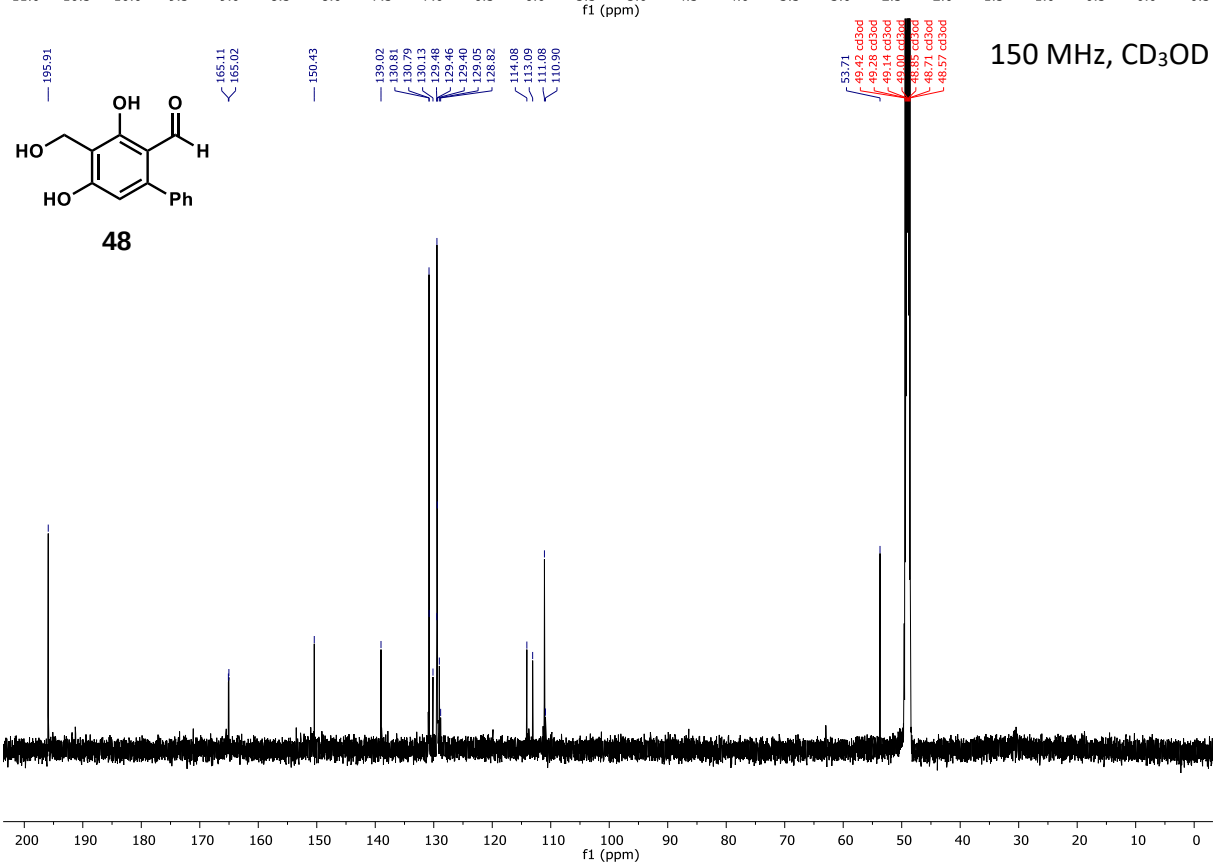
OH
O
HO
H
HO
Ph
48
150 MHz, CD3OD
195.91
165.11
165.02
150.43
139.02
130.81
130.79
130.13
129.48
129.46
129.40
129.05
128.82
114.08
113.09
111.08
110.90
53.71
49.42 cd3od
49.28 cd3od
49.14 cd3od
49.00 cd3od
48.85 cd3od
48.71 cd3od
48.57 cd3od
f1 (ppm)

400 MHz, CD_3OD

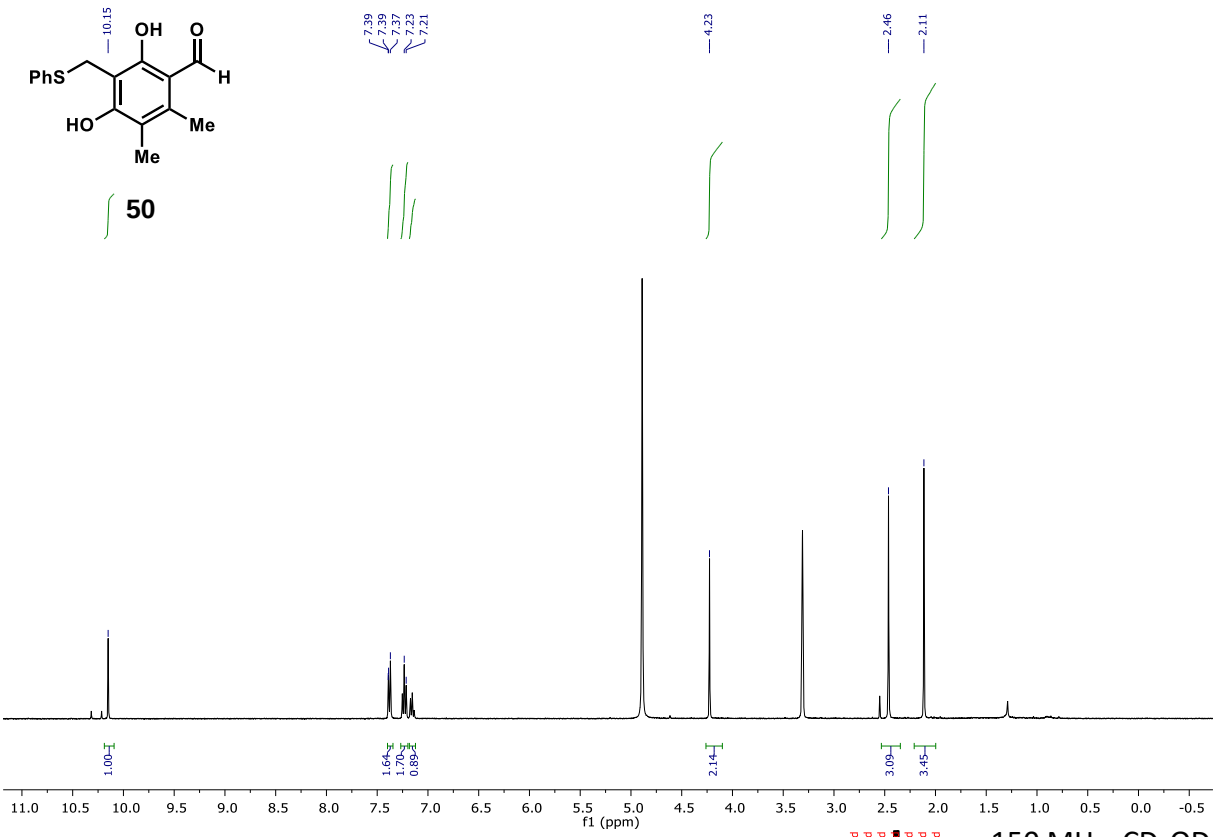

150 MHz, CD_3OD

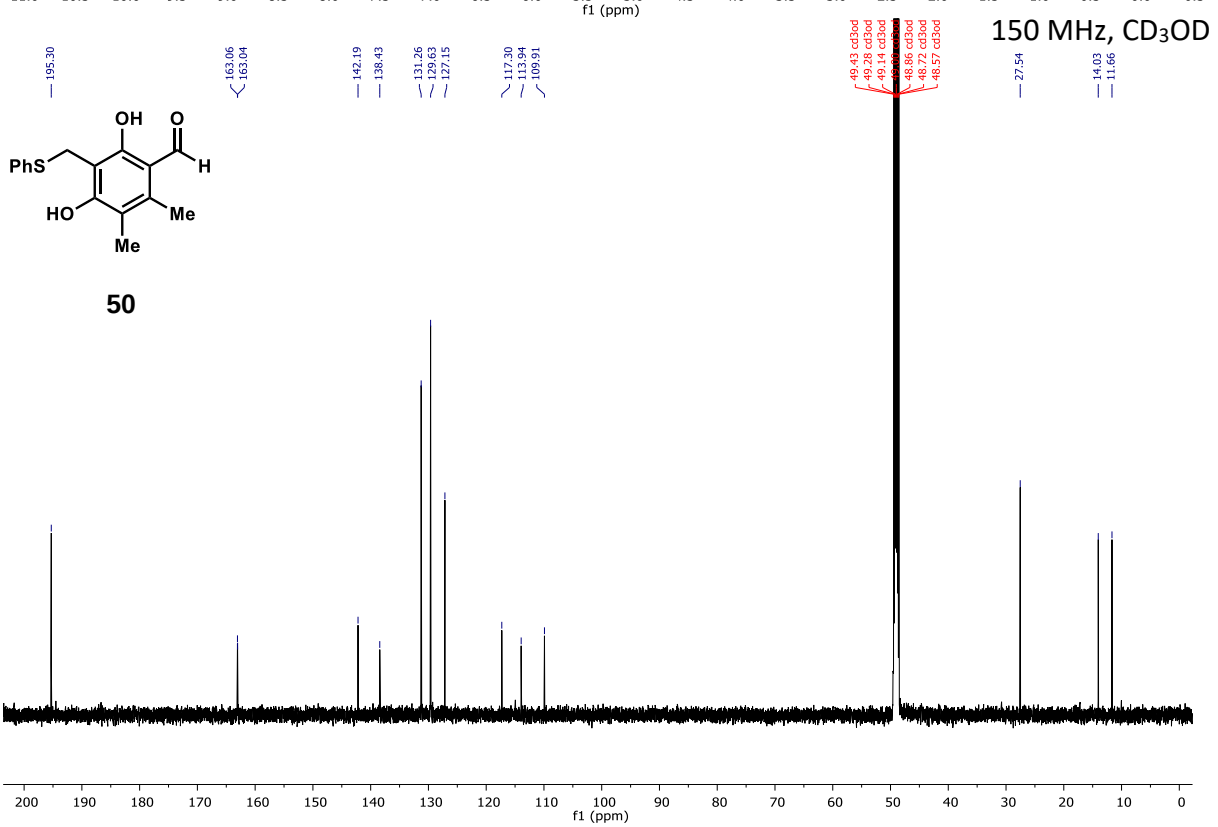

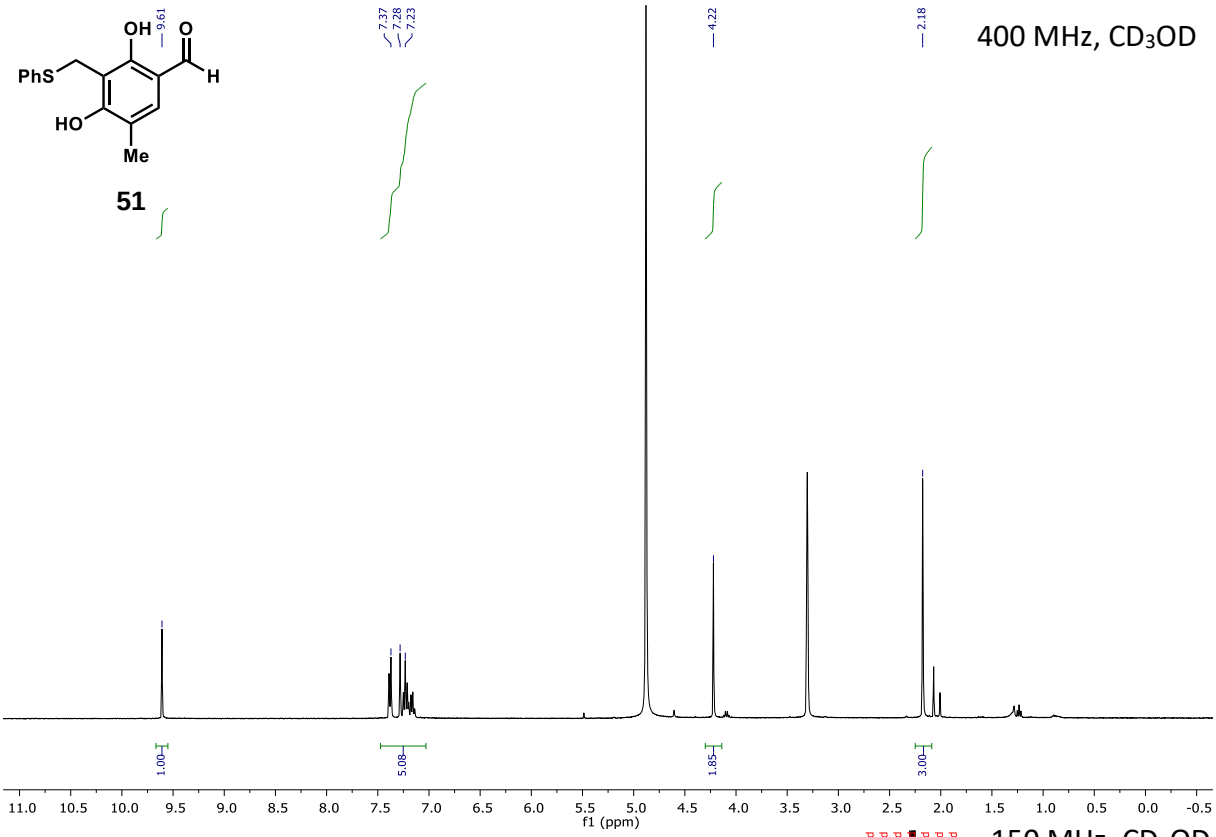
OH
O
PhS
H
HO
Me
51
9.61
7.37
7.28
7.23
4.22
2.18
400 MHz, CD3OD
1.00
5.08
1.85
3.00
f1 (ppm)

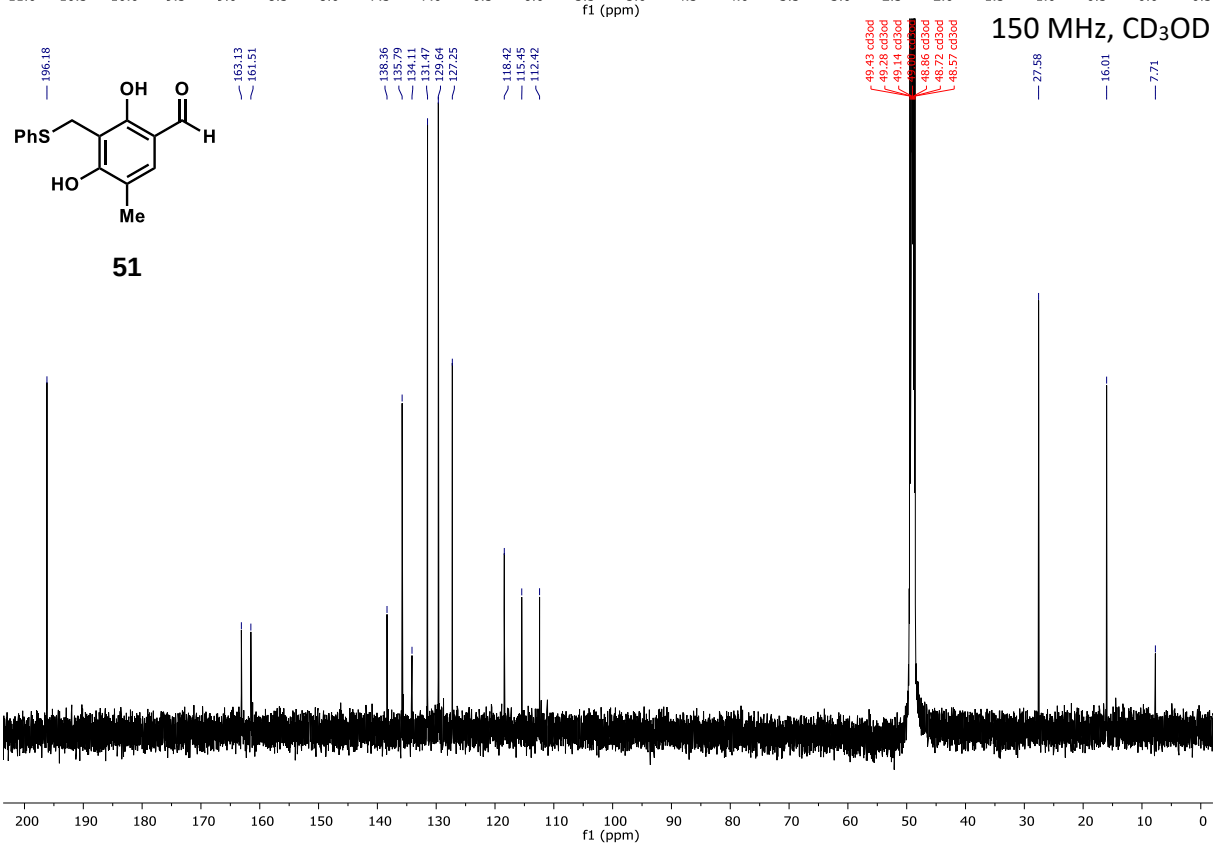
OH
O
PhS
H
HO
Me
51
196.18
163.13
161.51
138.36
135.79
134.11
131.47
129.64
127.25
118.42
115.45
112.42
49.43 cd3od
49.28 cd3od
49.14 cd3od
48.86 cd3od
48.72 cd3od
48.57 cd3od
27.58
16.01
7.71
150 MHz, CD3OD
f1 (ppm)

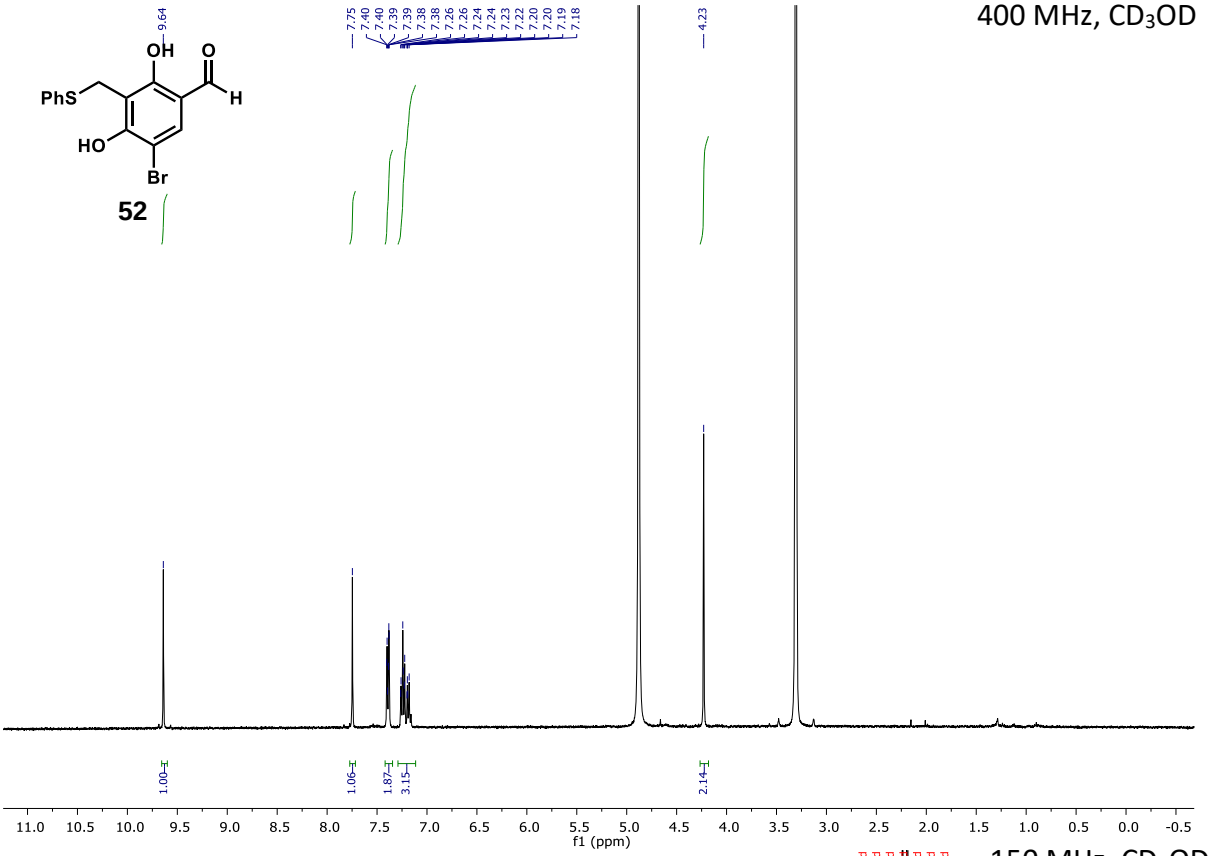
400 MHz, CD3OD
OH
O
PhS
H
HO
Br
52
9.64
7.75
7.40
7.40
7.39
7.39
7.38
7.38
7.26
7.26
7.24
7.24
7.23
7.22
7.20
7.20
7.19
7.18
4.23
1.00
1.06
1.87
3.15
2.14
f1 (ppm)

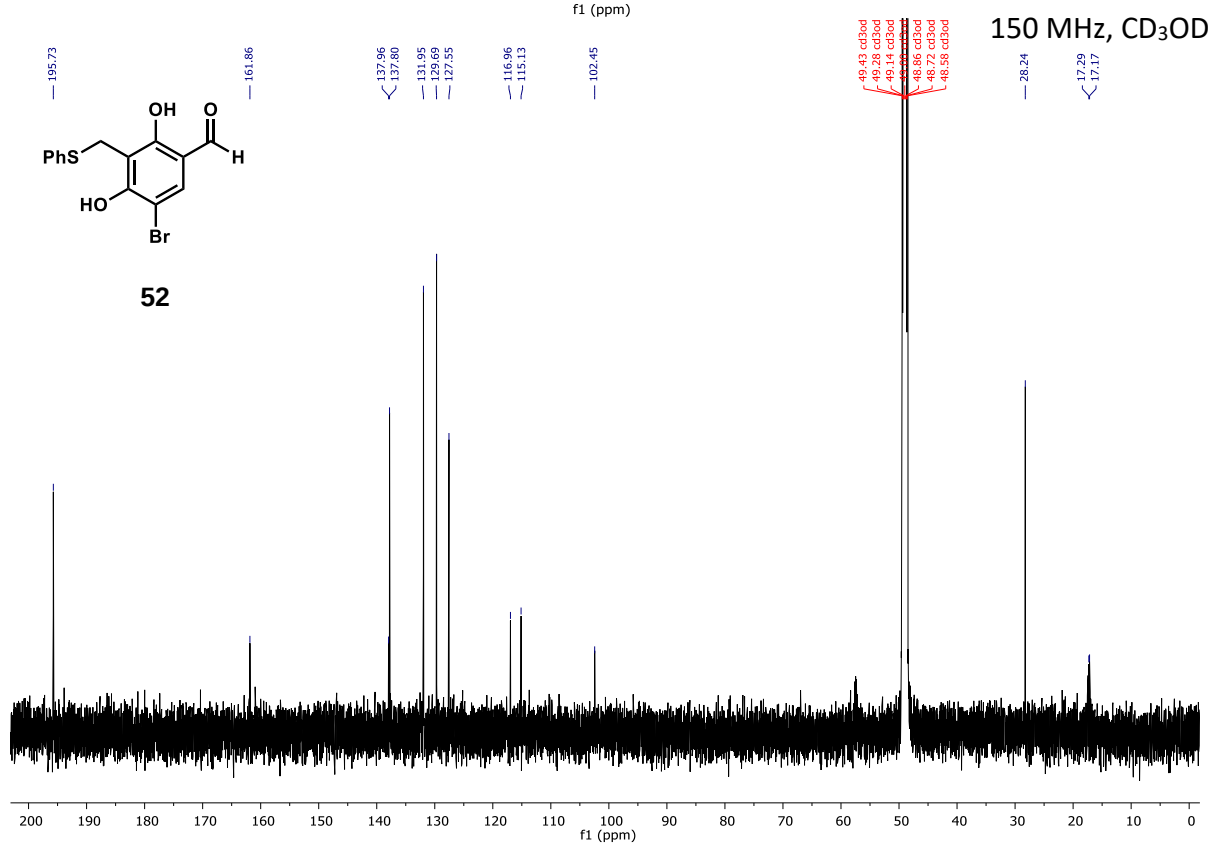
150 MHz, CD3OD
OH
O
PhS
H
HO
Br
52
195.73
161.86
137.96
137.80
131.95
129.69
127.55
116.96
115.13
102.45
49.43 cd3od
49.28 cd3od
49.14 cd3od
48.86 cd3od
48.72 cd3od
48.58 cd3od
28.24
17.29
17.17
f1 (ppm)

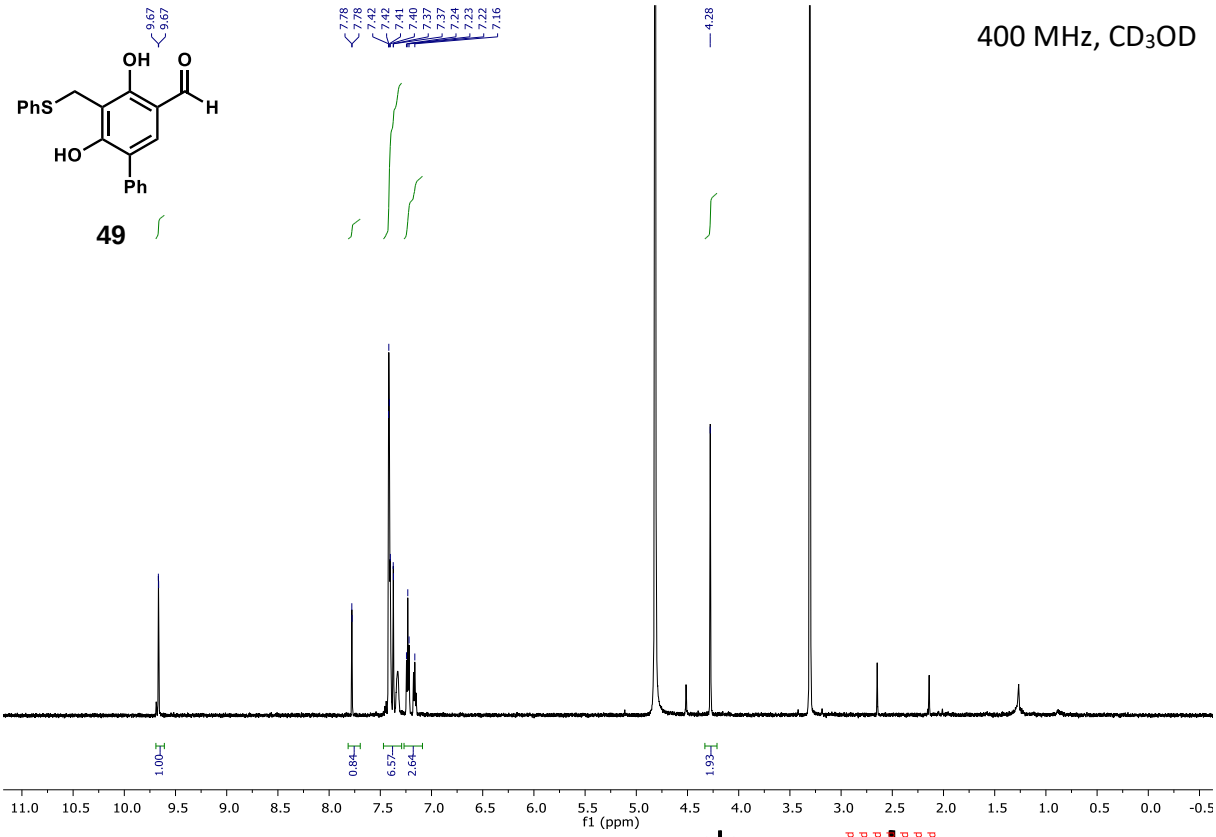
400 MHz, CD3OD
OH
O
PhS
H
HO
Ph
49
9.67
9.67
7.78
7.78
7.42
7.42
7.41
7.40
7.37
7.24
7.23
7.22
7.16
4.28
1.00
0.84
6.57
2.64
1.93
f1 (ppm)

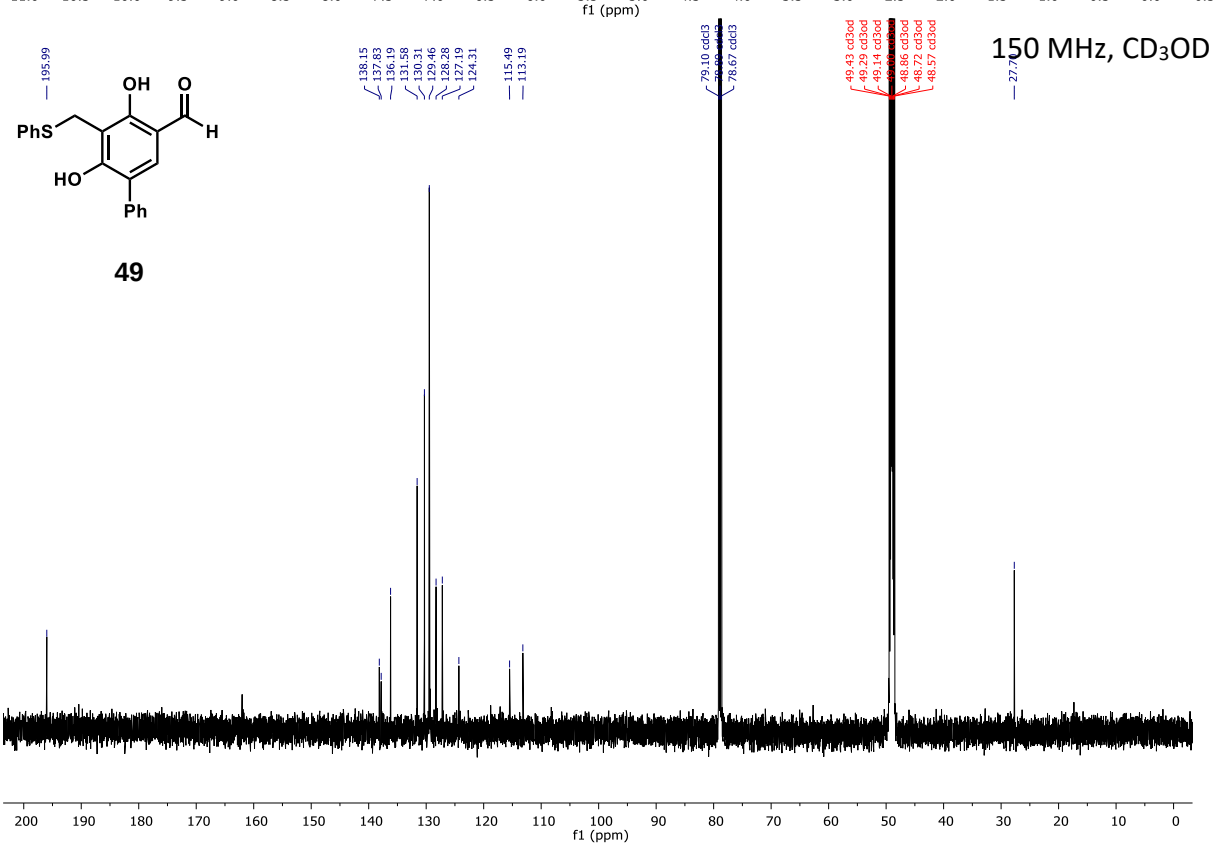
150 MHz, CD3OD
OH
O
PhS
H
HO
Ph
49
195.99
138.15
137.83
136.19
131.58
130.31
129.46
128.28
127.19
124.31
115.49
113.19
79.10 cdcl3
78.67 cdcl3
49.43 cd3od
49.29 cd3od
49.14 cd3od
48.86 cd3od
48.72 cd3od
48.57 cd3od
27.70
f1 (ppm)

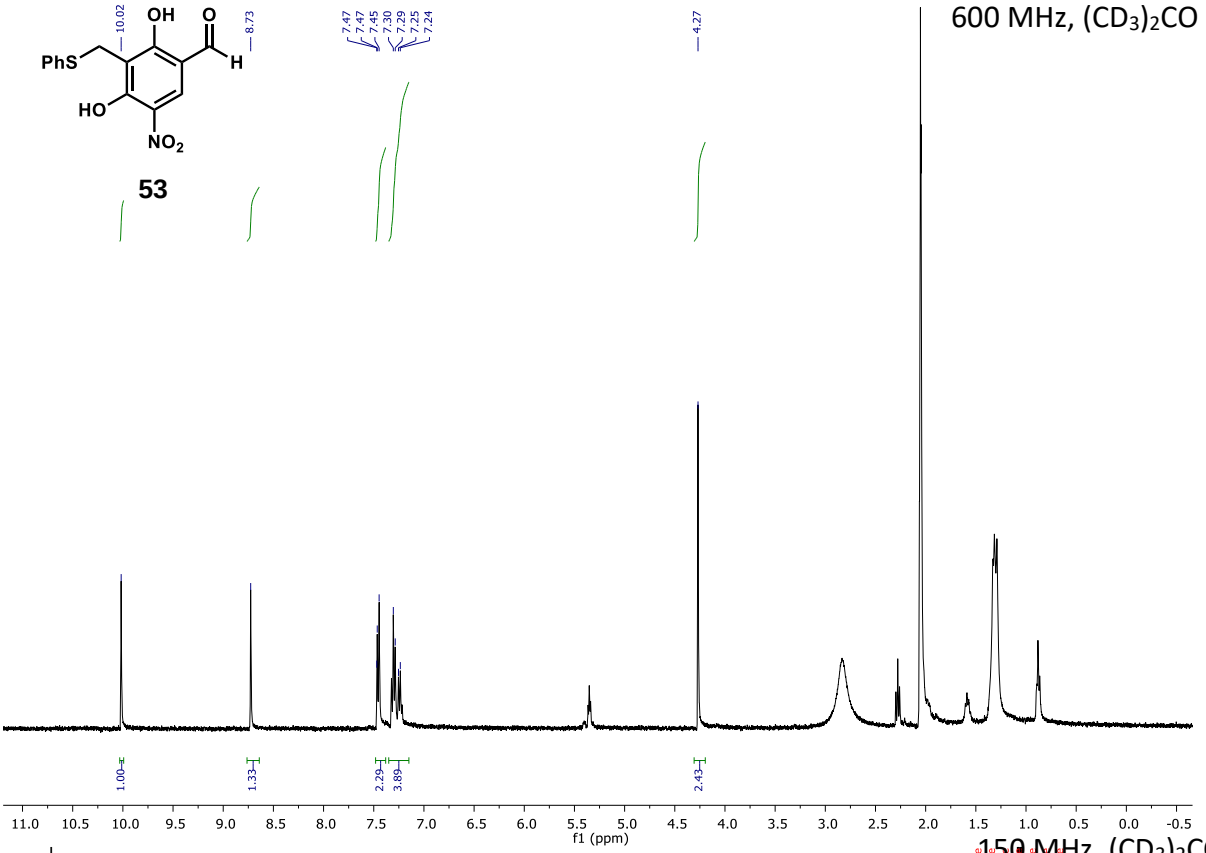
600 MHz, (CD3)2CO
PhS
OH
O
H
HO
NO2
53
10.02
8.73
7.47
7.47
7.45
7.30
7.29
7.25
7.24
4.27
1.00
1.33
2.29
3.89
2.43
f1 (ppm)

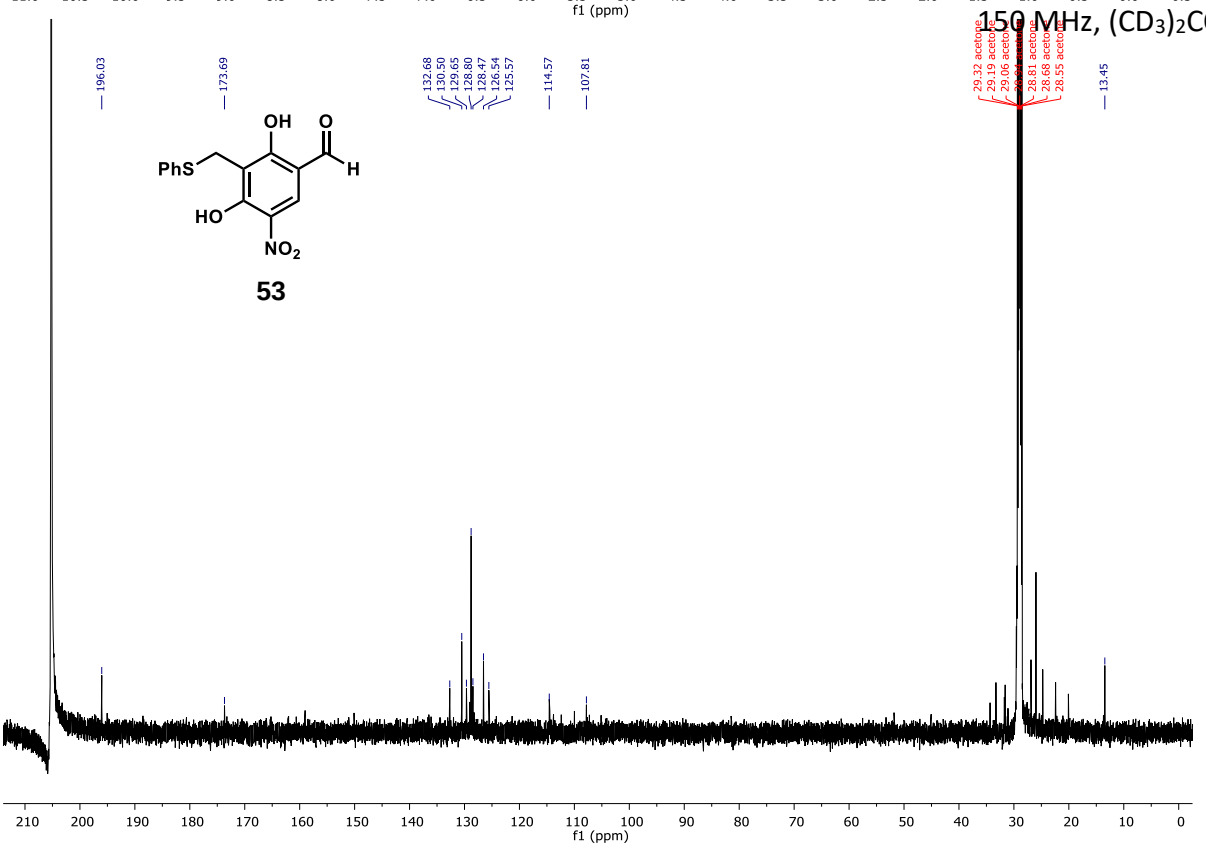
150 MHz, (CD3)2CO
PhS
OH
O
H
HO
NO2
53
196.03
173.69
132.68
130.50
130.65
128.80
128.47
126.54
125.57
114.57
107.81
29.32 acetone
29.19 acetone
29.06 acetone
28.81 acetone
28.68 acetone
28.55 acetone
13.45
f1 (ppm)

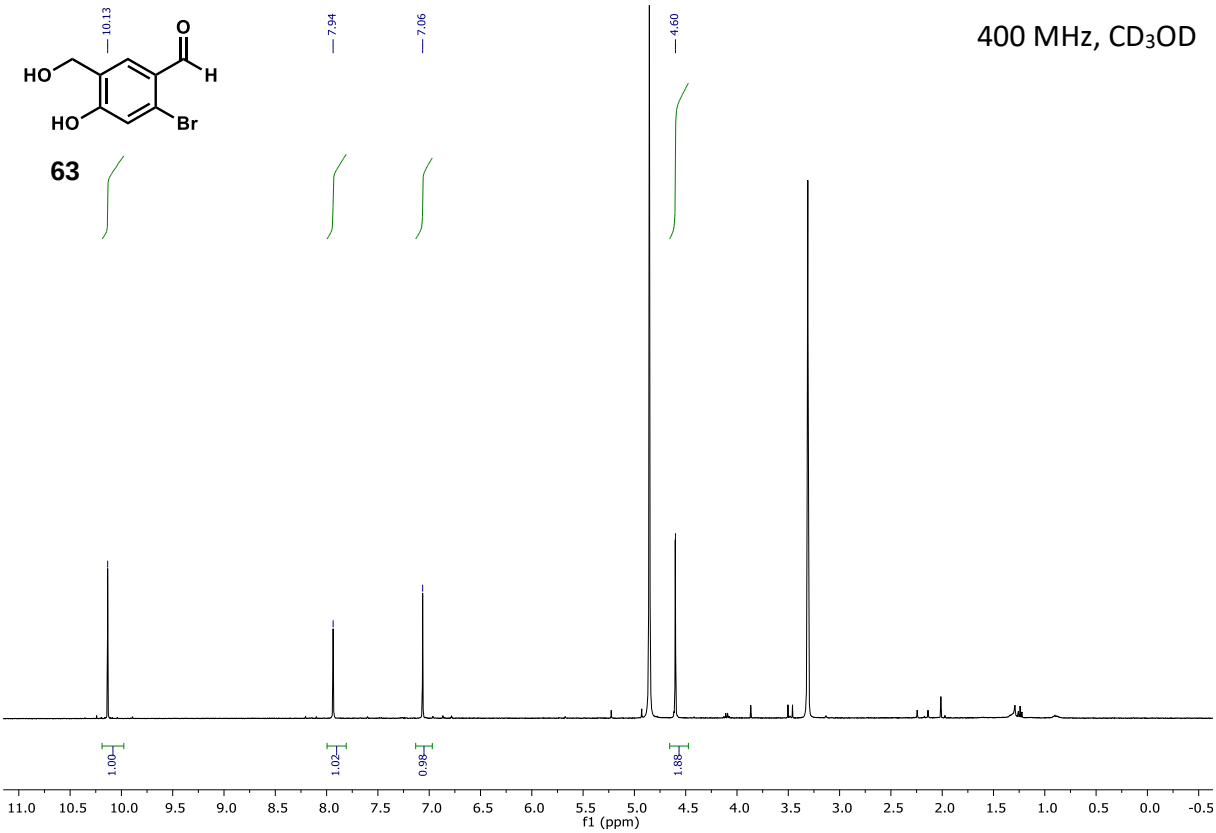
400 MHz, CD3OD
10.13
7.94
7.06
4.60
HO
O
H
HO
Br
63
1.00
1.02
0.98
1.88
11.0 10.5 10.0 9.5 9.0 8.5 8.0 7.5 7.0 6.5 6.0 5.5 5.0 4.5 4.0 3.5 3.0 2.5 2.0 1.5 1.0 0.5 0.0 -0.5
f1 (ppm)

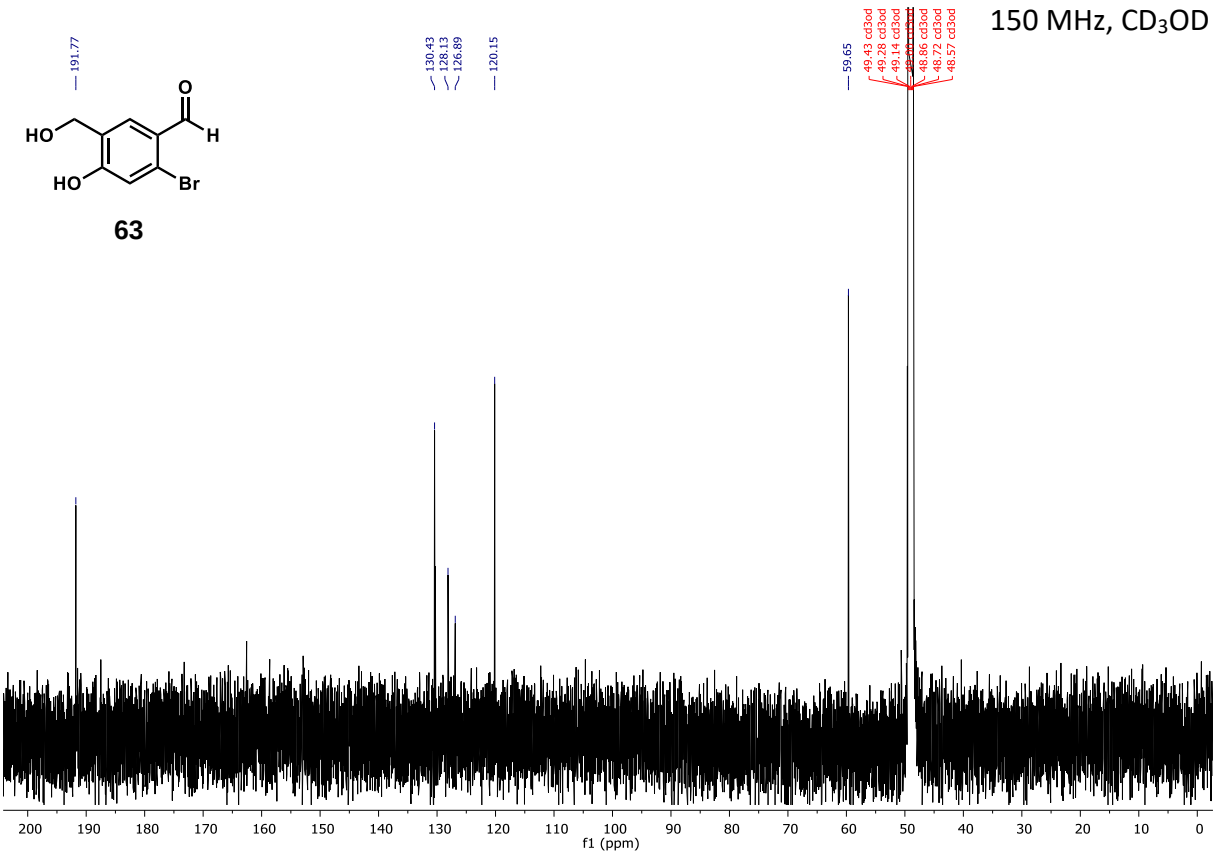
150 MHz, CD3OD
191.77
130.43
128.13
126.89
120.15
59.65
49.43 cd3od
49.28 cd3od
49.14 cd3od
48.86 cd3od
48.72 cd3od
48.57 cd3od
HO
O
H
HO
Br
63
200 190 180 170 160 150 140 130 120 110 100 90 80 70 60 50 40 30 20 10 0
f1 (ppm)

400 MHz, CD_3OD

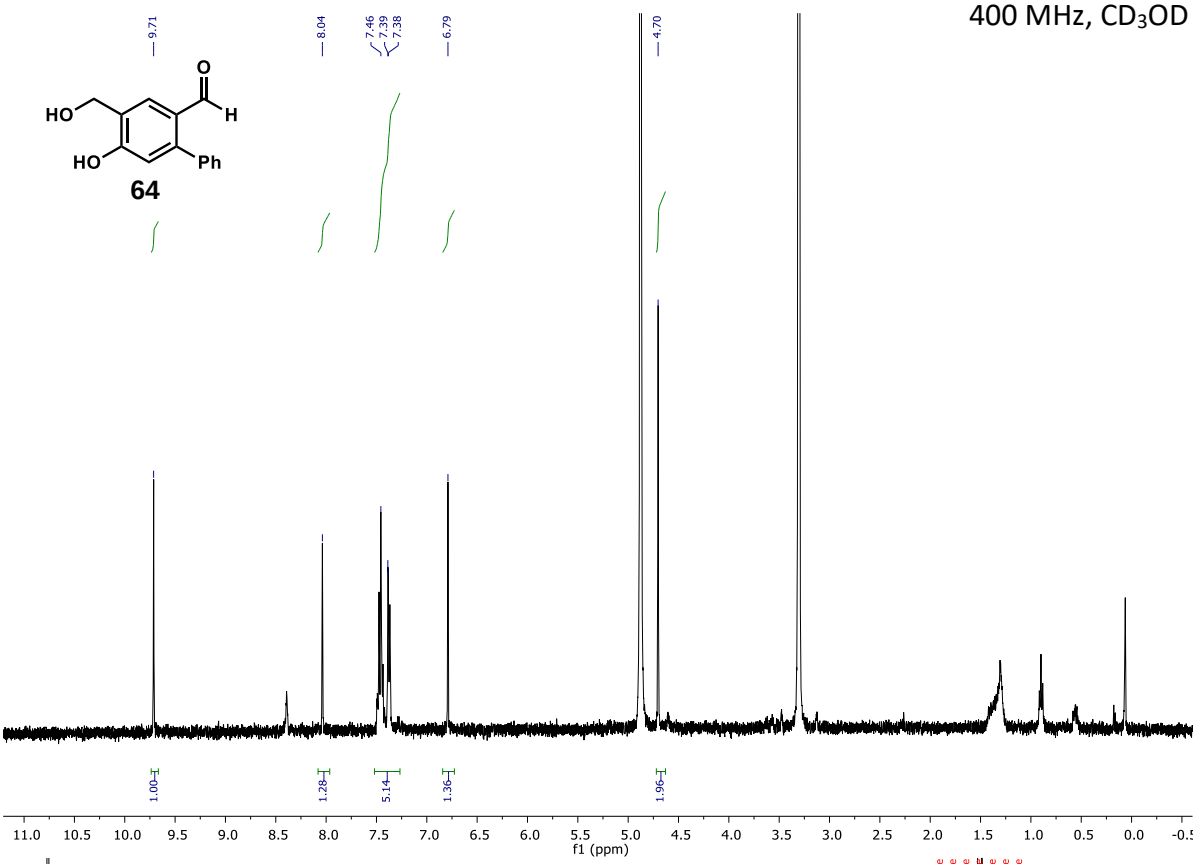

150 MHz, CD_3OD

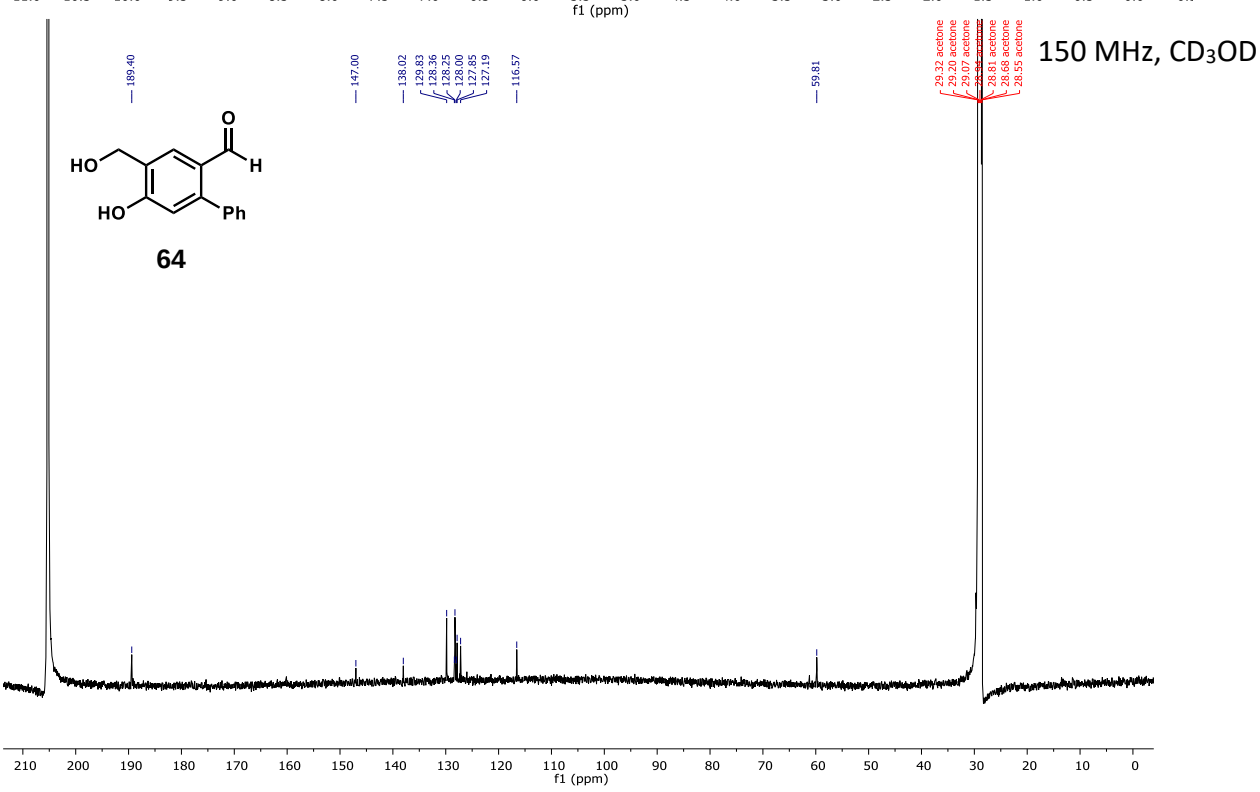

600 MHz, $(CD_3)_2CO$

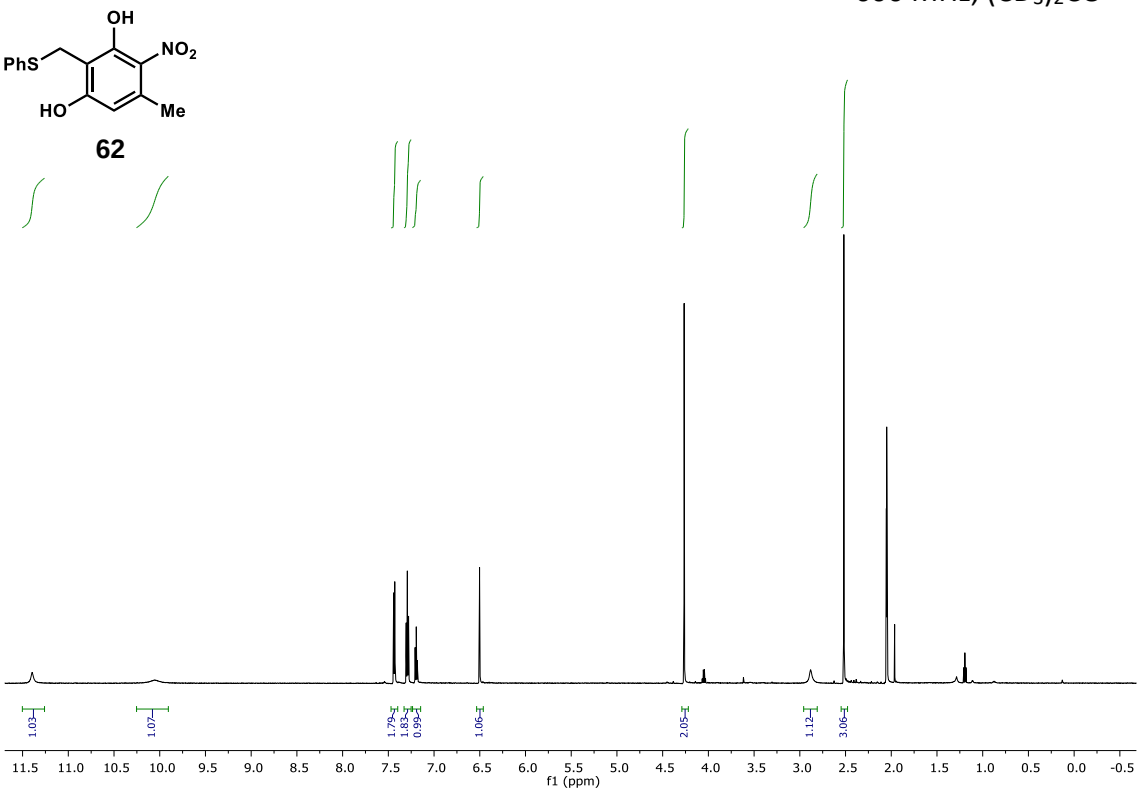

150 MHz, $(CD_3)_2CO$

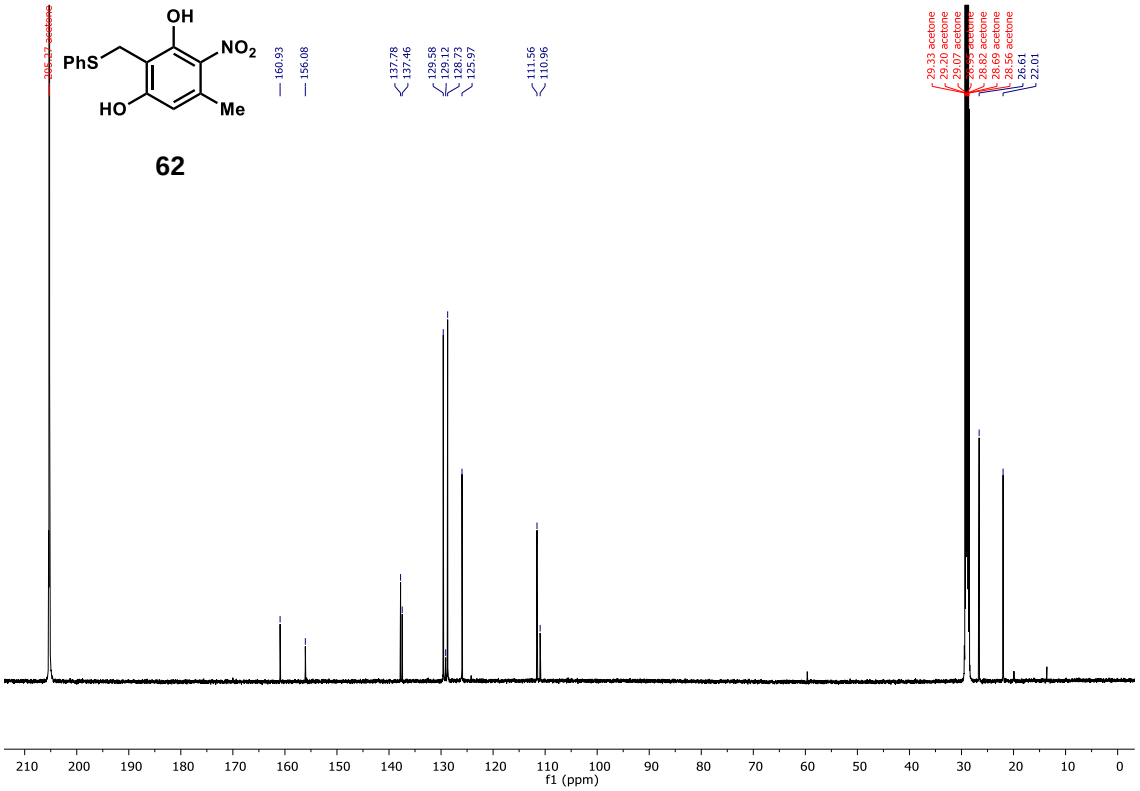

600 MHz, CD_3OD

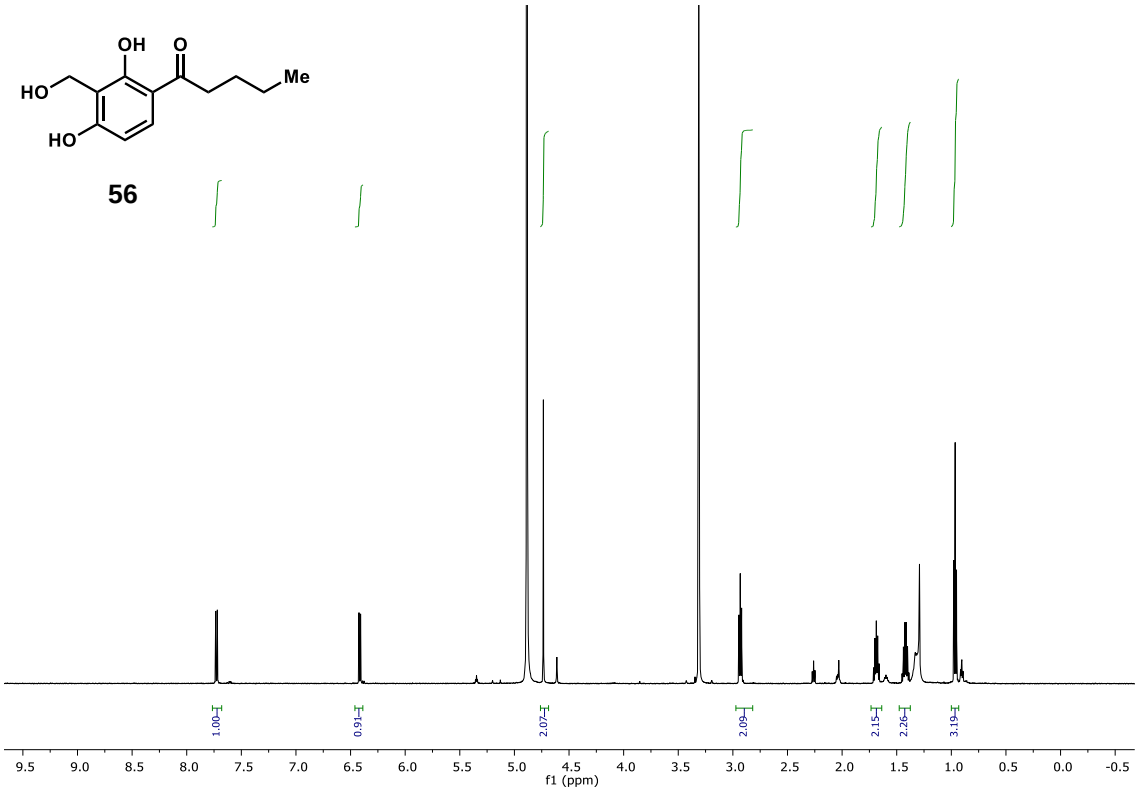

150 MHz, CD_3OD

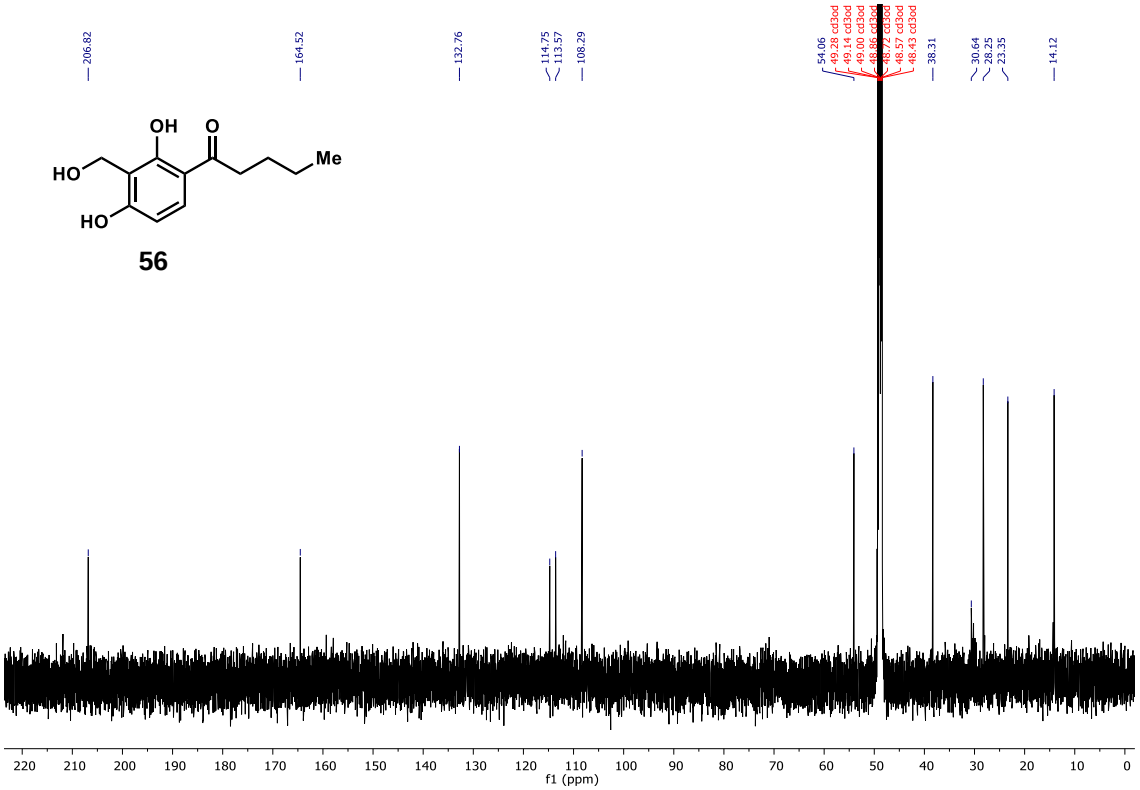

600 MHz, CD_3OD

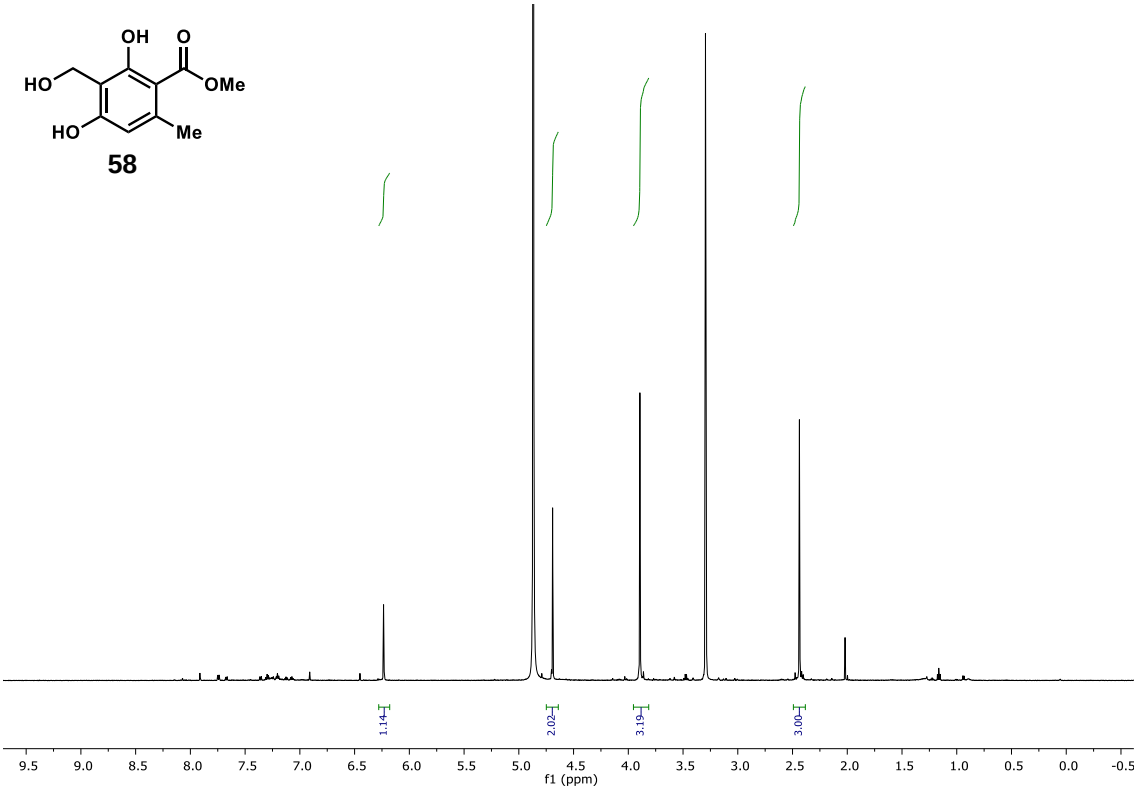

150 MHz, CD_3OD

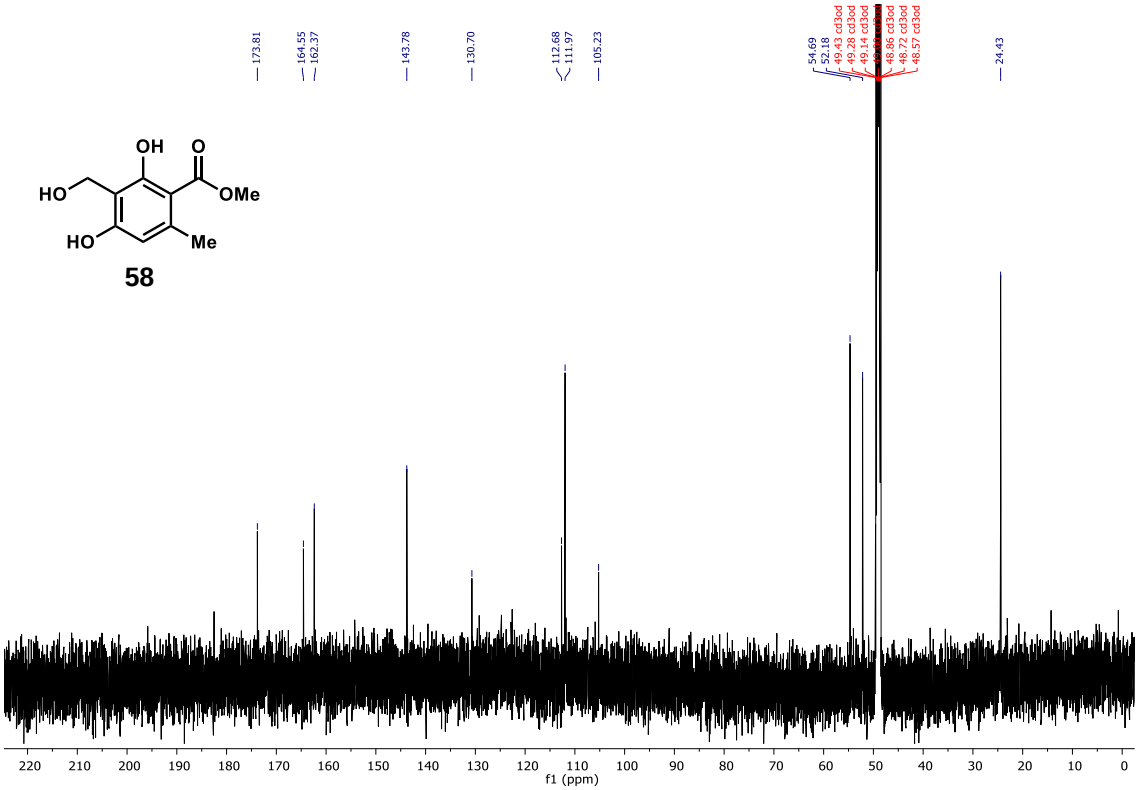

400 MHz, CD_3CN

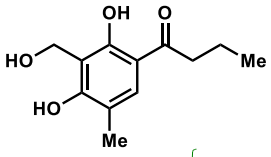

55

100 MHz, CD_3CN

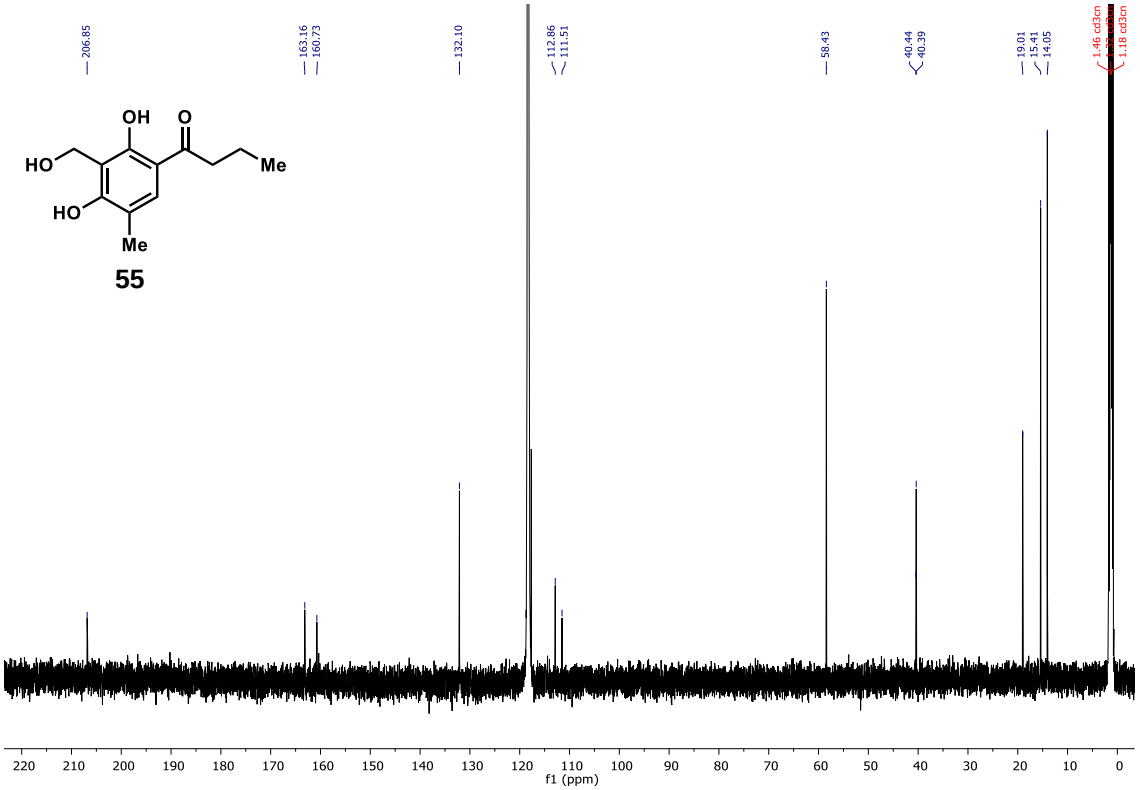

55

400 MHz, CD_3CN

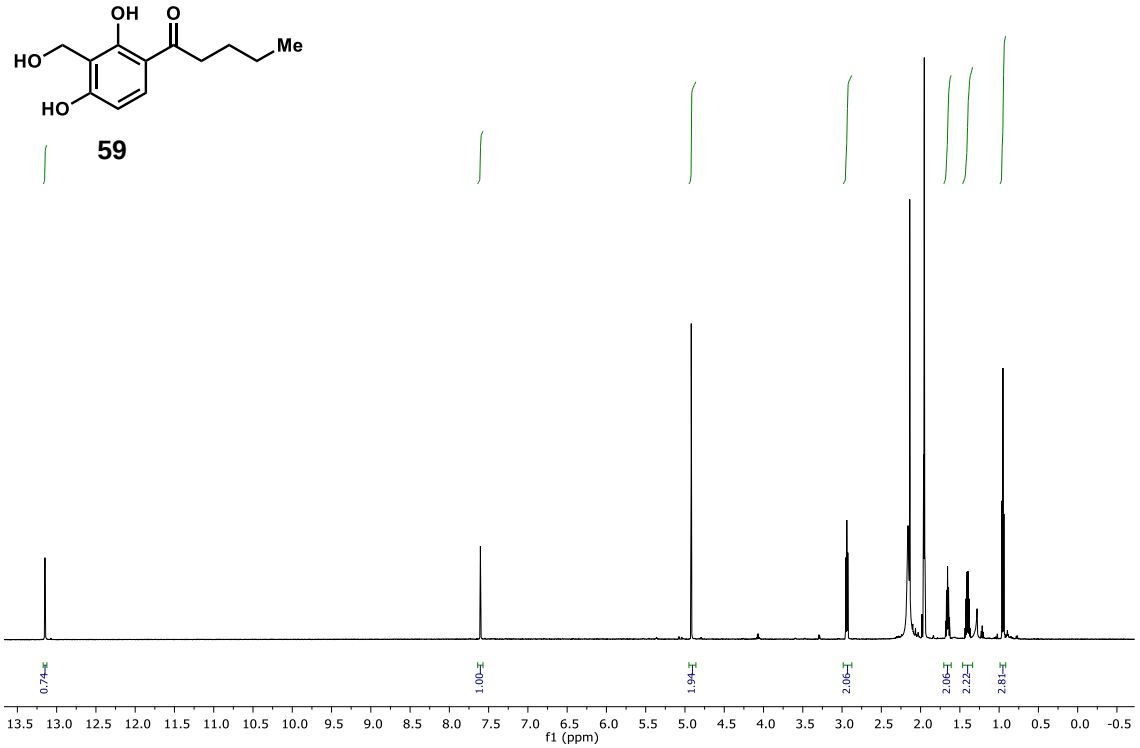

100 MHz, CD_3CN

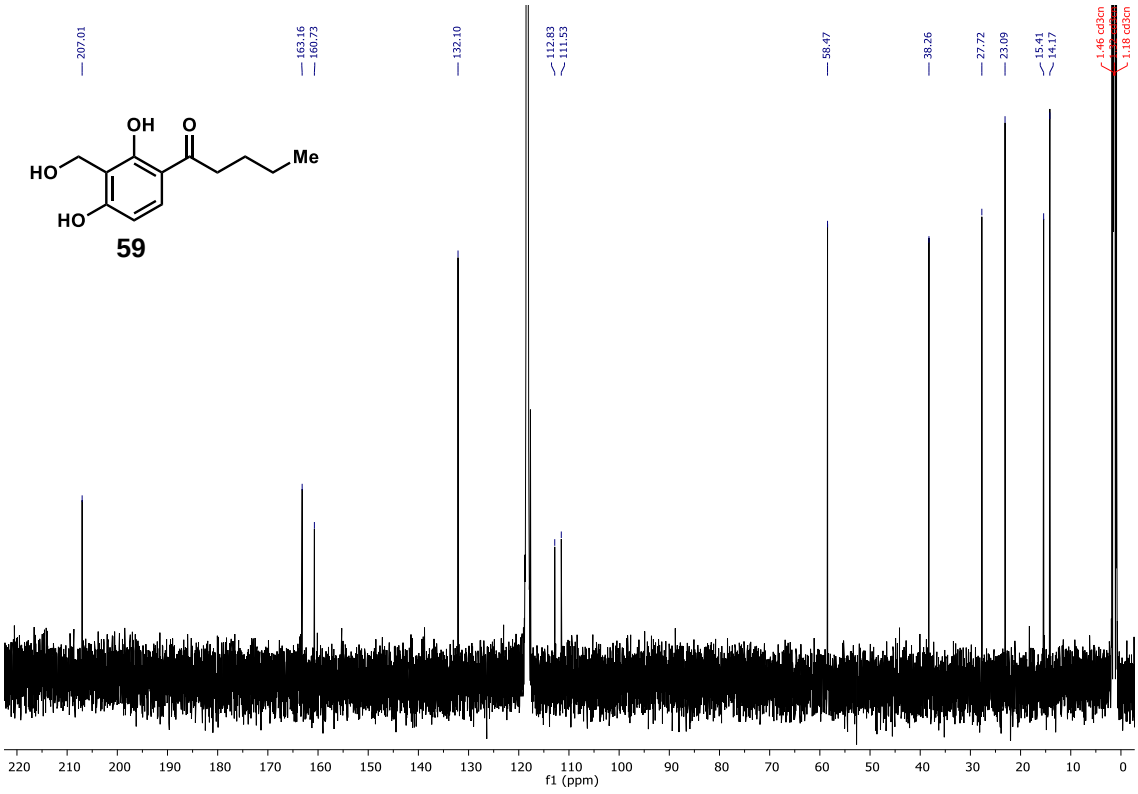

400 MHz, CD_3CN

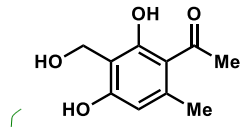

57

100 MHz, CD_3CN

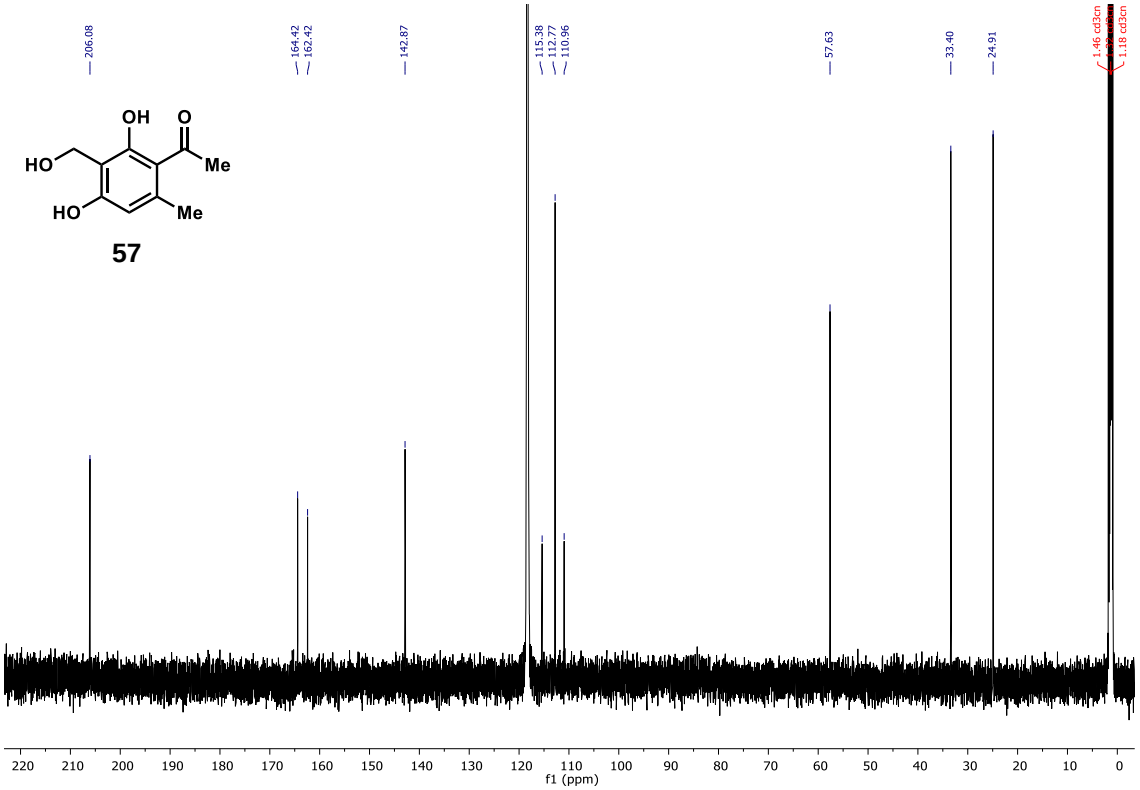

OH
O
HO
Me
HO
Me

57

400 MHz, CD_3CN

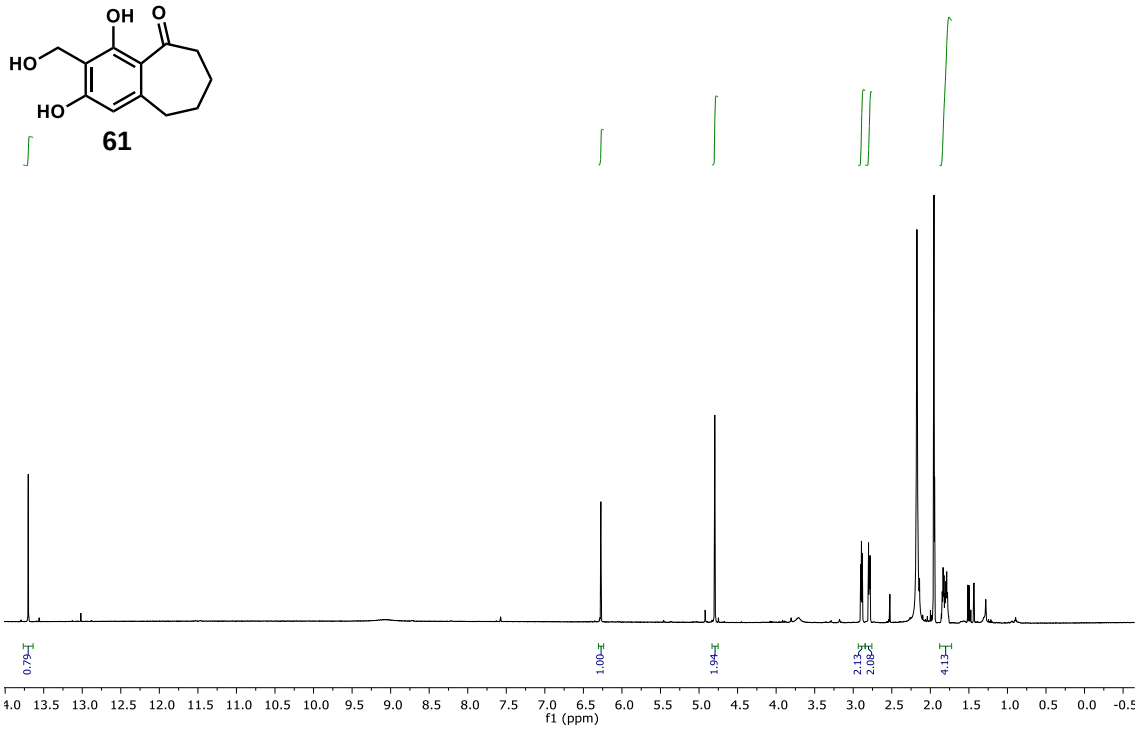

100 MHz, CD_3CN

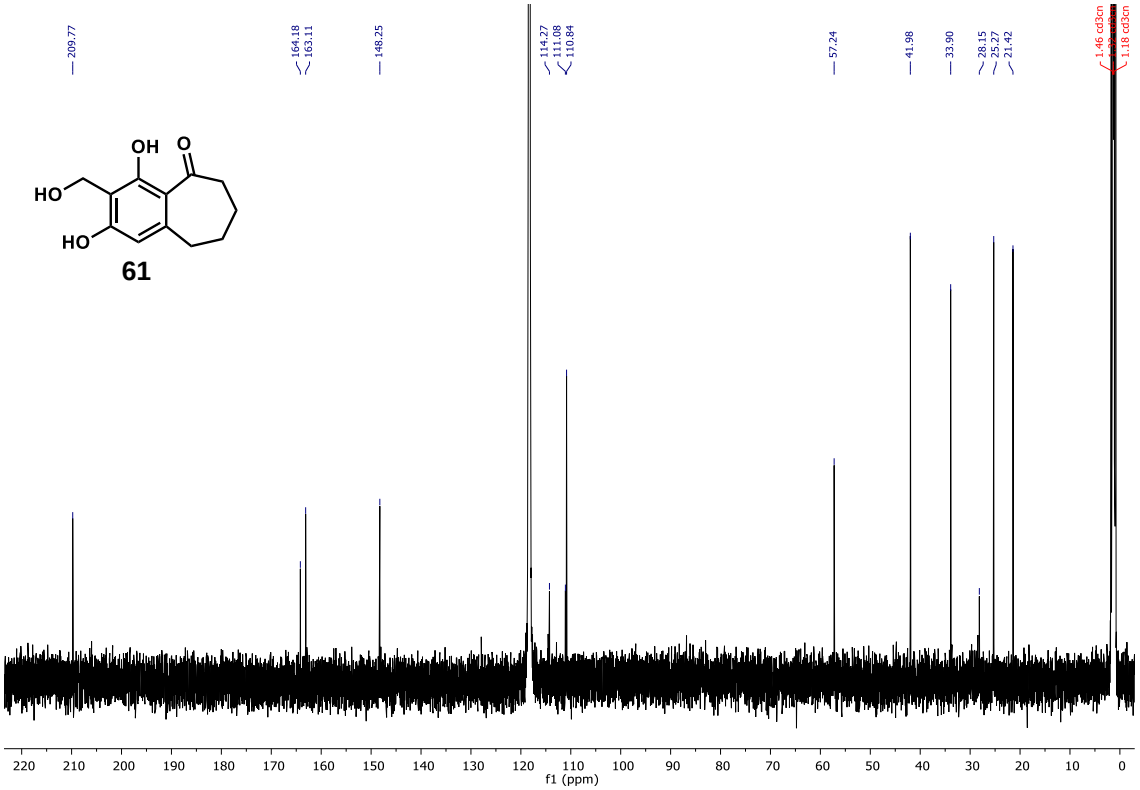

400 MHz, CD_3CN

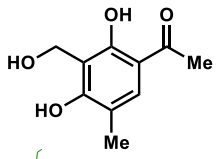

54

100 MHz, CD_3CN

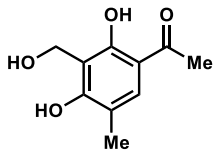

54

400 MHz, CD_3CN

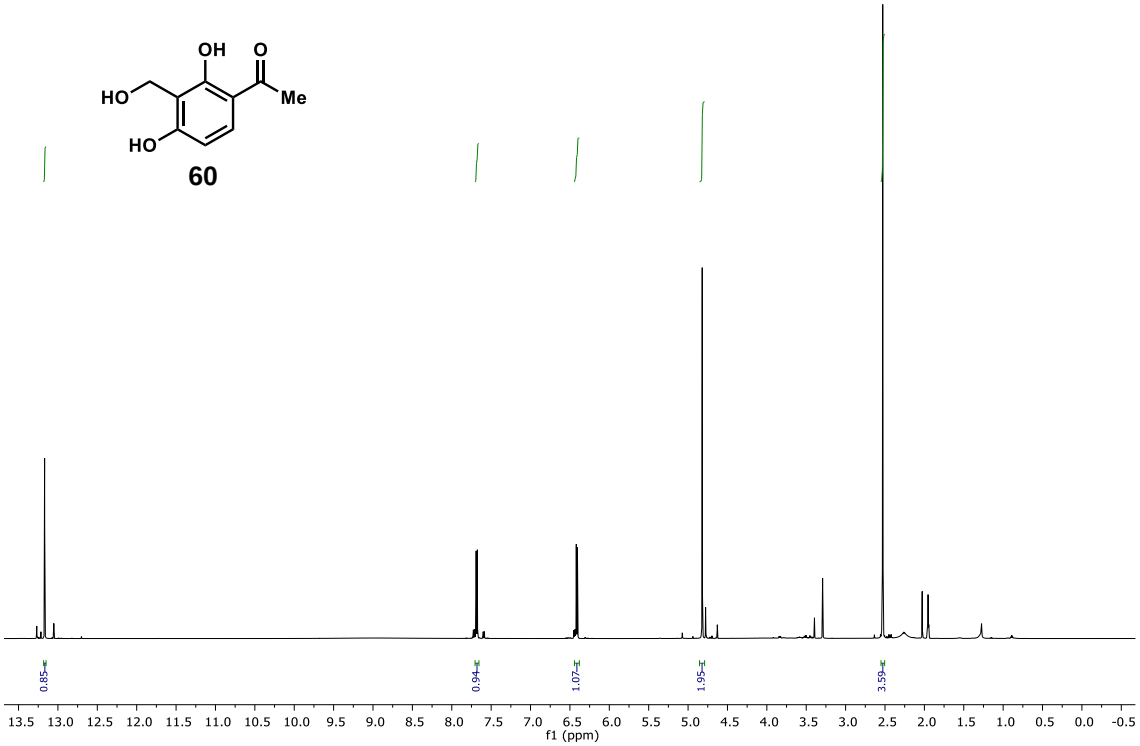

100 MHz, CD_3CN

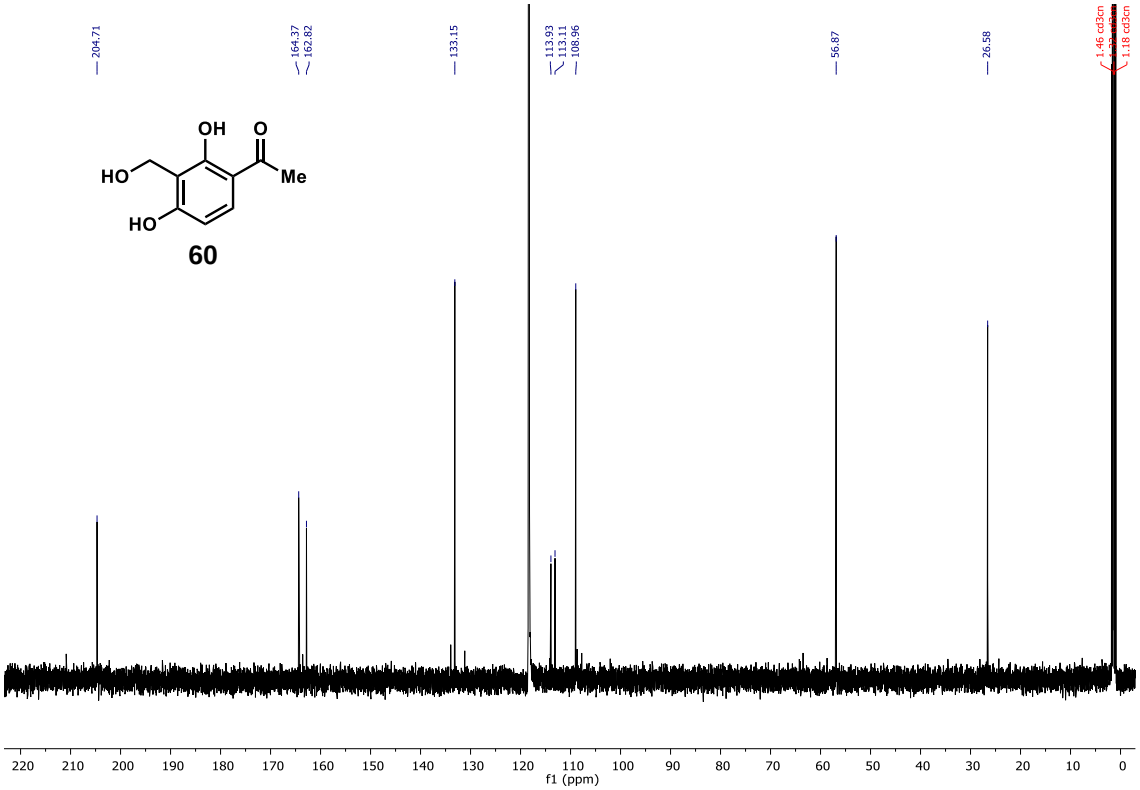

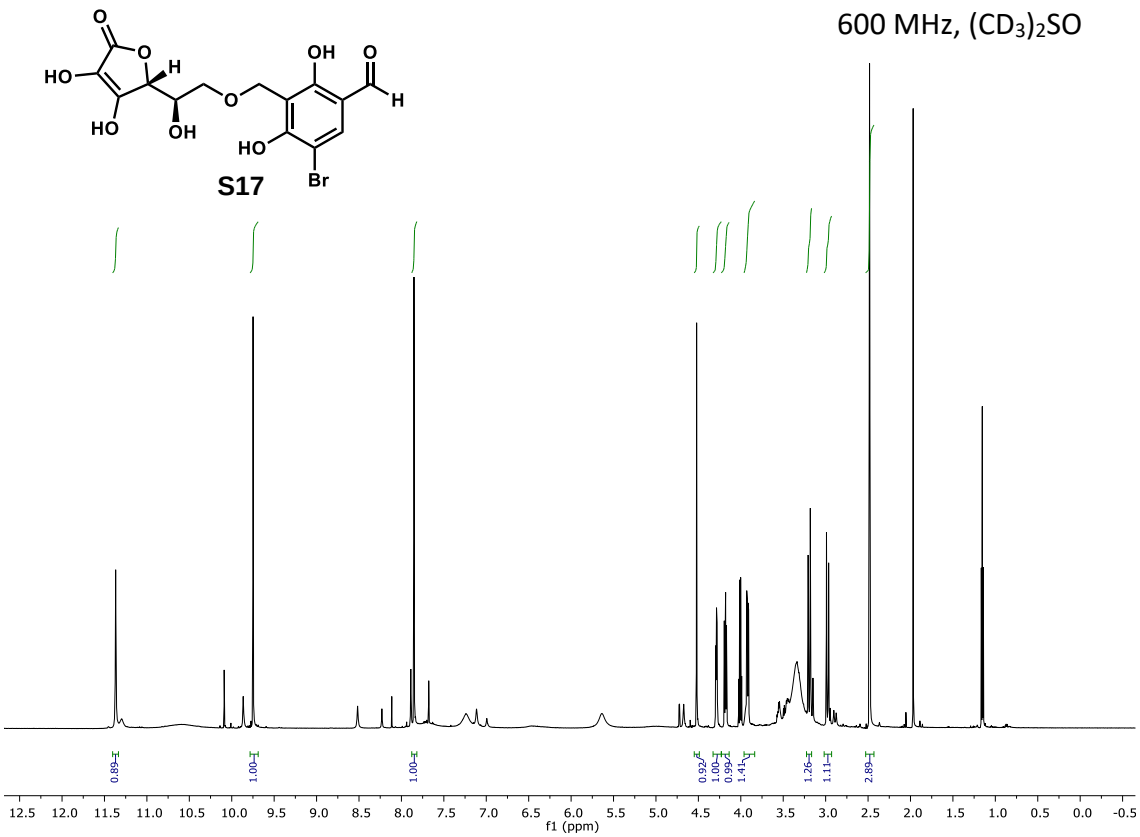
600 MHz, (CD3)2SO
S17
0.89
1.00
1.00
0.92
1.00
0.99
1.41
1.26
1.11
2.89
f1 (ppm)

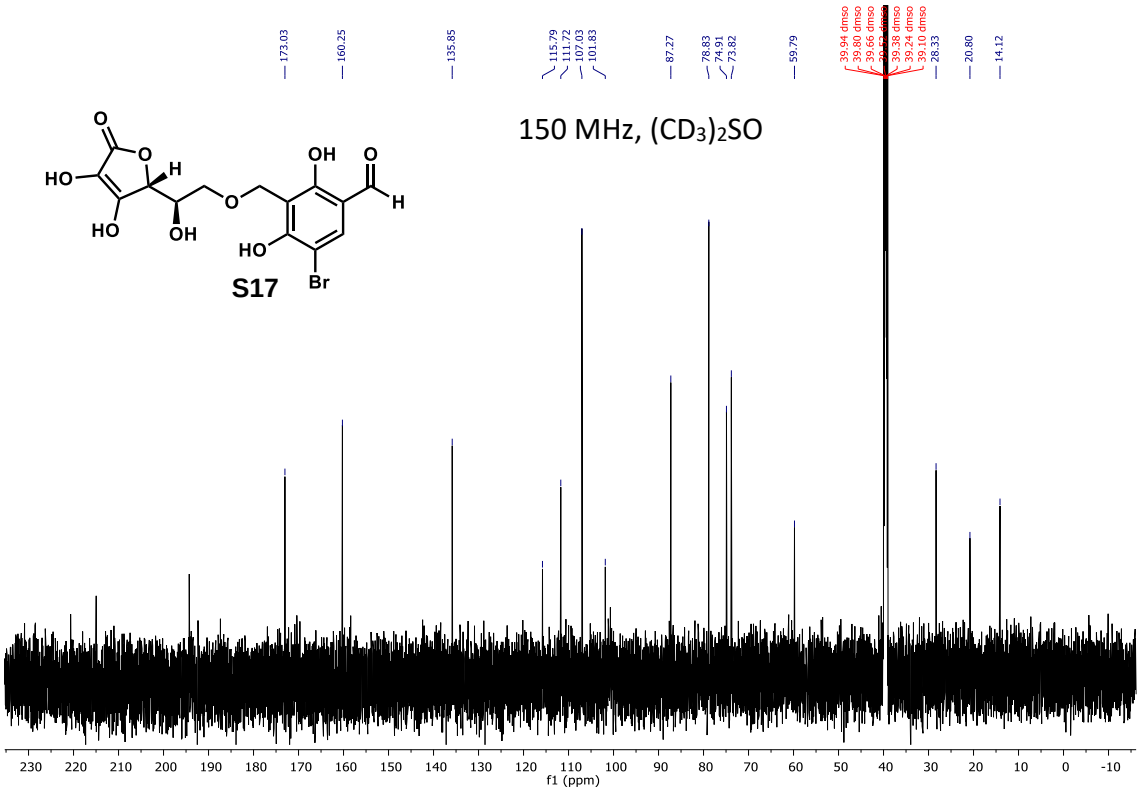
150 MHz, (CD3)2SO
S17
173.03
160.25
135.85
115.79
111.72
107.03
101.83
87.27
78.83
74.91
73.82
59.79
39.94 dmso
39.80 dmso
39.66 dmso
39.52 dmso
39.38 dmso
39.24 dmso
39.10 dmso
28.33
20.80
14.12
f1 (ppm)

Part XIII. Computational analysis of benzylic functionalization reactions

General computational information: All geometries and frequency computations were obtained using the unrestricted B3LYP density functional[9,10,11] and 6-311++G** basis set.[12,13] Reaction pathways were calculated using the single-ended growing string method.[14] All ground state geometries were confirmed to have no imaginary frequencies, and transition states were confirmed to have one imaginary frequency. Solvent corrections were performed using the SMD implicit solvent model (water)[15-17] and the cc-pVTZ basis set.[18-23] Reported energies are Gibbs free energies in solvent with gas-phase entropy and enthalpy corrections (at 298.15 K). Most simulations were performed using the Q-Chem 4.0 package,[24] except for the solvent computations, which were performed using ORCA 4.0.[25]

Thermodynamics of *ortho*-quinone methide generation and inverse-electron demand Diels-Alder (IEDDA) reactions: Supplementary Figure S68 depicts the potential energy diagram for the formation of the two possible *ortho*-quinone methides that can be accessed for benzylic alcohol **17**, and their subsequent reactions with ethyl vinyl ether or styrene. The model predicts moderate barriers for *ortho*-quinone methide generation and IEDDA reactions. Concerted, late transition states are seen for *ortho*-quinone methide generation (Supplementary Figure S69). For the C1 *ortho*-quinone methide, bonds between atoms $H1_a$ and $O1_a$ (C1-hydroxyl), $H2_a$ and $O2_a$ (water), and $O3_a$ and C7 (benzylic alcohol) are broken. Bonds between $H1_a$ and $O2_a$ (water) and $H2_a$ and $O3_a$ (new water) are formed. For C3 *ortho*-quinone methide, bonds between atoms $H1_b$ and $O1_b$ (C1-hydroxyl), $H2_b$ and $O2_b$ (water), and $O3_b$ and C7 (benzylic alcohol) are broken. Bonds between $H1_a$ and $O2_a$ (water) and $H2_a$ and $O3_a$ (new water) are formed. For the IEDDA reactions, the model shows concerted, asynchronous transition states for the IEDDA reactions (Supplementary Figure S70). For reactions with ethyl vinyl ether, changes in bond length are no greater than 0.996 Å (Supplementary Table S2). Reactions with styrene afford maximal bond length changes of 1.270 Å.

Supplementary Table S3. Changes in C-C and C-O bond lengths during IEDDA reactions with **17**.

Structure	Bond	Change in Bond Length (Å)
$TS2_{Ia}$	C-C	0.985
	C-O	0.541
$TS2_{IIa}$	C-C	0.996
	C-O	0.573
$TS2_{Ib}$	C-C	1.270
	C-O	0.815
$TS2_{IIb}$	C-C	1.212
	C-O	0.768

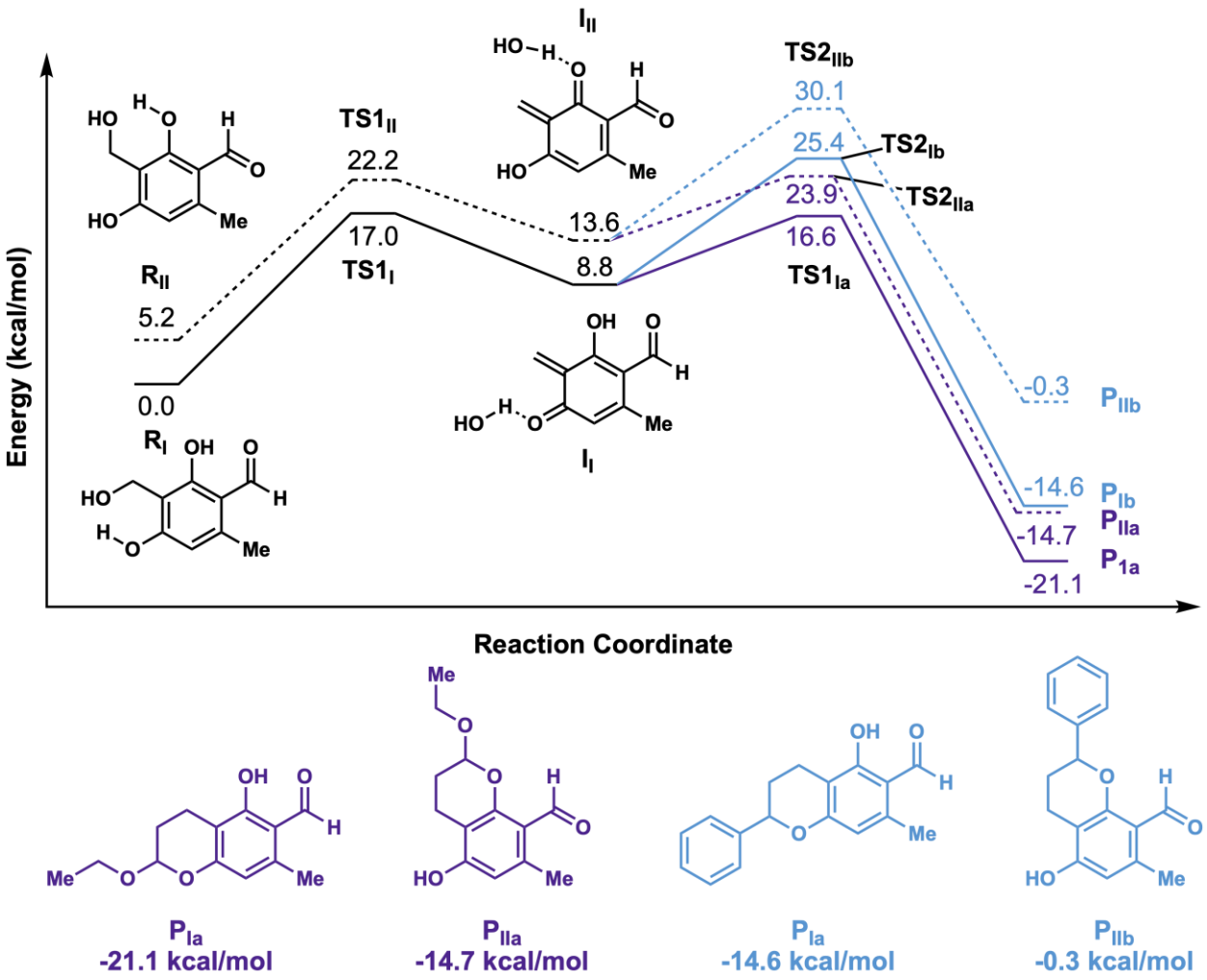

Supplementary Figure S82. Potential energy diagram for *ortho*-quinone methide (black) generation, and the subsequent IEDDA reactions with ethyl vinyl ether (purple) and styrene (light blue).

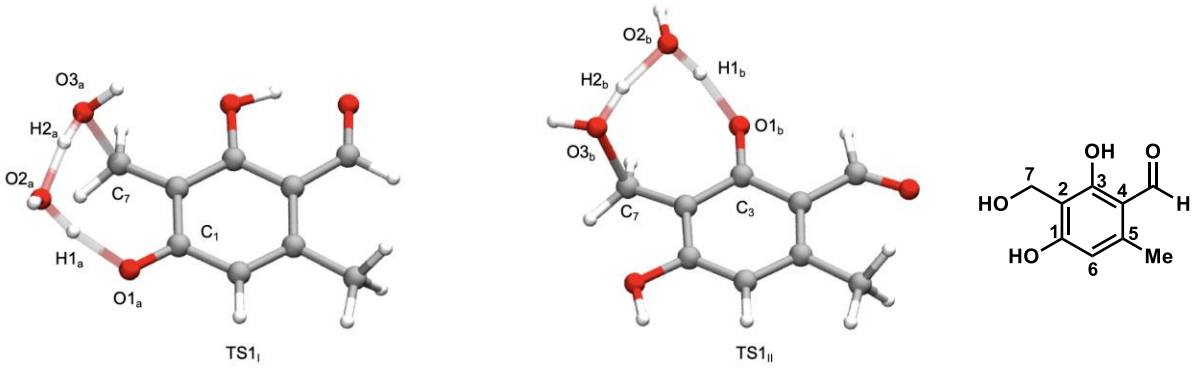

Supplementary Figure S83. 3D representations of transition states for both C1 and C3 *ortho*-quinone methides (I_I and I_{II} respectively). Both TS_I and TS_{II} structures undergo concerted, late stage transition states. Starting material (benzyl alcohol **17**) is depicted on the far right with the relevant carbons labelled.

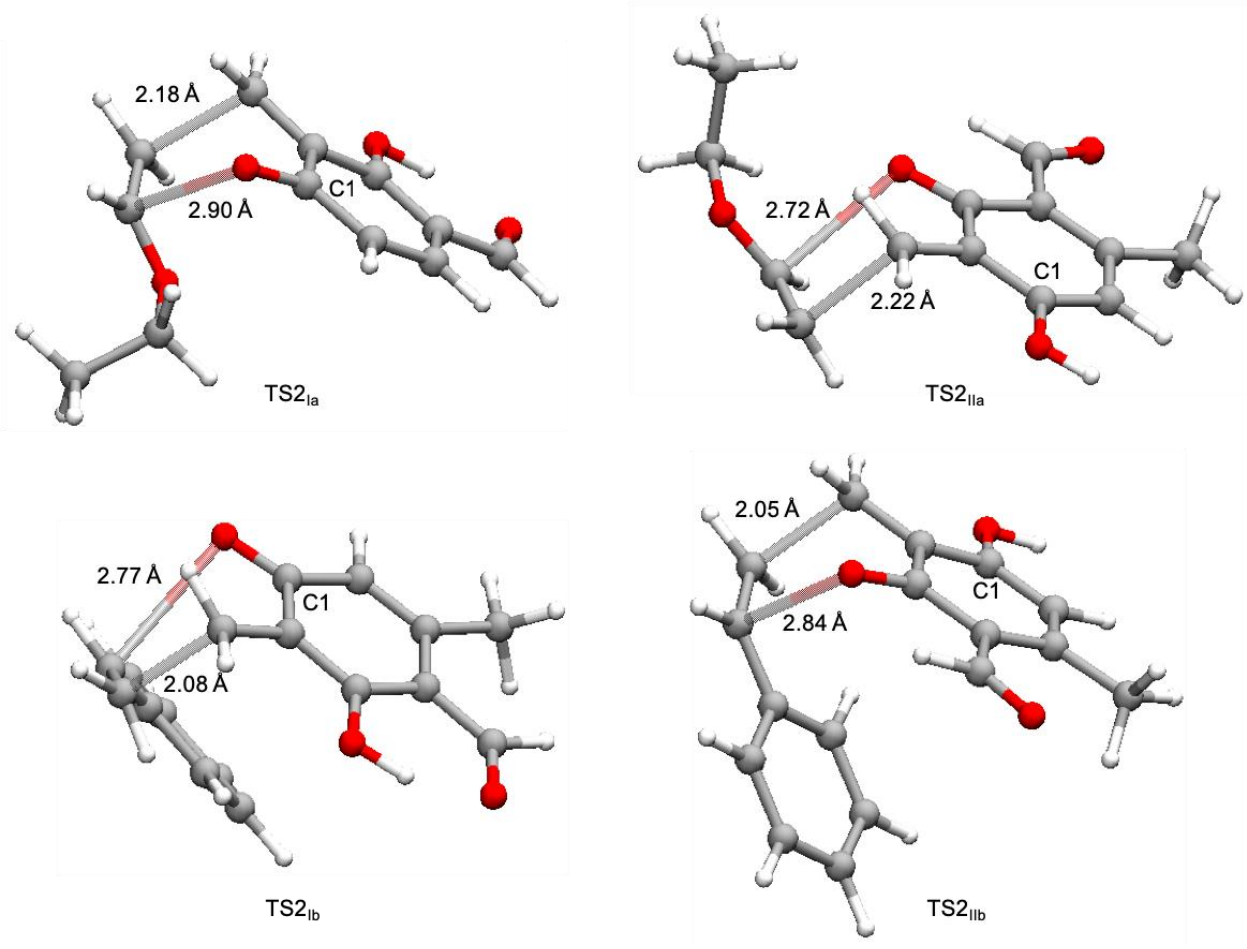

Supplementary Figure S84. Transition states for inverse electron-demand Diels-Alder reactions between I_I (left) and I_{II} (right) *ortho*-quinone methides with ethyl vinyl ether (top) and styrene (bottom). C-C distances are shorter than C-O distances for all transition states, which indicate asynchronous transition states.

Thermodynamic analysis of CitB-hydroxylated products: Experimental evidence from preparative-scale reactions with CitB suggested that benzylic alcohol products with C6-substitutents (**35**-**37** and **65**), particularly with electron-withdrawing substituents, were difficult to isolate without further elaboration to products downstream of *ortho*-quinone methide formation under the conditions of the CitB reaction. C5-substituted resorcinol substrates (**16** and **31**-**32**) did not typically exhibit this behavior under the same conditions. We conducted an analysis of the Gibbs free energies of CitB-generated benzylic alcohols of a panel of substrates (**16**, **31-32**, **35-37**, **65**, and **S18**-**S26**) to examine the impact of substitution pattern on benzylic alcohol stability. This analysis was carried out by comparing the Gibbs free energy for the benzylic alcohol products to their respective starting materials (ΔG_t). Mass balance was achieved by using a truncated 2-His-1-Asp non-heme iron system (Supplementary Figure S85).

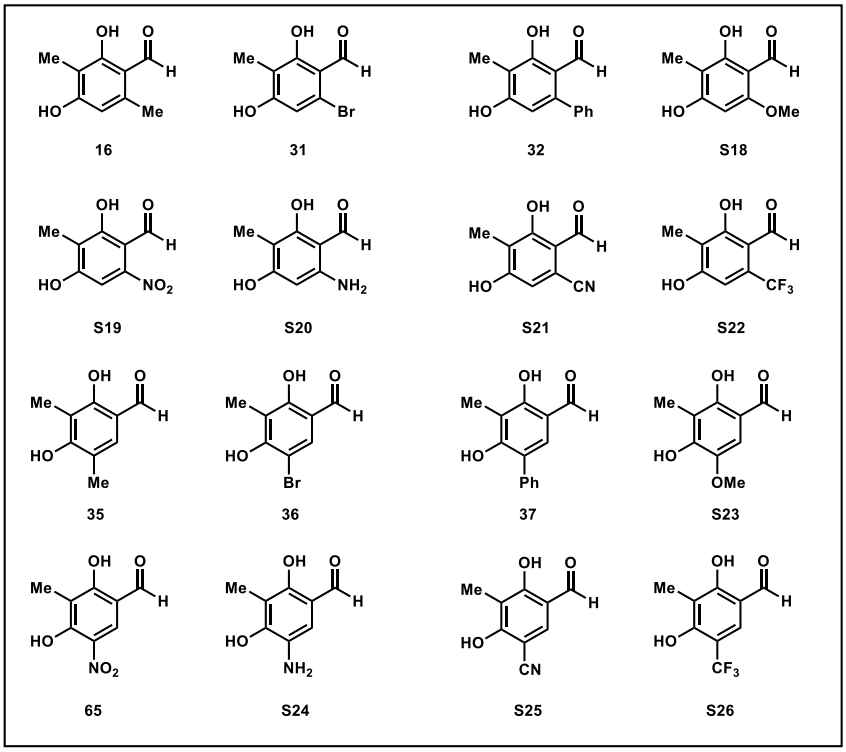

Supplementary Figure S85. Substrate panel used to develop thermodynamic relationships between starting material and products.

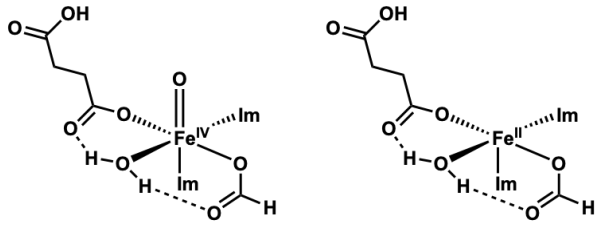

Supplementary Figure S86. Truncated 2-His-1-Asp non-heme iron system used for all thermodynamic calculations. Structure on left represents [Fe^{IV}] species and the structure on the right represents the [Fe^{II}] species. These structures were included to maintain atom balance between starting materials and benzylic alcohol products.

The ΔG_t of C6-substituted benzylic alcohols were spread over a relatively wide range of 5.1 kcal/mol, while the energies of the C5-substituted benzylic alcohols were nearly isoenergetic, with a range of 0.3 kcal/mol. This data indicated that the relative energies of these products was influenced by their substitution pattern. Further, we noted that benzylic alcohols containing inductively electron-withdrawing substituents in the C6-position generally tended to have higher energies, whereas the benzylic alcohol containing an inductively electron-donating substituent (R = methyl) had the lowest Gibbs free energy value in this substrate panel. This general trend is in agreement with our experimental observations, as **65**, which contains a nitro group at the C6 position, was quite reactive and difficult to isolate. Even upon isolation of the thiophenol adduct (**53**), we were required to use a non-nucleophilic NMR solvent for characterization, as MeOD quickly exchanged with thiophenol on the time-scale required for obtaining a ^{1}H NMR. In comparison, the analogous compound bearing a methyl group at C6 (**35**) could be transferred in MeOH and did not exchange with MeOD in the time required for full NMR characterization. To further investigate these observations, the Gibbs energies of thiophenol were analyzed in the same manner as the benzylic alcohol products. Through this analysis, we determined that thiophenol adducts of each CitB-hydroxylated product were lower in energy than their benzylic alcohol precursors (Supporting Fig. S88-S89). We also observed that the C6-nitro thiophenol adduct (**53**) had a relatively high Gibbs energy, which supported our observations that **65** exhibited reduced stability when compared to other isolated thiophenol adducts.

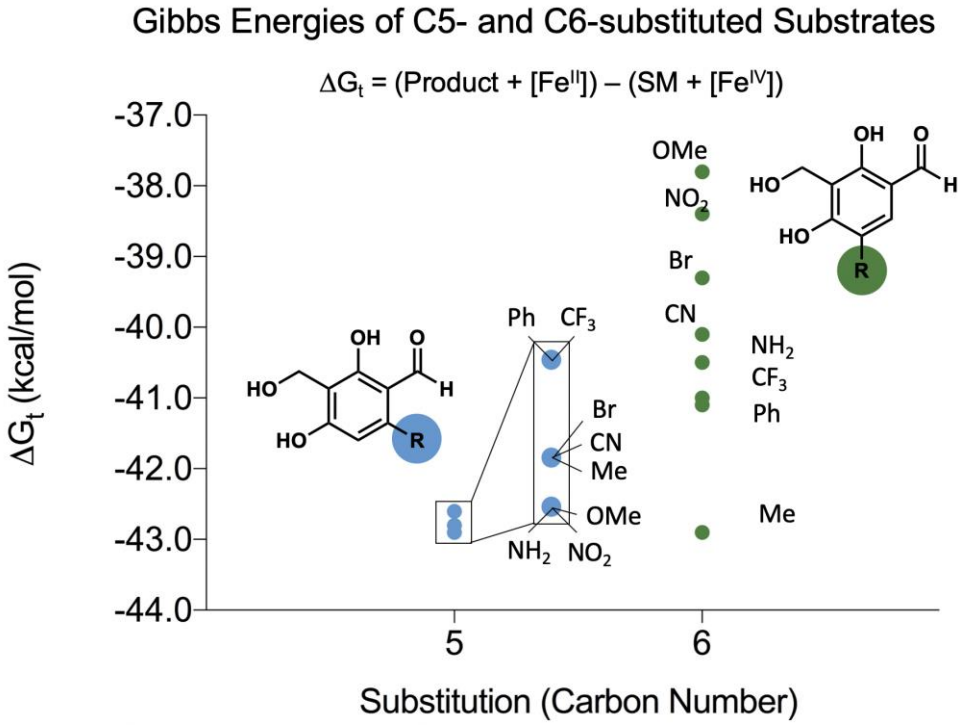

Supplementary Figure S87. Calculated thermodynamics (ΔG_t) of benzyl alcohol products, compared to their respective starting materials (SM). ΔG_t = (Product + [Fe^{II}]) – (SM + [Fe^{IV}]). Blue circles represent C5-substituted substrates and range from -43.6 to -43.9 kcal/mol. Green circles represent C6-substituted substrates and range from -37.8 to -42.9 kcal/mol.

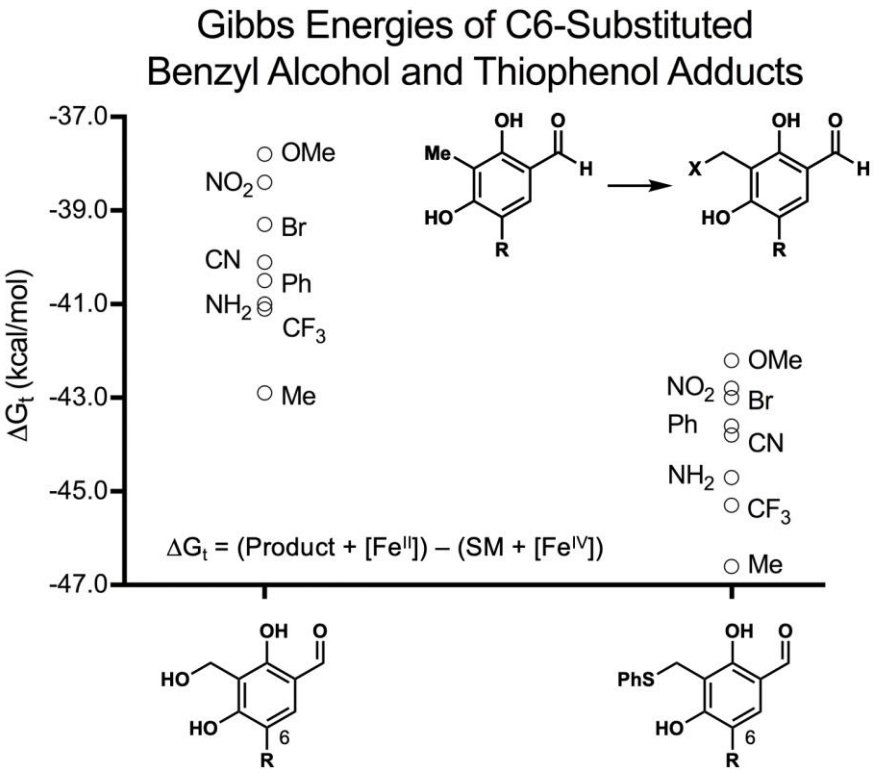

Supplementary Figure S88. Thermodynamic comparison of C6-substituted benzylic alcohols (left) and thiophenol products (right). All thiophenol products are lower in energy than the corresponding benzyl alcohol precursor. ΔG_t = (Product + [Fe^{II}]) – (SM + [Fe^{IV}]).

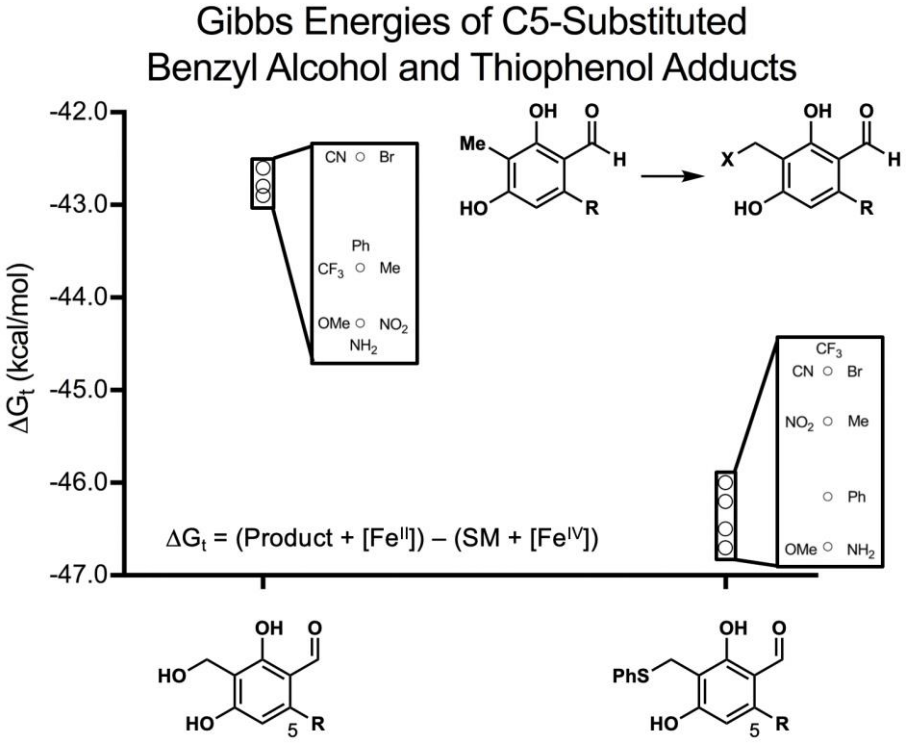

Supplementary Figure S89. Thermodynamic comparison of C5-substituted benzylic alcohols (left) and thiophenol products (right), compared to their respective starting material (SM). All thiophenol products are lower in energy than their benzylic alcohol precursors. ΔG_t = (Product + [Fe^{II}]) – (SM + [Fe^{IV}]).

Multivariable linear regression Hammett plot analysis: Intrigued by the apparent relationship between the free energy of C6-substituted substrates (**35**-**37**, **65**, and **S23**-**S26**) and the electronics of their substituents, we sought to define their Hammett relationship, which compares various electronic parameters (Hammett constants) based on substitution on an aryl ring. A relationship was found between the Hammett inductive (σ_I) and resonance (σ_R) constants and the Gibbs free energy of (ΔG_c) (Supplementary Figure S90). When plotting ΔG_c against ΔG_t, we observe a correlation with an R^2 of 0.7537. This correlation provides further support that electronics at the C6 position have an influence on the stability of the benzylic alcohol. An analysis of the coefficients of the regression reveals that σ_I has the larger coefficient than σ_R 7.7 and -4.7, respectively, and therefore is the most influential factor. Inspection of the σ_I and σ_R graphs against ΔG_t also confirms this conclusion (Supplementary Figures S91-S92).

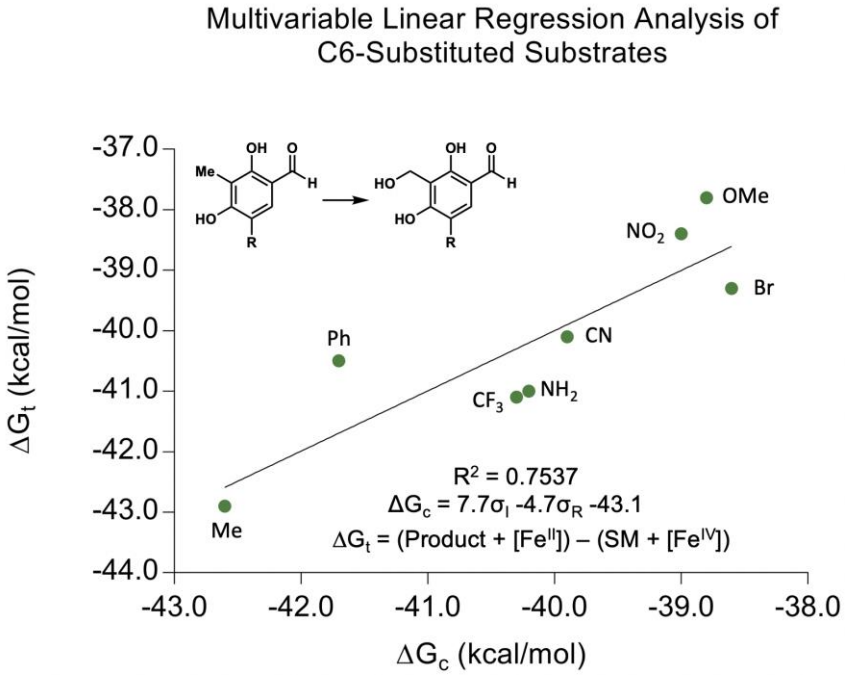

Supplementary Figure S90. Multivariable linear regression plot of combined inductive (σ_I) and resonance (σ_R) Hammett constants against calculated thermodynamics of C6-substituted substrates (see **xx**-**xx**, **xx**-**xx**) (ΔG_t). ΔG_t = (Product + [Fe^{II}]) – (SM + [Fe^{IV}]). A trend can be observed from inductively electron donating to inductively electron withdrawing. R^2 = 0.7537.

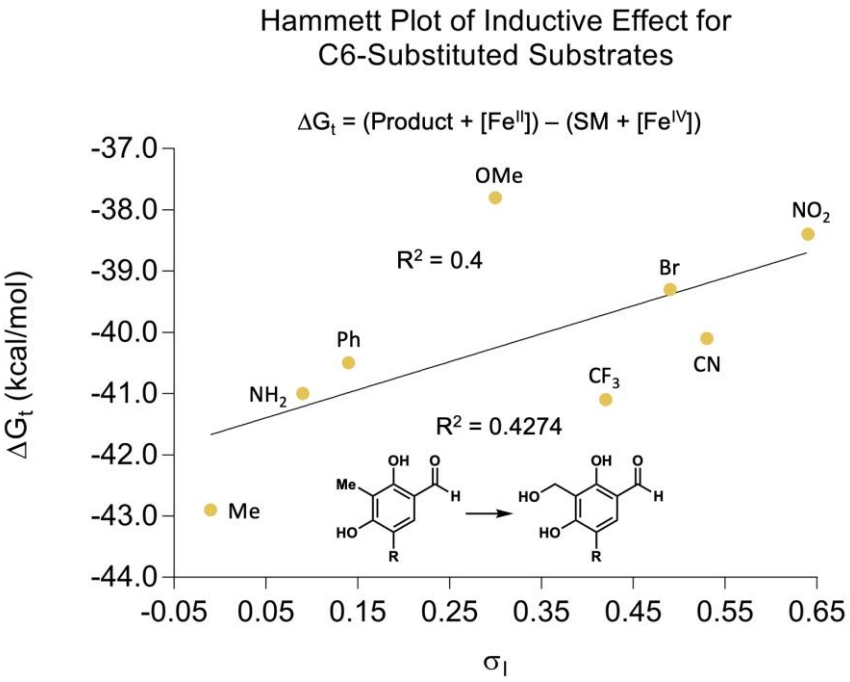

Supplementary Figure S91. Plot of the inductive Hammett constant (σ_I) against calculated thermodynamics (ΔG_t) of C6-substituted benzyl alcohol products compared to their respective starting materials. ΔG_t = (Product + [Fe^{II}]) – (SM + [Fe^{IV}]). ΔG_t ranges from -37.8 to -42.9 kcal/mol. R^2 = 0.424.

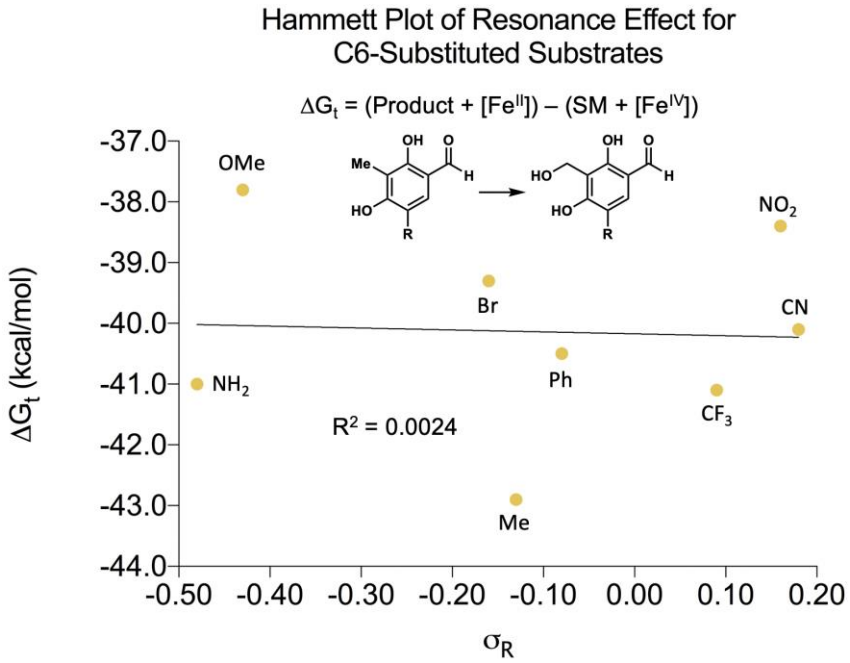

Supplementary Figure S92. Plot of the resonance Hammett constant (σ_R) against calculated thermodynamics (ΔG_t) of C6-substituted benzyl alcohol products compared to their respective starting materials.. ΔG_t = (Product + [Fe^{II}]) – (SM + [Fe^{IV}]). ΔG_t ranges from -37.8 to -42.9 kcal/mol. R^2 = 0.0024.

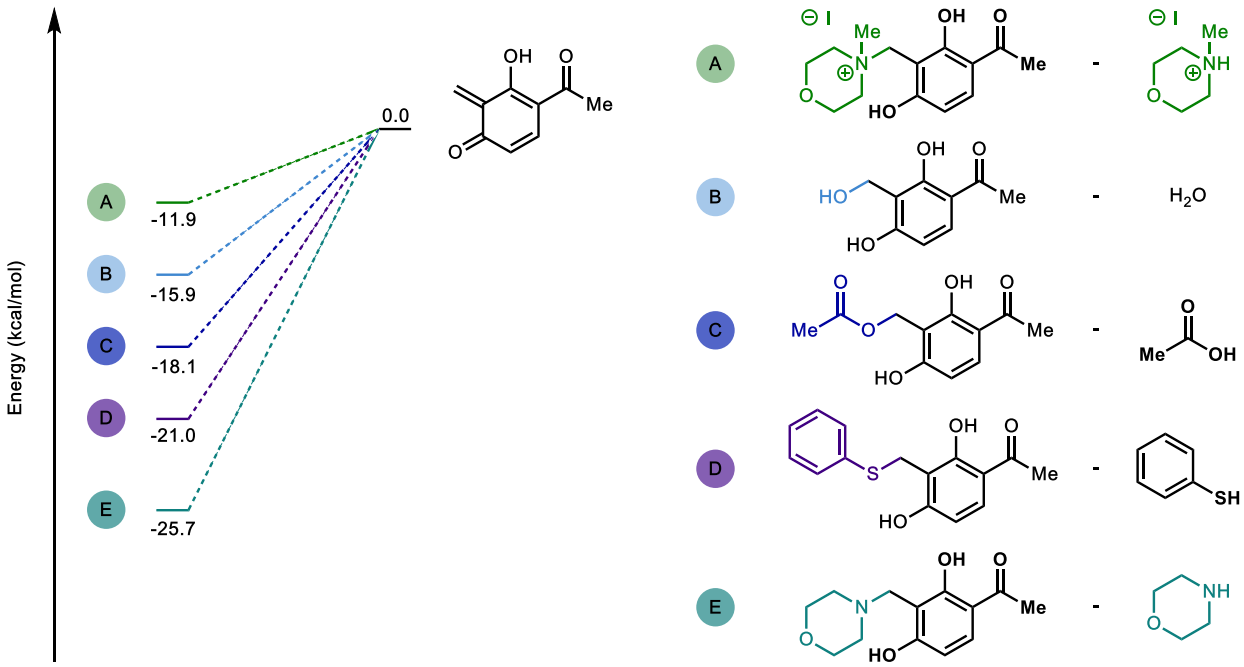

Supplementary Figure S93. Thermodynamic comparison of *ortho*-quinone methide precursors with a range of common leaving groups substituted at the benzylic position relative to the reactive *ortho*-quinone methide. This data shows that the benzylic alcohol (A) is higher in energy than other common leaving groups. This data also clearly shows why methylation of the morpholine adduct precursor used by Wilson and co-workers was necessary to observe *ortho*-quinone methide activity. Overall, this provides evidence as to why our enzymatically generated benzylic alcohol precursors can be used to access the *ortho*-quinone methide intermediates under such mild conditions.

Part XIV. XYZ coordinates of ortho-quinone methide and IEDDA transition states

$TS1_I$

H -4.9499456400 0.3051135600 0.4113060800
O -4.0414247800 0.1905241200 0.7316649200
H -3.7185704200 -0.7262253000 0.3535210500
C -2.8443859800 0.9804196500 -0.5535490500
H -2.8982343300 2.0398600900 -0.3262081000
H -3.4872014400 0.6268288300 -1.3533284500
O -2.8288415100 -1.7275963500 -0.3955920400
C -1.6393397800 0.2946932000 -0.3241739200
C -1.6906807200 -1.1569398800 -0.3862488800
O -0.4306888600 2.2663872900 0.1749792500
C -0.4274093000 0.9491992800 0.0104875200
C -0.4491738100 -1.8726385800 -0.3458470700
H -0.4907395000 -2.9525904900 -0.4402619200
H 0.5310208000 2.5221409900 0.3669362800
C 0.7392063900 -1.2273708300 -0.1049139400
C 0.7792546300 0.2024476000 0.0963095000
H 2.4888134500 -1.9392928100 0.9623600200
H 1.8051811700 -3.0951191200 -0.1884324400
C 2.0123708200 -2.0365368800 -0.0196777200
C 1.9892074500 0.9210841300 0.3723851700
O 2.0474349200 2.1565959800 0.5528138500
H 2.7457984200 -1.7139288300 -0.7673807000
H 2.9269280300 0.3453623700 0.4282085900

$TS1_{II}$

C 0.7609422300 0.1826692100 -0.1350069500
C -0.4964908500 0.8856089700 -0.1546474000
C -1.7258848300 0.1103971800 -0.1903379600
C -1.6772023100 -1.2857305800 0.0411133300
C -0.4530291600 -1.9336355000 0.1110299500
C 0.7594621700 -1.2197443900 0.0026149300
C -2.9128524600 0.8306537100 -0.4052586300
O -2.8796925500 2.1523788000 0.9999659900
O -2.8619882500 -1.9446020500 0.1171147800
O -0.6028285200 2.1579348100 -0.0720095800
C 2.0424029900 -2.0078820400 0.0633685700
C 1.9809787700 0.9937082200 -0.2035304900
O 3.1315683400 0.5696553400 -0.1979127100
H -3.8689494900 0.3410491300 -0.2553586700
H -3.4167840300 2.9079700900 0.7141229600
H -2.6927820400 -2.8869331400 0.2528852400
H -2.8928470200 1.6279710000 -1.1413423900
H -1.9066230500 2.3524182000 0.6613052800
H -0.4226526100 -3.0137369500 0.2324542800
H 1.8382503600 -3.0715753300 0.2132115500
H 2.6245371300 -1.8785628000 -0.8535223400
H 2.6898093800 -1.6438364000 0.8650917200

H 1.7830838200 2.0797994900 -0.2703474600

$TS2_{Ia}$

C -1.0362475800 0.3915354700 0.1127718900
C -2.0615369900 0.1378212700 1.0725993800
C -0.0597492100 -0.5883230500 -0.1641720100
C -0.1436962400 -1.8527799200 0.5091458900
C -1.1368341600 -2.1592796100 1.3890075100
C -2.1783460900 -1.1933113900 1.6999297900
H 0.6267831200 -2.5891380300 0.2836518800
H -1.1929744200 -3.1267625300 1.8779376600
C 0.9834671200 -0.3028425800 -1.1064803500
O 1.1034419600 0.7706324200 -1.7268151700
H 1.7244237900 -1.1066493800 -1.2807559800
O -1.0156784200 1.5790666500 -0.4947504200
O -3.1598839500 -1.4608426800 2.4283619100
C -3.0138825700 1.0977774500 1.4049750700
C -4.8437205100 0.8224115400 0.2447003600
H -2.8993381100 2.1125795500 1.0398365400
H -3.5530445300 0.9572028600 2.3335939000
C -5.0492786600 -0.5187795500 0.4351395700
H -4.4274862700 1.1631770900 -0.6973280000
H -5.4492681200 1.5227910700 0.8086404500
O -4.4938790600 -1.3977908900 -0.3844311100
H -5.5876000600 -0.9092717700 1.2958225800
H -0.2157145800 1.5704210300 -1.1031544200
C -4.6185120300 -2.8028294300 -0.0320072100
C -5.9827659900 -3.3543429000 -0.4152536300
H -6.0193004800 -4.4268427800 -0.1937596800
H -6.1754384200 -3.2159495900 -1.4839817400
H -6.7875383900 -2.8692274800 0.1482685500
H -4.3983097600 -2.8995740300 1.0356854600
H -3.8207333900 -3.2869228100 -0.5986686500

$TS2_{Ib}$

C -1.1226393400 0.4771206900 0.3527469300
C -2.2120106100 0.4039241900 -0.5616932000
C -0.2721416300 -0.6349971700 0.5572912100
C -0.5632216800 -1.8842882200 -0.1275907300
C -1.6552283100 -1.9951897400 -0.9387664200
C -2.5544406700 -0.8830068400 -1.1847780000
C 0.3396985900 -3.0794168800 0.0769665800
H -1.8947797700 -2.9328825600 -1.4310999600
C 0.8369690300 -0.4834008500 1.4561665900
O 1.1044273600 0.5629569700 2.0851172100
H 1.4981615000 -1.3533427900 1.6032346900
O -0.9197703700 1.6337977300 0.9874699100
O -3.5984034500 -0.9780117400 -1.8632513500
C -3.0365223100 1.4960453100 -0.8593276500
C -4.7863019700 1.4571353000 0.2066467100
H -3.5597654200 1.4417813800 -1.8070949000
H -2.7357836400 2.4810870700 -0.5160489400

C -5.3160086700 0.1829797300 0.0818792700
H -5.2571192100 2.2592739200 -0.3545150600
H -4.3441247900 1.7631078100 1.1497444700
H -5.9832313000 -0.0217203700 -0.7505884600
C -5.0291217300 -0.9304689700 0.9534445900
H -0.0944095300 1.5010391800 1.5532405600
C -4.1049026600 -0.8441494500 2.0185403000
C -5.6864753500 -2.1629981300 0.7358036800
C -5.4513617600 -3.2529684300 1.5606200500
C -3.8625849800 -1.9445608200 2.8364557600
C -4.5375094300 -3.1466547000 2.6166736400
H -3.5778012800 0.0842896400 2.2106592500
H -3.1469792800 -1.8624805800 3.6496698400
H -5.9708757900 -4.1901963800 1.3821240800
H -4.3514799500 -4.0005532800 3.2623996900
H -6.3790517300 -2.2482040000 -0.0972220800
H 1.3710855200 -2.8674232400 -0.2315179500
H -0.0162700300 -3.9314923200 -0.5080897500
H 0.3768056300 -3.3872254700 1.1295924300

$TS2_{IIa}$

C 1.3663481200 0.8862776400 0.6794257500
C 0.0739675900 0.2354337600 0.4151188100
C 2.5765996900 0.2267469900 0.1966877000
C 2.4802819100 -0.9561587200 -0.5451555000
C 1.2131151800 -1.5167931600 -0.8471165000
C 0.0446510800 -0.9313547000 -0.4041025500
H 1.1694713700 -2.4318909900 -1.4346299900
C 3.8507670900 0.8734376600 0.5186424700
O 4.9682919300 0.4846176100 0.1917999100
H 3.7360883000 1.7979606900 1.1151505700
O 1.3780583500 1.9979432800 1.2647325000
C -1.0779428100 0.8384189000 0.9101031300
C -1.5987970800 2.6437180000 -0.2694298100
H -0.9843355900 1.4793521800 1.7778721000
H -2.0401297600 0.3659645400 0.7446094300
C -0.6136810000 3.4930963900 0.1635385600
H -2.5926116100 2.7234478700 0.1599288100
H -1.5153371900 2.2134381700 -1.2596314300
O -0.7734149800 4.2077050900 1.2686333100
H 0.3389360100 3.5847645800 -0.3505804700
O -1.1831846400 -1.4448259400 -0.6912279800
C 3.6987185500 -1.6796834700 -1.0634888100
H 4.2822048600 -1.0396443400 -1.7325871100
H 3.4101751500 -2.5902761800 -1.5982089600
H 4.3800075700 -1.9397816200 -0.2481818200
H -1.0699674400 -2.2492892900 -1.2225538500
C 0.3763652800 4.9034843100 1.8129863000
C 0.5525250800 4.5074021000 3.2669427700
H 0.1696705700 5.9738690300 1.7043239400
H 1.2621005100 4.6405793500 1.2286608100
H -0.3588723600 4.7066594500 3.8403023000
H 1.3707554400 5.0874505200 3.7089355200
H 0.7994148600 3.4449303200 3.3295001100

$TS2_{IIb}$

C 1.0776353600 1.8739808300 -0.3393770100
C -0.0114023500 1.0045305600 0.1353536500
C 2.4492733000 1.3772349000 -0.2320166900
C 2.6918462100 0.1186801100 0.3232158500
C 1.6193084300 -0.6691403600 0.8216167000
C 0.3124637500 -0.2302909000 0.7637797400
H 1.8426930700 -1.6405329100 1.2590520500
C 3.5071395600 2.2606430600 -0.7310854500
O 4.7116308300 2.0253189700 -0.7242610900
H 3.1265411400 3.2153802900 -1.1387416700
O 0.7817387000 3.0092089400 -0.7772632500
C -1.3132370300 1.4913287000 -0.0067980000
C -1.7338153000 2.9518040500 1.4151011700
H -2.1494701300 0.8475312200 0.2473228700
H -1.4633571200 2.2024051300 -0.8101354200
C -0.7023248000 3.8754775400 1.3924754300
H -1.8237642500 2.2635336400 2.2501405100
H -2.6773182100 3.2315585800 0.9558029900
C 0.4977034200 3.8195029000 2.1962047100
H -0.7780233700 4.7180259100 0.7109601700
O -0.7302737900 -0.9531443600 1.2645062000
C 4.0826983400 -0.4566886400 0.4345712100
H 4.5569438300 -0.5368651100 -0.5484770500
H 4.0563829700 -1.4464955000 0.9017815800
H 4.7355387700 0.2006925500 1.0163531100
H -0.3897157100 -1.7907372700 1.6179999800
C 0.7927955400 2.7304215000 3.0440297000
C 1.4274425000 4.8814311400 2.1255758100
C 2.5916237400 4.8634750900 2.8807909900
C 1.9676044100 2.7101969200 3.7913817200
C 2.8670510700 3.7751089100 3.7174798900
H 2.1826248600 1.8603216000 4.4331784800
H 3.7817299400 3.7575060500 4.3034370700
H 1.2230721700 5.7155843200 1.4594676600
H 3.2936566800 5.6896618800 2.8133536600
H 0.1002894900 1.8989377500 3.1198977500

Part XV. References

1. Baker Dockrey, S. A.; Lukowski, A. L.; Becker, M. R.; Narayan, A. R. H., *Nat. Chem.* **2018,** *10*, 119.

2. Abood, A.; Al-Fahad, A.; Scott, A.; Hosny, A. E.-D. M. S.; Hashem, A. M.; Fattah, A. M. A.; Race, P. R.; Simpson, T. J.; Cox, R. J., *RSC Advances* **2015,** *5* (62), 49987-49995.

3. Backus, K. M.; Correia, B. E.; Lum, K. M.; Forli, S.; Horning, B. D.; González-Páez, G. E.; Chatterjee, S.; Lanning, B. R.; Teijaro, J. R.; Olson, A. J.; Wolan, D. W.; Cravatt, B. F., *Nature* **2016,** *534*, 570.

4. Li, L.; Liu, Y.; Wang, Q., *Eur. J. Org. Chem.* **2013,** *2013* (35), 8014-8021.

5. Zang, Y.; Song, X.; Li, C.; Ma, J.; Chu, S.; Liu, D.; Ren, Q.; Li, Y.; Chen, N.; Zhang, D., *Eur. J. Med. Chem.* **2018,** *143*, 438-448.

6. Cort, A. D.; Mandolini, L.; Panaioli, S., *Synth. Commun.* **1988,** *18* (6), 613-616.

7. Baciocchi, E.; Mandolini, L.; Rol, C., *J. Org. Chem.* **1980,** *45* (19), 3906-3909.

8. Vece, V.; Jakkepally, S.; Hanessian, S., *Org. Lett.* **2018,** *20* (14), 4277-4280.

9. Carter, D. V.; Charlton, P. T.; Fenton, A. H.; Housley, J. R.; Lessel, B., *J. Pharm. Pharmacol.* **1958,** *10* (S1), 149T-159T.

10. Becke, A. D. *J. Chem. Phys.* **1993**, *98*, 5648–5652.

11. Lee, C.; Yang, W.; Parr, R. G. *Phys. Rev. B* **1988**, *37*, 785–789.

12. Krishnan, R.; Binkley, J. S.; Seeger, R.; and Pople, J. A. *J. Chem. Phys.* **1980**, *72*, 650-654.

13. Clark, T.; Chandrasekhar, J.; Schleyer, P. v. R., *J. Comp. Chem.* **1983**, *4*, 294-301.

14. Zimmerman, P. M. *J. Comput. Chem.* **2015**, *36*, 601-611.

15. A. V. Marenich, R. M. Olson, C. P. Kelly, C. J. Cramer, and D. G. Truhlar, *J. Chem. Theory Comput.* **2007**, *3*, 2011-2033.

16. A. V. Marenich, R. M. Olson, C. P. Kelly, C. J. Cramer, and D. G. Truhlar, *J. Phys. Chem. B* **2009**, *113*, 6378-6396.

17. A. V. Marenich, C. J. Cramer, and D. G. Truhlar, *J. Chem. Theory Comput.* **2013,** *9*, 609-620.

18. Dunning, Jr., T.H. *J. Chem. Phys.* **1989**, *90*, 1007-1023.

19. Kendall, R. A.; Dunning, Jr., T.H.; and Harrison, R.J. *J. Chem. Phys.* **1992**, *96*, 6796-6806.

20. Woon, D. E. and Dunning, Jr., T. H. *J. Chem. Phys.* **1993**, *98*, 1358-1371.

21. Woon, D. E. and Dunning, Jr., T. H. *J. Chem. Phys.* **1994**, *100*, 2975-2988.

22. Wilson, A. K.; Woon, D.E.; Peterson, K.A.; Dunning, Jr., T.H. *J. Chem. Phys.* **1999**, *110*, 7667-7676.

23. Balabanov, N. B. and Peterson, K. A. *J. Chem. Phys.* **2005**,*123*, 064107.

24. Neese, F. *WIREs Comput. Mol. Sci.* **2012**, *2*, 73-78.

25. Shao, Y. et al. *Mol. Phys.* **2015**, *113*, 184–215.